Exploiting the geochemical attributes of migrated oils for an improved understanding of their sourcing facies

Lessons learned from the southeastern Caribbean and the Norwegian Barents and North Seas

Andrés Felipe Cedeño Motta

Thesis submitted in fulfilment of
the requirements for the degree of
PHILOSOPHIAE DOCTOR
(PhD)

Faculty of Science and Technology
Department of Energy Resources
2022

University of Stavanger
NO-4036 Stavanger
NORWAY
www.uis.no

ISBN: 978-82-8439-141-0
ISSN: 1890-1387
PhD Thesis UiS No. 678

Preface

This thesis is submitted in fulfilment of the requirements for the degree of Philosophiae Doctor (PhD) at the University of Stavanger (UiS), Norway. The research was completed between August 2018 and October 2022 and was founded by the LOCRA, JuLoCra (https://wp.ux.uis.no/julocra/) and CBTH (http://cbth.uh.edu/) projects. During this period, I worked as a research fellow at the Department of Energy Resources, Faculty of Science and Technology. My main supervisor is Professor Alejandro Escalona (UiS), and my co-supervisor is Professor Sverre Ohm (UiS). Collaboration was established with other UiS researchers: Luis Rojo and Guro Skarstein, Professor Nestor Cardozo, and Associated Professor Dora Marin. Adjunct Professor Thomas Demchuck at Louisiana State University and Professor Snorre Olaussen at UNIS were important collaborators. Additional industry collaboration was established with Eshita Narain (Staatsolie), Jan de Jager (independent consultant), Andrew Pepper (T!PS), and Elisabeth Roller (Belmont). During this time, I supported Professor Alejandro Escalona and Sverre Ohm in teaching the *Introductory Geology* bachelor course (GEO100) and the *Petroleum Systems* master course (GEO690), respectively. I occasionally supported Professor Escalona in teaching selected topics of the *Subsurface Interpretation* Master course (GEO600).

This research has resulted in five main publications, four as first author and one as a coauthor. They are published in two different journals: *American Association of Petroleum Geologist (AAPG) – Memoir 123* and *Marine and Petroleum Geology*. Besides these publications, I have authored other 2 papers and coauthored one more, which are complementary to the main publications (Annex 2). Likewise, I have presented several aspects of this research in academic and industry conferences.

The first chapter of this thesis introduces the main themes, objectives, implementation, database, results, discussion, conclusions, and recommendations. The second chapter is a compilation of the five papers constituting the main research production of this study.

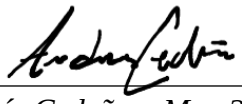

Andrés Cedeño – May 2022

Acknowledgements

First and foremost, I would like to express my deepest gratitude to my supervisors: Professors Alejandro Escalona and Sverre Ohm. Your guidance and support through the past four years have been essential to the completion of this work. I wholeheartedly appreciate your willingness and time for constructive discussions and feedbacks in no time. I tressure the freedom and flexibility you have granted me to make my own decisions and move across different disciplines.

A huge thank you to the sponsors of the CBTH and JuLoCrA consortia for providing essential economic support, without your contributions this research would not be possible. Projects' heads: professors Paul Mann (CBTH), Snorre Olaussen (JuLoCrA), and Alejandro Escalona (CBTH and JuLoCrA) are sincerely thanked. I am grateful to the Norwegian Petroleum Directorate, SINTEF, Staatsolie, and Barbados National Petroleum Company for facilitating the sediment and oil samples necessary to develop this research. Eshita Narain at Staatsolie is massively thanked for her efforts in providing data. I thank Integrated Geochemical Interpretation for providing academic licenses of their software, Alex Zumbergue at GeoMark Research for access to their oil data base, and Applied Petroleum Technologies for analytical studies, especially Per Erling Johansen. An enormous thank goes to Andreas Habel at UiS for his constant IT support.

Many thanks to my research fellows Ivan, Luis, Sayyid, Bereke, Xiaoan, Guro, Solveig, and Camilo for all the technical contributions, laughs, and support. Special thanks go to Associate Professor Dora Marin and Professor Nestor Cardozo at UiS for their technical contributions, teaching, and friendship through the years. Gunardi Sulystio at BHP and Andrew Pepper at T!PS are sincerely thanked for voluntarily sharing their knowledge and

experience during their free time. My geochemical knowledge grew exponentially through our discussions on the GoM and circum-Caribbean.

Finally, but most importantly, I would like to express my gratitude to my mother, sisters, and girlfriend. Your love, patience, and support have been an endless source of motivation during this journey.

Andrés Cedeño – May 2022

Summary

Assessing the geochemistry of oils and the source rock facies from which they originated is crucial in petroleum systems analysis. Crude oils are usually available for geochemical characterization, but pertinent source rock data is often scarce or absent because exploratory drilling mostly targets reservoirs in structurally elevated areas and fails to sample the deeply buried, prolific basinal source facies. Explorationists, unable to perform direct oil-to-source correlations, must rely on source rock inferences drawn from oil geochemistry, a practice named geochemical inversion.

This work focuses on organic geochemical investigations in the southeastern Caribbean-Atlantic margin and selected areas of the Norwegian Continental Shelf. These geologically distinct regions were selected as natural laboratories because their different data sets and geochemical commonalities offer a unique arena to explore the successes and pitfalls of selected geochemical proxies in geochemical inversion. A variety of techniques are employed to: (1) Review the accuracy of stable carbon isotopes in assessing organofacies in source rocks and oils; (2) Explore the utility of inverting oil biomarker composition to source rock organofacies and associated kinetic; and (3) Appraise the validity of selected biomarker ratios employed in age and lithofacies determination.

Paper I combines maceral descriptions, TOC and Rock-Eval, carbon isotopes, and palaeogeographical considerations. Integration of this data resulted in a subregional to regional characterization of organofacies and sedimentary environment changes through the Upper Jurassic to Lower Cretaceous Hekkingen Formation in the Norwegian Barents Sea. Importantly, this paper documents a poor correlation between maceral compositions and stable carbon isotopes of source rock extracts. It is

tentatively explained as the result of varying degrees of diagenetic alteration of the organic matter.

Paper II builds on Paper I and evaluates the petroleum generation potential of the Hekkingen Formation using pyrolysis gas chromatography, bulk kinetics, and micro-scale sealed vessel pyrolysis analyses. This article demonstrates how the source rock thermal stability and the character of the generated hydrocarbon blend varies with regard to maceral assemblages.

Paper III collects Upper Jurassic source rocks across the northern North Sea. The samples were analysed for TOC and Rock-Eval, carbon isotopes, and maceral compositions, and the results are integrated to produce a regional organofacies interpretation. The isotopic and biomarker composition of 120 oils distributed across the North Sea is utilized for organofacies assessment of their source facies and subsequent comparison with the interpreted source rock variability. This work finds that carbon isotopes of both source rocks and oils become progressively heavier with increasing terrestrial detritus as per macerals and biomarkers, respectively.

Paper IV uses biomarker and isotope data to perform a geochemical characterization of oils onshore Barbados. Interpretations suggest that these liquids were derived from a Cretaceous deep marine shale source rock. This manuscript also compares the Barbados dataset with publicly available data to establish possible relationships between the facies sourcing the Barbados oils and well-understood source rocks in the region. The studied oils, as well as most oils used for the regional comparison, exhibit high concentrations of extended tricyclic terpanes. This publication argues that the elevated abundance of these markers in the region may be circumstantial evidence to date Upper Cretaceous-sourced oils.

Paper V evaluates the molecular and carbon isotopic composition of fifteen heavy oils onshore Suriname. Oils produced from Cenozoic reservoirs

(Group A) possess compositional attributes characteristic of oils generated from a distal marine shale, possibly the Upper Cretaceous shales of the Canje Formation. These oils possess varyingly high abundances of extended tricyclic terpanes. In contrast, Group B oils occur in Late Cretaceous beds and have biomarker relationships diagnostic of oils derived from a proximal marine depositional system rich in terrestrial organic matter. These oils exhibit isotopic values that are in average 3‰ heavier than the Group A oils.

This thesis provides clear observations, conclusions, and recommendations that can help optimize the use of selected geochemical proxies in inverting oil compositions to source rock attributes. The results have direct implications for understanding source rocks in the southern Caribbean-Atlantic margin and elsewhere when pertinent data is absent.

Table of Contents

List of Papers

Paper I: ***Upper Jurassic to Lower Cretaceous source rocks in the Norwegian Barents Sea, part I: Organic geochemical, petrographic, and paleogeographic investigations.***

Andrés Cedeño, Sverre Ohm, Alejandro Escalona, Dora Marín, Snorre Olaussen, Thomas Demchuck.

2021, *Marine and Petroleum Geology*, 134
doi.org/10.1016/j.marpetgeo.2021.105342

Paper II: ***Upper Jurassic to Lower Cretaceous source rocks in the Norwegian Barents Sea, part II: Insights from open- and closed-system pyrolysis experiments.***

Andrés Cedeño, Sverre Ohm, Alejandro Escalona, Dora Marín, Snorre Olaussen, Thomas Demchuck.

2021, *Marine and Petroleum Geology*, 134
doi.org/10.1016/j.marpetgeo.2021.105343

Paper III: ***Facies Variations in the Upper Jurassic Source Rocks of the Norwegian North Sea; From Micro to Macro Scale*.**

Guro Skarstein, Sverre Ohm, Andrés Cedeño, Alejandro Escalona.

2022, Marine and Petroleum Geology, 145
doi.org/10.1016/j.marpetgeo.2022.105856

Paper IV: ***Barbados petroleum and its role in understanding distribution of Cretaceous source rocks in the southeastern Caribbean margin: insights from an organic geochemistry study.***

Andrés Cedeño, Sverre Ohm, Alejandro Escalona

2021, AAPG – Memoir 123, 441- 467
DOI: 10.1306/13692254M1233854

Paper V: Source rocks in the Guyana basin: insights from geochemical investigation of 15 heavy oils from onshore Suriname.

Andrés Cedeño, Sverre Ohm, Alejandro Escalona, Eshita Narain, and Jan de Jager.

2021, AAPG – Memoir 123, 749 – 775
DOI: 10.1306/13692312M1233854

Conference presentations and posters

Cedeño, A., Pepper, A., Ohm, S., Escalona, A., Narain E., and Roller, L., 2021. Source Rocks in The Guyana Basin: An Organic Geochemistry Study on and Offshore Suriname. IMAGE SEG-AAPG, September 26th-October 1st, Denver-Colorado & Online. (*Talk*)

Cedeño, A., Pepper, A., Ohm, S., Escalona, A., Narain E., and Roller, L., 2021. Oil and Source Rock Geochemistry of The Guyana Basin. 3rd HGS/EAGE Conference on Latin America, November 8th-10th November, Houston, Texas & Online. (*Talk*)

Cedeño, A., Ohm, S., Escalona, A., Olaussen, S., 2021. Facies and source rock variations within the Hekkingen Formation. Petroleum System Conference, Norwegian Petroleum Society, February 2nd, Oslo, Norway. (*Talk*)

Cedeño, A., Ohm, S., Escalona, A., and Narain E., 2019. Petroleum system (s?) in the Guyana-Suriname basin: insights from a geochemical study onshore Suriname. 29th International Meeting on Organic Geochemistry (IMOG), September 2nd, Gothenburg, Sweden, DOI: 10.3997/2214-4609.201902838. (*Talk*)

Cedeño, A., Ohm, S., and Escalona, A., 2019. Facies variations within the Hekkingen formation: an interdisciplinary approach. 29th International Meeting on Organic Geochemistry (IMOG), September 2st, Gothenburg, Sweden, DOI: 10.3997/2214-4609.201902713. (*Poster*)

Other Papers

Tectono-Stratigraphic Evolution of the Western Barbados Accretionary Prism and the Eastern Tobago Basin: Implications for Petroleum Systems.
Andrés Cedeño, Mudussar Ahmed, Alejandro Escalona and Peter Abrahamson.

2021, *AAPG – Memoir 123*, 649 – 675.
DOI: 10.1306/13692261M1233854

The Middle Jurassic to lowermost Cretaceous in the SW Barents Sea: Interplay between tectonics, coarse-grained sediment supply and organic matter preservation.
Dora Marín, Solveig Helleren, Alejandro Escalona, Snorre Olaussen, Andrés Cedeño, Henrik Nøhr-Hansen, Sverre Ohm.

2020, *Basin Research*; 00:1–23.
DOI: 10.1111/bre.12504

The impact of salt tectonics on the thermal evolution and the petroleum system of confined rift basins: insights from basin modeling of the Nordkapp Basin, Norwegian Barents Sea.
Andrés Cedeño, Luis Alberto Rojo, Néstor Cardozo, Luis Centeno and Alejandro Escalona.

2019, *Geosciences*, 9 (7), 316.
doi.org/10.3390/geosciences9070316

Chapter 1

1. Introduction

Assessing the geochemistry of oils, as well as the source rock facies from which they originated, is of crucial importance in petroleum systems analysis. Such assessment involves the use of multiple geochemical techniques, some of which are exclusive to either sediments or oils and others that are applicable to both. Bulk and pyrolytic source rocks analyses such as TOC, Rock-Eval, Py-GC, and kinetic are employed to address variations in the organic matter make-up and petroleum generative potential. Molecular analyses of crude oils and source rock extracts are instrumental in investigating the character (i.e., marine versus terrestrial), age, and maturity of the organic matter as well as in inferring depositional conditions during its sedimentation. Stable carbon isotopes of both liquids and extracts have also been exploited as an organofacies diagnostic parameter. As such, molecular and isotopic techniques provide tools to perform oil-to-source and oil-oil correlations with certain confidence.

Crude oil samples are usually available for geochemical characterization and correlation, but pertinent source rock data is often scarce or absent because exploratory drilling mostly targets reservoirs in structurally elevated areas and fails to sample the deeply buried, prolific basinal source facies. Therefore, explorationists are unable to perform direct oil-to-source correlations and must rely on source rock inferences drawn from oil geochemistry, a practice named "geochemical inversion" by Bissada et al. (1993). That is the case in the southeastern Caribbean-Atlantic margin (Figure 1A). The organic facies sourcing the Woodbourne Field onshore Barbados remains undrilled due to structural complexity while correlation of the distinct oil families to their parent source in the neighboring Guyana Basin is imperfectly understood.

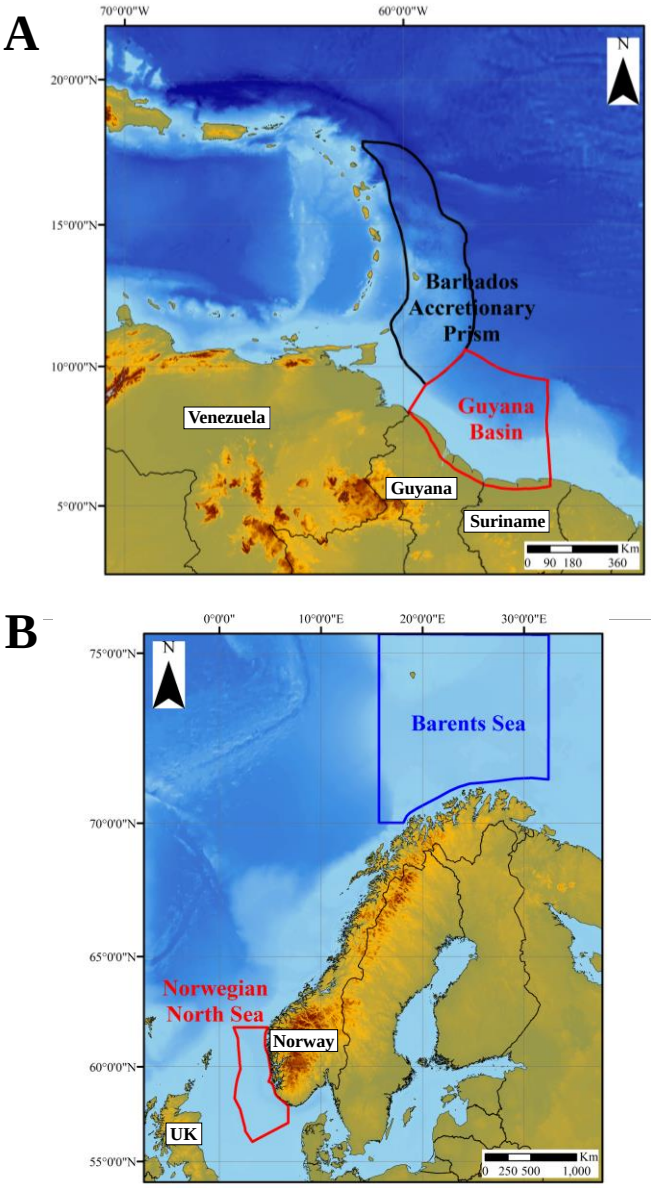

Figure 1. Map of the southeastern Caribbean-Atlantic margin (**A**) and the Norwegian Continental Shelf (**B**) outlining the study areas in this study.

In areas like the Norwegian Barents and North seas (Figure 1B), the different source rock intervals are extensively drilled, and sampling materials are accessible. These provinces also enjoy vast volumes of oil and source rock data readily available in public and proprietary data bases. Lessons learned from these data-rich regions can assist in inverting the geochemical characteristics of migrated oils to specific attributes of the source rock in the southeastern Caribbean-Atlantic margin and elsewhere when pertinent data is absent.

This work utilizes the southeastern Caribbean-Atlantic margin and selected areas of the Norwegian Continental Shelf as natural laboratories with the aim of exploring the successes and pitfalls of selected geochemical proxies in predicting source rock attributes. It focuses on the use of stable carbon isotopes and specific biomarkers in inferring source organofacies and associated kinetics, age, and sedimentary conditions grouped in the three following themes.

1.1. Theme 1: Stable carbon isotopes in organofacies assessment

In petroleum geochemistry, stable carbon isotopes (i.e., $\delta^{13}C$) have been suggested to reflect the composition of the organic matter in the source rock facies (Craig, 1953; Sofer 1984). Isotopically heavy oils are attributed to terrestrially dominated sources whereas lighter oils are ascribed to marine dominated sources (Yeh and Epstein 1981). Other authors have associated oils of a heavy isotope composition (i.e., -18 to -24 ‰) to deep-water facies, and lighter compositions (i.e., -26 to -32 ‰) to shallower-water facies (Bissada et al., , 1993). If the criteria for inferring sedimentary environments and affiliated organic inputs are assumed to be intimately related, i.e., deep marine facies contain mostly marine inputs, the findings by the different authors are essentially contradictory.

While it is fact that the composition of the primary organic matter imparts specific attributes to the general isotopic character, numerous factors alter it during and immediately after deposition, transformation into petroleum, and migration (Galimov 2006). Biochemical research on modern sediments has demonstrated that several fractionation mechanisms acting together alter the $\delta^{13}C$ of the primary organic materials differently during diagenesis, leading to selective preservation of the less reactive organic compounds (Freudenthal et al., 2002; Lehmann et al., 2002; Galimov 2006). The $\delta^{13}C$ composition inherited from the diagenetic stage is additionally modified by thermal stress and eventually by hydrocarbon biodegradation. The overlapping effects of all these factors partly outweigh each other and may eventually obscure the original $\delta^{13}C$ of the source material. Historically, most workers, unable to perform direct oil-to-source correlations, have oversimplified this matter and the variability is solely attributed to changes in organic inputs and sedimentary environment.

1.2. Theme 2: Geochemical inversion to source rock organic composition and kinetics

The sedimentary organic matter occurring in a source rock has characteristic biochemical attributes inherited from the unique mixture of organisms coexisting in the ecosystem. The resulting organic make-up can consist entirely of bacterial, algal, planktonic, or land-plant derived materials, or consist of a mixture of various organic components as most commonly occur (Behar and Vandenbroucke, 1987). Each of the organic matter types possesses different oil and gas generative capabilities and transforms into hydrocarbons at different temperatures (i.e. thermal lability; Tegelaar and Noble, 1994; Eglington et al., 1990). This transformation proceeds through a multitude of quasi-irreversible, parallel and consecutive reactions governed by chemical kinetics (Dieckmann et al., 1998).

The relative abundance of terrestrial plant detritus versus aquatic organics determines both the kinetics of petroleum generation and the character of the generated hydrocarbon blend. For example, hydrogen-poor terrestrial kerogens, which are at best only gas & condensate prone, are thermally very stable and require higher activation energies to generate than do labile, oil-expulsive marine kerogens (Eglington et al., 1990; Braun et al., 1991; Tegelaar and Noble, 1994). These complexities cause every source rock, or facies of a single source, to be kinetic and compositionally unique. If source rock samples are absent, so are the pertinent kinetic parameters needed for simulating the petroleum generation and explorationists must rely on selecting a set of kinetics from analogue source rocks.

The characteristic biochemical attributes of the organic matter in a source rock are transferred to the migrated oils in the form of molecular fossils or biomarkers. Thus, examining the biomarker distribution provides a strategy by which the relative contribution of aquatic marine versus terrestrial plant materials to the kerogen mix can be qualitatively estimated. This in turn provides a quick means of inverting the composition of the accumulated liquids to approximate kinetic properties of their sourcing facies.

1.3. Theme 3: Selected biomarkers in age and lithology determinations

The advent of Gas Chromatography Mass Spectrometry during the 60s prompted the development, and implementation, of the biomarker concept (Hunt et al., 2002). Since then, biomarkers have been crucial to the geochemist in deriving clues about the sedimentary environment, lithology, age, organic matter composition, and maturity of source rocks. The concept capitalizes on the fact that certain organic compounds in the original source material preserve most of their initial structural signature and stereochemistry in the migrated oils (Tissot and Welte, 1978).

In the Norwegian Barents Sea, the presence of high quantities of extended tricyclic terpanes is associated with Triassic or older source rocks and oils (Figure 2A), being characteristically low in Upper Jurassic-sourced oils (Ohm et al., 2008). Caribbean-Equatorial oils in which these markers are high, like in the Barbadian and Surinamese crudes (Figure 2B and C), are interpreted as having originated in upwelled source rock systems of Cretaceous age (Zumberge et al., 2007).

The distribution of tricyclic terpanes and the abundance of diasteranes relative to regular steranes in some crude oils from the Guyana Basin are typical of generation from a mixed clastic and carbonate source facies. Despite biomarkers consistently diagnosing a mixed source, bulk oil properties such as the sulfur weight percent of these oils (i.e. 0.2 wt%) fail to support the biomarker interpretation and instead support a clastic source. These ambiguities seemingly demonstrate that the significance of specific biomarkers vary due to attributes intrinsic to the organic source materials and the local environmental conditions in which the organisms are deposited. Under certain circumstances, for instance, organic input or lithology diagnostic parameters can overlap with those sensitive to age or water oxygenation conditions.

1.4. Research objectives and implementation

This PhD project focuses on organic geochemical investigations in the southeastern Caribbean-Atlantic margin (Papers IV and V) and selected areas of the Norwegian Continental Shelf – Barents (Papers I and II) and North (Paper III) seas. These geologically distinct regions were selected as natural laboratories because their different data sets and geochemical commonalities offer a unique arena to explore the successes and pitfalls of selected geochemical proxies in geochemical inversion. For such purpose,

this work adopts an interdisciplinary approach and defines the following objectives:

1. Review the accuracy of stable carbon isotopes in assessing organofacies in source rocks and oils.
2. Explore the utility of inverting oil biomarker composition to source rock organofacies and associated kinetic.
3. Appraise the validity of selected biomarker ratios traditionally employed in age and lithofacies determination.

The current study comprises five publications related to the three fundamental objectives described above. **Paper I** combines maceral and mineral descriptions, TOC and Rock-Eval, carbon isotopes, and palaeogeographical considerations. Integration of this data resulted in a subregional to regional characterization of organofacies and sedimentary environment changes through the Upper Jurassic to Lower Cretaceous Hekkingen Formation in the Norwegian Barents Sea. Importantly, this manuscript discusses the relationship between isotopes of source rock extracts and maceral compositions. **Paper II** builds on Paper I and evaluates the petroleum generation potential of the Hekkingen Formation using bulk and quantitative pyrolysis analysis. This article demonstrates how the source rock thermal stability and the character of the generated hydrocarbon blend varies with regard to maceral assemblages. **Paper III** implements a workflow similar to that in Paper I but evaluates Upper Jurassic source rocks in the northern North Sea. In addition, this publication discuses oil isotopes and their relationship with source rock organofacies. **Paper IV** uses biomarker and isotope data to perform a geochemical characterization of petroleum occurrences onshore Barbados and speculates on their generating facies. This manuscript also compares the Barbados dataset with publicly available data in an attempt to establish possible relationships between the facies sourcing the Barbados oils and well-understood source rocks in the

region. **Paper V** evaluates the geochemical composition of fifteen heavy oils onshore Suriname and draws inferences on possible sourcing facies based on various geochemical attributes. Like Paper IV, this work discusses the existence of varyingly high abundances of extended tricyclic terpanes and their possible significance.

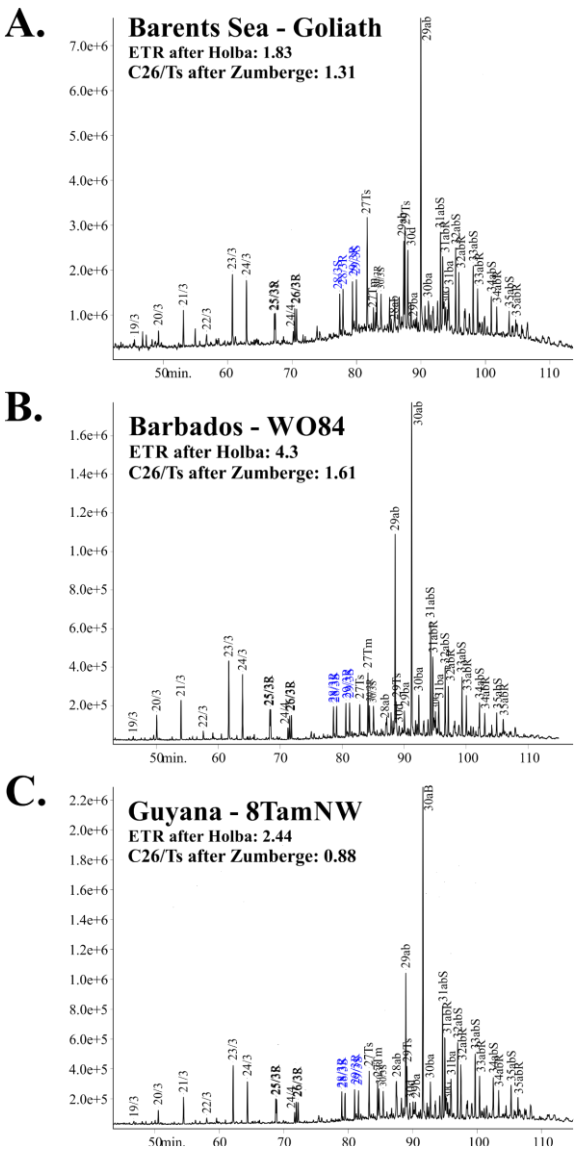

Figure 2. Mass chromatograms of terpanes (*m/z* 191) of a representative oil from the Norwegian Barents Sea (**A**), Barbados (**B**), and Suriname (**C**). The extended tricyclic terpane ratio after both Holba and Zumberge are annotated for each oil.

2. Study area and geological setting

This study involves two different geological regions: (1) the southeastern Caribbean-Atlantic margin comprising the Barbados Accretionary Prism and the adjacent Guyana Basin (Figure 1A); and (2) the Norwegian Barents and North seas (Figure 1B). This chapter briefly introduces the most important aspects of the regional geology with a focus on source rock development.

2.1 Southeastern Caribbean-Atlantic margin

2.1.1 The Barbados Accretionary Prism – A mid to Upper Cretaceous, La Luna-Like source rock (?)

The present-day tectonic setting in the southeastern Caribbean is controlled by eastward motion of the Caribbean plate relative to South America at a rate of about 20 mm/yr (Mann, 1999; Weber et al., 2001). This eastward movement began in the late Eocene and was fully established by the late Oligocene (Malfait and Dinkelman, 1972; Escalona and Mann, 2011; Figure 3). The Barbados Prism developed at the leading edge of the Caribbean plate because of offscraping of sediments that were previously deposited on the proto-Caribbean and Atlantic oceanic floor (Escalona and Mann, 2011; Escalona et al., 2021a, b; Cedeño et al., 2021a). Brown and Westbrook (1987) subdivided the accretionary prism into four zones based on the dominant structural style. From east to west these zones are as follows: zone of initial accretion, zone of stabilization, zone of supra complex basins, and the Barbados Ridge (Figure 4A). The ridge is characterized by uplift and westward thrusting of the prism complex over the Tobago Basin (Brown and Westbrook, 1987). Consequently, it is the topographically highest part of the prism and is the region along which the island of Barbados is emergent.

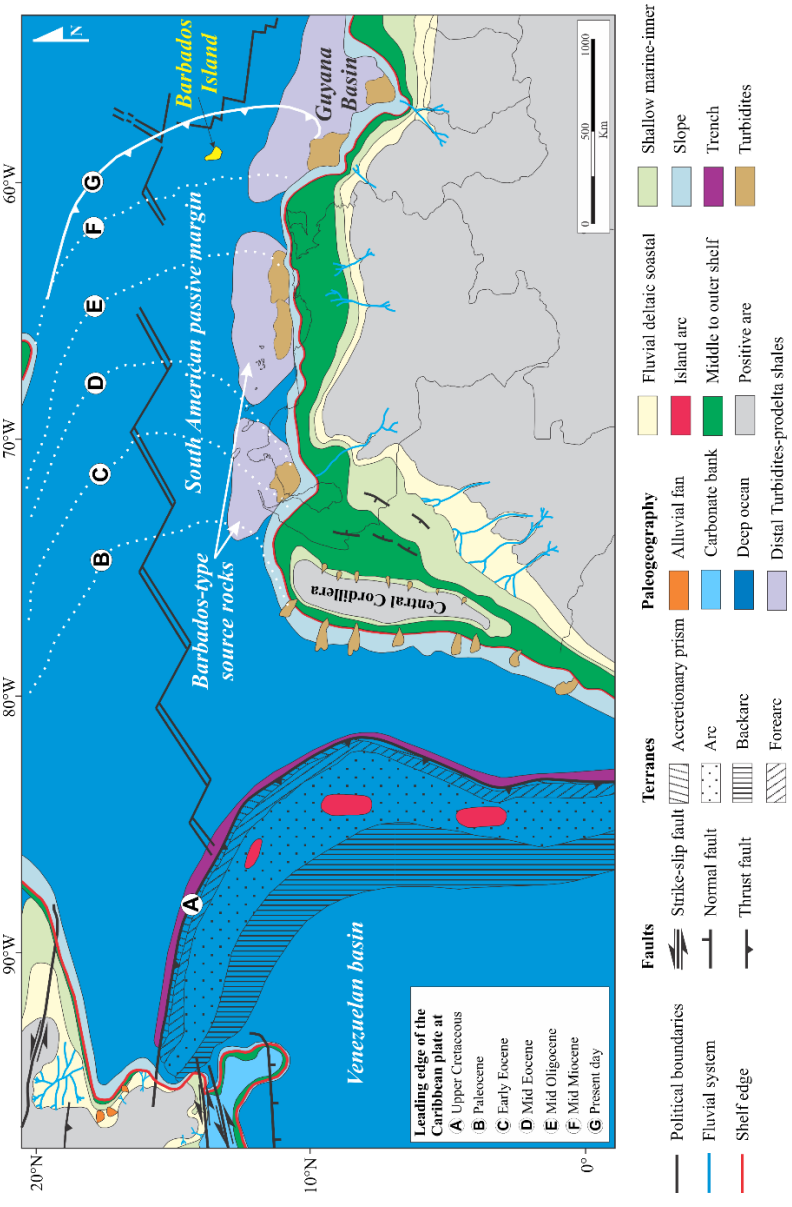
90°W
80°W
70°W
60°W
20°N
10°N
0°
Barbados Island
Guyana Basin
South American passive margin
Barbados-type source rocks
Central Cordillera
Venezuelan basin
A
B
C
D
E
F
G
0
500
1000
Km
Leading edge of the Caribbean plate at
A Upper Cretaceous
B Paleocene
C Early Eocene
D Mid Eocene
E Mid Oligocene
F Mid Miocene
G Present day
Political boundaries
Fluvial system
Shelf edge
Faults
Strike-slip fault
Normal fault
Thrust fault
Terranes
Accretionary prism
Arc
Backarc
Forearc
Paleogeography
Alluvial fan
Carbonate bank
Deep ocean
Fluvial deltaic soastal
Island arc
Middle to outer shelf
Positive are
Distal Turbidites-prodelta shales
Shallow marine-inner shelf
Slope
Trench
Turbidites

Figure 3. Upper Cretaceous paleogeographic map of northern South America. Dotted lines show the position of the leading edge of the Caribbean plate through time. Relevant geological provinces are indicated. Deposition of the Barbados-type source rocks occurred along most of the distal areas of the passive South American margin. Modified from Escalona et al. (2021a).

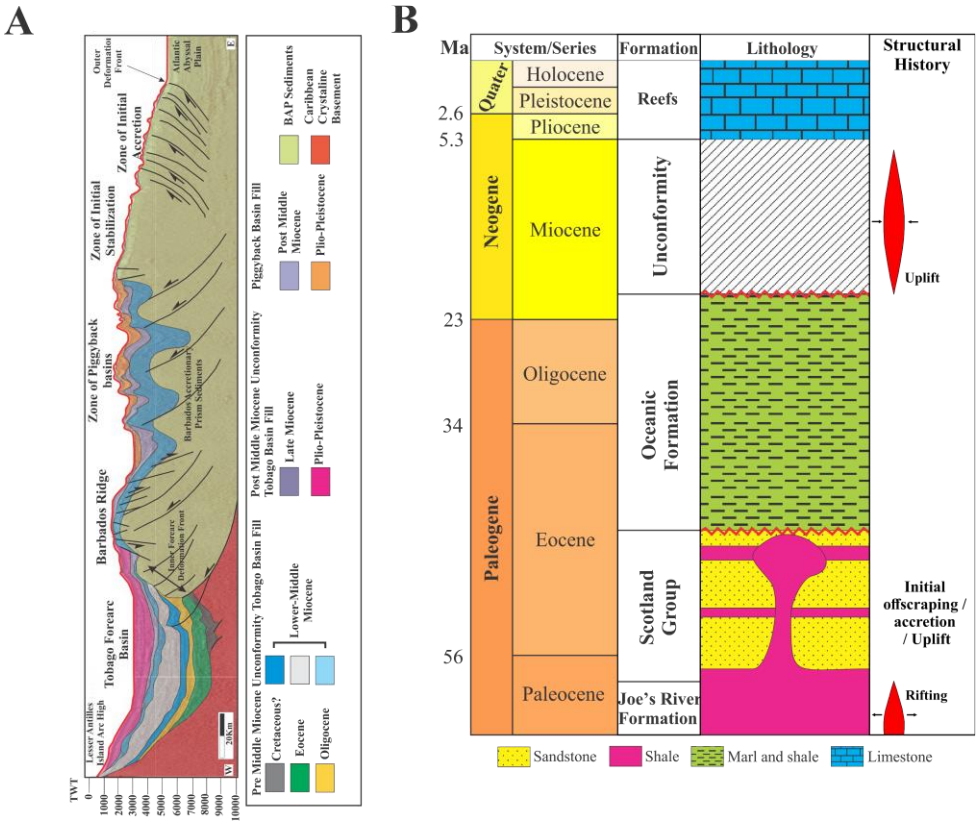

Figure 4. A. East–west seismic line showing the stratigraphy and structural provinces of the Barbados accretionary prism based on the dominant structural style. Modified from Chaderton (2005). **B.** Generalized stratigraphic column of the Barbados Island. Modified from Deville and Mascle (2012). The main structural events described in the text are annotated.

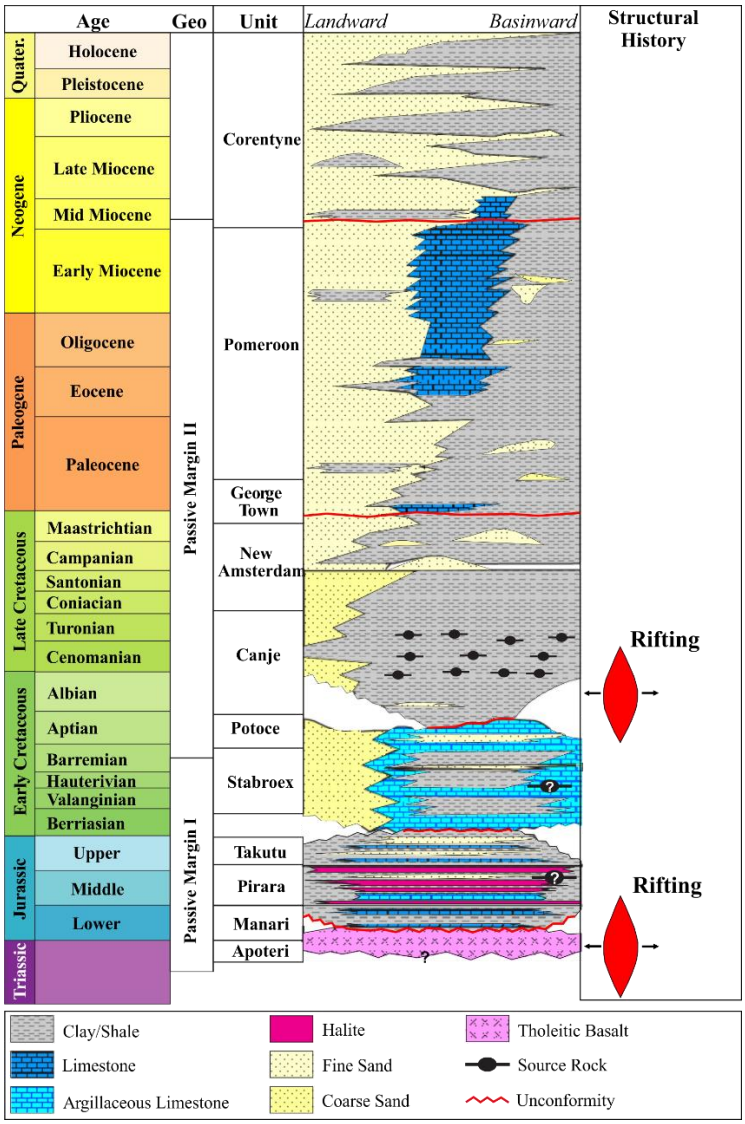

Figure 5. Generalized stratigraphic column of the Guyana Basin. The main structural events described in the text are annotated. Modified from Bihariesingh (2014) and Crawford et al. (1985). The Triassic–Jurassic stratigraphy of the Takutu Graben as described by Crawford et al. (1985) is assumed.

The offshore stratigraphy of the prism is poorly understood due to its extreme structural complexity. It has been correlated to four lithostratigraphic units outcropping in the island of Barbados (Barker and Poole, 1983, Figure 4B). The basal unit is composed of deepwater turbiditic sand–shale beds called the Scotland Group of late Paleocene to middle Eocene age (Chaderton, 2055 and 2009; Deville and Mascle, 2012). The Scotland Group is intruded by paleo diapirs called Joe's River Formation. Nannofossils found in the clasts of the formation yielded an age of late Campanian–early Maastrichtian (Deville and Mascle, 2012). Overlying the Scotland Group is the Oceanic Formation of middle Eocene to late Oligocene, which consists of pelagic marl, chalk, and volcanic ashes (Speed et al., 1989). Pleistocene limestones cap the island of Barbados.

Hill and Schenck (2005) suggested that oil occurrences onshore Barbados originated from a mid-Cretaceous La Luna-like source, but as of today the late Paleocene to middle Eocene turbiditic deposits of the Scotland Group are the oldest drilled sediments. Escalona and Mann (2011) and Cedeño et al. (2021a) proposed that late Albian-Turonian source rocks deposited on the Atlantic oceanic floor (i.e., Figure 3) were tectonically incorporated into the prism during the eastward movement of the Caribbean plate.

2.1.2 Guyana Basin, mid to Upper Cretaceous source rock

The Guyana Basin is located along the passive margin of northeastern South America – adjacent to the Barbados Prism (Figure 1A and 3). The tectonic development of the basin started with the Late Triassic–Early Jurassic north–south rifting and establishment of a first passive margin stage (Figure 5; Erlich and Barrett, 1994; Gouyet et al., 1994; Kean et al., 2007; Yang and Escalona, 2011a). In the Barremian, South America and Africa commenced to drift apart, resulting in two conjugate margins (Pindell, 1991; Erlich and Barrett, 1994; Mann et al., 1995; Nemcŏk et al., 2015). Passive margin

sedimentation was reestablished, and the organic-rich Canje Formation deposited during a long-lived, regional flooding event that lasted from the late Albian until the Turonian (Lindseth and Beraldo, 1985; Erlich et al., 2003). The Canje Formation is a black shale with TOC values between 2% and 15% (Schwarzer and Krabbe, 2009; Yang and Escalona, 2011b; Cedeño et al., 2021b and c). Organic enrichment and preservation were favored by upwelling and several Oceanic Anoxic Events (OAE), and restricted water circulation in the basin (Erlich et al., 2003; Meyers et al., 2006). Early Cenozoic carbonate shelf deposits unconformably overlay the Upper Cretaceous clastic sediments (Campbell, 2005). Carbonate deposition ceased in the middle–late Miocene because of an increase in the clastic inputs (Yang and Escalona, 2011a).

2.2 Selected areas of the Norwegian Continental Shelf

2.2.1 Barents Sea, a multi-source rock system

In the Late Devonian-early Carboniferous, crustal extension caused the initiation of several basins across the western Barents Shelf (Steel & Worsley 1984; Gudlaugsson et al., 1998). Sedimentation was predominantly siliciclastic with localized coaly source rock deposition within half grabens on the Finnmark Platform (Bugge et al. 1995; Ehrenberg et al., 1998; Figure 6). TOC in these coal-bearing strata ranges between 2 and 4 wt.% and HI values are overall less that 200mgHC/gTOC (Henriksen et al., 2011a; Ohm et al., 2008).

A regional sag basin developed over most of the Barents Shelf during the late Carboniferous-early Permian (Gudlaugsson et al., 1998). Warm-water carbonate sedimentation took place (Stemmerik et al., 1999) and local source rocks developed near bioherms (Henriksen et al., 2011a; Figure 6).

Ohm et al., (2008) reported average TOC and HI values of 2.1% and 200 mgHC/gTOC, respectively. Better source rocks likely deposited in the western Barents Shelf as Permian carbonate to evaporitic sediments reportedly charged the Gotha discovery in the Loppa High (Matapour and Karlsen, 2017; Figure 7A). The Late Permian represents a shift from carbonate to clastic deposition due to rapid changes in oceanographic conditions (Stemmerik & Worsley 2005). The late Permian through Triassic period was tectonically quiet with sedimentation of marine and deltaic sediments (Faleide et al., 1993; Figure 6). Triassic source rocks deposited nearby the Svalis Dome (i.e., Steinkobbe Formation, TOC=3.88% and HI=3 68mgHC/gTOC) and Svalbard (i.e., Botneheia Formation; TOC=4.26% and HI=459mgHC/gTOC; Abay et al., 2017). Fluvio-deltaic type III kerogen is recorded in the Kobbe Formation in Nordkapp Basin and Bjarmaland Platform.

In the Late Jurassic-Early Cretaceous, renewed extension and high global eustatic sea levels caused flooding and deposition of organic rich sediments over most of the Barents shelf (Figure 6; Sund et al., 1986; Berglund et al., 1986; Faleide et al., 1993; Gernigon et al., 2014; Serck et al., 2017; Rojo et al., 2019; Kairanov et al., 2021). These sediments are collectively known as the Hekkingen Formation, which in turn is subdivided into a basal, shale-rich member and an overlying siltier member. TOC values are typically higher in the basal Alge Member (i.e., >7%) relative to the overlying Krill Member but both units record HI values that oscillate between 30 and 450 mgHC/gTOC (Ohm et al., 2008; Henriksen et al., 2011a; Abay et al., 2017). Across the southwestern Barents Shelf, long-term Cenozoic uplift associated to the opening of the North Atlantic has resulted in net erosion that varies from 0 to more than 3000m (Riis, 1996; Cavanagh et al., 2006; Henriksen et al., 2011b).

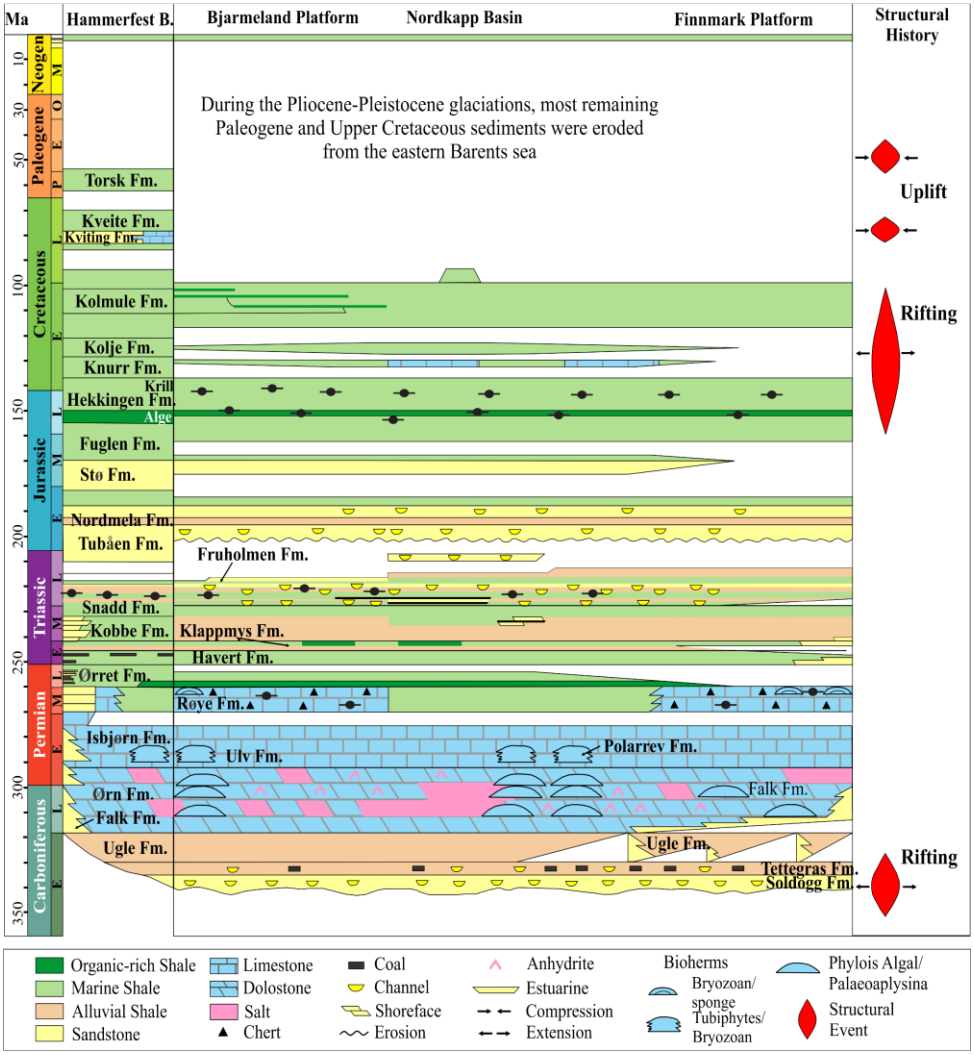

Figure 6. Stratigraphic chart illustrating the main lithologies in the Hammerfest Basin, Bjarmeland Platform, Nordkapp Basin, and Finnmark Platform of the Norwegian Barents Sea. The main structural events and source rocks described in the text are annotated. Modified from Ohm et al., (2008).

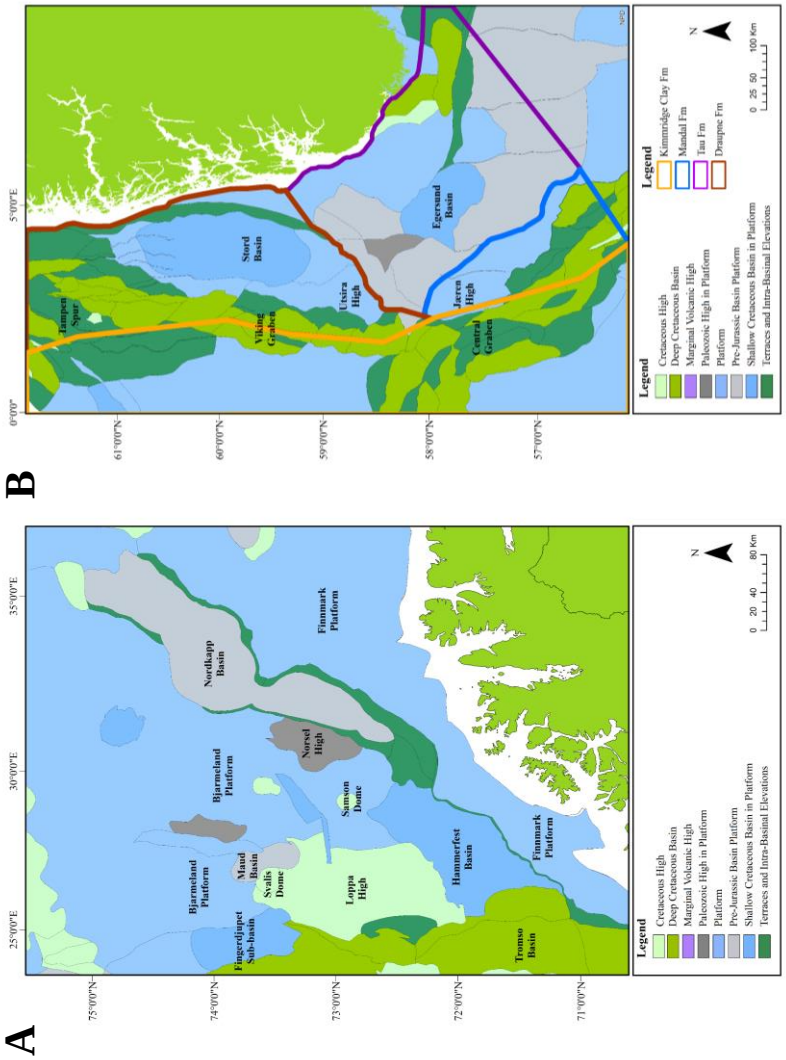

Figure 7. Maps of the southwestern Barents Sea (A) and the northern North Sea (B) displaying the main structural elements. In figure B, the Kimmeridge Clay in the |UK sector and its Norwegian equivalents are outlined. Modified from the NDP fact pages and Skarstein et al., (2022).

2.2.2 North Sea, Upper Jurassic source rocks

The North Sea is a post-Caledonian graben system (Færseth, 1996). The present-day structural setting developed during two major extensional phases in the Permo-Triassic and the middle Jurassic-Early Cretaceous (Ziegler, 1992; Figure 8), followed by thermal cooling and subsidence (Badley et al., 1988, Færseth, 1996). The Middle Jurassic to Early Cretaceous rift phase represents a change from fluvio-deltaic to deep marine depositional environments resulting from a major marine transgression (Nøttvedt et al., 1995; Mannie et al., 2014). During this period, organically enriched clays were deposited. These sediments constitute the Kimmeridge Clay in the UK sector and equivalent Mandal, Draupne, and Tau formations in the Norwegian Sector (Figures 7 and 8; Gautier, 2005;). The Mandal and Tau formations in the southern part of the Norwegian sector record TOC and HI values oscillating between 2 to 13% and 350 to 800 mgHC/gTOC, respectively (Petersen et al., 2013; Ritter et al., 1987). Goff (1983) and Thomas et al. (1985) documented TOC values of up to 12 wt.% and HI of up to 600 mg HC/g for the Draupne Formation in the Viking Graben.

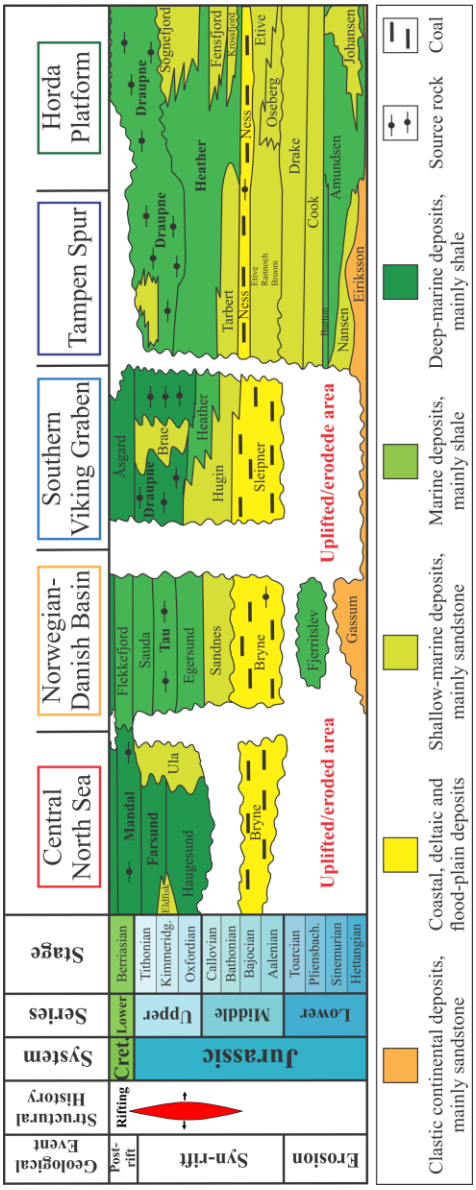

Figure 8. Stratigraphic chart illustrating the main lithologies in the Central North Sea, Norwegian-Danish Basin, Southern Viking Graben, Tamper Spur, and Horda Platform in the Norwegian North Sea. The main structural events and source rocks described in the text are annotated.

3. State of the art

3.1 Stable carbon isotopes as organofacies parameter

Stable carbon isotope compositions (reported as $\delta^{13}C$) represent the deviation from the $^{13}C/^{12}C$ ratio of the standard carbonate-carbon in the Pee Dee Belemnite expressed in units per mill ‰ (Urey et al., 1951). Since the early times of petroleum geochemistry, many workers have considered oil isotope variability to result from changes in the character of the organic precursors that contributed to the source. Craig (1953), Silverman and Epstein (1958), Hunt (1970), Tissot and Welte (1978), and Rogers (1980) suggested that oils sourced by terrestrial-rich organofacies are isotopically lighter than marine sourced oils. Yeh and Epstein (1981) contradicted that view because they studied marine derived oils that are isotopically lighter than terrestrial derived oils. Sofer (1984) developed an interpretation scheme for discriminating between terrestrial-sourced oils from marine-source oils. He argued that the differences in isotopic compositions between terrestrial and marine-sourced oils do not manifest themselves in the absolute $\delta^{13}C$ values of a single fraction but in the relationship between the aromatic and saturate fractions. To understand the possible reasons behind the reported contradictions, it is pertinent to review the multiple processes that have the potential to modify the $\delta^{13}C$ of sedimentary organic matter in a source rock during sedimentation, diagenesis, and thermal maturation.

3.1.1 The journey of organic matter from sedimentation to petroleum

Galimov (1980 and 2006) explained that the $\delta^{13}C$ signature of sedimentary organic carbon accumulated in a potential source rock results from a complex interaction of factors. In short, the $\delta^{13}C$ of the organic matter

available for transformation into petroleum depends on its original $\delta^{13}C$ value and on the isotopic, naturally-occurring fractionation affecting the organic matter during formation, sedimentation, and diagenetic evolution.

Galimov (1980) documented that in natural systems there exists a thermodynamically ordered intra- and intermolecular carbon isotope distribution prompted exclusively by biosynthesis. If the biological isotope effects are thermodynamically ordered, the carbon isotopes will be regulated between and within biomolecules. Such a process is governed by the thermodynamic isotope exchange properties of each molecule, known as the *ß*-factor. The larger the value of the factor, the greater the concentration of the heavy ^{13}C isotope is. Because the *ß*-factor is temperature-dependent, the $\delta^{13}C$ of organisms also depends on the temperature of the biosynthesis. During formation of the organisms and subsequent chemical evolution (i.e., life cycle, early diagenesis), removal of functional groups with ^{13}C enriched carbon like formyl or carboxyl leads to enrichment of the organic matters in the light ^{12}C isotope. Conversely, elimination of methoxy or methyl groups results in organic matter enriched in the heavier ^{13}C isotope.

Marine plants are enriched in the heavier ^{13}C relative to land plants. A similar isotopic trend is also observed when shifting depositional facies from marine to proximal (Galimov et al., 1998; Galimov, 2004 and 2006). The $\delta^{13}C$ values of planktonic species decrease with increasing water depth and latitude (i.e. -18‰ to -20‰ in the equator to -23‰ to -26‰ in high latitudes) in response to isotopically lighter CO_2 with depth and higher CO_2 solubility in colder waters, respectively (Calvert and Fontugne, 1987; Freeman et al., 1994; Rau et al., 1989). The $\delta^{13}C$ of intact organic particles reaching the bottom is closely similar to that of their biological source (Kodina et al., 1994, 1996; Galimov, 1995). Galimov (2006) argued that the $\delta^{13}C$ of land-derived organic carbon has remained relatively similar through geological time, but that of marine organic carbon has progressively become enriched

in light ^{12}C towards present time. Thus, marine organic carbon older than Oligocene is overall isotopically lighter than the terrestrial-derived carbon.

During diagenesis, several processes mediated by the action of aerobic and anaerobic microbes act together and result in sedimentary organic matter with a remarkably different $\delta^{13}C$ relative to the original biomass (Harvey et al., 1995; Freudenthal et al., 2002; Lehmann et al., 2002; Galimov 2006). Three main processes act together and partially outweigh each other: isotope fractionation during the initial break-down of complex organic compounds, selective preservation of isotopically different fractions of organic matter, and bacterial biosynthesis (Lehmann et al., 2002). The overall decrease in the $\delta^{13}C$ of the bulk organic matter during diagenetic alteration is in the range of 0 to 2 ‰ relative to the initial value of the accumulated biomass (Freudenthal et al., 2002; Lehmann et al., 2002; Galimov 2006; Figure 9). This change depends essentially on the balance between heavier ^{13}C isotope enrichment caused by degradation of labile compounds and simultaneous lighter isotope increase due to selective preservation of resistant ^{13}C-depleted organic compounds (Freudenthal et al., 2002). Diagenetic fractionation of specific components like proteins and carbohydrates proceeds through pathways that are greater in magnitude and different in the direction of isotope shifts with respect to the host organic matter (Harvey et al., 1995; Galimov 2006). Chemically resistant components such as algaenans (i.e., sporopollenin in dinoflagellate cysts), spores, and higher plant leaf cutans may eventually preserve their chemical structures (Skopintsev, 1981; Freudenthal et al., 2002; Lehmann et al., 2002)

In anoxic environments, the accumulated organic matter can be additionally depleted in heavier ^{13}C due to the contribution of chemosynthetic bacteria, whose isotope fractionation is greater than that of photosynthetic bacteria by 4–6‰ (Ruby et al., 1987). In environments with sulfate reduction, carbon isotope fractionation varies in magnitude and direction according to the

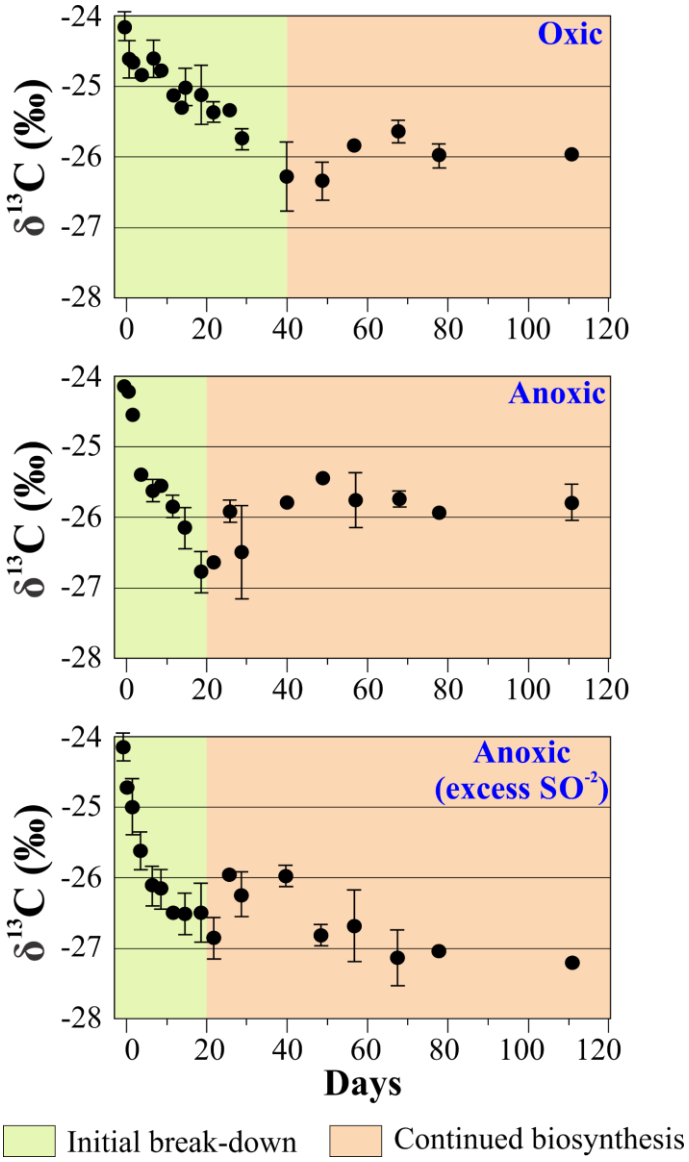

Figure 9. Variation of $\delta^{13}C$ of particulate organic matter during experimental oxic, anoxic, and anoxic excess SO^{-2} microbial decomposition of plankton. Modified from Lehmann et al., (2002).

sulfate-reducing bacterial community oxidizing acetate and its different metabolic pathways (Londry Des Marais, 2003; Habicht and Canfield, 2003, Goevert and Conrad , 2008).

Thermal maturation of the organic materials causes its enrichment in ^{13}C, leading to an isotopically heavier (i.e., 1 to 2‰) residue due to the kinetic isotope effect (Figure 10; Chung and Sackett; 1979; Galimov, 1980; Peters et al., 1981; Galimov and Simoneit 1982; Lewan, 1983; Tocque et al., 2005). Therefore, the expelled hydrocarbon products are isotopically lighter relative to the source material: the lower the molecular weight of the generated hydrocarbon products, the isotopically lighter they become. Simultaneously, the expelled products are enriched in the heavier ^{13}C with increasing maturity (Lewan, 1983; Tocque et al., 2005).

Andrusevich et al. (1998) used the $\delta^{13}C$ of the saturate fraction of oils and recognized a systematic enrichment in ^{13}C of oils with decreasing geologic age, which is overall independent of source rock type (i.e., organic matter and lithology). This fortified the findings by Stahl, (1977), Grizzle et al. (1979), and Chung et al. (1992).

3.1.2 Carbon isotopes in the Norwegian Continental Shelf

Karlsen et al. (1995) and Karlsen and Skeie (2006) associated the westwards shift from heavier to lighter whole oil isotopes in the Haltenbanken Terrace with a change from terrestrially dominated kerogens to more algal-bacterial-amorphous kerogens. Odden et al. (2002) found that kerogen pyrolysates from marine shales of the Spekk Formation possess $\delta^{13}C$ values lighter than pyrolysates from the coaly shales of the Åre Formation. These observations imply that a positive feedback exists between lighter isotopes and marine kerogens in the Norwegian North Sea.

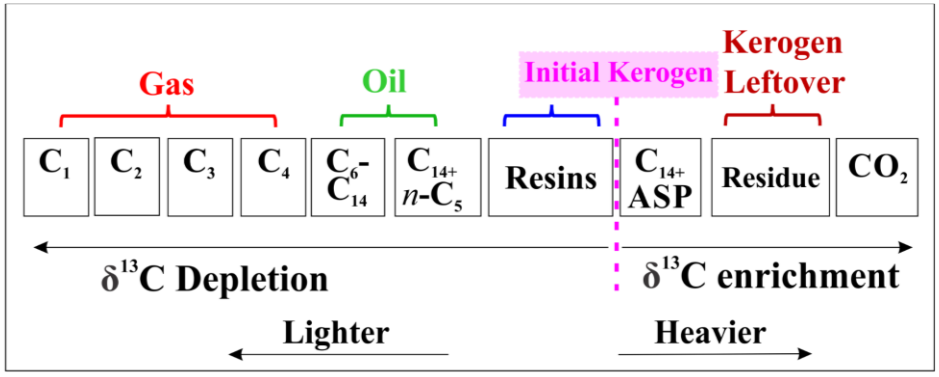

Figure 10. Simplified scheme for carbon isotopic fractionation of kerogen pyrolysis products. Modified from Toque et al., (2005).

In the Norwegian Barents Sea, Ohm et al. (2008) presented a detailed organic geochemical evaluation of oils and source rocks and implemented the age approach of Andrusevich et al. (1998) to date various oil tribes. They proposed that the isotopically heaviest oils (i.e., overall heavier than 29‰) originated from the Upper Jurassic Hekkingen Formation, oils with $\delta^{13}C$ lightest values (i.e., overall lighter than 30‰) originated from Upper Paleozoic sources, and those with intermediate $\delta^{13}C$ values originated from Triassic sources.

3.2 Oil and source rock kinetics

The kinetic behavior of naturally occurring kerogens depends essentially on two main factors: the character of the primary biomass and the diagenetic incorporation of sulfur (Tegelaar and Noble, 1994; di Primio and Horsfield, 1996). Inherently, varying proportions of aquatic (i.e., marine or lacustrine) and terrestrial macerals in most sources invokes heterogeneity in kerogen kinetic stability (Tegelaar and Noble, 1994).

The first of the two factors dictates the initial kinetic diversity, and, importantly, the gross composition of generated petroleum (Demaison and

Moore, 1980; di Primio and Horsfield, 2006). Tegelaar and Noble (1994) presented a discussion on kinetic reactions as a function of kerogen composition using analyzes for 70+ source rock samples from different depositional environments and ages. They explained that kinetic parameters only poorly correlate with hydrogen indexes because chemical characteristics fail to adequately reflect the molecular make-up of kerogen. They found that Py-GC and a set of derived diagnostic indices provide a more accurate view of the kerogen composition and determined a number of end-member kerogen types, each with their own distinctive kinetic properties. These findings provide a means of inverting pyrolysates composition to kinetics of source rocks, which sets a precedent for the work in this study.

Many workers have taken interest and discussed the effects of kerogen types on the kinetic reactions of petroleum generation adopting hydrogen indexes as the only kerogen diagnostic. This has resulted in the recognition of distinctive activation energy distributions for different sedimentary environments (Braun et al., 1991; Hartwig et al., 2012; Ziegs, 2013; Abbasi et al., 2014 and 2016). Petersen et al. (2010) expanded their view and documented the relationship between kinetic measurements (i.e., activation energies distribution and frequency factors) and maceral compositions using a global set of type I /I-II source rocks (Figure 11). di Primio et al. (2000) studied the kinetic properties of petroleum asphaltenes and the structural similarity of asphaltenes to the parent kerogen. They concluded that the kinetic of petroleum asphaltenes can assist in determining the temperature of the actual source rock at the time of expulsion of the analyzed oil. This work and Petersen's et al. 2010 also go directly to the issue of relating maceral compositions and oils to kinetic properties in this research.

The second factor, namely diagenetic sulfurization of the organic matter, causes a reduction in kerogen stability, resulting in kerogen decomposition

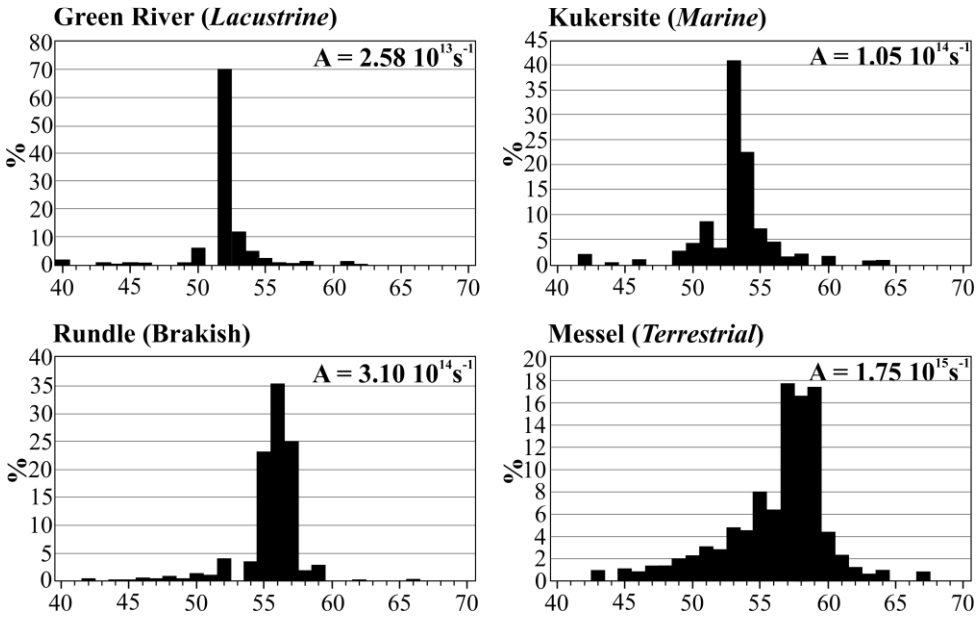

Figure 11. Activation energy distributions (Ea) and frequency factors (A) of four representative source rocks. Modified from Petersen et al., (2010).

under less intense thermal stress (Orr, 1986; di Primio and Horsfield, 1996). The generation of petroleum at relatively low levels of maturity is ascribed to the preferential cleavage of weak sulphur-sulphur and carbon-sulfur bonds (Orr, 1986). This phenomena is known to preferentially occur in carbonate-rich environments where reactive detrital iron is scarce and reduced sulfide is plentiful (Benner 1984; di Primio and Horsfield, 1996). Results presented in this study, however, indicate that incorporation of sulfur into the organic matter network can also occur in oxygen-deprived, clastic source rock systems lacking detrital iron.

3.3 Selected biomarkers in source rock age and lithology determinations

3.3.1 Selected biomarkers as lithofacies parameters

Tricyclic terpanes are ubiquitous in source rocks and oils from a wide variety of geological ages and depositional environments (Aquino Neto et al., 1982 and 1983; Moldowan et al., 1983; De Grande et al., 1993; Zumberge 1987; Tao et al., 2015). Therefore, they are routinely trusted for predicting lithological source rock characteristics. The diagram plotting the C_{24}/C_{23} tricyclic terpane ratio as a function of the C_{22}/C_{21} tricyclic terpane ratio (after Peters et al., 2005; Figure 12A) is perhaps the most common approach using these markers for lithology assessment. The C_{27} Ts and Tm norhopanes are probably as widespread in crude oils as tricyclic terpanes. Their ratio (i.e., Ts/Ts+Tm) can be used in tandem with the abundance of rearranged steranes relative to regular steranes (i.e., diasteranes /diasteranes + steranes) to define source rock lithology (Seifert and Moldowan, 1978; McKirdy et al., 1983; Mello et al., 1988).

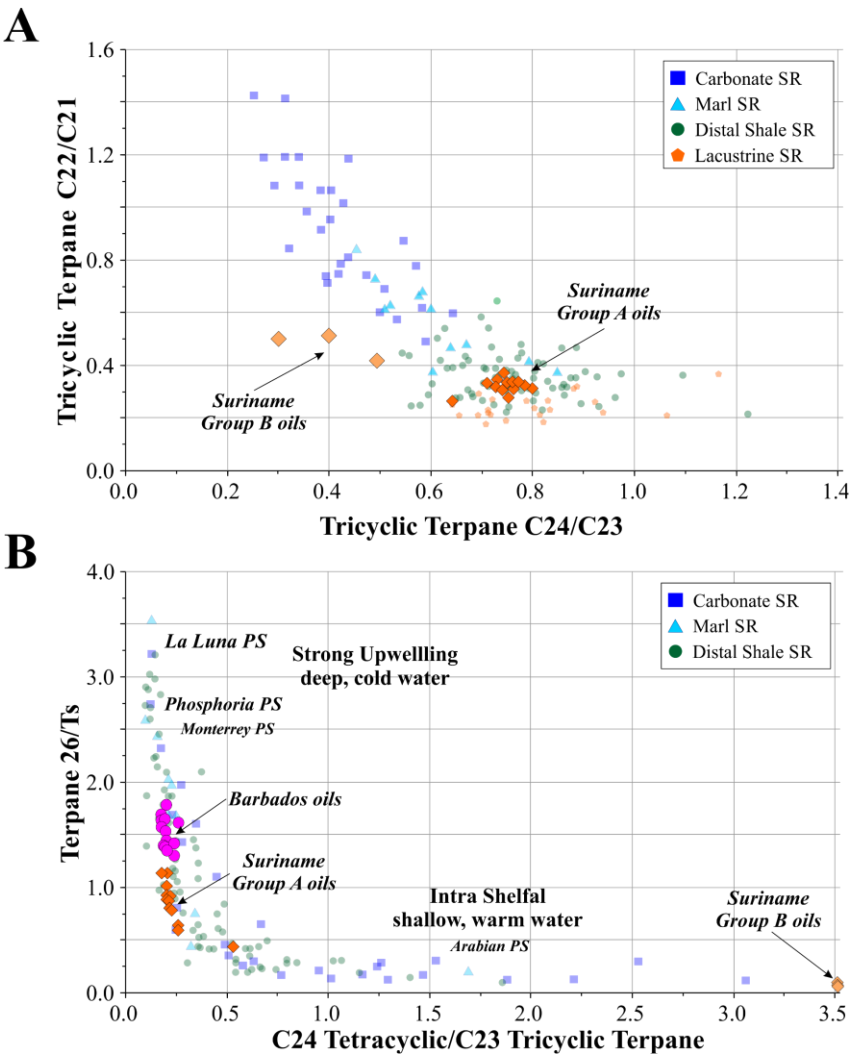

Figure 12. Cross-plots of terpane ratios comparing the Suriname and Barbados oils to a cosmopolitan dataset (in Zumberge et al., 2016) of petroleum systems from known source rock lithofacies. A. C24/C23 versus C22/C21 (after Peters et al., 2005) used for source rock lithology assessment. B. C24 tetracyclic/C23 tricyclic terpane vs C26 tricyclic/Ts (after Zumberge et al., 2016) employed for assessing upwelling in the source rock sedimentary environment.

3.3.2 Extended tricyclic terpanes in oil geochemistry

The biological source and precursor molecule of the extended tricyclic terpane series (i.e., C_{27} - C_{54}; ETR) remains poorly understood with the potential to occur in multiple biological sources (Liyanage et al., 2019; Peters et al., 2005). Consequently, their interpretations in oil geochemistry can be ambiguous - as is the case in this study. In the Norwegian Barents Sea, ETR have been traditionally exploited as an age-sensitive parameter to discriminate between Jurassic and pre-Jurassic oils. The age determination potential of ETR does not enjoy much contemporary support in the southeastern Caribbean-Atlantic margin where ETR are associated with mid-Cretaceous upwelling conditions.

3.3.2.1 ETR as age-sensitive parameters

Holba et al. (2001) recognized elevated concentrations of ETR relative to hopanes in many Triassic marine sourced oils whereas Middle and Late Jurassic marine oils are depleted in these compounds. They proposed the ratio of the extended tricyclic doublets for C_{28} and C_{29} over Ts (i.e., ETR_{RH}) to discriminate between the mentioned ages. The coincidental development of oceanographic conditions and the consequences of global mass extinctions, which may have had an impact on the principal biological sources of tricyclic terpanes, are suggested as the explanation for high ETR_{RH} values (i.e. > 2) in the Triassic marine sourced oils. It is worth noticing that most Triassic oils enriched in ETR in their original study derive from high paleo-latitudes, i.e. Barents Sea (Norway), Alberta and Sverdrup basins (Canada), and Alaskan North Slope.

In the Norwegian Barents Sea, Ohm et al. (2008) separated oils originating in the Upper Jurassic Hekkingen Formation from Triassic and Paleozoic sourced oils on the basis of the ETR_{RH} (i.e. Goliath oil in Figure 2A). Although some of their age determinations are supported by the work of

Matapour and Karlsen (2017), the authors highlighted that ETR in the Barents Sea could also be influenced by facies and maturity rather than being strictly age diagnostic. Similarly, they concluded that the abundance of ETR in some of the studied oils may be altered by varying degrees of intra-reservoir mixing.

3.3.2.2 ETR as upwelling-diagnostic parameters

Holba et al. (2003) described a connection between oils originating from source rocks accumulated near strong or persistent upwelling conditions and the relative abundance of ETR. Zumberge et al. (2007) observed an exceptionally strong relationship between upwelling sites predicted by oceanographic models and the occurrence of Late Cretaceous source rocks and oils with distinctive terpane distributions. Using a variation of the ratio to estimate upwelling (i.e., Tricyclic C_{26} S+R /C_{27} Ts), they showed that the Upper Cretaceous La Luna Formation and its regional equivalents (i.e. Querecual, Naparima Hill, and Canje) of northwestern South America were deposited under varying upwelling intensities (Figure 12B). Therefore, the generated oils possess distinctively high C_{26}/Ts ratio values (i.e., > 2). Such diagnostic characteristic should also be manifest as high C_{28} and C_{29} extended tricyclic doublets as noted by Holba. Erlich at al., (2003) predicted strong upwelling environments across the northeastern corner of South America, including the Barbados Accretionary Prism and the Guyana Basin. Source rocks deposited in epicontinental basinal or semi-closed settings such as the Upper Cretaceous Tuscaloosa and Eagle Ford display considerably lower values for C_{26}/Ts (i.e., < 1.5) (Zumberge et., 2007 and 2016).

4. Data and methods

The data used in this study comprises source rocks and oils analyzed using several standard petroleum geochemical methods. The majority of the data was acquired through the Jurassic-Lower Cretaceous Basin Studies of the Artic (JuLoCrA; https://wp.ux.uis.no/julocra/) and Conjugate Basins Tectonics and Hydrocarbons (CBTH; http://cbth.uh.edu/) consortia for the purpose of this study. Data in Paper III, which I coauthor, belongs to the Paleozoic Basins project (PABAS; https://wp.ux.uis.no/pabas/). Table 1 summarizes all analyses acquired for this study organized by paper.

All geochemical analyses were performed by Applied Petroleum Technologies (https://www.apt-int.com/) and follow the Norwegian Industry Guide to Organic Geochemical Analyses - NIGOGA (Weiss et al., 2000). The flow chart in Figure 13 summarizes the analytical techniques used in this study. The petrographic analyses were conducted by an external contractor from the RPS Group (https://www.rpsgroup.com/), namely Thomas Demchuck. Detailed description of the chemical analytical methods and petrographic workflows are presented in Appendix I.

Analysis	Paper I	Paper II	Paper III	Paper IV	Paper V
TOC	320	320	35		
Rock-Eval	320	320	35		
Maceral	320	320	35		
Source Rock Isotopes	140		15		
Py-GC		15			
Kinetic		15			
MSSV		5			
Extract GC-MS	15			4	
API					15
Sulfur wt.%					15
Oil GC / GC-MS			29[1]	7	15
Oil Isotopes			29[1]	11	15

Table 1. Geochemical and petrographic analyses employed in this study discriminated by paper.

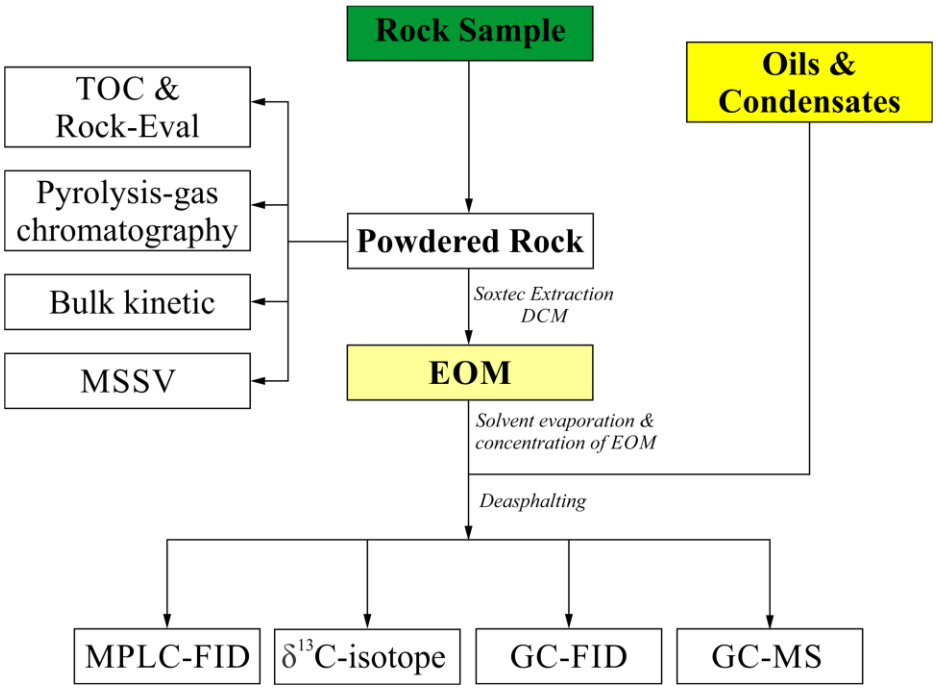

Figure 13. Flow chart of the geochemical analytical methods employed in this study.

4.1 Source rocks

Sample material was collected from the Norwegian Petroleum Directorate (NPD) well repository in Stavanger, Norway. Thirty and fourteen oil wells were sampled for the Norwegian Barents (Figure 14A) and North Sea-PaBas (Figure 14B) studies, respectively. In addition, sediments from five shallow stratigraphic wells (i.e., IKU now SINTEF https://www.sintef.no/en/) were included for the Barents Sea study. Wells were chosen to cover the study areas as extensively as possible. The sampled intervals were selected based on the stratigraphic boundaries as defined by the NPD and preexisting

geochemical studies from well completion reports. Sample selection was designed to ensure regular sampling intervals and prioritize core material over cuttings.

For Papers I and III, source rocks were subjected to Rock-Eval, TOC, and petrographic organic and inorganic analyses (Table 1). Selected source rocks were extracted and analyzed for stable carbon isotopes of the saturate, aromatic, and asphaltene (i.e. SARA) fractions. Open and closed-system pyrolysis techniques (i.e., pyrolysis-gas chromatography Py-GC, bulk kinetics, microscale sealed vessel pyrolysis MSSV) were used to investigate the generative potential of selected samples with distinctively different maceral assemblages in Paper II.

Fifteen source rock extracts with known maceral assemblages were submitted for molecular analyses. Py-GC and bulk kinetic analytical data were acquired for nine representative samples. This data is included in the chapter 6 of this thesis with the purpose of enhancing the discussion on geochemical inversion, but it is not published in the papers due to confidentiality restrictions.

4.2 Crude oils and oil-stained samples

For Paper III, twenty-nine crude oils were provided by the NPD (Table 1). Samples come from different producing wells and reservoirs. These oils, as well as those in papers IV and V, were subjected to molecular and isotopic analyses. Additional analytical data for 91 oils was retrieved from the Diskos database for broader coverage of the Norwegian North Sea (Paper III). Likewise, oil analytical data for selected samples from the GeoMark's (https://geomarkresearch.com/) Gulf of Mexico data base is utilized for testing the isotope findings in this study.

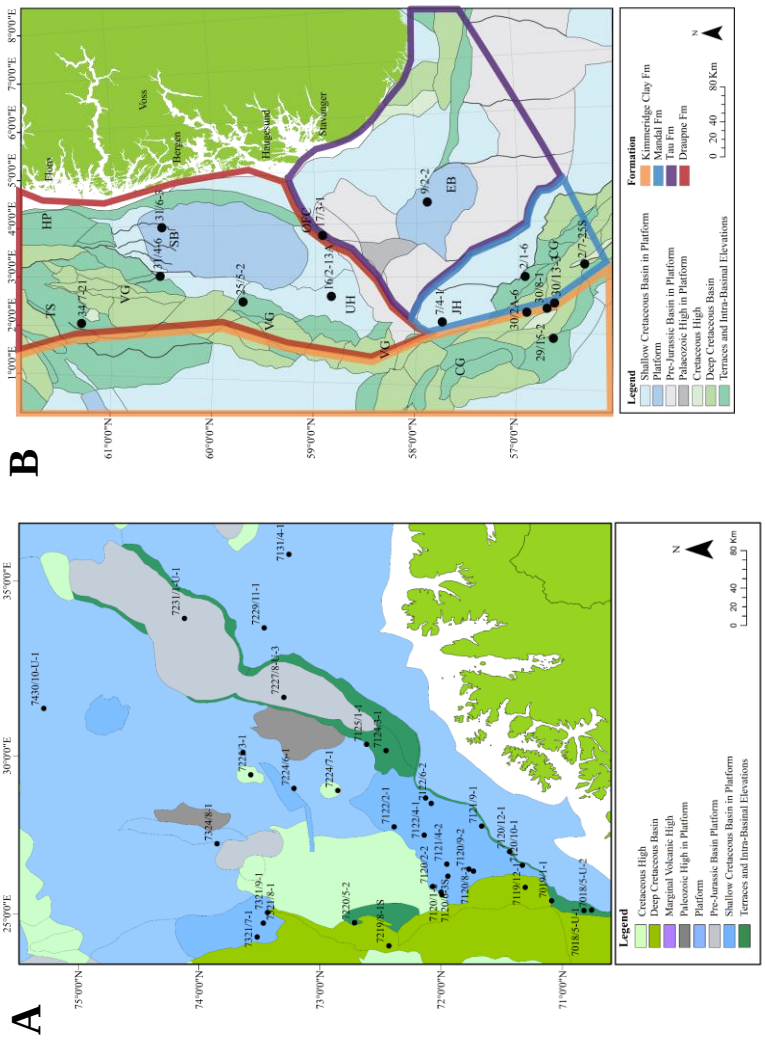

Figure 14. A. Map of the southwestern Barents Sea displaying the wells used in this study. **B**. Map of the northern North Sea illustrating the location of sampled wells and the different Kimmeridge Clay Formation equivalents. CG=Central Graben, JH=Jæren High, EB=Egersund Basin, UH=Utsira High, ØFC=Øygarden Fault Complex, VG=Viking Graben, SB=Stord Basin, TS=Tampen Spur, HP=Horda Platform.

For Paper IV, six crude oils were sampled from the wellheads of different producing wells within the Woodbourne field onshore Barbados (Figure 15A). The samples were taken from different reservoir units and depths within the Scotland Group (Figure 4B). In addition, an active oil seep (Figure 16A) and four oil-saturated sands were collected from the Shale Quarry in the northern part of the island (Figure 15A). At this location, semisolid bitumen occurs in isolated beds and stains as seen from ongoing leakage through severely deformed sediments (Figure 16B).

For Paper V, fifteen heavy oils from onshore Suriname wells were provided by Staatsolie (https://www.staatsolie.com/) in sealed glass bottles (Figure 16C). Nine oil samples were collected from the heads of various producing wells in the Tambaredjo (four oils), Calcutta (two oils), and Tambaredjo Northwest (three oils) fields (Figure 15B). These samples were produced from different clastic reservoirs of the Cenozoic age according to Staatsolie. The remaining six oils were sampled from exploration wells within the Weg Naar Zee (two oils), Uitkijk (two oils), Commewijne (one oil), and Coronie (one oil) exploration blocks. These oils were recovered from both the Cenozoic and Upper Cretaceous sand-rich formations during drillstem tests.

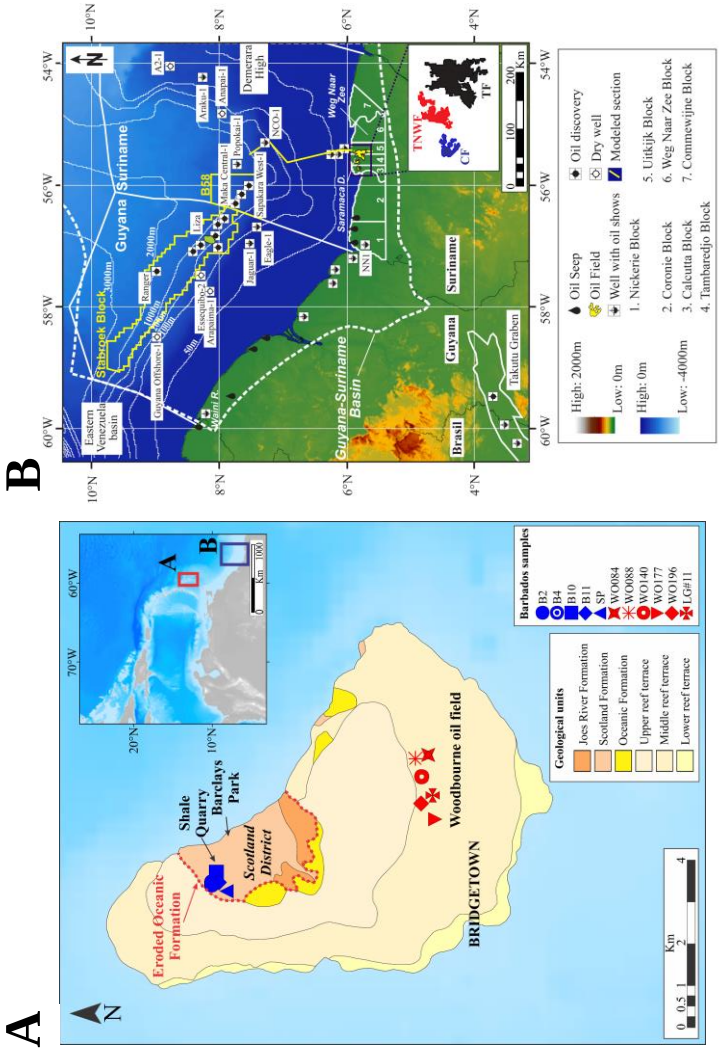

Figure 15. A. Geological map of the Barbados Island, southeastern Caribbean margin, showing the location of samples analyzed in this study; **B.** Topographic–bathymetric map showing the location of the study area and the main geological features of the region. In addition, oil fields and discoveries, oil shows, and relevant exploration blocks are displayed.

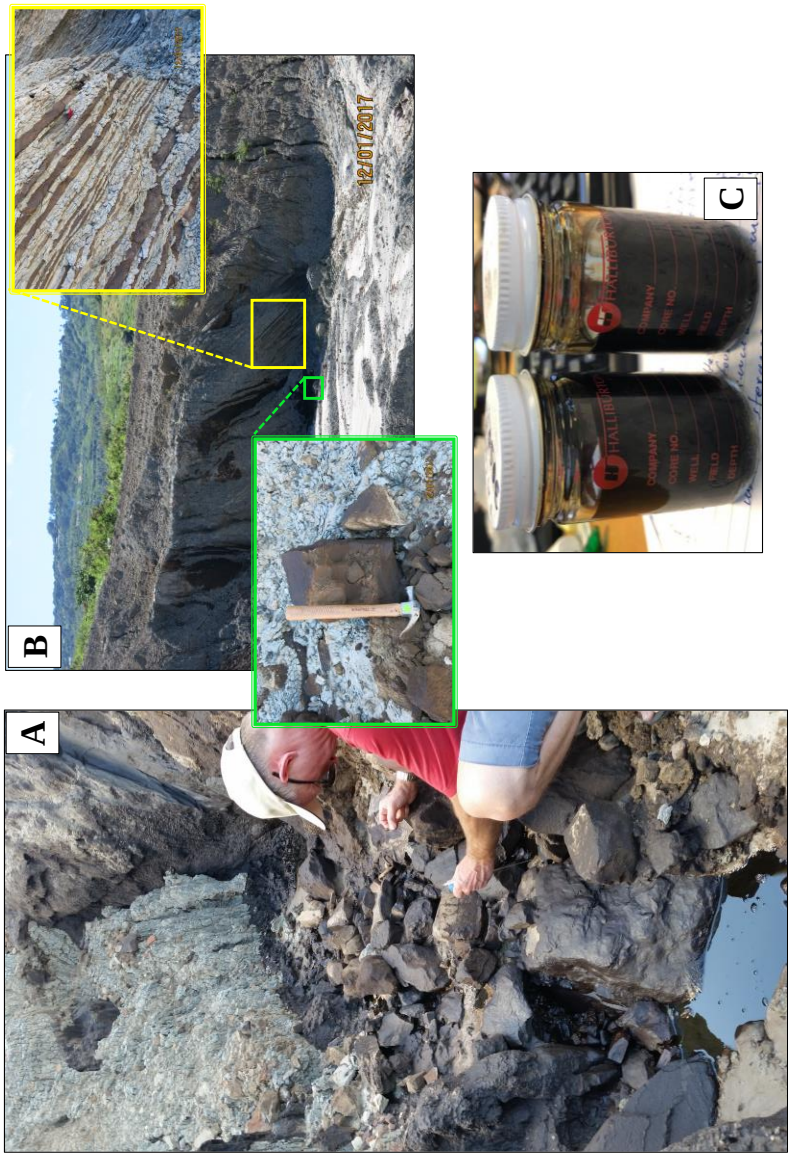

Figure 16. Active oil seep (**A**) and semi-solid bitumen (**B**) in severely deformed sediments of the Scotland Group at the Shale Quarry, northern Barbados Island. **C.** Black, heavy oil samples in sealed glasses from onshore Suriname.

5. Summary of Papers

5.1 Paper I. Upper Jurassic to Lower Cretaceous source rocks in the Norwegian Barents Sea, part I: Organic geochemical, petrographic, and paleogeographic investigations

Paper I provides a subregional to regional characterization of organofacies changes within the Hekkingen Formation in relationship to paleoenvironmental and paleogeographic conditions (Figure 17). To serve such purpose, this paper integrates various geochemical and petrographic analyses with paleogeographic models.

The Hekkingen Formation is subdivided into two units: the Alge and Krill members. The proportion of terrestrially derived macerals was found to be higher in the Krill Member relative to the underlying Alge Member (Figure 17). There is a greater proportion of marine macerals within distal areas of the Hammerfest Basin and well 7218/1-S in the southern Bjørnøyrenna Fault Complex. This shift in the relative proportion of marine and terrestrial macerals is ascribed to changes in the location of the depositional sites with respect to the sources of the terrestrial materials.

The Alge Member features the highest levels of total organic carbon (TOC ≥7 wt %), but the more discrete and organically poorer beds of the Krill Member still remain sufficiently rich to be considered petroleum source rocks (TOC ≥2 wt %). In immature to marginally mature (i.e., Tmax ≤ 435ºC) localities, the entire formation records hydrogen indices (HI) between 50 and 400 mg HC/g TOC, indicating that both members, upon maturation, can generate oil and gas. These low to moderate HI values are indicative Type III to II-III kerogens and are generally consistent with the high proportions of terrestrial macerals. Prior to thermal maturation, marine

type II kerogens (i.e. ≥ 400 mgHC/gTOC) probably existed in the marine liptinite-rich rocks in the distal Hammerfest Basin and Bjørnøyrenna Fault Complex. At least three factors are interpreted to have controlled the detected variability in geochemical parameters: dilution rates of organic matter, varying inputs of terrestrial versus marine organic matter, and the degree of preservation.

Pyrite contents and carbon isotopes of source rock extracts suggest that the degree of anoxia and bacterial sulfate reduction decreased gradually from south to north. This zonation in redox conditions is more prominent in the Alge Member. Importantly, this paper found a poor correlation between stable carbon isotopes of the saturate, aromatic and asphaltene (i.e., SARA) fractions and maceral compositions (Figure 18) and tentatively explained it as the result of varying degrees of bacterial sulfate reduction.

5.2 Paper II. Upper Jurassic to Lower Cretaceous source rocks in the Norwegian Barents Sea, part II: insights from open- and closed-system pyrolysis experiments

Paper II builds on Paper I and evaluates the petroleum generation potential of the Hekkingen Formation using bulk and quantitative pyrolysis analysis. Fifteen thermally-immature samples with differing organic facies were selected for total organic carbon, Rock-Eval pyrolysis, pyrolysis gas chromatography, bulk kinetics, and micro-scale sealed vessel pyrolysis analyses. The results were employed to characterize differences in source rock kerogens, gross petroleum type, and the compositional evolution of the generated fluids as well as their physical properties (i.e. gas to oil ratio, saturation pressure, and formation volume factor) as a function of increasing maturity.

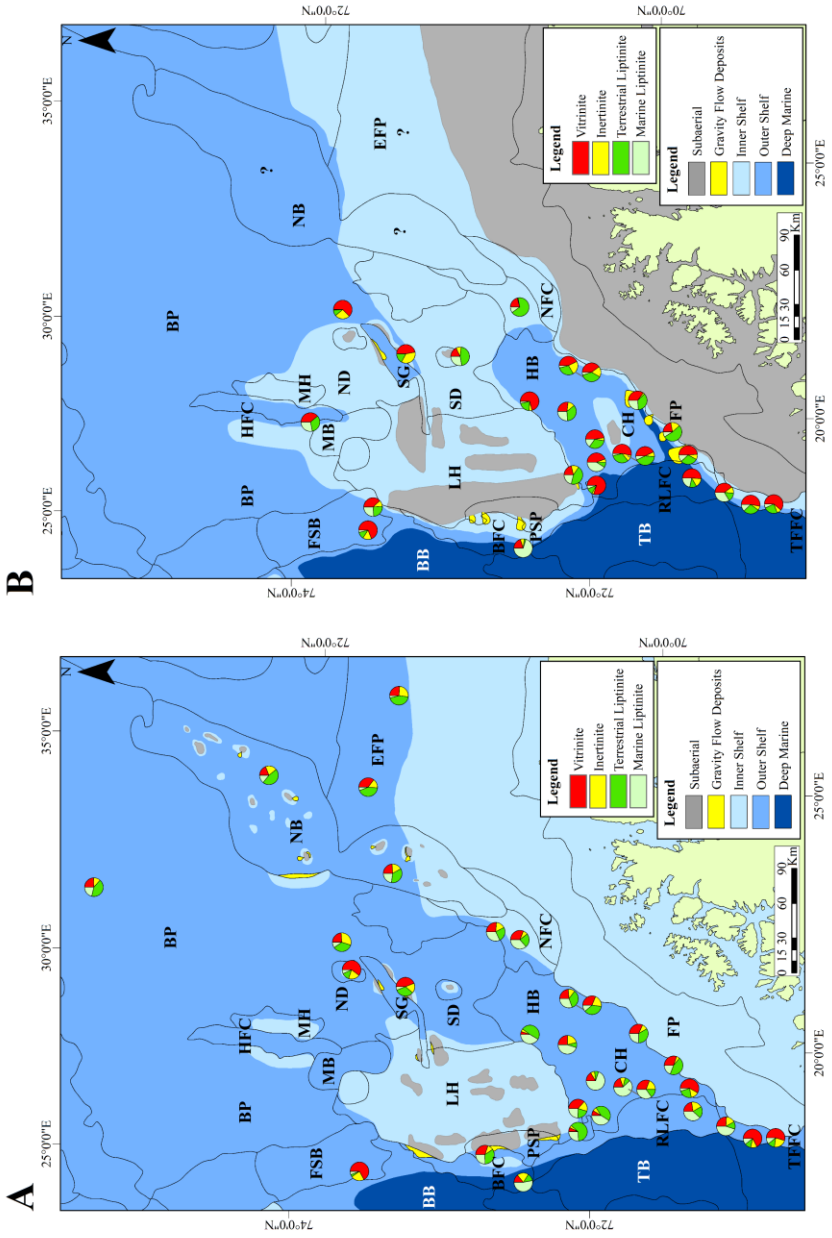
B
A
N
35°0'0"E
30°0'0"E
25°0'0"E
20°0'0"E
72°0'0"N
74°0'0"N
70°0'0"N
BP
NB
EFP
?
HFC
MB
MH
ND
SG
SD
LH
HB
NFC
CH
FP
RLFC
TFFC
TB
BFC
PSP
BB
FSB
Legend
Vitrinite
Inertinite
Terrestrial Liptinite
Marine Liptinite
Subaerial
Gravity Flow Deposits
Inner Shelf
Outer Shelf
Deep Marine
0 15 30 60 90 Km

Figure 17. Paleogeographic maps of the southwestern Barents Sea illustrating the variability in sedimentary environments within the Alge (**A**) and Krill (**B**) members. The paleogeographic maps are modified from Marin et al., (2020). The pie diagrams represent the average (i.e., per well) maceral compositions calculated from the microscopic analysis. Refer to Figure 1 in Paper I for abbreviations of geological provinces.

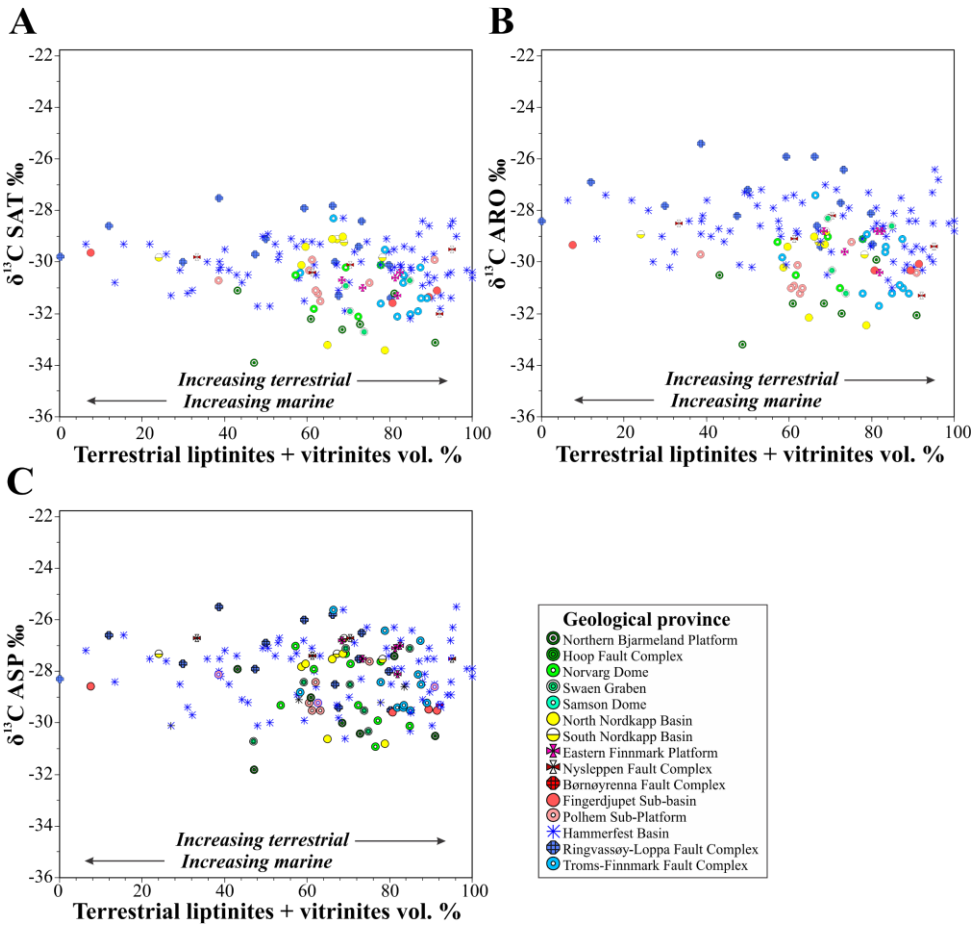

Figure 18. Volume percentage of terrestrial macerals (i.e., vitrinite + terrestrial liptinites) cross-plotted versus carbon isotope values of the δ^{13}C saturate (δ^{13}C SAT) (**A**), aromatic saturate (δ^{13}C ARO) (**B**), and asphaltenes saturate (δ^{13}C ASP) (**C**) fractions of extracted source rock samples. Samples are color-coded based on geological provinces.

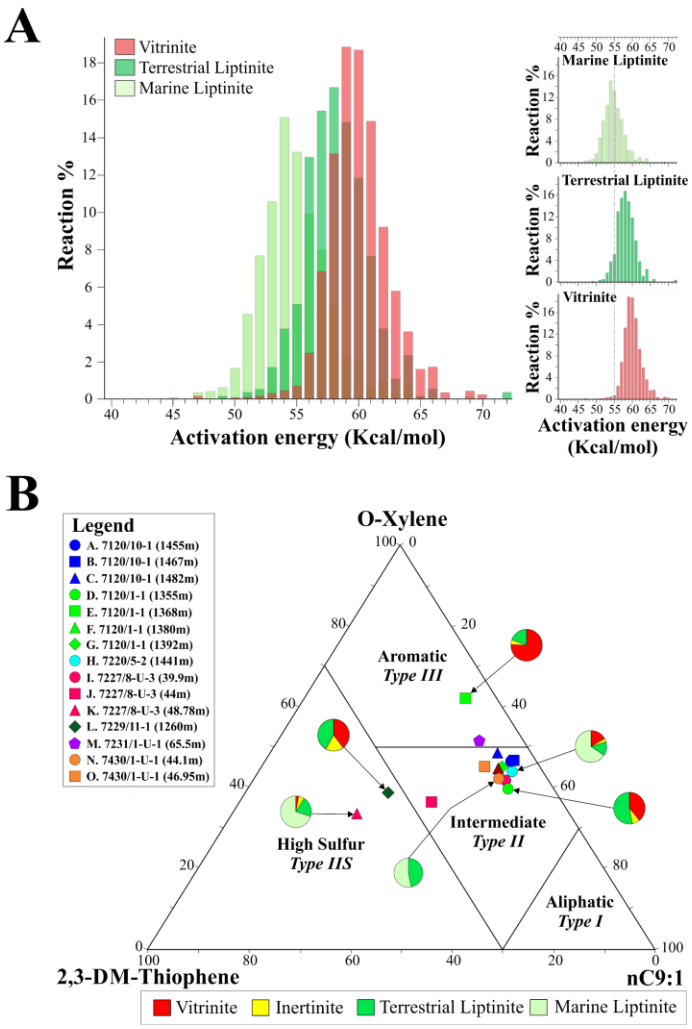

Figure 19. A. Average activation energy distributions computed according to the volumetrically predominant maceral (i.e., marine liptinites, terrestrial liptinites, vitrinites) in each sample in Paper II. Vitrinite subset = A, B, E; terrestrial liptinite subset = D, G, I, J, M, N; marine liptinite subset = C, F, H, K, N. See Table 1 in Paper II for maceral assemblages of individual samples. **B.** Ternary diagram of n-C9 alkene (n-C9:1), ortho-xylene (O-Xylene), and 2,3 dimethyl-thiophene (2,3-DM-Thiophene) used for kerogen classification according to Eglinton et al. (1990).

Heterogeneity in the kerogen mix resulted in different orders of kinetic stability (Figure 19A), with the predicted onset of petroleum generation spread over a relatively high and wide temperature range from 123ºC to 144ºC (at 3.3Cº/Ma). This temperature range equates to a difference of up to 700 m of burial if a thermal gradient of 30ºC is assumed. Reduced kerogen stability associated with elevated sulfur contents is documented in a few samples.

The majority of the analyzed samples possess the potential to generate low GOR oils of an intermediate to aromatic, low wax paraffinic-naphthenic-aromatic (P-N-A) composition and variable amounts of wet gas (Figure 19B). Petroleums of similar compositional and physical properties are predicted to have been generated from the natural maturation sequence of various organic facies in thermally mature areas of the Hammerfest Basin and the Ringvassøy-Loppa High and Bjørnøyrenna fault complexes. Vitrinite-rich sources in the Fingerdjupet Sub-basin and the Troms-Finnmark Fault Complex have potential for gas and condensate generation.

Finally, this paper utilizes the mapping of organic matter changes in Paper I and produces a map that illustrates the variation in kinetic properties and predicted petroleum types generated from the natural maturation series of various organic facies across the southwestern Barents Sea.

5.3 Paper III. Facies Variations in the Upper Jurassic Source Rocks of the Norwegian North Sea: From Micro to Macro Scale (*Skarstein et al., 2022*)

Paper III collects Upper Jurassic source rock samples from fourteen wells across the northern North Sea, including samples from the British and Norwegian Central Graben, Ling Depression, Egersund Basin, Viking Graben, Tampen Spur, and Horda Platform areas (Figure 14B). The samples

were analysed for organic richness and generation potential (i.e., TOC and Rock-Eval), carbon isotopes, and maceral and mineral content (petrography). Subsequently, the results were integrated to produce a holistic organofacies interpretation. The overall maceral composition was found to be consistent with Rock-Eval and isotope data.

In addition, the isotopic and biomarker composition of 120 oils distributed across the North Sea was utilized for organofacies assessment of the parental source and subsequent comparison with the observed source rock variability. Most importantly, this work found that carbon isotopes of both source rock extracts (Figure 20A) and oils (Figure 20B) become progressively heavier with increasing terrestrial detritus as per maceral and biomarker compositions, respectively.

Integration of all available data in a map (Figure 21) suggests generation from more oxic and terrestrially influenced organofacies in the southern part of the Central Graben, North Viking Graben and Horda Platform areas, and comparatively more anoxic and marine in the northern part of the Central Graben and South Viking Graben areas.

5.4 Paper IV. Barbados Petroleum and Its Role in Understanding Distribution of Cretaceous Source Rocks in the Southeastern Caribbean Margin: Insights from an Organic Geochemistry Study

In Paper IV, petroleum from onshore Barbados is analyzed geochemically and the results are compared to similar analytical data of source rocks and oils from Venezuela and Trinidad. This work goes directly to the issue of understanding petroleum sources within the Barbados Accretionary Prism and complements the work in Cedeño et al. (2021a).

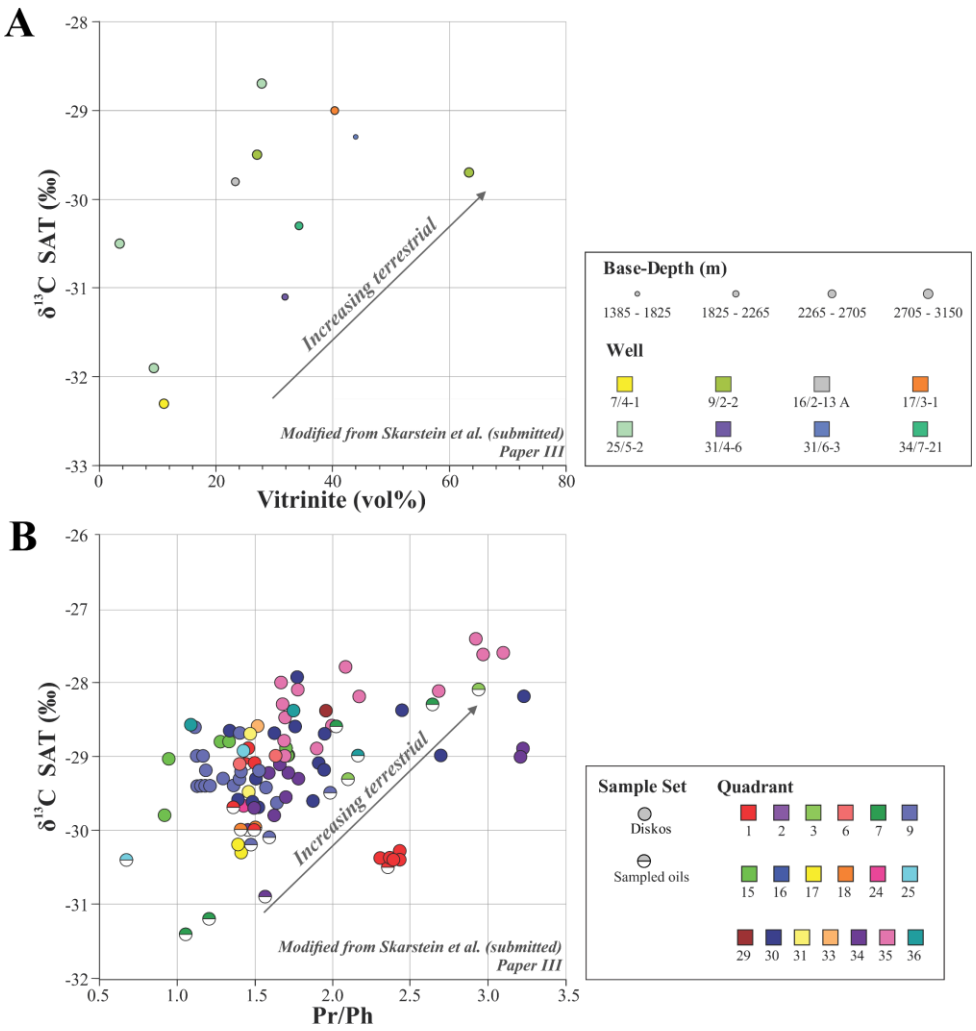

Figure 20. **A**. Vitrinite volume percentage (vol%) plotted against carbon isotope values of the saturate fraction (δ^{13}C SAT) of source rock extracts. Isotope compositions are seen to become isotopically heavier with increasing vitrinite content. **B**. Pristane/phytane (Pr/Ph) ratios cross-plotted against δ^{13}C SAT of oils from the Norwegian North Sea. δ^{13}C values are seen to become increasingly heavier with increasing Pr/Ph ratios. Figures are modified from Paper III by Skarstein et al., (2022).

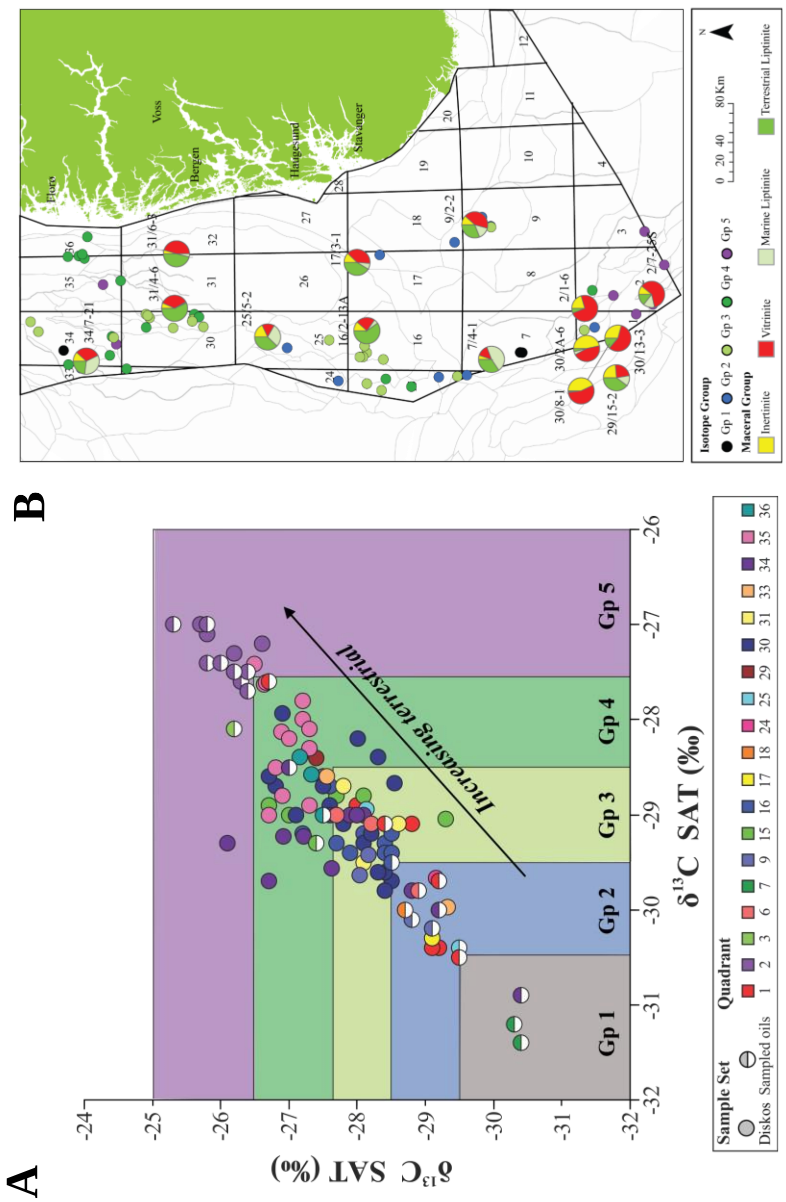
A
B
Gp 1
Gp 2
Gp 3
Gp 4
Gp 5
Increasing terrestrial
δ13C SAT (‰)
Sample Set
Diskos
Sampled oils
Quadrant
Isotope Group
Maceral Group
Inertinite
Vitrinite
Marine Liptinite
Terrestrial Liptinite
Bergen
Stavanger
Haugesund
Voss

Figure 21. **A**. Cross-plot of carbon isotopes of the saturate (δ^{13}C SAT) and aromatic (δ^{13}C ARO) fractions of oils from the Norwegian North Sea in Skarstein et al., (2022). The oil data set was divided into five groups (Gp): Gp 1 has the isotopically lightest composition while Gp 5 has the isotopically heaviest composition. Gp 1 oils are associated with generation from source rocks enriched in marine organic inputs. Gp 5 oils are associated with generation from source rocks comparatively enriched in terrestrial organic inputs. **B**. Map of the North Sea showing the average maceral composition of the studied wells and the distribution of studied oils colored after the grouping in A. Modified from Skarstein et al., (2022).

Interpretations suggest that petroleum onshore Barbados was derived from a Cretaceous deep marine shale source rock deposited under oxic-to-dysoxic conditions with varying contributions of marine and land plant-derived organic matter. This petroleum can be categorized into two groups. Group A petroleum was generated and expelled at the early oil window from an interval of the shale source rock containing predominantly marine organic matter. By contrast, petroleum in group B was generated at the peak of the oil window from a more proximal interval of the same source rock containing comparatively higher input of terrestrial-derived organics. These observations could imply the existence of the shale source rock at different maturities within a possible multiple-stacked source rock system in the prism. Oils in both groups, as well as most oils used for the regional comparison, display high concentrations of extended tricyclic terpanes (i.e., Figure 2B). Hence, this publication argues that the elevated abundance of extended tricyclic terpanes in the region may be circumstantial evidence to date empirically Upper Cretaceous-sourced oils.

Our interpretations suggest that reservoirs at the Woodbourne field have received at least two charges of hydrocarbons recognizable at present day. A first filling event is interpreted to have charged the reservoirs with the lower maturity petroleum (group A) after the middle Miocene uplift of the Barbados Ridge. Oils in reservoirs above 1000 m (3280 ft) depth are moderately biodegraded, whereas more deeply buried oils are only slightly biodegraded. The second more recent charge consists exclusively of light hydrocarbons (n-C3 to n-C9) expelled from the source rock at maturity levels similar to those determined for group B petroleum. This charging event is inferred to be triggered by the Pliocene–Pleistocene tectonic event.

Finally, the regional comparison using facies-sensitive biomarkers shows that Barbados petroleum was sourced by clastic facies similar to those sourcing petroleum in the northern part of the Eastern Venezuelan Basin,

Gulf of Paria, and Trinidad (Figure 22). These organic-carbon rich strata were speculatively incorporated into the western margin of the Barbados prism during the early stages of accretion (Paleocene–Eocene).

5.5 Paper V. Source Rocks in the Guyana Basin: Insights from Geochemical Investigation of 15 Heavy Oils from Onshore Suriname

This paper presents an overview of the geochemical composition of 15 heavy oils from producing and exploration wells onshore Suriname aiming to determine the organic facies generating them. The inferred facies are integrated with the geologic framework of the Guyana Basin in a two-dimensional basin model to further assess their thermal history in the shelfal area of the basin.

Detailed biomarker and carbon isotope geochemistry reveals the existence of two compositional groups onshore Suriname. Oils produced from Cenozoic reservoirs (Group A) possess compositional attributes characteristic of oils generated from a distal marine shale (Figure 12A). Their composition suggests the Upper Cretaceous shales of the Canje Formation as their potential source. Group A oils possess varyingly high abundances of extended tricyclic terpanes with values for the ETRs ratio (after Holba et al., 2001) oscillating between 1.87 and 3.37 (Figure 2C). In contrast, Group B oils occur in siliciclastic reservoirs of Late Cretaceous age and have biomarker relationships diagnostic of oils derived from a proximal marine depositional system rich in terrestrial organic matter. Uncertainty exists as to the age and spatial distribution of this organic facies. A Late Jurassic–Early Cretaceous age is provisionally proposed. It is worth noticing that the carbon isotope composition of the Group B oils was found to be in average 3‰ heavier than that of the Group A oils (Figure 23).

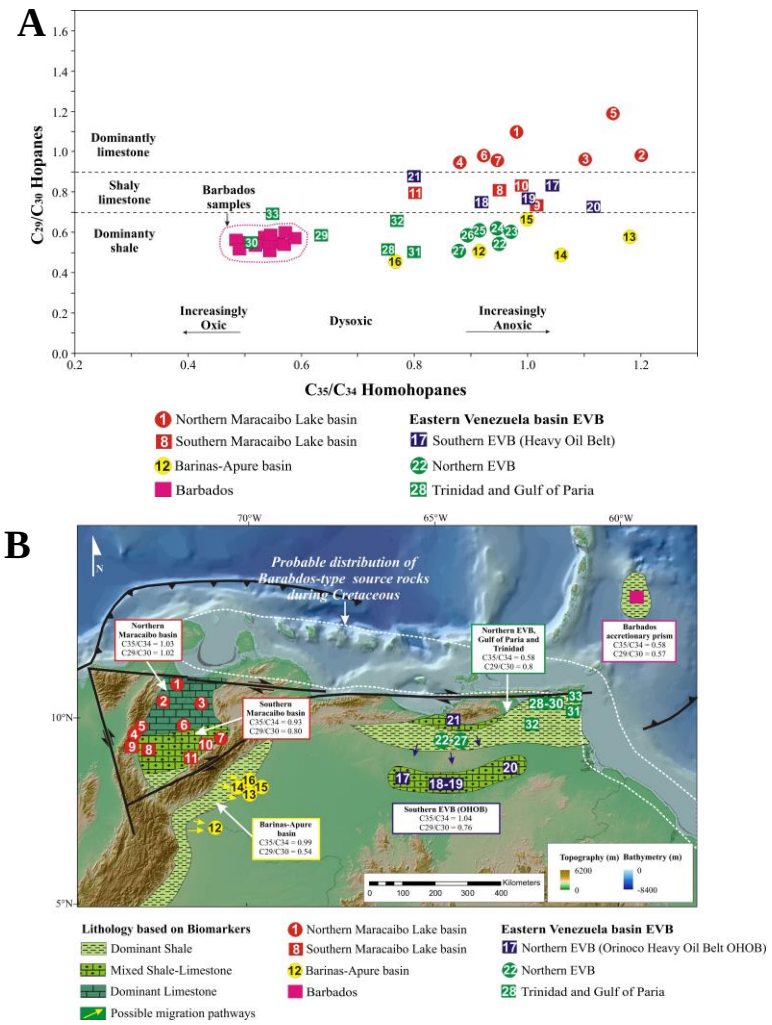

Figure 22. A. Cross plots of C35/ C34 homohopanes versus C29/ C30 hopanes ratios showing facies variations in several basins and comparing them with the Barbados sample set. **B.** Map showing regional variations in lithology and redox conditions during deposition of Cretaceous source rocks. Average calculated ratios C29/C30 hopanes (lithology) and C35/C34 homohopanes (redox conditions) are displayed for every basin.

Oil-maturity estimates indicate generation from source rocks at the mid-oil window for all the sample set. 2D Basin modeling suggests that generation from the Upper Cretaceous (Canje Formation) and Upper Jurassic–Lower Cretaceous source rock facies started in the early Oligocene. The Upper Cretaceous clay-rich facies has only transformed 30% of its potential in the shelf with expulsion starting in the middle Pliocene. Accordingly, entrapment of Canje-generated oils in the onshore Tambaredjo trapping structure is suggested to be younger than the middle Pliocene. The Upper Jurassic–Lower Cretaceous facies in most of the shelf area has nearly reached peak generation with expulsion commencing in the late Miocene given the input parameters. In the shelf area, up dip migration of hydrocarbon expelled from these two organic facies is dominant and terminates around the onshore Tambaredjo area.

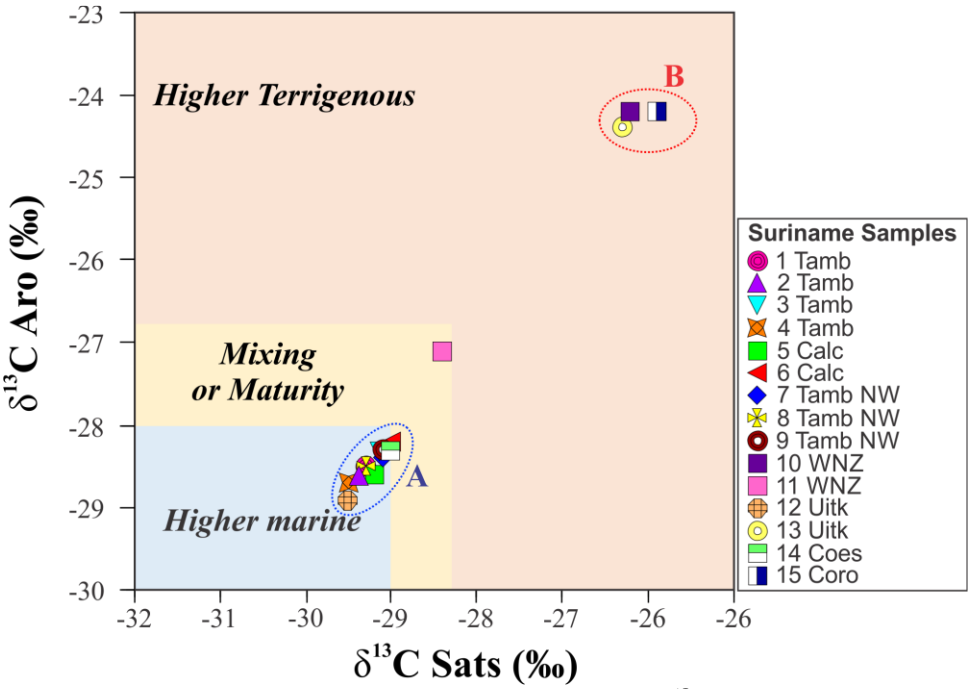

Figure 23. Plot of stable carbon isotopes of the saturate (δ^{13}C SAT) versus aromatic fractions (δ^{13}C ARO) displaying two distinct populations of samples in the Suriname data set. Template is after Integrated Geochemical Interpretations.

6. Discussion

This section highlights the main findings and contributions of this PhD study to geochemical inversion in terms of: 1 – stable carbon isotopes as organofacies indicators, 2 - biomarkers for kinetics predictions, and 3 – pitfalls of selected biomarkers in age and lithofacies determinations.

6.1 Implications for stable carbon isotopes as organofacies indicators

The composition of stable carbon isotopes (i.e., $\delta^{13}C$) of source rocks and oils is traditionally assumed to reflect that of the organic matter, and so it is exploited as a proxy to determine the relative contributions of marine versus terrestrial organic materials. Isotope analyses of Upper Jurassic source rock extracts in the Barents Sea and source rock extracts and oils in the North Sea (Papers I and III, respectively) contribute to such topic.

In Figure 18, the $\delta^{13}C$ of the various fractions is plotted as a function of maceral composition for the Hekkingen Formation data set. The poor correlation observed fails to reproduce what is expected from generalizations such as "marine organic materials are isotopically lighter than terrestrial organics" or vice versa. Paper I interprets this as the result of diagenetic transformation (i.e., fractionation) of the organic matter possibly related to varying degrees of sulfate-reducing bacteria under different redox conditions. This process may have modified the $\delta^{13}C$ of the various components of the kerogen mix differently because of varying stabilities, imparting a "homogenizing" effect that partly obscures the organofacies-related variability in $\delta^{13}C$ of the original biomass. The effects of other altering processes that are not revealed by the methods employed in this study such as differential aerobic bacterial degradation cannot be discarded. These modifications of the $\delta^{13}C$ result from thermodynamically ordered

isotope re-distribution within the kerogen network. Paper I thus demonstrates that after diagenesis the $\delta^{13}C$ of the organic matter preserved in the sedimentary record has been modified, setting a "new" post-diagenetic $\delta^{13}C$ that would be inherited by the generated fluids.

Figure 20A shows a plot similar to that in Figure 18 but for samples from the Upper Jurassic source rocks of the Norwegian North Sea in Paper III. Opposite to the scenario described in the Hekkingen case, the isotopic composition of the saturate fraction (i.e., $\delta^{13}C_{Sat}$) is gradually depleted in lighter ^{12}C (i.e. becomes isotopically heavier) as the content of vitrinitic macerals increases. Biomarker and isotope data for the North Sea oil data base in Paper III reveals that progressively heavier $\delta^{13}C_{Sat}$ values are also associated with increasing terrestrial organic inputs (Figure 20B) to the source rock depositional site. The maceral composition of the analyzed source rocks and $\delta^{13}C$ of the oils displayed on a map (Figure 21B) indicate that the liquids grossly reflect the organic matter composition of the sources. Marine sourced oils being isotopically lighter than terrestrial-sourced oils have also been documented in other areas of the Norwegian Continental Shelf (i.e., Haltenbanken Terrace Karlsen et al., 1995). Paper V also documents heavy isotope values in oils originating from source rocks enriched in terrestrial organics, as per biomarker data, in the Guyana Basin (Figure 23).

In attempt to test if the isotope-organofacies relationship discussed in the preceding paragraph is universally applicable, this work utilizes a set oils affiliated to the Paleocene Wilcox Group in the US Gulf of Mexico. This unit is known to transition from non-marine/transitional to lower slope and abyssal facies (Pepper et al., 2017). In Figure 24, the $\delta^{13}C$ of the saturate and aromatic fractions of oils acknowledged to have been sourced by the Wilcox are cross-plotted against tricyclic (A and B) and acyclic isoprenoid (C) parameters sensitive to organofacies. These cross-plots show that the $\delta^{13}C$

becomes progressively lighter with increasing terrestrial signatures - a trend that is essentially opposite to that documented for the North Sea and the Guyana Basin cases in Papers III and V, respectively. Increasing thermal maturation is acknowledged to shift the $\delta^{13}C$ of oils to heavier values (i.e., isotopically heavier), and, thus, has the potential to mask organic matter signatures. Although the impact of maturity is inherent to generation, it does not appear to be the main factor controlling the $\delta^{13}C$ of the oil data set as indicated by the weak correlation between $\delta^{13}C_{sat}$ and a maturity-diagnostic parameter in Figure 24D.

Assuming that conditions affecting the isotope composition of carbon in ancient biospheres are similar to those in today's biosphere, it is reasonable to infer that multiple processes must have altered the $\delta^{13}C$ of the sedimentary organic matter sourcing today's oil. These complexities and ambiguities show that the use of generalizations in inverting isotopes to a single attribute of a source rock, i.e. organofacies, needs to be done with caution because of the overlapping effect of various primary and secondary factors affecting organic pools differently. Naturally, this could lead to the marine or terrestrial character of a given source rock to be overstated.

6.2 Implications for biomarkers in predicting source rock kinetic properties

The transformation of sedimentary organic matter to hydrocarbons occurs at different temperatures and rates depending on the liability of the different components in the kerogen mix (Tissot and Welte, 1978; Tegelaar and Noble, 1994; Braun et al., 1991; Petersen et al., 2010). Pyrolytic experiments in Paper II show vertical and lateral variations in kinetic and petroleum products as a function of organofacies changes, even when the gross sedimentary environment remains broadly similar. Figure 19 illustrates that the thermal stability of the source rock and the generated hydrocarbon blend

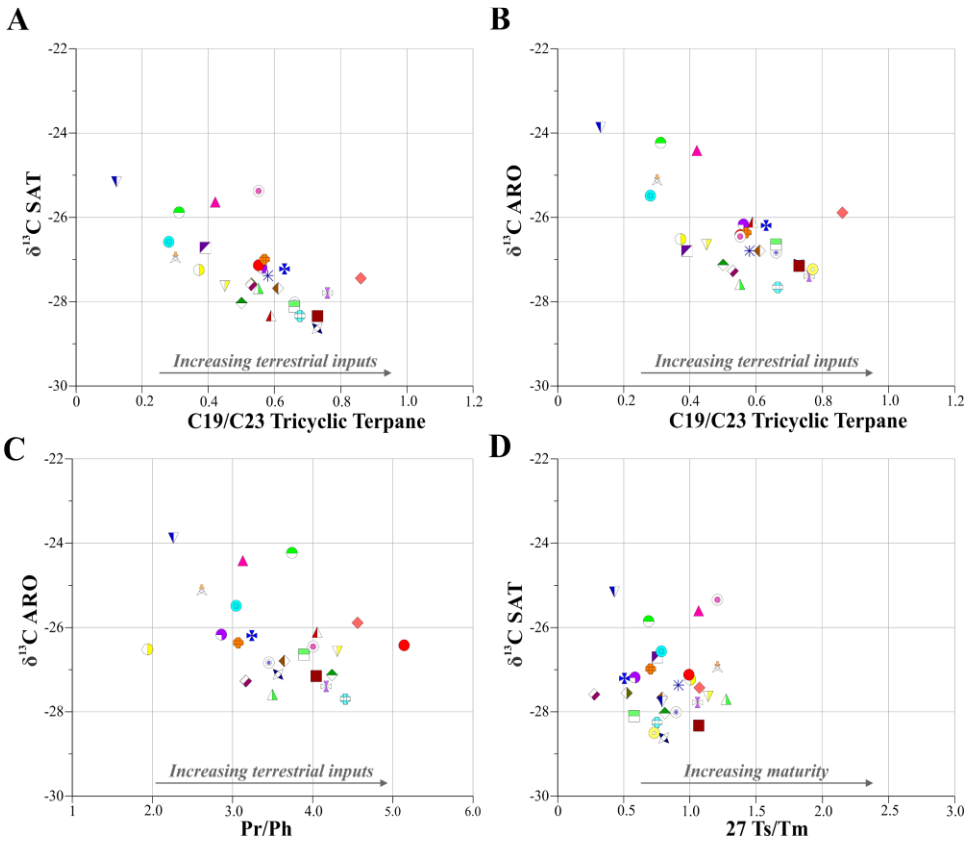

Figure 24. Common organofacies biomarker ratios (**A**, **B**, and **C**) plotted against stable carbon isotopes of the saturate (δ^{13}C SAT) and aromatic fractions (δ^{13}C ARO) for a set of Wilcox-derived oils. The cross-plots show a trend towards lighter δ^{13}C values with increasing terrestrial inputs. **D**. C27 Ts/Tm versus δ^{13}CSAT showing a weak correlation between maturity and δ^{13}C values.

(i.e., saturate rich, aromatic rich, or intermediate composition) relates closely to its maceral composition. Thus, maceral data could assist in estimating comparative kinetic of petroleum generation for source rock samples that have not been subjected to direct kinetic experiments. Elevated concentrations of sulfur detected in a few pyrolysates suggests that diagenetic sulfurization of organic matter can also occur in clastic environments if conditions are viable, most importantly, regardless of the source rock maceral composition (i.e., Sample L in Figure 19B and Figure 8 in Paper II). Consequently, early petroleum generation due to thermally labile sulfur-sulfur and sulfur-carbon bounds can also occur in clastic sources opposite to conventional wisdom.

Paper I, II, and III prove that within a single source vertical organofacies and intrinsic kinetic variations can occur over a few meters. This ubiquitous heterogeneity cannot be described by bulk and quantitative pyrolysis analysis of a few samples at different depths; even more closely-spaced sampling would only partly reproduce such variability. Zumberge et al. (2016) explained that oils represent an average compositional view of their sourcing organic matter. Therefore, flash liquids often reflect the compositional characteristics of their parental sources more efficiently than do single, or a set of rock extracts. In line with the "averaging perspective", Paper II argues that for a more pragmatic use, the kinetics of petroleum generation within a heterogenous source could also be modeled as an average.

A potential tool for inverting oil compositions to their approximate parent source rock kinetics capitalizes on the above simplifications and exploits the correlations in Figure 25. It cross-plots biomarker data for the North Sea oil data base in Paper III and corresponding analytical data for selected sediments extracts with both maceral and kinetic analyses from the Barents Sea data base in Paper II. It is intended only as a preliminary review for

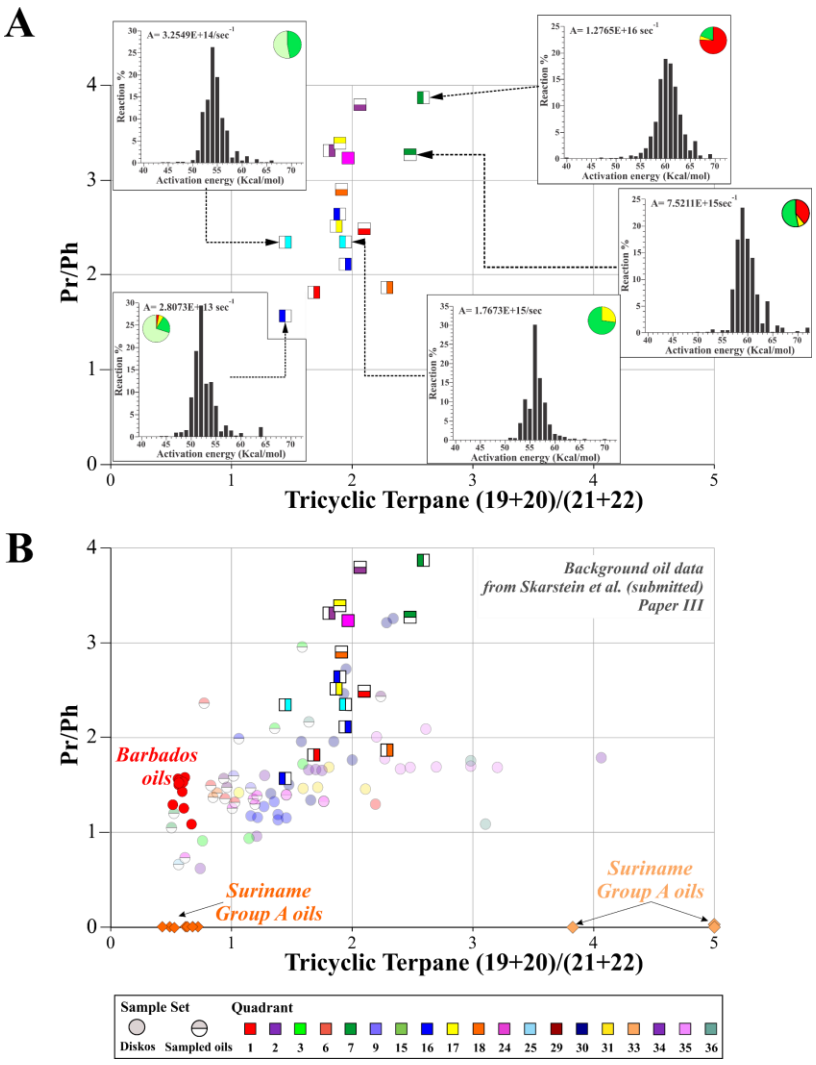

Figure 25. A. Cross plot of (C19/C20)/(C21+C22) tricyclic terpanes versus pristane/phytane (Pr/Ph) ratios for selected source rock extracts from the Hekkingen Formation with distinctive maceral compositions and kinetic properties. **B.** Hekkingen source rock extracts integrated with Barbados, Suriname, and North Sea (background) oil data sets as a potential proxies for inverting oil biomarker to source rock kinetics.

marine sourced oils and inferences drawn from it must be taken as probabilistic rather than absolute.

Crude oils exhibiting values ≥ 3 for the Pristane/Phytane (Pr/Ph) and ≥ 2 for the (C_{19}+C_{20})/(C_{21}+C_{22}) tricyclic terpane (TT) ratios compare most favorably to extracts from kinetically stable sources (i.e., peaking at 58-61 kcal/mol) enriched in terrestrial plant detritus (i.e., vitrinite and terrestrial liptinite; Figure 25A). Such organic matter, in turn, implies relatively oxidizing conditions and proximity of the depositional site to a source of land-plant remnants, i.e. a proximal marine or coal-bearing delta plain environments. Although the Surinamese Group B oils (Paper V) lack values for the Pr/Ph ratio due to degradation, TT ratios in the range of 3.8 to 6.2 suggest inversion to terrestrial-rich, kinetically stable sources (Figure 25B). In fact, similar kinetic parameters to that resulting from the inversion are reported for the lower section of the Upper Cretaceous source rock system modeled in Paper V.

Oils with lower Pr/Ph and TT ratios (i.e., < 2) plot most closely similar to extracts from thermally labile sediments containing predominantly marine macerals with varying but subordinate terrestrial detritus (Figure 25A). These sediments show less stable kinetic properties with varyingly low peaking maxima (i.e., peaking at 51-53 kcal/mol) depending on the proportions of terrestrial inputs. This kerogen mix is interpreted to indicate sedimentation within mid-distal shelfal environments with normal-marine redox conditions. Examples of oils with these characteristics are the Barbadian oils in Paper IV and North Sea oils from blocks 17, 18, and 31 among others (Figure 25B). A large spread in the TT values at similar Pr/Ph ratios could signify generation from organic matter consisting of distinct proportions of marine and terrestrial particles deposited under similar redox conditions. Samples N and O in Figure 25A are examples of differing organic matter composition (i.e., as per macerals) with similar Pr/Ph ratios.

These initial results show that further work is needed to refine this tool and understand what factors underlie variability with greater clarity.

6.3 Implications for the applicability of selected biomarkers in age and lithology determinations

Unlike other source rock attributes, absolute age is particularly challenging to invert from oil biomarker compositions. Only in few exceptional cases, does age impart a distinctive characteristic to oil fingerprints. The principal influence of age is in the origination, evolution, and extinction of organisms that constitute the organic matter budget available for sedimentation, burial, and ultimately transformation to petroleum (Bissada et al., 1993). As a consequence, biomarker parameters employed to infer source age typically overlap with those related to lithology, environment, and organic inputs as discussed in Papers IV and V.

Oils enriched in extended tricyclic terpanes (i.e., ETR) occur in the Norwegian Barents Sea (Figure 2A). Ohm et al. (2008), using the rationale in Holba et al. (2001), associated high ETR_{HR} (i.e., ≥ 2) with Triassic and possibly Paleozoic-aged sources. Interestingly, they also reported extracts from immature Triassic sources with $ETR_{HR} \approx 0$ and potential Triassic oils with $ETR_{HR} < 2$. High concentrations of extended tricyclic terpanes also occur in sources and oils of the southeastern Caribbean-Atlantic margin, including Barbados and Suriname (Figure 2B and C). If the ETR age concept of Holba et al. (2001) was universally applicable as it stands, one could incorrectly conclude that the source of these oils is of Triassic age, not the Albian-Turonian Canje Formation. In Papers IV and V, such high values are explained in the context of varyingly high upwelling conditions known to have occurred in the region (Erlich et al., 2003; Zumberge et al., 2007). The ambiguity discussed above illustrates that the significance assigned to high

ETR abundance differs from one geographic location to another, and, therefore, their universal use needs careful consideration and calibration.

Although extended tricyclic terpanes are not entirely independent of thermal and bacterial degradation, their enrichment appears to be intimately linked with changes in sedimentary conditions over a narrow geographic and stratigraphic range which in turn trigger local changes in the biological sources of terpanes (Holba et al., 2001 and 2003; Zumberge et al., 2007; Dutta et al., 2006). Consequently, it is likely that high ETR occur recurrently when and where the conditions for their sources are viable. High ETR may thus reflect the approximate timing of the changes rather than being strictly age deterministic in themselves and may instead be regarded as a facies diagnostic proxy. Their relative abundance may be interpreted to indicate the extent of upwelling in the system - if oils are of comparable maturity. It implies that ETR within a single source, and so that transferred to the generated oils, can vary considerably, even if the gross organofacies remains broadly similar.

Mid to Upper Cretaceous-sourced oils from Barbados in Paper IV exhibit ETR_{HB} values that are overall higher than those in the Suriname oils in Paper V (i.e., 3.1 - 4.3 and 1.87 - 3.37, respectively; Figure 2B and C). Values calculated for the ratios proposed in Zumberge et al. (2007) (i.e., C_{24}/C_{23} and C_{26}/Ts) for the same oil data set substantiate such difference (Figure 12B). At the regional level, these varying proportions could signify generation from facies of the same source deposited under different upwelling intensities as recognized by Zumberge at al., (2007) – stronger for the facies sourcing the Barbados oils. Over an area the size of the Norwegian Barents Sea (Figure 1A and 7A), considerable lateral variations in sedimentary and upwelling environments during the various periods of source deposition likely occurred. Thus, it is reasonable to suggest that not all oils expelled from the Triassic source in the Norwegian Barents Sea, or elsewhere, must

have ETR_{HR} values greater than 2 to be characterized as Triassic - a reflection similar to that discussed by Ohm et al. (2008). Based on the above observations, the ETR signature of an oil originating in an upwelled source rock system would be dependent on the location of its sourcing facies within the system.

Similarly, biomarkers can "mimic" the fingerprints of a distinctively different lithology creating inconsistencies between and among biomarkers inferences and bulk oil attributes. The biomarker character of the Group B oils onshore Suriname (Paper V) is that of many oils and source rocks deposited in marl sedimentary systems (Figure 12A); however, their low to very low sulfur content (i.e. 0.18-0.22 wt.%; Figure 26A) fails to reflect the higher values expected from the marl biomarker geochemistry and suggest a clastic source. The high contributions of terrestrial organic inputs also seems inconsistent with the marine-dominated kerogen observed in marl depositional systems. In fact, these oils compare most favorably to oils originating from terrestrial-rich D/E organofacies (Figure 26B and C) in the tricyclic terpanes profile. These contradictions manifest that some biomarkers in migrated liquids bear no relation to the source organic materials, but perhaps originate from secondary alteration of organic compounds. Regardless of the mechanism (s) driving these inconsistencies, this study highlights that biomarkers are not universally applicable as well as the need for holistic geochemical interpretations.

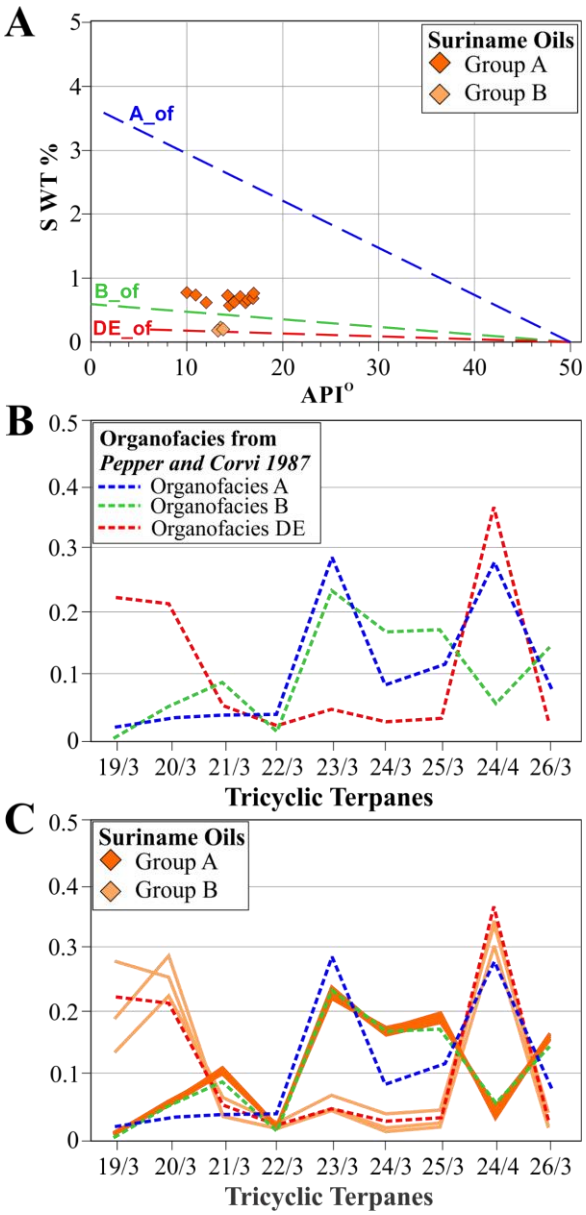

Figure 26. **A**. Cross plot of API gravity versus sulfur weight percent (S WT%) for the Suriname data set. Average API-S WT% trends for marine clay-poor organofacies A (A_of), marine clay-rich organofacies B (B_of), and terrestrial-rich organofacies DE (DE_of) are displayed for comparison. **B**. Tricyclic and tetracyclic terpane profiles for an end-member oil originating from organofacies A, B, and DE. **C**. Tricyclic and tetracyclic terpane profiles of the Suriname oils compared to organofacies end-members in B. Organofacies scheme after Pepper and Corvi (1987).

6.4 Limitations

Whereas this study has drawn important observations with direct implications for geochemical inversion in the study areas and elsewhere, it is important to recognize that there are limitations related to the data set itself and those that are intrinsic to source rocks and oils under natural subsurface conditions. Rising awareness of these limitations is crucial for understanding the applicability of the findings as well as provide the foundations for future work.

6.4.1 Source rock data

Most wells being preferentially drilled in structural highs limits the ability to understand syn- and post-sedimentary processes controlling the development of organically-richer basinal source facies. The lack of such sampling materials precludes the acquisition of maceral, kinetic, isotope, and molecular data for true deep-marine facies and their use in the different proxies discussed in this work. Consequently, source rock attributes assigned to the distal basinal areas are, at best, estimations based on the maceral data. In some wells, sampling material was only available every 10-15 meter with high chances of mixing during drill cuttings recovery.

6.4.2 Oil data

Intermediate to heavy bacterial degradation of oils in the southeastern Caribbean-Atlantic margin hinders the use of common molecular parameters such as Pr/Ph, which could provide a broader overview of the whole oil composition and could complement isotope interpretations.

7. Recommendations for future work

7.1 Continued work on stable carbon isotopes of oils as organofacies indicators

Future research can be oriented towards an in-depth assessment of the influence of diagenetic carbon isotope alteration of the primary biomass in the ultimate $\delta^{13}C$ of the generated oil. Evaluating the character of the diagenetic alterations can be performed by complementing source rock stable carbon isotopes with isotopic studies of sulfur and nitrogen as well as with inorganic geochemical analysis of trace (i.e., molybdenum, uranium, vanadium, chromium) and major (i.e., iron, sulfur) elements. Incubation studies can help simulate various diagenetic scenarios. Subsequent hydrous pyrolysis of samples with distinct diagenetic histories and maceral assemblages could provide insight into the $\delta^{13}C$ of the generated fluids, which can, in turn, be related to the source organic components and compared to the pre- and post-diagenetic $\delta^{13}C$. Such work would provide valuable supporting information to reappraise more confidently the value of carbon isotopes in inverting to source rock organofacies.

7.2 Continued work on inverting biomarkers to source rock kinetics

The preliminary results presented in this study highlight the potential of this approach, yet extensive work remains to be done. Observations from the data set used may be directly applicable to marine source rocks but may not be as directly pertinent to source rocks deposited in other sedimentary environments. Future research should focus on supplementing the data set with maceral, kinetic, and extractions for deep-marine clay-rich, marine clay-poor, lacustrine clay-poor and clay-rich, and coal source rock end-members. Source rocks containing bacteria-rich and degraded marine

organic materials also need to be added. Efforts are also urged to better understand the overall contribution of the different maceral groups in the source rock, particularly that of the terrestrial particles, to the generated oil biomarker composition. Likewise, kinetics of petroleum asphaltenes derived from known organofacies could valuably contribute because they represent an average compositional view of the source.

Further work could also be done concerning compositional Microscale Sealed Vessel pyrolysis experiments for samples that are representative of the different source rock environments and organic matter mixtures. With that, the proposed approach could be enhanced to provide information on the gross relative proportions of liquids and gas in the generated hydrocarbon blend and its main physicochemical properties.

7.3 Continued work on evaluating extended tricyclic terpanes

Although the results in this study do not claim universal validity, it is apparent that extended tricyclic terpanes can be used as an upwelling diagnostic parameter - a topic that deserves further investigation. Systematic extraction of sediments from an upwelled source rock system like that contained in the Albian-Cenomanian-Turonian La Luna Formation of northern South America would permit studying how the geochemical attributes of extensively upwelled systems compare to those of more localized, smaller-scale upwelling systems. That research could also benefit from analyses of trace (i.e., molybdenum, uranium, vanadium, chromium) and major (i.e., iron, sulfur) elements as a means of determining sedimentary conditions. Finally, a similar workflow could be applied to the multiple source rock intervals in the Norwegian Barents Sea, which would assist in delineating the contribution of the different sources to the petroleum system.

8. Conclusions

This work adopted an interdisciplinary approach consisting of isotope, molecular, pyrolytic, and petrographic analyses to draw observations concerning the successes and pitfalls of selected geochemical proxies in inverting oil composition to their parental source rock. The results have direct implications for understanding source rocks not only in the study areas but also elsewhere when pertinent data is scarce or absent.

1. The observed variability in stable carbon isotopes of source rock extracts and oils does not always correlate with changes in the proportions of marine and terrestrial organic components. Multiple fractionation processes acting together during diagenesis alter the organic components differently. Depending on the intensity, diagenetic changes may outweigh the isotopic difference between the original organic components. Consequently, estimating the contribution of marine and terrestrial organics in the source rock based solely on stable carbon isotopes is uncertain. Carbon isotopes are a recommendable tool only if validated by molecular and bulk parameters.

2. The thermal stability of a given kerogen mix and the generated hydrocarbon blend are closely related to the maceral composition. This allows the maceral assemblage of a source rock to be exploited as a rapid means of assigning comparative gross kinetic properties to samples that have not been subjected to direct kinetic experiments. An exception to this observation occurs if the organic matter has undergone significant diagenetic sulfurization because the incorporated sulfur reduces the kerogen thermal stability regardless

of the maceral composition. Opposite to common wisdom, sulfurization can also occur in clastic systems.

A preliminary test combining maceral composition, molecular, and kinetic data for organically different marine source rocks demonstrates that oil biomarker compositions can be inverted to the kinetic properties of the source rock facies. Conclusions and inferences drawn from this approach must be taken as probabilistic rather than absolute.

3. Extended tricyclic terpanes are not strictly age deterministic in themselves as formerly interpreted. Increased concentrations of these compounds reflect changes in the biological sources of terpanes that occur at specific locations and times under suitable conditions. Such conditions are reportedly mediated by strong and persistent upwelling in the system. Thus, their age-diagnostic potential should only indicate the approximate timing of changes in the local sedimentary environment, which may, however, occur recurrently when and where conditions are viable. It is proposed that extended tricyclic terpanes could be regarded as a facies diagnostic proxy and their relative abundance may provide clues as to the extent of upwelling in the sedimentary system.

4. Despite occasional ambiguities in their interpretation, stable carbon isotopes and biomarkers provide valuable supporting information for inverting source rock facies. Importantly, they need to be calibrated as their significance may vary from one basin/paleo-latitude to another. Interpretations should therefore integrate bulk, molecular, and isotopic data in conjunction with geological observations.

9. References

Abbassi, S., Edwards, D.S., George, S.C., Volk, H., Mahlstedt, N., di Primo, R., and Horsfield, B., 2016. Petroleum potential and kinetic models for hydrocarbon generation from the Upper Cretaceous to Paleogene Latrobe Group coals and shales in the Gippsland Basin, Australia. Org. Geochem., 91, 54-67.

Abbassi, S., George, S.C., Edwards, D.S., di Primo, R., Horsfield, B., and Volk, H., 2016. Generation characteristics of Mesozoic syn- and post-rift source rocks, Bonaparte Basin, Australia: New insights from compositional kinetic modelling. Marine and Petroleum Geology, 50, 148-165.

Abay, T.B., Karlsen, D.A., Pedersen, J.H., Olaussen, S., and Backer-Owe, K., 2017. Thermal maturity, hydrocarbon potential and kerogen type of some Triassic-Lower Cretaceous sediments from the SW Barents Sea and Svalbard. Petroleum Geosciences, 24, 349–373.

Andrusevich, V.E., Engel, M.H., Zumberge, J.E., and Brothers, L.A. 1998. Secular, episodic changes in stable carbon isotope composition of crude oils. Chemical Geology, 152, 59–72.

Aquino Neto, F. R., Restle, A., Connan J., Albrecht P., and Ourisson, G., 1982. Novel tricyclic terpanes (C19, C20) in sediments and petroleums. Tetrahedron Lett. 23, 2027-2030.

Aquino Neto, F. R., Trendel J. M., Restle, A., Connan J., and Albrecht, P., 1983. Occurrence and formation of tricyclic and tetracyclic terpanes in sediments and petroleum. In Bjoröy, M. , eds., Advances in Organic Geochemistry 1981, 659-667. Wiley, Chichester.

Badley, M., Price, J., Dahl, C.R., and Agdestein, T., 1988. The structural evolution of the northern Viking Graben and its bearing upon extensional modes of basin formation. Journal of the Geological Society, 145, 455-472.

Barker, L. H., and Poole, E. G.,1981. Geology and mineral resource assessment of the Island of Barbados: The Government of Barbados, Bridgetown, 109 p.

Behar, F and Vandenbroucke M., 1987. Chemical modeling of kerogen. Organic Geochemestry, 11, 15-24.

Berglund, L., Augustson, J., Færseth, R., Gjelberg, J., and Ramberg-Moe, H., 1986. The evolution of the Hammerfest Basin. Habitat of hydrocarbons on the Norwegian continental shelf. Norsk Petroleumsforening, 319–338.

Berner, R.A., 1984. Sedimentary pyrite formation: an update. Geochem. Cosmochim. Acta 48, 605–615.

Bihariesingh, V., 2014. Is the cretaceous an effective petroleum system offshore Suriname? (abs.): GTW Deep Horizon and Deep Water Frontier Exploration in Latin American and the Caribbean, Port of Spain, Trinidad, March 9–11, 2014.

Bissada, K.K, Elrod L.W., Robison C.R., Darnell L.M., Szymczyk H.M., and Trostle J.L. 1993. Geochemical inversion - A modem approach to inferring source-rock identity from characteristics of accumulated oil and gas. Energy Exploration & Exploitation 11, 3/4, Special Issue: Hydrocarbon Exploration (1993), 295-328.

Brown, K., and Westbrook, G., 1987. The tectonic fabric of the Barbados Ridge accretionary complex. Marine and Petroleum Geology, 4, 71–81.

Braun, R.L., Burnham, A.K., Reynolds, J.G., and Clarkson, J.E., 1991. Pyrolysis kinetics for lacustrine and marine source rocks by programmed micropyrolysis. Energy Fuel., 5, 192–204.

Bugge, T., Mangerud, G., Elvebakk , G., Mørk , A., Nilsson, I., Fanavoll, Stein, and Vigran, J.O., 1995. The Upper Paleozoic succession on the Finnmark Platform, Barents Sea. Norwegian Journal of Geology, 75, 3–30.

Calvert, S.E., and Fontugne, M.R., 1987. Stable carbon isotopic evidence for the marine origin of the organic matter in the Holocene Black Sea sapropel. Isot. Geosci. 66, 315–322.

Campbell, A., 2005. Shelf-geometry response to changes in relative sea level on a mixed carbonate-siliciclastic shelf in the Guyana Basin. Sedimentary Geology, 175, 259 - 275.

Cavanagh, A.J., di Primio, R., Scheck-Wenderoth, M., and Horsfield, B., 2006. Severity and timing of cenozoic exhumation in the southwestern Barents Sea. Journal of the Geological Society, 163, 761–774.

Cedeño, A., Ahmed, M., Escalona, A., and Abrahamson, P., 2021a. Tectono-stratigraphic evolution of the western Barbados Accretionary Prism and the eastern Tobago Basin: Implications for petroleum systems. In C. Bartolini, (Eds.), South America–Caribbean–Central Atlantic plate boundary: tectonic evolution, basin architecture, and petroleum Systems. American Association of Petroleum Geologists Memoir 123, 649–676.

Cedeño, A., Pepper, A., Ohm, S., Escalona, A., Narain E., and Roller, L., 2021b. Source Rocks in The Guyana Basin: An Organic Geochemistry Study on and Offshore Suriname. IMAGE SEG-AAPG, September 26th-October 1st, Denver-Colorado & Online.

Cedeño, A., Pepper, A., Ohm, S., Escalona, A., Narain E., and Roller, L., 2021c. Oil and Source Rock Geochemistry of The Guyana Basin. 3rd HGS/EAGE Conference on Latin America, November 8th-10th November, Houston, Texas & Online.

Chaderton, N., 2005. Evolution of the Tobago Forearc Basin: Implications for sedimentation and hydrocarbon prospectivity, M.S. thesis, The University of Texas at Austin, Austin, Texas, 99 p.

Chaderton, N., 2009. Sedimentation within the Tobago Forearc Basin with implications for the evolutionary history of the Southern Barbados

Accretionary Margin, Ph.D. thesis, The University of Texas at Austin, Austin, Texas, 203 p.

Chung, H.M., and Sackett, W.M., 1979. Use of carbon isotope composition of pyrolytically derived methane as maturity indices for carbonaceous materials. Geochimica et Cosmochimica Acta 43, 1979–1988.

Chung, H.M., Rooney, M.A., Toon, M.B., and Claypool, G.E., 1992. Carbon isotope composition of marine crude oils. American Association of Petroleum Geology Bulletin, 76, 1000–1007.

Craig, H., 1953. The geochemistry of the stable carbon isotopes. Geochimica et Cosmochimica Acta 3, 53–92.

Crawford, F. D., Szelewski, C. E., and Alvey, G. D., 1985. Geology and exploration in the Takutu graben of Guyana and Brazil: Journal of Petroleum Geology, 8, 5–36.

De Grande, S.M.B., Aquino Neto, F.R., and Mello, M.R., 1993. Extended tricyclic terpanes in sediments and petroleums. Org Geochem., 20, 7, 1039-1047.

Demaison, G.J., Moore, G.T., 1980. Anoxic environments and oil source bed genesis. American Association of Petroleum Geologists Bulletin, 64, 1179–1209.

Deville, E., and Mascle, A., 2012. The Barbados ridge: A mature accretionary wedge in front of the Lesser Antilles active margin. In D. G. Bally and A. W. Roberts, (Eds.), Regional geology and tectonics: Principles of geologic analysis: Amsterdam. Elsevier, 580–607.

di Primio, R., and Horsfield, B., 1996. Predicting the generation of heavy oils in carbonate/evaporitic environments using pyrolysis methods. Org. Geochem., 24, 10/11, 999-1016.

di Primio, R., Horsfield, B., and Guzman-Vega, M.A., 2000. Determining the temperature of petroleum formation from the kinetic properties of petroleum asphaltenes. Nature, 406, 173-176.

di Primio, R., and Horsfield, B., 2006. From petroleum-type organofacies to hydrocarbon phase prediction. American Association of Petroleum Geologists Bulletin, 90, 1031–1058.

Dutta, S., Greenwood, P.F., Brocke, R., Schaefer, R.G., and Mann, U., 2006. New insights into the relationship between Tasmanites and tricyclic terpenoids. Org. Geochem., 37, 1, 17–34.

Eglinton, T.I., Sinninghe Damst´e, J.S., Kohnen, M.E.L., de Leeuw, J.W., Larter, S.R., and Patience, R.L., 1990. Analysis of maturity-related changes in the organic sulfur composition of kerogens by flash pyrolysis–gas chromatography. In: Geochemistry of Sulfur in Fossil Fuels. American Chemical Society, 529–565.

Ehrenberg, S. N., Nielsen, E. B., Svånå, T. A., and Stemmerik, L. 1998. Depositional evolution of the Finnmark carbonate platform, Barents Sea: results from wells 7128/6-1 and 7128/4-1. Norwegian Journal of Geology, 78, 185–224.

Erlich, R. N., and Barrett, S. F., 1994. Petroleum geology of the eastern Venezuela foreland basin. In R. W. McQueen and D. Leckie, (Eds.), Foreland basins and fold belts. American Association of Petroleum Geologists Memoir 55, 341–362.

Erlich, R. N., Villamil, T., and Keens-Dumas, J., 2003. Controls on the deposition of Upper Cretaceous organic carbon - rich rocks from Costa Rica to Suriname. In C. Bartolini, R. T. Buffler, and J. Blickwede, eds., The Circum-Gulf of Mexico and the Caribbean: Hydrocarbon habitats, basin formation, and plate tectonics. American Association of Petroleum Geologists Memoir 79, p. 1–45.

Escalona, A., and Mann, P., 2011. Tectonics, basin subsidence mechanisms, and paleogeography of the Caribbean-South American plate boundary zone. Marine and Petroleum Geology, 28, 8–39.

Escalona, A., Norton, I. O., Lawver, L. A. , and Gahagan, L., 2021a. Quantitative plate tectonic reconstructions of the Caribbean region, from

Jurassic to present. In C. Bartolini, (Eds.), South America–Caribbean–Central Atlantic plate boundary: Tectonic evolution, basin architecture, and petroleum systems. American Association of Petroleum Geologists Memoir 123, 239–264.

Escalona, A., Ahmad, S. S., and Watson, L., 2021b. Late Cretaceous–Pliocene paleogeography of the circum-Caribbean region based on quantitative plate reconstruction and georeferenced databases. In C. Bartolini, (Eds.), South America–Caribbean–Central Atlantic plate boundary: Tectonic evolution, basin architecture, and petroleum systems. American Association of Petroleum Geologists, 513–538.

Faleide, J.I., Vågnes, E., and Gudlaugsson, S.T., 1993. Late Mesozoic-Cenozoic evolution of the southwestern Barents Sea in a regional rift-shear tectonic setting. Marine and Petroleum Geology, 10, 186–214.

Freeman, R.H., Wakeham, S.G., Hayes, J.M., 1994. Predictive isotopic biogeochemistry: hydrocarbon from anoxic marine basins. Org. Geochem. 21, 629– 644.

Freudenthal, T., Thomas Wagner, T., Wenzhöfer, F., Zabel, M., Wefer, G., 2002. Early diagenesis of organic matter from sediments of the eastern subtropical Atlantic: evidence from stable nitrogen and carbon isotopes. Geochimica et Cosmochimica Acta, 65, 11, 1975-1808.

Færseth, R., 1996. Interaction of Permo-Triassic and Jurassic extensional fault-blocks during the development of the northern North Sea. Journal of the Geological Society, 153, 931-944.

Galimov, E.M., 1980. C^{13}/C^{12} in Kerogen. In: Durand, B., (Eds.), Kerogen: insoluble organic matters from sedimentary rocks. Editions Technip, 27, Paris, pp. 271-299.

Galimov, E.M., and Simoneit, B.R.T., 1982. Geochemistry of interstitial gases in sedimentary deposits of the Gulf of California. In: Curray, J.R., Moore, D.G., et al. (Eds.), Initial Reports of Deep Sea Drilling Project, 64. US Government Printing Office, Washington, pp. 781–788.

Galimov, E.M., 1995. Fractionation of carbon isotopes on the way from living to fossil organic matter. In: Wada, E. et al. (Eds.), Stable Isotopes in the Biosphere. Kyoto University Press, Kyoto, 133–170.

Galimov, E.M., Kodina, L.A., Zhiltzova, L.I., Tokarev, V.G., Vlasova, L.N., Bogacheva, M.P., Korobeinik, G.S., and Vaisman, T.I., 1998. Organic carbon geochemistry in the N–W Black Sea– Danube River system. In: Martin, J.M. (Ed.), Report of the International Project EROS-21. JRS, Ispra, It, 18–28.

Galimov, E.M., 2004. The pattern of δ 13Corg versus HI/OI relation in recent sediments as an indicator of geochemical regime in marine basins: comparison of the Black Sea, Kara Sea, and Cariaco Trench. Chemical Geology, 287-301.

Galimov, E.M., 2006. Isotope organic geochemistry. Organic Geochemistry, 37, 1200-1262.

Gautier, D.L., 2005. Kimmeridgian shales total petroleum system of the North Sea graben province. USGS Bulletin, 1–24.

Gernigon, L., Brönner, M., Roberts, D., Olesen, O., Nasuti, A., and Yamasaki, T., 2014. Crustal and basin evolution of the southwestern Barents Sea: from Caledonian orogeny to continental breakup. Tectonics, 33, 347–373.

Goevert, D., and Conrad, R., 2008. Carbon Isotope Fractionation by Sulfate-Reducing Bacteria Using Different Pathways for the Oxidation of Acetate. Environ. Sci. Technol, 42, 21 7813-7817.

Gouyet, S., Unternehr, P., and Mascle, A., 1994. The French Guyana margin and the Demerara Plateau: Geological history and petroleum plays. In A. Mascle, (Eds.), Hydrocarbon and petroleum geology of France. European Association of Petroleum Geoscientists Special Publication, 4, 411–422.

Goff, J.C., 1983. Hydrocarbon generation and migration from Jurassic source rocks in the E Shetland Basin and Viking Graben of the northern North Sea.

Grizzle, P.L., Coleman, H.J., Sweeney, R.E., and Kaplan, I.R., 1979. Correlation of crude oil source with nitrogen, sulfur, and carbon stable isotope ratio. Am. Chem. Soc. Meeting, April 1979, 39–51.

Gudlaugsson, S. T., Faleide, J. I., Johansen, S. E., and Breivik, A. J., 1998. Late Paleozoic structural development of the South-western Barents Sea. Marine and Petroleum Geology, 15, 73–102.

Habicht, K.S., and Canfield, D.E., 2001. Isotope fractionation by sulfate-reducing natural populations and the isotopic composition of sulfide in marine sediments. Geology, 29, 555–558.

Hartwig, A., di Primio, R., Anka, Z., Horsfield, B., 2012. Source rock characteristics and compositional kinetic models of Cretaceous organic rich black shales offshore southwestern Africa. Org. Geochem. 51, 17–34.

Harvey, H. R., Tuttle, J. H., and Belll, J. T., 1995. Kinetics of phytoplankton decay during simulated sedimentation: Changes in biochemical composition and microbial activity under oxic and anoxic conditions. Geochim. Cosmochim. Acta 59, 16, 3367–3377.

Henriksen, E., Bjørnseth, H.M., Hals, T.K., Heide, T., Kiryukhina, T., Kløvjan, O.S., and Larssen, G.B., 2011b. Uplift and erosion of the greater Barents Sea: impact on prospectivity and petroleum systems. In: Spencer, A.M., Embry, A.F., Gautier, D.L., Stoupakova, A.V., Sørensen, K. (Eds.), Arctic Petroleum Geology. Geological Society, 35, 271–281.

Henriksen, E., Ryseth, A., Larssen, G., Heide, T., Rønning, K., Sollid, K., and Stoupakova, A., 2011a. Tectonostratigraphy of the greater Barents Sea: implications for petroleum systems. In: Spencer, A.M., Embry, A.F., Gautier, D.L., Stoupakova, A.V., Sørensen, K. (Eds.), Arctic Petroleum Geology. Geological Society, 35, 163–195.

Hermeston, and L. Ledvéniová, (Eds.), Transform margins: Development, controls and petroleum systems. Geological Society (London) Special Publication 431, 199–917.

Hill, R. J., and Schenk, C. J., 2005. Petroleum geochemistry of oil and gas from Barbados: Implications for distribution of Cretaceous source rocks and regional petroleum prospectivity. Marine and Petroleum Geology, 22, 917–943.

Holba, A. G., Ellis, L., Dzou, I. L., Hallam, A. , Masterson, W. D. , Francu, J., and Fincannon, A. L., 2001. Extended tricyclic terpanes as age discriminators between Triassic, Early Jurassic, and Middle–Late Jurassic oils. (abs.): 20th International Meeting on Organic Geochemistry, September 10–14, 2001, Nancy, France, v. 1, p. 464.

Holba, A. G., Zumberge, J. E., Huizinga, B. J., Rosenstein, H., and Dzou, L. I., 2003. Extended tricyclic terpanes as indicators of marine upwelling. (abs.): 21st International Meeting on Organic Geochemistry, Krakow, Book of Abstracts, p. 131.

Hunt, J.M., Philp, R.P. and Kvenvolden, K.A., 2002. Early developments in petroleum geochemistry. Organic Geochemistry, 33, 1025–1052.

Hunt, J. M., 1970. The significance of carbon isotope variations in marine sediments, in G. D. Hobson and G. C. Speers, eds., Advances in organic geochemistry, 1966: New York, Pergamon Press, 27-35.

Kairanov, B., Escalona, A., Norton, I., and Abrahamsson, P., 2021. Early cretaceous evolution of the Tromsø Basin, SW Barents Sea. Marine and Petroleum Geology, 123.

Karlsen, D. A., Nyland, B., Flood, B., Ohm, S.E., Brekke, T., Olsen, S., and Backer-Owe, K., 1995. Petroleum geochemistry of the Haltenbanken, Norwegian continental shelf. In J. M. Cubitt and W. A. England, eds., The geochemistry of reservoirs. Geological Society Special Publication 86, 203 - 256.

Karlsen, D. A., and Skeie, J.E., 2006. Petroleum migration, faults and overpressure: 1. Calibrating basin modeling using petroleum in traps - A review. Journal of Petroleum Geology, 29, 3, 227–256.

Kean, A., Brisson, I., Preston, C., Colmenares, J., Connolly, D., Sikora, P., Legarretti, L., 2007. Reducing geologic risk in frontier deep water exploration of the Paleogene, Suriname, South America. In L. Kennan, J. Pindell and N. C. Rosen, (Eds.), The paleogene of the Gulf of Mexico and Caribbean basins, processes, events, and petroleum systems. SEPM Society for Sedimentary Geology, 27, 586–617.

Kodina, L.A., Lyutsarev, S.V., Bogacheva, M.P., and Galimov, E.M., 1994. On the role of particulates in vertical transport of material to the bottom as deducted from the carbon isotope composition of particles and bottom sediments exemplified by the study of the brine-bearing deep hole Bannok (Mediterranean). Geokhimiya 2, 174–180.

Kodina, L.A., Bogacheva, M.P., and Lyutsarev, S.V., 1996. Particulate organic carbon in the Black Sea: isotopic composition and origin. Geokhimiya 9, 884–890.

Lehmann, M.F., Bernasconi, S.M., Barbieri, A., Judith A McKenzie, J.A., 2002. Preservation of organic matter and alteration of its carbon and nitrogen isotope composition during simulated and in situ early sedimentary diagenesis. Geochimica et Cosmochimica Acta, 66, 20, 3573-3584.

Lewan, M.D., 1983. Effects of thermal maturation on stable organic carbon isotopes as determined by hydrous pyrolysis of Woodford Shales. Geochimica Cosmochimica Acta, 47, 1471–1479.

Lindseth, R. O., and Beraldo, V. L. A., 1985. Late Cretaceous submarine canyon in Brazil, in A. J. Tankard, R. Suarex Soruco, and H. J. Welsink, (Eds.), Petroleum basins of South America. American Association of Petroleum Geologists Bulletin Memoir 62, 168–181.

Liyanage, T.M., van Maldegem, L. M., Boreham, C., Hope, J. M., and Brocks, J.J., 2019. The occurrence of extended tricyclic terpanes in the Proterozoic and Paleozoic. (abs.): 29th International Meeting on Organic Geochemistry, September 1 - 6, 2019, Gothenburg, Sweden.

Londry, K.L., and Des Marais, D.J., 2003. Stable Carbon Isotope Fractionation by Sulfate-Reducing Bacteria. Applied and Environmental Microbiology, 69, 5, 2942-2949.

Mannie, A.S., Jackson, C.A.-L., and Hampson, G.J., 2014. Structural controls on the stratigraphic architecture of net-transgressive shallow-marine strata in a salt-influenced rift basin: Middle-to-Upper Jurassic Egersund Basin, Norwegian North Sea. Basin Research, 26, 675-700.

Malfait, B. T., and Dinkelman, M. G., 1972. Circum-Caribbean tectonic and igneous activity and the evolution of the Caribbean plate. Geological Society of America Bulletin, 83, 2, 251–272.

Mann, P., Taylor, F. W. , Lawrence, R., and Ku, T., 1995. Actively evolving microplate formation by oblique collision and sideways motion along strike-slip faults: an example from the northeastern Caribbean plate margin. Tectonophysics, 246, 1–69.

Mann, P., 1999. Caribbean sedimentary basins: Classification and tectonic setting from Jurassic to present. In P. Mann, (Eds.), Caribbean basins: Elsevier Sedimentary Basins of the World, 4, 3–31.

Matapour, Z., and Karlsen, D.A., 2017. Ages of Norwegian oils and bitumen based on age-specific biomarkers. Petroleum Geoscience, 24, 1, 92 - 101.

Marín, D., Helleren, S., Escalona, A., Olaussen, S., Cedeño, A., Nøhr-Hansen, H., Ohm, S., 2020. The Middle Jurassic to lowermost Cretaceous in the SW Barents Sea: interplay between tectonics, coarse-grained sediment supply and organic matter preservation. Basin Res.

McKirdy, D. M., Aldridge, A. K., and Ypma, P. J. M., 1983. A geochemical comparison of some crude oils from Pre-Ordovician carbonate rocks. In: Advances in Organic Geochemistry 1981 (M. Bjorøy, C. Albrecht, C. Cornford, et al., eds.), John Wiley & Sons, New York, 99–107.

Mello, M. R., Telnaes, N., Gaglianone, P. C., et al. (1988) Organic geochemical characterization of depositional paleoenvironments in Brazilian marginal basins. Org. Geochem., 13, 31–46.

Meyers, A. P., Stefano, B. M., and Astrid, F., 2006. Origins and accumulation of organic matter in expanded Albian to Santonian black shale sequences on the Deremara Rise, South American margin. Org. Geochem, 37, 1816–1830.

Moldowan, J. M., Seifert, W. K., and Gallegos, E.J., 1983. Identification of an extended series of tricyclic terpanes in petroleum. Geochim. Cosmochim. Acta, 47, 153l-1534.

Nemcŏk, M., Rybár, S., Ekkertová, O., Kotulová, J., Hermeston, S. A., and Jones, D., 2015. Transform-margin model of hydrocarbon migration: The Guyana–Suriname case study. In M. Nemcŏk, S. Rybar, S. T. Sinha, S. A.

Nøttvedt, A., Gabrielsen, R., and Steel, R., 1995. Tectonostratigraphy and sedimentary architecture of rift basins, with reference to the northern North Sea. Marine and Petroleum Geology, 12, 881-901.

Ohm, S.E., Karlsen, D.A., Austin, T., 2008. Geochemically driven exploration models in uplifted areas: Examples from the Norwegian Barents Sea. America Association of Petroleum Geologists Bulletin, 92, 1191-1223.

Odden, W., Bart, T., Talbot, M.R., 2002. Compound-specific carbon isotope analysis of natural and artificially generated hydrocarbons in source rocks and petroleum fluids from offshore Mid-Norway. Organic Geochemistry, 33, 1, 47-65.

Orr, W.L.,-1986. Kerogen/asphaltene/sulfur relationships in sulfur-rich Monterrey oils. Org. Geochem., 10, 499-516.

Pepper, A.S., and Corvi, P.J., 1995. Simple kinetic models of petroleum formation. Part I: oil and gas generation from kerogen. Marine and Petroleum Geology, 12, 291–319.

Pepper, A., Ahmad, N., and Doebbert, A., 2017. Upper Paleocene–Lower Eocene 'Wilcox'-Sourced Petroleum Systems of the Gulf of Mexico Basin: A Re-Evaluation and Comparison with the Coeval Patala Formation Sourced Petroleum System in the Upper Indus Basin, Pakistan. Abs. Gulf Coast

Association of Geological Societies. San Antonio, Texas, November 3rd, 2017.

Peters, K.E., Rohrback, B.G., and Kaplan, I.R., 1981. Carbon and hydrogen stable isotope variations in kerogen during laboratory simulated thermal maturation. American Association of Petroleum Geologists Bulletin, 65, 501–508.

Peters, K. E., Walters, C. C., and Moldowan, J. M., 2005. The Biomarker Guide, Volume 2: Biomarkers and Isotopes in the Petroleum Exploration and Earth History, vol. 2. New York: Cambridge University Press.

Petersen, H.I., Bojesen-Koefoed, J.A., and Mathiesen, A., 2010. Variations in composition, petroleum potential and kinetics of Ordovician – Miocene type I and type I-II source rocks (oil shales): implications for hydrocarbon generation characteristics. Journal of Petroleum Geology, 33, 1, 19-42.

Petersen, H., Holme, A., Andersen, C., Whitaker, M., Nytoft, H., and Thomsen, E., 2013. The source rock potential of the Upper Jurassic–lowermost Cretaceous in the Danish and southern Norwegian sectors of the Central Graben, North Sea. First Break 31.

Pindell, J., 1991. Geologic rationale for hydrocarbon exploration in the Caribbean and adjacent regions. Journal of Petroleum Geology, 14, 237–257.

Rau, G.H., Takahashi, T., and Des Marais, D.J., 1989. Latitudinal variations in plankton δ13C: implications for CO2 and productivity in past oceans. Nature 341, 516–518.

Riis, F., 1996. Quantification of Cenozoic vertical movements of Scandinavia by correlation of morphological surfaces with offshore data. Global Planet. Change, 331–357.

Ritter, U., Leith, T.L., Griffiths, C.M., and Schou, L., 1987. Hydrocarbon generation and thermal evolution in parts of the Egersund Basin, Northern North Sea. In: Beaumont, C., Tankard, A.J. (Eds.), Sedimentary Basins and

Basin Forming Mechanism. Canadian Society of Petroleum Geology Calgary, 75-85.

Rogers, M. A., 1980. Application of organic facies concepts to hydrocarbon source rock evaluation, in Proceedings of the 10th World Petroleum Congress 1979, 2: London, Heyden and Son Ltd., 22-30.

Rojo, L.A., Cardozo, N., Escalona, A., Koyi, H., 2019. Structural style and evolution of the Nordkapp Basin, Norwegian Barents Sea. American Association of Petroleum Geologists Bulletin, 103, 9, 2177–2217.

Ruby, E.G., Jannasch, H.W., and Denser, W.G., 1987. Fractionation of stable isotopes during chemoautotrophic growth of sulfuroxidizing bacteria. Applied and Environmental Microbiology, 53, 1940–1943.

Schwarzer, D., and Krabbe, H., 2009. Source rock geochemistry and petroleum system modeling in the Guyana basin, offshore Suriname (abs.). American Association of Petroleum Geologists Search and Discovery Article #90091.

Seifert, W. K., and Moldowan, J. M., 1978. Applications of steranes, terpanes and monoaromatics to the maturation, migration and source of crude oils. Geochimica et Cosmochimica Acta, 42, 77–95.

Serck, C.S., Faleide, J.I., Braathen, A., Kjølhamar, B., Escalona, A., 2017. Jurassic to early cretaceous basin configuration(s) in the Fingerdjupet subbasin, SW Barents Sea. Marine and Petroleum Geology, 86, 874–891.

Silverman, S.R., and Epstein, S., 1958. Carbon isotopic compositions of petroleum and other sedimentary organic materials. AAPG Bulletin, 42, 998-1012.

Silverman, S.R., 1964. Investigations of petroleum origin and evolution mechanisms by carbon isotope studies. In: Craid, H., Miller, S.L., Wesserburg, G.J. (Eds.), Isotopic and Cosmic Chemistry. North-Holland, Amsterdam, 92–102.

Speed, R., Torrini, R., and Smith, P.L., 1989. Tectonic evolution of the Tobago Trough forearc basin. Journal of Geophysical Research: Solid Earth, 94, 2913–2936.

Stahl, W. J., 1977. Carbon and nitrogen isotopes in hydrocarbon research and exploration. Chemistry, 20, 121-149.

Steel, R. J., and Worsley, D., 1984. Svalbard's post-Caledonian strata – an atlas of sedimentational patterns and palaeogeographic evolution. In: Spencer, A. M. (Eds.), Petroleum Geology of the North European Margin. Graham and Trotman, London, 109–135.

Stemmerik, L., and Worsley, D., 2005. 30 years on – Arctic Upper Paleozoic stratigraphy, depositional evolution and hydrocarbon prospectivity. Norwegian Journal of Geology, 85, 151–168.

Stemmerik, L., Elvebakk, G., and Worsley, D. 1999. Upper Paleozoic carbonate reservoirs on the Norwegian Arctic Shelf: delineation of reservoir models with application to the Loppa high. Petroleum Geoscience, 5, 173–187.

Sofer, Z., 1984. Stable Carbon Isotope Compositions of Crude Oils: Application to Source Depositional Environments and Petroleum Alteration. AAPG Bulletin, 68, 1, 31- 49.

Skopintsev, B. A., 1981. Decomposition of organic matter of plankton, humification and hydrolysis. In: E. K. Duursma and R. Dawson (Eds.), Marine organic chemistry: evolution, composition, interactions and chemistry of organic matter in seawater, Elsevier, 31, 125–177.

Sund, T., Skarpnes, O., Jensen, L.N., and Larsen, R.M., 1986. Tectonic development and hydrocarbon potential offshore Troms, northern Norway. In: Halbouty, T.H. (Eds.), Future Petroleum Provinces of the World, 40. American Association of Petroleum Geologists Special Volumes.

Tao, S., Wang, C., Du, J., Liu, L., and Z. Chen, Z., 2015. Geochemical application of tricyclic and tetracyclic terpanes biomarkers in crude oils of NW China. Marine and Petroleum Geology, 67, 460-467.

Tegelaar, E. W., and Noble, R. A., 1994. Kinetics of hydrocarbon generation as a function of the molecular structure of kerogen as revealed by pyrolysis-gas chromatography. Organic Geochemistry, 22, 543-574.

Thomas, B., Møller-Pedersen, P., Whitaker, M., and Shaw, N., 1985. Organic facies and hydrocarbon distributions in the Norwegian North Sea. In Thomas, B.M., Dore, A.G., Eggen, S.S., Home, P.C., Larsen, R.M. (Eds.), Petroleum geochemistry in exploration of the Norwegian Shelf. Graham & Trotman London.

Tissot, B. P., and Welte, D. H., 1978. Petroleum formation and occurrence: A new approach to oil and gas exploration, Berlin, Heidelberg, Springer.

Tocque, E., Behar, F., Budzinski, H., Lorant, F., 2005. Carbon isotopic balance of kerogen pyrolysis effluents in a closed system. Organic Geochemistry, 36, 893–905.

Urey, H.C., Lowenstam, H.A., Epstein, S., and McKinney, R., 1951. Measurement of paleotemperatures and temperatures of the Upper Cretaceous of England, Denmark, and the southeastern United States. Bulletin of the Geological Society of America. 62, 399 -416.

Weber, J., Dixon, T., C. DeMets, C., Ambeh, W., Jansma, P., Mattioli, G., Saleh, J., Sella, G., Bilham, R., and Perez, O., 2001. GPS estimate of relative motion between the Caribbean and South American plates, and geologic implications for Trinidad and Venezuela. Geology, 29, 75–78.

Weiss, H.M., Wilhelms, A., Mills, N., Scotchmer, J., Hall, P.B., Lind, K., Brekke, T., 2000. NIGOGA-The Norwegian Industry Guide to Organic Geochemical Analyses (online). Edition 4.0, published by Norsk Hydro, Statoil, Geolab Nor, SINTEF Petroleum Research and the Norwegian Petroleum Directorate, 102 pp.

Yang, W., and Escalona, A., 2011a. Basin modelling and source rock evaluation in the Guyana Basin: First Break, 29, 10, 59–69.

Yang, W., and Escalona, A., 2011b. Tectonostratigraphic evolution of the Guyana Basin. American Association of Petroleum Geologists Bulletin, 5, 8, 1339–1368.

Yeh, H. W, and Epstein S., 1981. Hydrogen and carbon isotopes of petroleum and related organic matter: Geochimica et Cosmochimica Acta 45, 753-762.

Ziegler, P., 1992. North Sea rift system. Tectonophysics, 208, 55-75.

Ziegs, V., 2013. Development of a compositional kinetic model for primary and secondary petroleum generation from Lower Cretaceous Wealden Shales, Lower Saxony Basin, Northern Germany. Master thesis, Freiberg University of Mining and Technology, Freiberg, p. 82.

Zumberge, J.E., 1987. Terpenoid biomarker distributions in low maturity crude oils. Org. Geochem., 11, 6, 479–496.

Zumberge, J., Lillich H., and Scotese C., 2007. Biomarkers from marine crude oils reflect modeled climatic/oceanographic conditions for the Late Cretaceous. 23rd International Meeting on Organic Chemistry, Abstract of Reports, 23, 555.

Zumberge, J., Harold, I., and Lowell, W., 2016. Petroleum geochemistry of the Cenomanian–Turonian Eagle Ford oils of south Texas. In: Breyer, J.A. (Eds.), The Eagle Ford Shale: A Renaissance in U.S. Oil Production. American Association of Petroleum Geologists Memoir 110, pp. 135–165.

Intentionally left blank

Chapter 2

Paper I

Upper Jurassic to Lower Cretaceous source rocks in the Norwegian Barents Sea, part I: Organic geochemical, petrographic, and paleogeographic investigations

Andrés Cedeño [a], Sverre Ohm [a], Alejandro Escalona [a], Dora Marín [a], Snorre Olaussen [b], Thomas Demchuk [c]

[a] University of Stavanger, Norway

[b] The University Centre in Svalbard, Norway

[c] Louisiana State University, USA

Marine and Petroleum Geology 134 (2021) 105342
https://doi.org/10.1016/j.marpetgeo.2021.105342

Paper I

Marine and Petroleum Geology 134 (2021) 105342

Contents lists available at ScienceDirect

Marine and Petroleum Geology

journal homepage: www.elsevier.com/locate/marpetgeo

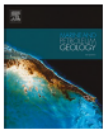

Upper Jurassic to Lower Cretaceous source rocks in the Norwegian Barents Sea, part I: Organic geochemical, petrographic, and paleogeographic investigations

Andrés Cedeño [a,*], Sverre Ohm [a], Alejandro Escalona [a], Dora Marín [a], Snorre Olaussen [b], Thomas Demchuk [c]

[a] University of Stavanger, Norway
[b] The University Centre in Svalbard, Norway
[c] Louisiana State University, USA

ARTICLE INFO

Keywords:
Source rock
Organofacies variations
Barents Sea
Macerals
Carbon isotopes
Generation potential

ABSTRACT

This study provides a subregional to regional characterization of organofacies changes within the two members of the Upper Jurassic to Lower Cretaceous Hekkingen Formation (i.e. Alge and Krill) by integrating geochemical and petrographic analysis with paleogeographic models.

The gross kerogen composition of the Hekkingen Formation is dominated by terrestrial macerals. This preponderance of land-derived particles is more pronounced in the Krill Member than in the underlying Alge Member. There is a greater proportion of marine macerals within distal areas of the Hammerfest Basin and well 7218/1-5 in the southern Bjørnøyrenna Fault Complex. This shift in the relative proportion of marine and terrestrial macerals is ascribed to changes in the location of the depositional sites with respect to the sources of the terrestrial materials.

The Alge Member features the highest levels of total organic carbon (TOC ≥7 wt %), but the more discrete and organically poorer beds of the Krill Member still remain sufficiently rich to be considered petroleum source rocks (TOC ≥2 wt %). Hydrogen indices (HI) between 50 and 400 mg HC/g TOC recorded throughout the entire formation indicate that the kerogen within both members has similar oil and gas generation capabilities. These low to moderate HI values are indicative of immature Type III to II-III kerogens and are generally consistent with the high proportions of terrestrial macerals. Prior to thermal maturation, marine type II kerogens (i.e. ≤ 400 mgHC/gTOC) probably existed in the marine liptinite-rich rocks in the distal Hammerfest Basin and Bjørnøyrenna Fault Complex. At least three factors controlled the detected variability in geochemical parameters: dilution rates of organic matter, varying inputs of terrestrial versus marine organic matter, and the degree of preservation. The documented variability in organic-rich facies assists in reducing source rock risk in the study area, but also helps explorationists understand source rock distribution across other shelfal areas.

1. Introduction

During the Late Jurassic, high rates of organic carbon burial and petroleum source rock formation were globally widespread (Leith et al., 1993; Klemme, 1994; Weissert and Mohr, 1996; Berner and Kothavala, 2001). Upper Jurassic deposits of the Hanifa-Arab Formation in the Arabian-Iranian Basin, the Bazhenov Formation in West Siberia, the Smackover and Tuaman formations in the Gulf of Mexico, and the Kimmeridgian Shale in the Northwestern European Shelf are prime archives of increased accumulation of organic carbon leading to prolific source rocks (Klemme, 1994). Most of these shale and carbonate units are characterized by the occurrence of type II organic matter (Klemme, 1994) resulting from a significant rise in global eustatic sea level and widespread establishment of epicontinental seas in coexistence with the advent of skeletonized planktonic organisms (Klemme, 1994).

The Hekkingen Formation, stratigraphically equivalent to the Kimmeridgian Shale, records intensified carbon productivity and sedimentation within a Late Jurassic epeiric sea in the Norwegian Barents Sea

* Corresponding author.
E-mail address: andres.f.cedenomotta@uis.com (A. Cedeño).

https://doi.org/10.1016/j.marpetgeo.2021.105342
Received 9 April 2021; Received in revised form 31 August 2021; Accepted 22 September 2021
Available online 29 September 2021

(Worsley, 2008; Henriksen et al., 2011a; Marin et al., 2020) (Fig. 1A). As a unit, it extends from the Tromsø Basin northwards into the Bjarmeland Platform (Fig. 1B) and the Svalbard Archipelago, where it is named the Agardhfjellet Formation. The Hekkingen Formation consists of a lower succession (i.e. Alge Member) of black shales featuring the highest total organic carbon (TOC) values, and an upper succession (i.e. Krill Member) of siltstones featuring lower TOC values (Dalland et al., 1988; Mørk et al., 1999; Henriksen et al., 2011a; Georgiev et al., 2017). Rock-Eval hydrogen indices (HI) in both members are seen to be highly variable at the same maturity level (i.e. same Tmax in Fig. 2). The documented variability in organic matter quantity and quality suggests that the Hekkingen Formation is not a homogenous entity and contains varying proportions of marine and terrestrial kerogens. This condition implies paleogeographic and palaeoceanographic controls on deposition of the sedimentary organic matter. As with this study, previous geochemical work, using analogous analytical data has also documented source rock variability within this formation (Bjorøy et al., 1983; Smelror et al., 2001; Ohm et al., 2008; Henriksen et al., 2011a; Abay et al., 2017; Helleren et al., 2020).

Rock-Eval and TOC analysis constitute the conventional approach to assessing the total generative potential of petroleum source rocks and predicting the nature of their kerogen. Importantly, this chemical approach lacks the qualitative information of the organic precursors (i.e. macerals or organic matter type) provided by maceral microscopic analysis and disregards the inorganic aspects of the sediment matrix. The purpose of this paper is to characterize subregional to regional organofacies variations within the Hekkingen Formation in relationship to paleoenvironmental and paleogeographic conditions by integrating geochemical and petrographic analyses with paleogeographic models. Through implementing this integrated approach, this study augments the earlier geochemical work that recognized variations in organofacies within the Hekkingen Formation and provides the basis for assessing changes in the petroleum generative potential (see Cedeño et al., 2021). The latter has direct implications for prospectivity studies of the southwestern Barents Sea.

2. Structural and stratigraphic framework

Multiple studies have recognized the Middle Jurassic to Early Cretaceous as a period of renewed tectonic activity in the southwestern Barents Sea characterized by extensional and strike slip faulting, halokinesis, and uplift of local highs (Sund et al., 1986; Berglund et al., 1986; Faleide et al., 1993; Gernigon et al., 2014; Serck et al., 2017; Rojo et al., 2019; Kairanov et al., 2021). Tectonic activity concentrated mostly along local to semi-regional fault complexes such as Troms-Finnmark, Ringvassøy-Loppa, Bjørnøyrenna, Nysleppen, and Hoop (Fig. 1B). These diachronous fault systems controlled subsidence of the basins (i.e. Hammerfest, Tromsø, Bjørnøya, Nordkapp, and Fingerdjupet) and uplift of the structural highs (Clark et al., 2014; Blaich et al., 2017; Indrevær et al., 2017; Mulrooney et al., 2017; Serck et al., 2017; Kairanov et al., 2019; Faleide et al., 2019; Tsikalas et al., 2021). From the Cretaceous to the Holocene, the greater Barents Sea region underwent different magnitudes of uplift and erosion (Riis, 1996; Doré et al., 2000; Cavanagh et al., 2006; Henriksen et al., 2011b). The combined effects of the opening of the Atlantic and Artic oceans and the Pliocene-Pleistocene glacial-interglacial cycles have resulted in net

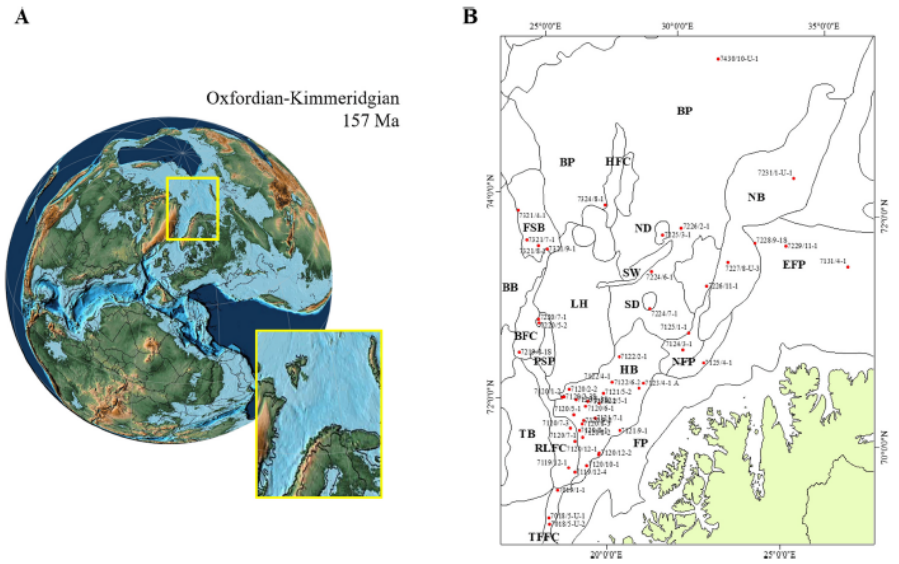

Fig. 1. **A.** Paleogeographic location of the Barents Sea within the northwestern European Shelf at the Oxfordian-Kimmeridgian boundary (Paleomap Project; Scotese, 2016). **B.** Map of the southwestern Barents Sea displaying the main structural elements and wells used in this study. BP= Bjarmeland Platform, HFC= Hoop Fault Complex. MB = Maud Basin, MH = Mercurius High, NB= Nordkapp Basin, EFP = eastern Finnmark Platform, ND= Norvarg Dome, SG= Swaen Graben, SD= Samson Dome, FSB= Fingerdjupet Sub-basin, BB= Bjørnøya Basin, BFC= Bjørnøya Fault Complex, PSP= Polhem Sub-platform, LH = Loppa High, NFC= Nysleppen Fault Complex, HB= Hammerfest Basin, CH= Central High, RLFC = Ringvassøy-Loppa Fault Complex, TB = Tromsø Basin, FP= Finnmark Platform, TFFC = Troms–Finnmark Fault Complex.

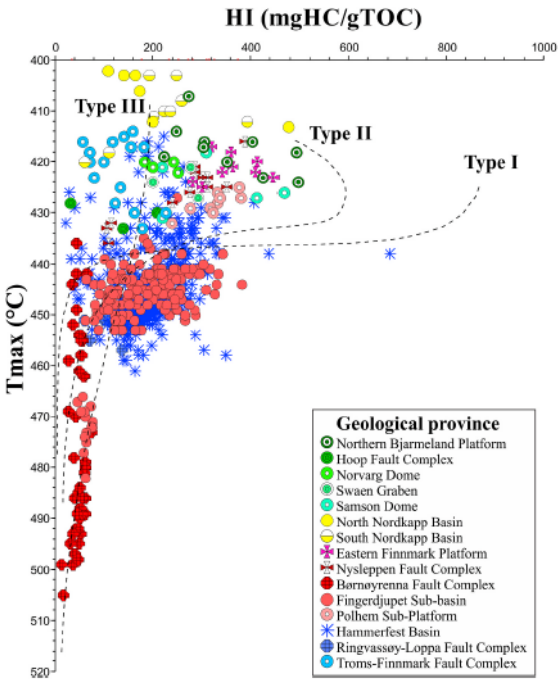

Fig. 2. Hydrogen index (HI) versus Tmax Rock-Eval (Tmax) plot of samples from the Hekkingen Formation. Samples from this study and from the IGI (Integrated Geochemical Interpretations) database are plotted. Maturation pathways for the three main kerogen types are shown after Cornford (1988). Samples are color-coded based on geological provinces. (For interpretation of the references to color in this figure legend, the reader is referred to the Web version of this article.)

erosion values varying from 0 to more than 3000 m (Faleide et al., 1984; Riis and Fjeldskaar, 1992; Johansen et al., 1992; Knies et al., 2009; Henriksen et al., 2011b).

During the Late Jurassic, most of the Barents Sea shelf was flooded, and deposition was controlled by regional transgression and gradual landwards migration of the shorelines (Henriksen et al., 2011a; Marín et al., 2020). The Late Jurassic is known to be a period of global eustatic sea level rise and high burial rates of organic carbon in the oceans (Schlanger and Jenkyns, 1976; Weissert et al., 1979; Leith et al., 1993; Klemme, 1994; Weissert and Mohr, 1996; Georgiev et al., 2017).

Several aspects of Late Jurassic geological and oceanographic conditions are manifest in the sedimentary record of the Barents Sea. The Oxfordian marks a clear lithological shift from the silty-mudstones and marls of the Fuglen Formation to the organic-rich shales of the Hekkingen Formation (Dalland et al., 1988; Mørk et al., 1999; Smelror et al., 2001; Henriksen et al., 2011a). A widespread middle Oxfordian hiatus is known to record this mineralogical shift (Bugge et al., 2002; Smelror et al., 2001; Wierzbowski and Smelror, 2020). Contiguous units on the Russian shelf include the Bazhenov Formation in the South Barents Sea, Timan Pechora, and West Siberian basins (Grace and Hart, 1986; Gavshin and Zakharov, 1996; Henriksen et al., 2011a).

The Hekkingen Formation consists of two members according to the TOC content and well log character: the Alge Member and the overlying Krill Member (Fig. 3). Biostratigraphically controlled age dates indicate a Late Oxfordian? To late Kimmeridgian age for the Alge Member and a Kimmeridgian to Ryazanian age for the Krill Member (Dalland et al., 1988; Georgiev et al., 2017; Mørk et al., 1999; Smelror et al., 2001). Costa and Davey (1992) and Smelror and Below (1993) argued that the Alge rocks in the Polhem Sub-platform are slightly older, spanning from Callovian to early Kimmeridgian. The boundary between these two units is interpreted as diachronous (Leith et al., 1993; Marín et al., 2020), i.e. its age and stratigraphic position may vary across the different structural provinces. The top of the Hekkingen Formation is informally known as the Base Cretaceous Unconformity, a hiatus ranging in age from Kimmeridgian to early Barremian (Århus, 1991; Bugge et al., 2002; Marín et al., 2018; Wierzbowski and Smelror, 2020).

The Alge Member is composed of black shale and typically displays high gamma ray (GR) values (Fig. 3). Geochemical and elemental analysis show that this member contains the highest levels of TOC (Ohm et al., 2008; Henriksen et al., 2011a; Abay et al., 2017). The Alge Member varies in thickness from 185 m (well 7129/8-1-s) in the Bjørnøyrenna Fault Complex to around 35 m in the Hammerfest Basin (Mørk et al., 1999; Marín et al., 2020). Localized sand injectites and thin turbiditic sandstone have been described along the boundary between the Hammerfest Basin and the Bjørnøyrenna Fault Complex and in the Bjørnøya Basin (Dalland et al., 1988; Mørk et al., 1999; Smelror et al., 2001; Bugge et al., 2002; Henriksen et al., 2011a; Helleren et al., 2020). Mørk et al., (1999) interpret the Alge Member to have been laid down

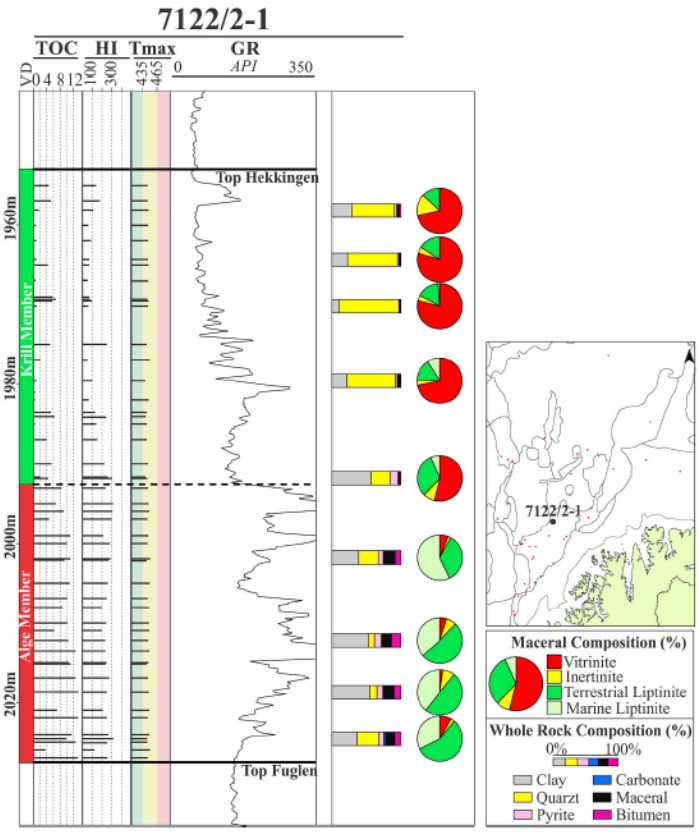

Fig. 3. Typical gamma ray (GR) log of the Hekkingen Formation at well 7122/2-1 displaying source rock analytical data (i.e. TOC, Tmax, HI). Mineral and maceral compositions of studied samples at different depths are also shown.

within a shelf environment with anoxic bottom water conditions. Helleren et al., (2020) recognize short phases of more oxygenated bottom water during deposition of this member.

The Krill Member consists of silt, silty shales, and very fine sand. Total organic carbon values within this member are diminished relative to the underlying Alge Member (Mørk et al., 1999; Ohm et al., 2008; Henriksen et al., 2011a; Abay et al., 2017). The thickness of the Krill Member varies considerably across the Barents Sea, from more than 600 m within the Bjørnøyrenna Fault Complex to virtually absent in some wells of the Hammerfest Basin (Marín et al., 2020). Deposition of this unit is interpreted to have occurred in a wide range of water depth conditions ranging from shallow shelf to possibly deep marine systems (Mørk et al., 1999; Marín et al., 2020). Variations in paleobathymetric conditions and thickness of the Krill Member were controlled by widespread tectonic activity (Marín et al., 2020). Around the buried Mjølnir crater, the Upper Volgian-Ryazanian Ragnarok Formation and the Sindre Bed consist of breccias, pebbles, sand, and mud ejected by the Mjørnir impact (Gudlaugsson, 1993; Tsikalas et al., 1999; Dypvik et al., 2004).

3. Materials and methods

3.1. Thickness maps

The thickness map for each of the members was built using publicly available well log data retrieved from the Diskos data base (NPD, 2021). To calculate sedimentary rates, a one-dimensional decompaction process was carried out using the Sclater-Christie equation $\phi(z) = \phi_0 e^{-cz}$, where $\phi(z)$ is the porosity at any depth, ϕ_0 is the depositional porosity of a lithology, c is the porosity depth coefficient (km^{-1}), and z is depth (m). ϕ_0 values were adopted from the North Sea study by Sclater and Christie (1980). The shale-rich sediments of the Alge Member were assigned a $\phi_0 = 0.63$, whereas a lower value of 0.56 (an average between sand $\phi_0 = 0.49$ and shale $\phi_0 = 0.63$) was assigned to the siltier sediments of the

Krill Member. The compaction curves employed to back-calculate initial thicknesses are considered to be an exponential relationship as defined by Sclater and Christie (1980). All present-day depths were corrected to account for the Late Cretaceous-Holocene erosion using the regional map of net erosion by Henriksen et al. (2011b).

3.2. Sample material

The rock material used in this research includes a total of 320 conventional core and drilling cutting samples from 35 oil and stratigraphic (i.e. IKU Stratigraphic Drilling Projects) wells located across the southwestern Barents Sea (Fig. 1; Table 1). Sample material was collected from the Norwegian Petroleum Directorate (NPD) and the SINTEF well repositories in Stavanger and Trondheim, Norway, respectively. The sampled intervals were selected based on the stratigraphic boundaries of the Hekkingen Formation as defined by the NPD and preexisting geochemical studies from well completion reports. Sample selection was designed to ensure regular sampling intervals and prioritize core material over cuttings.

3.3. Chemical analyses

All samples described in section 3.2. were divided into subsets; one sample subset for organic geochemical studies (i.e. TOC, Rock-Eval, and isotope analysis) and the other sample subset for microscopy (i.e. organic and inorganic components). For geochemical analysis, all samples were mechanically ground to powder. A split of the powdered sample was treated with hydrochloric acid to remove carbonate minerals and combusted in a LECO SC-632 oven. The amount of carbon in the sample was measured as carbon dioxide by an IR-detector. A second split of the powdered sample was pyrolyzed using a Rock-Eval 6 instrument, allowing direct measurement of free hydrocarbons (S_1), remaining hydrocarbon generative potential (S_2), carbon dioxide (CO_2) content produced during thermal cracking (S_3), and temperature of S_2 maxima (T_{max}). The pyrolysis programme started at 300 °C (held for 3 min) and increased to 650 °C (held for 0 min) at 25 °C/min.

The remaining portion of selected powdered samples was used for measuring the carbon isotopic composition ($\delta^{13}C$) of the saturate, aromatic, and asphaltene (i.e. SARA) fractions. Isolation of the extractable organic matter (EOM) was performed using a Soxtec Tecator instrument. Thimbles were pre-extracted in dichloromethane with 7 % (vol/vol) methanol, 10 min boiling and 20 min rinsing. The sample was weighed accurately in the pre-extracted thimbles and boiled for 1 h and rinsed for 2 h in approximately 80 cc of dichloromethane with 7 % (vol/vol) methanol. Copper blades activated in concentrated hydrochloric acid were added to the extraction cups to cause free sulfur to react with the copper.

For deasphaltening, extracts were evaporated almost to dryness before a small amount of dichloromethane (3 times the amount of EOM) was added. Pentane was added in excess (40 times the volume of EOM and dichloromethane) and the solution was stored for at least 12 h in a dark place before the solution was filtered or centrifuged and the weight of the asphaltenes measured. The deasphaltened samples were then loaded into an automatic sampler and placed in a combustion reactor (Thermo Fisher Scientific Elemental Analyzer) held at 1020 °C. The produced water was trapped on Magnesium Perchlorate. CO_2 was separated by column and flashed into Delta V Plus Isotope Ratio Mass Spectrometer (IRMS, Thermo Fisher Scientific) via Conflo IV.

3.4. Petrographic analyses

The sample subset for microscopy was crushed and sieved through a 16-mesh sieve, and then embedded in thermoplastic epoxy in 2.54 cm molds. The pellets were ground and polished according to ASTM standards (ASTM, 2011). All samples were investigated under both white- and UV-light using a Zeiss Axio-Scope A1 at 500× (10× eyepiece, and 50× objective) in immersion oil. White- and UV-light was provided by an X-Cite 120 LED light source. Point-counts were conducted using a proprietary automated point-counter attached to the stage of the Zeiss Axio-Scope. As macerals and minerals were identified under the cross-hairs in the field of view, data were captured using proprietary software: once the petrographer made a count, the computer and motorized stage would then automatically move step-wise to a new, random field of view. Three-hundred counts of macerals and minerals were made for each sample. If there was insufficient organic matter after the 300 counts, counting was continued until 100 total counts of organic matter were collected. The resolution of the microscope is 1 μm (≥1 μm).

4. Results

4.1. Thickness map and whole rock constituents

4.1.1. The Alge member

The thickness map of the Alge Member shows that sediments accumulated preferentially within downthrown blocks of the Bjørnøyrenna Fault Complex (Fig. 4A). Decompaction estimations for the 185 m shale-rich succession in well 7219/8-1 S yield an initial thicknesses of roughly 430 m, which equates to sedimentation rates of approximately 86 m per million years (m/Ma). An average decompacted thicknesses of 55 m is estimated for most of the Hammerfest Basin, whereas a slightly higher average thickness of 60 m is calculated for the southern portion of the Bjarmeland Platform, the Nordkapp Basin, and the eastern Finnmark Platform. These figures imply sedimentary rates of roughly 11 and 12 m/Ma, respectively.

The average whole rock composition (i.e. per well) of the Alge Member consists of, in descending order, clay, sand, organic particles (i.e. macerals and solid bitumen), pyrite, and carbonate grains (Table 1). The clay content varies between 31 % and 64 % and the quartz content between 9 and 50 %. The relative abundance of sand increases in the eastern margin of the Hammerfest Basin, the Nysleppen Fault Complex, the eastern Finnmark Platform, and around the Norvarg Dome (Fig. 4A). The total content of macerals ranges between 6 and 18 %, while the content of solid bitumen ranges from 5 to 26 % (Table 1). The average pyrite content, in the form of framboids, typically accounts for less than 10 %, but occasionally reach up to 18 % in individual samples.

4.1.2. The Krill Member

The thickness map of the Krill Member (Fig. 4B) reveals that the fault-controlled depocenter in the southern end of the Bjørnøyrenna Fault Complex continued to be active during the sedimentation of the Krill Member. A present-day thickness of up to 680 m in well 7219/8-1 S translates into roughly 1300 m of decompacted sediments, indicating sedimentation rates of up to 130 m/My. Another major north-east-south-west oriented depocenter, presently containing up to 310 m of sediments, developed along the Troms-Finnmark Fault Complex and extended over the southern half of the Hammerfest Basin. Decompaction of this succession yields an initial thickness of 540 m, implying a sedimentary rate of 54 m/My. The remaining western and northern areas of the Hammerfest Basin show a present-day average thickness of 40 m, which equates to a decompacted thicknesses of nearly 70 m and to a sedimentary rate of 7 m/My. Across the southern Bjarmeland Platform, the Krill Member exhibits an average thickness of about 35 m. This suggests that initial accumulation of over 55 m of clastic detritus occurred at a rate of around 6 m/My.

Sedimentary rates presented in the ongoing study are only approximate partly because of poor age control and partly because some of the wells used in this study were drilled in or around structural highs, where sedimentary units are thinner or eroded, or both. The Krill Member, for example, is known to have been partly eroded, at least locally, by the regionally-extended Base Cretaceous Unconformity. Either scenario could be advocated to explain the absence of the Krill Member in the Nordkapp Basin and the adjacent eastern Finnmark Platform.

Table 1
Well identification, whole rock constituents, maceral composition, and bulk source rock geochemical data (i.e. total organic carbon = TOC; hydrogen index = HI; Tmax Rock Eval = Tmax) of the studied wells discriminated by member. Composition and source rock data represent average values calculated for each well. Maceral compositions are shown in normalised percentage. NP= Hekkingen member is not present. Refer to Fig. 1 for abbreviations of geological provinces.

Well name	Geo. province	Alge member										
		Whole rock constituents						Normalised maceral composition %				TOC/Rock-Eval
		% Clay	% Quartz	% Pyrite	% Carbonates	% Macerals	% Bitumen	Marine Lip	Terres Lip	Inertinite	Vitrinite	TOC (wt %)
7018/5-U-1	TFPC	60	9	12	1	8	9	11	11	11	68	7
7018/5-U-2	TFPC	51	10	3	3	7	26	11	32	23	35	12
7019/1-1	RLPC	43	29	10	0	13	5	45	13	16	26	9
7119/12-1	RLPC	46	25	12	1	9	8	30	18	19	33	9
7120/1-2	HB	41	20	12	0	16	10	25	60	4	7	9
7120/10-1	HB	60	14	8	2	8	7	5	23	14	58	9
7120/12-1	HB	35	26	10	4	11	14	19	45	6	30	10
7120/2-2	HB	54	18	8	0	7	14	42	21	17	20	11
7120/2-3 S	HB	37	16	17	1	18	11	41	43	7	9	11
7120/6-3 S	HB	NP	NP	NP	NP	NP	NP	NP	NP	NP	NP	NP
7120/8-3	HB	54	11	11	0	10	14	35	15	19	31	12
7120/9-2	HB	31	30	11	0	13	14	62	9	9	20	10
7121/4-2	HB	35	14	16	3	13	20	69	7	7	16	10
7121/9-1	HB	40	32	9	1	12	7	25	34	10	32	9
7122/2-1	HB	46	20	8	1	15	11	41	48	5	5	11
7122/4-1	HB	44	12	12	3	10	18	45	9	21	25	10
7122/6-2	HB	50	12	9	1	10	19	11	37	21	31	12
7123/4-1 A	HB	41	36	1	0	11	11	31	35	12	24	11
7124/3-1	NPC	22	48	8	0	8	14	36	24	8	31	7
7125/1-1	NPC	14	7	2	8	26	0	32	25	16	26	13
7131/4-1	RPC	28	50	6	0	7	10	4	44	26	26	9
7219/8-1 S	BPC	42	20	7	2	11	17	53	13	20	14	7
7220/5-2	PGP	44	41	5	0	5	4	25	34	10	30	4
7224/6-1	ND	64	15	6	0	6	10	6	33	17	44	11
7224/7-1	SM	NP	NP	NP	NP	NP	NP	NP	NP	NP	NP	NP
7225/3-1	ND	40	38	7	0	6	9	7	13	20	61	9
7226/2-1	SG	48	31	2	0	7	12	10	35	31	24	8
7227/8-U-3	NB	52	12	7	1	8	20	27	43	14	17	12
7229/11-1	EFP	48	23	7	1	7	15	6	42	16	35	11
7231/1-U-1	NB	48	22	4	1	7	18	14	47	20	19	11
7321/7-1	FGB	45	26	7	1	5	17	5	4	23	67	9
7321/8-1	FGB	NP	NP	NP	NP	NP	NP	NP	NP	NP	NP	NP
7321/9-1	FGB	NP	NP	NP	NP	NP	NP	NP	NP	NP	NP	NP
7324/8-1	MH	NP	NP	NP	NP	NP	NP	NP	NP	NP	NP	NP
7430/10-U-1	BP	47	18	4	1	14	16	21	42	12	24	13

Compositionally, clay is the dominant constituent of the Krill Member in most of the Hammerfest Basin and the Ringvassøy-Loppa and Troms-Finnmark fault complexes with volume percentages of around 40 % or higher (Table 1; Fig. 4B). This clay-dominated composition contrasts with the significantly higher quartz content in the depocenter west of the Central High that reaches up to 89 %. In the most northernly parts of the Hammerfest Basin, the Fingerdjupet Sub-basin, and the Bjarmeland Platform, quartz is the predominant constituent. Similar proportions of clay and quartz particles occur in the Bjørnøyrenna Fault Complex. Total maceral content varies between 2 and 10 % whereas solid bitumen typically shows lower values than in the Alge Member, varying between 1 and 10 % (Table 1). Pyrite rarely constitutes 10 % of the whole rock.

4.2. Visual kerogen analysis

Under incident light microscopy, most of the organic materials (i.e. macerals + solid bitumen) in the studied samples appear to be recognizable as particles larger than the resolution of the microscope, i.e. ≥ 1 μm. This is substantiated by a correlation of the volume percentage of organics to the weight percentage of total organic carbon (TOC) in Fig. 5. As expected in the absence of large amounts of submicroscopic organic matter, the computed regression line for the dataset yields a roughly 2:1 relationship of the volume percentage of organics to the weight percentage of TOC (Scheidt and Littke, 1989).

The maceral analysis from kerogen microscopy indicates that both members contain significant proportions of terrestrial macerals, i.e. vitrinite and terrestrial-derived liptinites (Figs. 6 and 7; Table 1). Particles of vitrodetrinite and primary vitrinite constitute the bulk of the vitrinite group (Fig. 6A and B), but the relative abundance of the former is commonly triple that of the later. The terrestrial liptinite sub-group comprises mainly particles of sporinite, occasional cutinite, and rarely occurring resinite (Fig. 6G and H). Colonial alginite, also included in the terrestrial liptinite sub-group, corresponds to debris of lacustrine or shallow marine colonial algae of which *Botryococcus* is the most representative (Fig. 6E). The marine liptinite sub-group consists mainly of alginite particles (i.e. lamalginite, tasmanites, dinoflagellates; Fig. 6F); locally, fluorescing amorphinite occurs as the dominant marine maceral. Importantly, the composition of the various kerogen groups in samples of the Alge Member are overall similar to those in the Krill Member samples. This implies that sedimentary organic matter in the two members derived essentially from the same kinds of organisms, and that no significant or permanent changes occurred in the biota sourcing the organic matter during Alge and Krill times. The difference in the relative

Alge member		Krill member												
TOC/Rock-Eval		Whole rock constituents						Normalized maceral composition %				TOC/Rock-Eval		
HI (mgHC/gTOC)	Tmax (°C)	% Clay	% Quartz	% Pyrite	% Carbonates	% Macerals	% Bitumen	Marine Lip	Terres Lip	Inertinite	Vitrinite	TOC (wt %)	HI (mgHC/gTOC)	Tmax (°C)
117	416	54	28	5	1	7	5	12	28	7	53	3	128	426
181	417	54	21	8	2	5	10	7	24	8	61	5	127	419
122	449	43	41	5	0	8	3	34	15	11	40	4	139	450
113	452	56	26	9	0	4	4	19	12	16	52	3	172	448
203	432	5	89	4	0	2	0	6	11	3	80	1	111	438
184	418	42	32	9	1	10	6	12	30	9	49	5	200	422
266	423	41	34	12	1	7	6	9	52	16	22	6	321	428
175	448	59	16	8	0	9	8	24	42	14	21	4	199	448
260	434	NP	NP	NP	NP	NP	NP	NP	NP	NP	NP	NP	NP	NP
NP	NP	13	71	6	1	7	2	41	9	6	44	2	257	309
183	434	63	17	8	0	7	4	7	42	8	43	4	183	439
407	434	9	72	10	0	6	4	4	32	11	54	6	287	432
188	445	64	14	7	2	9	4	15	33	5	48	3	184	445
280	432	41	40	6	1	9	3	26	36	3	35	4	301	433
265	440	28	64	4	0	2	2	4	20	5	71	2	133	440
203	452	62	17	9	0	7	5	26	35	12	27	4	226	441
272	434	63	17	6	0	8	5	5	37	18	40	5	287	435
261	434	11	81	1	1	5	1	4	30	24	43	2	190	436
295	422	14	70	4	0	10	1	9	62	1	19	4	191	430
315	423	NP	NP	NP	NP	NP	NP	NP	NP	NP	NP	NP	NP	NP
361	322	NP	NP	NP	NP	NP	NP	NP	NP	NP	NP	NP	NP	NP
12	514	38	33	6	2	15	6	70	3	7	20	3	71	387
328	428	NP	NP	NP	NP	NP	NP	NP	NP	NP	NP	NP	NP	NP
238	423	43	49	3	0	4	1	0	17	36	47	4	293	427
NP	NP	39	29	9	2	12	9	28	45	9	18	3	290	424
250	421	NP	NP	NP	NP	NP	NP	NP	NP	NP	NP	NP	NP	NP
191	421	23	72	1	0	4	1	1	10	26	62	3	254	426
238	408	NP	NP	NP	NP	NP	NP	NP	NP	NP	NP	NP	NP	NP
373	422	NP	NP	NP	NP	NP	NP	NP	NP	NP	NP	NP	NP	NP
162	407	NP	NP	NP	NP	NP	NP	NP	NP	NP	NP	NP	NP	NP
61	477	NP	NP	NP	NP	NP	NP	NP	NP	NP	NP	NP	NP	NP
NP	NP	30	53	7	0	4	6	4	12	15	69	3	174	448
NP	NP	29	52	8	1	6	4	26	25	11	38	3	224	444
NP	NP	13	76	4	0	3	3	19	22	0	26	2	298	286
366	417	NP	NP	NP	NP	NP	NP	NP	NP	NP	NP	NP	NP	NP

abundance of macerals groups is ascribed instead to changes in the location of the depositional sites with respect to the sources of the terrestrial materials.

4.2.1. Northern areas: Bjarmeland and eastern Finnmark platforms and Nordkapp Basin

Fig. 7 shows the general distribution of the maceral groups across the study area. High concentrations of vitrinitic and terrestrial liptinitic macerals are characteristic of the Alge Member samples in the southern Bjarmeland and eastern Finnmark platforms (Figs. 7A and 8D). Inertinite is the next most abundant maceral and marine liptinitic particles are only of subordinate abundance (i.e. ≤10 %; Table 1). The overlying Krill Member is virtually depleted of marine debris with only localized occurrences in the Samson Dome and the area between the Maud Basin and the Hoop Fault Complex (Figs. 7B and 8D). The Alge Member in the eastern Finnmark Platform is, compared with the southern Bjarmeland, richer in terrestrial liptinites. The maceral composition of the Alge samples within the Nordkapp Basin is slightly enriched in marine liptinites relative to the surrounding platforms (Fig. 7A).

4.2.2. Central-southern areas: Hammerfest Basin, Ringvassøy-Loppa and Troms-Finnmark fault complexes

The Alge Member along the south-west-north-east boundary of the Finnmark Platform exhibits varying maceral assemblages overall dominated by land-derived particles (Fig. 7A; Table 1). The organic fraction in the southern portion of this boundary, i.e. Troms-Finnmark Fault Complex and the southern end of the Hammerfest Basin, consists mostly of vitrinites and terrestrial liptinites (Fig. 9A). The content of inertinites rarely exceeds 15 % and only trace amounts of marine liptinites occur. Stratigraphically equivalent sediments in the eastern Hammerfest Basin (Fig. 9B) and northwards in the Nysleppen Fault Complex show a higher content of liptinitic material (Fig. 7A). Nevertheless, the Alge Member in the Nysleppen Fault Complex is richer in marine liptinites than it is in the eastern and northeastern Hammerfest Basin. The amount of marine macerals increases considerably in the central and western areas of the Hammerfest Basin and moderately in the Ringvassøy-Loppa Fault Complex (Figs. 7A and 9C-D; Table 1). The average content (i.e. per well) of marine liptinites commonly exceeds 30 % and reaches distinctively high values of up to 65 % in the central parts of the Hammerfest Basin. Vitrinitic material constitutes the main terrestrial input and only rarely exceeds 25 %. Grains of finely disseminated alginite dominate the marine organic fraction. Only in the wells

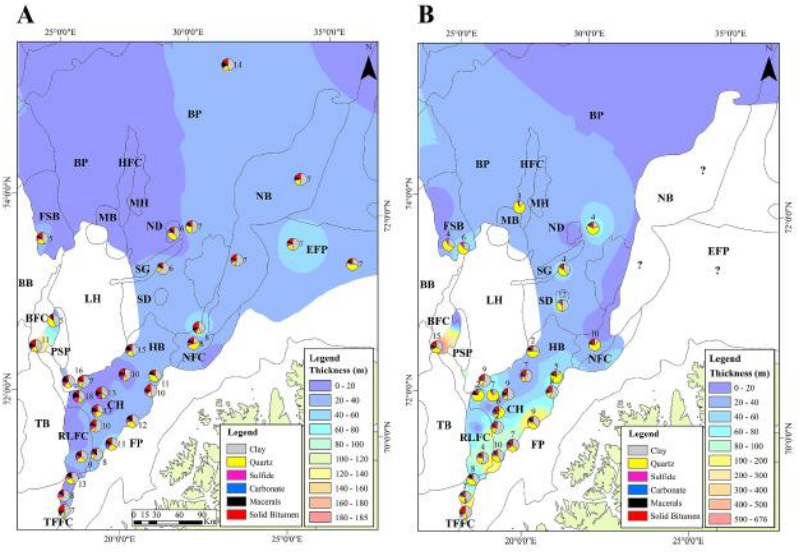

Fig. 4. Thickness maps of the Alge (**A**) and Krill (**B**) members. The pie diagrams represent the average (i.e. per well) whole rock compositions calculated from the microscopic analyses. Accompanying labels represent the average volume percentage of macerals in the whole rock. See Table 1 for the plotted values.

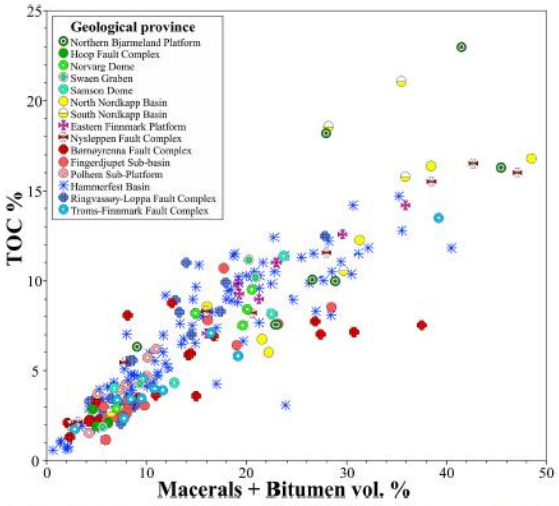

Fig. 5. Relationship between volume percentage of organic particles (i.e. macerals + bitumen) in whole rock versus total organic carbon (TOC) weight percent for each of the studied samples. Samples are color-coded based on geological provinces. (For interpretation of the references to color in this figure legend, the reader is referred to the Web version of this article.)

from the Ringvassøy-Loppa Fault Complex and the southernmost well in central Hammerfest does amorphinite predominates over alginite. Alge Member shales from areas of the Hammerfest Basin adjoining the Loppa High record an increased content of terrestrial liptinites (Figs. 3 and 7A). In this case, the land-derived liptinitic fraction has less sporinite and cutinite than in most other localities and consists predominantly of colonial alginite (Fig. 6E).

Rocks of the Krill Member in the Hammerfest Basin and the Ringvassøy-Loppa High and Nysleppen fault complexes record higher proportions of vitrinite and terrestrial liptinite relative to the underlying Alge Member (Figs. 7B and 9). This condition causes the westwards increase in marine particles observed in the Alge Member rocks of the Hammerfest Basin to be less pronounced and restricted to fewer central-western localities. Remarkably high vitrinite contents (i.e. ≥ 70 %) are also detected in some sites neighboring the Loppa High (Fig. 3).

4.2.3. Western areas: Bjørnøyrenna Fault Complex and Fingerdjupet Sub-basin

Marine-derived liptinites predominate over terrestrial macerals in the southern end of the Bjørnøyrenna Fault Complex, accounting for up to 70 % of the average maceral composition in the overlying Krill Member (Figs. 7 and 8A). The marine organic fraction is predominantly composed of granular and finely disseminated fluorescent amorphinite, opposite to the high alginite inputs detected in most of the Hammerfest Basin. Northwards, the overall character of the kerogen in the Alge Member changes substantially and terrestrial macerals make up to 70 % of the organic fraction in the boundary between the Bjørnøyrenna Fault Complex and the Polhem Sub-platform (Figs. 7A and 8B).

The composition of the organic matter within both members in the western sites of the Fingerdjupet Sub-basin is essentially the same (Fig. 7). Vitrinite predominates and makes up to 70 % of the organic matter fraction (Fig. 8C). The next most abundant maceral is inertinite. Only few terrestrial liptinites are found while marine liptinites are nearly absent. Liptinitic particles increase to nearly 50 % within the Krill Member in the eastern part of the sub-basin (Fig. 7B). Marine and terrestrial liptinites occur in approximately equal abundance.

4.3. Source rock generative potential

4.3.1. TOC and Rock-Eval pyrolysis

TOC data for the Hekkingen Formation shows values from 0.45 to 24 wt % (Fig. 5). The distribution of TOC in a 65 m Hekkingen core is displayed in Fig. 3 and demonstrates some of the stratigraphic attributes previously described. There is a sudden downwards increase in TOC to values ≥ 7 wt %, which is, in most cases, coincident with the top of the discussed GR deflection. TOC values between 8 and 12 wt % are predominant within the organically richer Alge Member. The fine-grained sediments in the Polhem Sub-platform (Fig. 8B) are an exception to this generalization because TOC contents are lower than 7 %, but biostratigraphically controlled ages confirm they were laid down during Alge times (i.e. Callovian to early Kimmeridgian; Costa and Davey, 1992; Smelror and Below, 1993).

Total organic carbon contents within the Krill Member are diminished relative to the underlying Alge Member but are still sufficiently high to be considered petroleum source rocks (i.e. ≥2 wt %; Zumberge et al., 2012, Figs. 7–10). Values between 2 and 5 wt % occur more often. Organic-rich intervals alternate with only modestly enriched intervals, revealing the oscillatory nature of organic carbon sedimentation within the Krill Member (Fig. 3). This attribute of the Krill Member reflects a more discrete distribution of the organic matter when compared to the more consistent distribution observed throughout the Alge Member. It is noteworthy to highlight that some wells, particularly in the southern areas of the Bjarmaland Platform (Fig. 1), were drilled in or adjacent to structural highs, some of which are known to have been topographically higher during sedimentation of the Hekkingen Formation. TOC and HI values recorded in these locations probably represent minimum values owning to a systematic decrease in organic matter sedimentation, poor preservation conditions, and selective preservation of hydrogen poor particles.

The generative potential of thermally immature samples (e.g. Tmax <435 °C) can be assessed based on the hydrogen index (HI). This parameter is the result of S2 divided by TOC (i.e. S2/TOC x 100). In Fig. 10, the majority of the HI values are in the range of 50 and 450 mgHC/gTOC, indicating that the kerogen within both members has comparable oil and gas generation capabilities.

4.3.2. Relationships between geochemical and petrographic data

Because of the high percentage of particles visible under the microscope (i.e. Fig. 5), the maceral composition is expected to be reflected by bulk geochemical parameters (i.e. TOC and HI). A diagram of HI as a function of the relative abundance of liptinites (marine + terrestrial) provides the basis for comparing geochemical and petrographic data. In Fig. 11, there seems to be an overall positive correlation between HI and increasing contents of liptinites. Alge Member samples from the eastern Finnmark Platform show higher HI values than other samples containing comparable amounts of liptinites (Fig. 11A). Accordingly, this area records some of the most oil prone source rocks (i.e. among immature samples) as defined by average HI values of 373 and 387 mg HC/g TOC (Fig. 7A), which are typically associated with Type II/III kerogens. Alge samples from the Polhem Sub-platform also display HI values that are slightly higher than other samples with compositionally similar kerogen assemblages. An average HI value of 328 mg HC/g TOC in well 7220/5-2 is indicative of type II-III kerogen in this area.

The highest average (i.e. per well) TOC levels, i.e. 13 %, are recorded for the Alge Member rocks at the boundary between the Bjarmeland Platform and the Nysleppen Fault Complex and in the Northern Bjarmeland Platform (Fig. 7; Table 1). Average HI values of 315 and 366 mg HC/g TOC were computed for these two areas, respectively, which suggests the presence of kerogen type II/III.

Some Alge samples in the Nordkapp Basin possess moderately high TOC levels paired with HI values that are lower than expected from the overall TOC-HI relationships in Fig. 10A. Such low HI values also seem to be inconsistent with the relatively high content of liptinites in these samples (Fig. 11A). This discrepancy can be interpreted as reflecting oxidation or bacterial reworking of the organic matter, or both, leading to the formation of hydrogen-lean type III kerogen, which are at best only gas-prone. Early generation is ruled out as a possible cause because of the low Tmax values of 410 °C measured in these samples (Table 1). The Alge and Krill members contain mostly a mixed type III/II kerogen (i.e. 200 to 300 mgHC/gTOC) across the southern Nordkapp Basin and the adjacent southern Bjarmeland Platform (i.e. Norvarg and Samson domes, Swaen Graben, Hoop Fault Complex). This only modest generative potential appears to be consistent with the predominance of terrestrial organic particles.

In the southern end of the Hammerfest Basin and in the adjacent Troms-Finnmark Fault Complex, both the Alge and Krill members have average HI values generally less than 200 mg HC/g TOC (Figs. 7 and 9A). This might have been anticipated because of the high concentrations of humic kerogen of a vitrinitic nature. Hydrogen-poor, type III kerogen also occurs within Krill Member sediments deposited in the northeastern corner of the Hammerfest Basin (i.e. average HI 190 mgHC/gTOC) and the neighboring Nysleppen Fault Complex (i.e. HI 191 mgHC/gTOC) (Fig. 7B). Along the eastern margin of the Hammerfest Basin, the Alge Member displays average TOC values ranging from 9 to 13 %; and the Krill Member shows lower average values ranging from 4 to 6 wt % (Fig. 7). The preferential accumulation of land-derived organic particles is reflected in only moderate HI values spanning from 260 to 280 mg HC/g TOC and from 287 to 321 mgHC/gTOC, respectively.

4.3.3. Estimations of initial generative potential in thermally mature areas

Hydrogen indices in the central and western areas of the Hammerfest

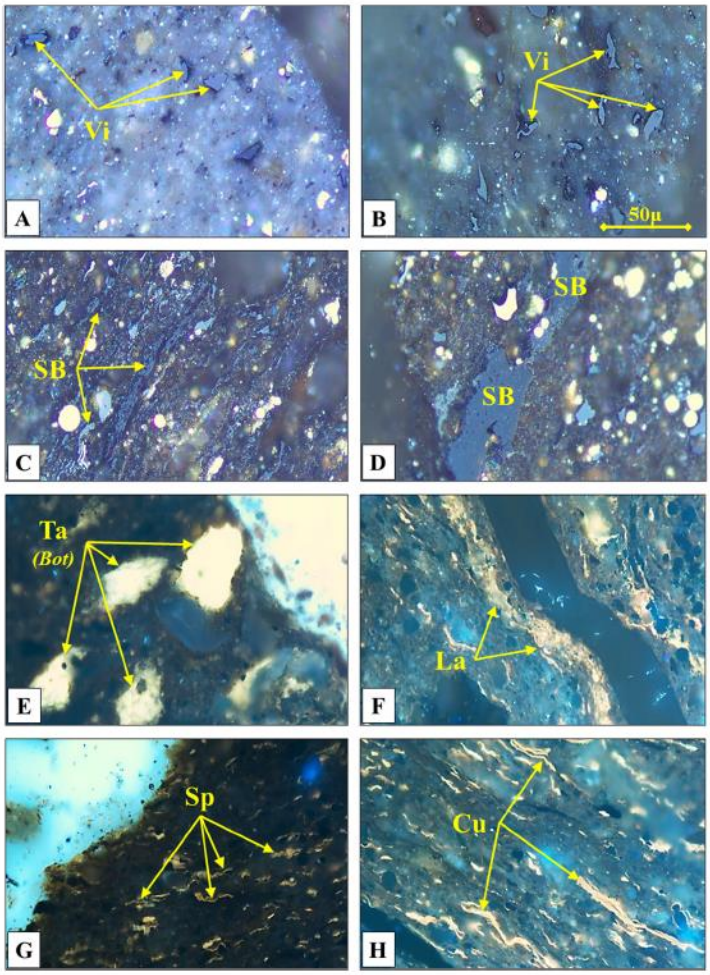

Fig. 6. Photomicrographs of representative maceral types in the dataset taken at 500X magnification. **A and B.** Photos in white-light of vitrinite maceral, and vitrodetrinite (Vi), within a mineral matrix mostly composed of quartz. Vitrodetrinite particles are those defined as being smaller than 10μ in size. Photo A: well 7120/1–2 at 1912m; Photo B: well 7119/12-1 at 2511 m. **C and D.** Photos in white-light of granular solid bitumen (SB) illustrating dark grey to light grey reflectance. Solid bitumen is differentiated from in-situ vitrinite by its granular appearance and generally lower reflectance (darker grey color). Photo C: well 7119/12-1 at 2595 m; Photo D. well 7120/2-2 at 2144 m. **E.** Photo in UV-light of telalginite maceral (Ta) in this instance Botryococcus-like colonial algae. Note the feathery edges of the colonial algae characteristic of this maceral. The bright yellow fluorescence indicates relatively low maturity. Well 7120/2-3 S at 2005.93 m. **F.** Photo in UV-light of lamalginite (La) illustrating the laminated nature of the fluorescing organic matter. Well 7120/2-3 S at 2005.93 m. **G:** Photo in UV-light of fluorescing sporinite (Sp). In these instances the fluorescing material is likely terrestrial pollen. Well 7120/2-3 S at 2005.93 m. **H.** Photo in UV-light of fluorescing material, most importantly cutinite (Cu) which are the fluorescing cuticles in terrestrial plant material. Note the abundant other fluorescing organic matter including sporinite (terrestrial pollen) and liptodetrinite (fluorescing organic matter smaller than 10μ in size). Well 7120/2-3 S at 2005.93 m. (For interpretation of the references to color in this figure legend, the reader is referred to the Web version of this article.)

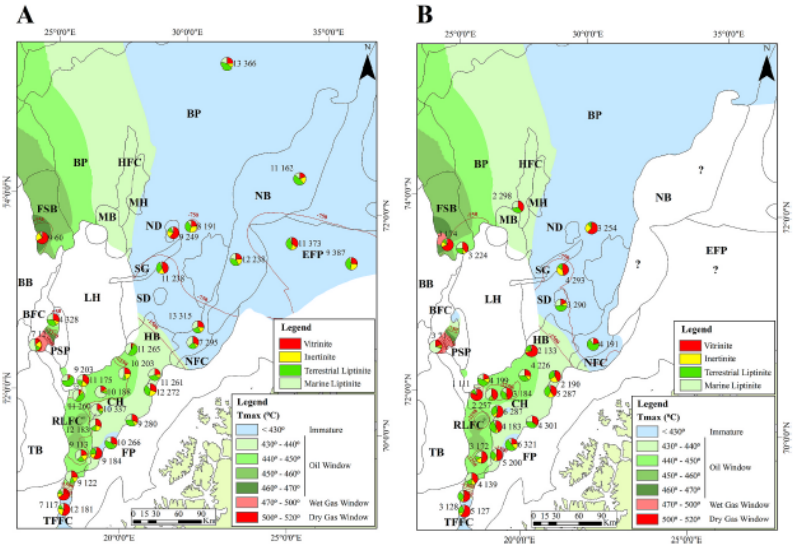

Fig. 7. Map of the southwestern Barents Sea illustrating the variability in maceral compositions within the Alge (**A**) and Krill (**B**) members. The pie diagrams represent the average (i.e. per well) maceral compositions calculated from the microscopic analysis. Accompanying labels represent the average (i.e. per well) total organic carbon (TOC) and hydrogen index (HI). A present-day maturity overlay of the Hekkingen Formation calculated from Tmax Rock-Eval data is also displayed. See Table 1 for plotted values. Refer to Fig. 1 for abbreviations of the different geological provinces.

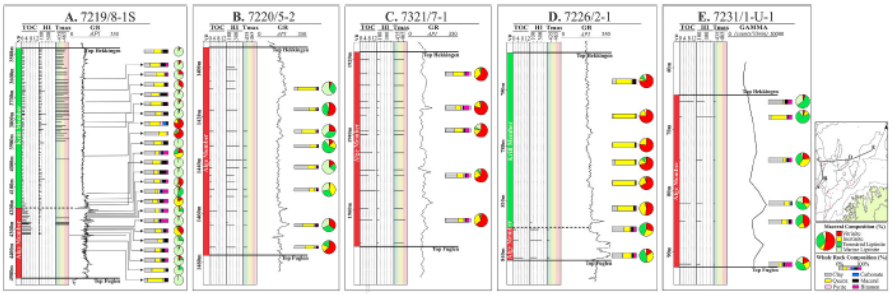

Fig. 8. Gamma ray (GR) logs, source rock geochemical data (i.e. TOC, HI, Tmax), and maceral and mineral composition of studied Hekkingen samples from different wells: **A.** 7219/8-1 S = Bjørnøyrenna Fault Complex; **B.** 7220/5-1 = Polhem Sub-platform; **C.** 7321/7-1 = Fingerdjupet Sub-basin; **D.** 7226/2-1 = Southern Bjarmeland Platform; **E.** 7231/1-U-1 = Nordkapp Basin. See inset map for well locations.

Basin, the Ringvassøy-Loppa and Bjørnøyrenna fault complexes, and the Fingerdjupet Sub-basin are diminished because of the marginal to mature nature of the Hekkingen Formation (Fig. 7). Thermal stress has probably led to different levels of hydrogen losses considering the thermal stability of the various maceral types. An average initial hydrogen richness (HIi) range is estimated by integrating observations from maceral composition and back-calculation. A HIi range is obtained empirically from comparing the HI of thermally mature samples with that of immature samples of similar maceral composition. A second range is calculated by translating the measured HI of mature samples along the maturation pathways on a Tmax versus HI cross-plot. Modestly elevated HIi values between 350 and 400 mg HC/g TOC are tentatively estimated for the marine liptinite rich kerogens within the Alge Member shales in the central Hammerfest Basin (i.e. Figs. 7 and 9C). Maceral assemblages made up of roughly equal proportions of marine and terrigenous liptinites in the Alge Member shales neighboring the Loppa High (i.e. Fig. 3) are assigned HIi values between 280 and 330 mgHC/gTOC. Lower HIi values between 250 and 300 mg HC/g TOC are

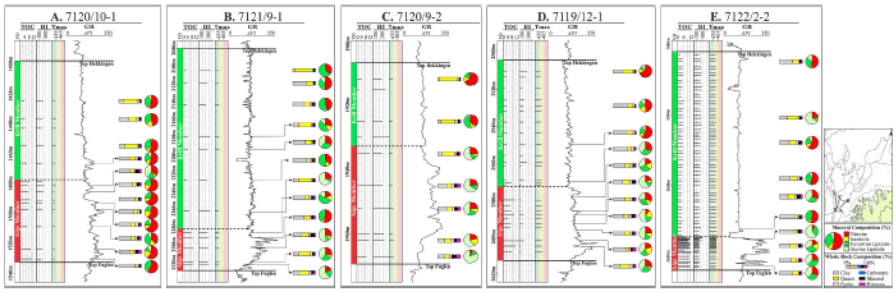

Fig. 9. Gamma ray (GR) logs, source rock geochemical data (i.e. TOC, HI, Tmax), and maceral and mineral composition of studied Hekkingen samples from different wells: A. 7120/10-1 = Southern Hammerfest Basin; B. 7121/9-1 = Eastern Hammerfest Basin. C. 7120/9-2 = Central Hammerfest Basin; D. 7119/12-1 = Ringvassøy-Loppa Fault Complex; E. 7122/2-2 = Western Hammerfest Basin. See inset map for well locations.

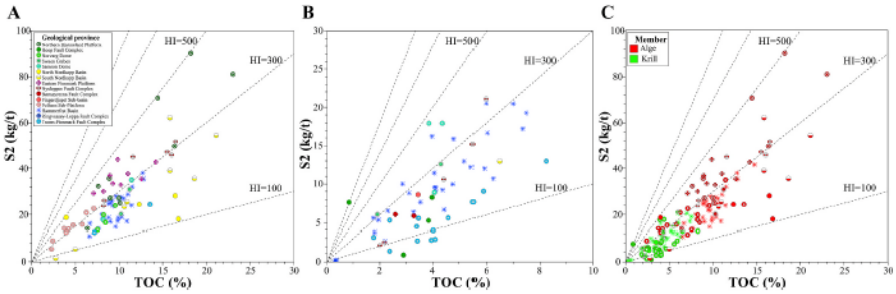

Fig. 10. Total organic carbon (TOC) versus Rock-Eval S2 peak (S2) cross-plot of thermally immature (i.e. < Tmax 430 °C) samples from the Algae (**A**) and Krill (**B**) members. **C.** Combined data from both members. Samples are color-coded based on geological provinces (i.e. A and B) or Hekkingen members (i.e. C). The complete dataset with Tmax values is displayed in Fig. 2. (For interpretation of the references to color in this figure legend, the reader is referred to the Web version of this article.)

estimated for the more terrestrially influenced kerogens within the overlying Krill Member (Fig. 9). Southwards into the Ringvassøy-Loppa Fault Complex, initial hydrogen richness is estimated to have been between 270 and 320 mg HC/g TOC for both members. As will be discussed in section 4.4, sedimentary organic matter in these areas, particularly within the Alge Member, is suspected to have been differentially affected by the action of sulfate-reducing bacteria. This condition may in turn have depressed the original hydrogen richness of the organic materials to different extends, leading to HIi lower than estimated.

Original HI values lower than 200 mg HC/g TOC are estimated for the vitrinitic kerogen in the western localities of the Fingerdjupet Subbasin (i.e. Figs. 7 and 8C) and some Krill sites in the west of the Hammerfest Basin (i.e. Fig. 3). The high quantities of oil-prone, fluorescent amorphous macerals in the Bjørnøyrenna Fault Complex (i.e. Fig. 8A) is indicative of accumulation of "authentic" marine type II kerogen containing elevated hydrogen indexes. Based on analog data from discrete, amorphinite-rich intervals documented in the Polhem sub-platform, a feasible prognosis of HIi for such maceral characteristics would be around 400–500 mgHC/gTOC, or even higher depending on syn- and post sedimentary alteration.

4.4. Sedimentary conditions during sedimentation

4.4.1. TOC versus pyrite

Under marine, oxygen-limited conditions, sulfate-reducing bacteria utilizes sulfate as their main source of oxygen (Berner, 1984). The reduced inorganic sulfide is largely fixed as pyrite (FeS_2) depending on the supply of both reactive iron and bacterially decomposable organic matter, which acts as both a reductant for sulfate and as an oxygen-consuming barrier that prompts anoxic conditions (Berner, 1984). This premise permits the relationship between sedimentary pyrite and TOC to be used as a qualitative tool to evaluate the redox state of the depositional environment (Berner and Raiswell, 1983; Leventhal, 1983; Berner, 1984). Fig. 12 compares samples from the Alge (A) and Krill (B) members in terms of TOC content (wt %) and volume percentage of pyrite from the microscopic analyses. TOC and pyrite correlate positively with one another for Krill samples (Fig. 12B). This is characteristic of sediments deposited in normal marine (i.e. moderately low oxygen content) bottom waters (Berner, 1984; Raiswell et al., 1988; Lückge et al., 2002). Under such conditions, dissolved sulfide and reactive detrital iron minerals are plentiful and, hence, the major control on pyrite formation is the available amount and reactivity of decomposable organic matter.

In the Alge samples, pyrite displays a weaker correlation with TOC

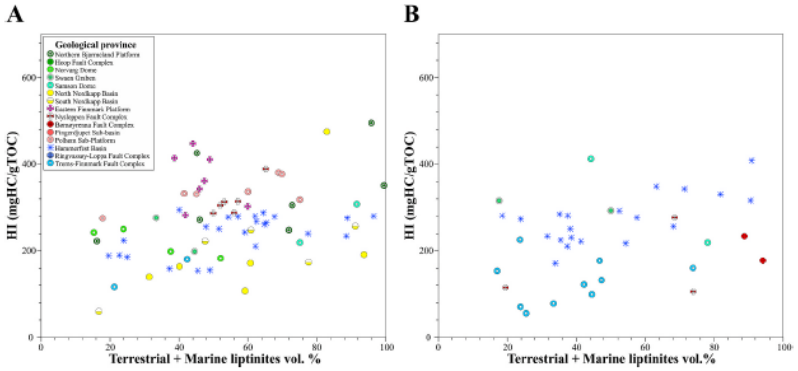

Fig. 11. Relationship between volume percentage of liptinitic macerals (i.e. marine + terrestrial liptinites) and hydrogen index (HI) of thermally immature (i.e. < Tmax 430 °C) samples from the Alge (**A**) and Krill (**B**) members. Samples are color-coded based on geological provinces. (For interpretation of the references to color in this figure legend, the reader is referred to the Web version of this article.)

and its concentration seems independent of TOC (Fig. 12A). This attribute of the Alge Member is typical of accumulation and burial of organics in anoxic settings (Berner, 1984). There, a plentiful supply of organic carbon and sulfide leads to the formation of high concentrations of pyrite, which is in this case limited by the amount of reactive iron-minerals and, importantly, time for reaction. Similar to the Krill Member, highest pyrite concentrations (up to 18 wt %) occur preferentially in samples from the most southernly located areas, i.e. Hammerfest Basin and Ringvassøy Fault Complex. Samples from other locations with comparable TOC levels exhibit a lower pyrite content. This possibly results from the coincidental development of relatively more anoxic bottom waters and stronger inputs of reactive iron minerals in the southern depositional sites. Under strongly anoxic conditions, sulfide occurs in the bottom water and in the upper few meters of the sediments (Sweeney and Kaplan, 1980; Berner, 1984) and even the slowly reacting iron compounds have sufficient time to react with high concentrations of sulfide (Leventhal, 1983).

4.4.2. Carbon isotopes of the SARA fractions

The carbon isotopic composition of the $\delta^{13}C$ saturate (C_{sat}), aromatic (C_{aro}) and asphaltene (C_{asp}) fractions (i.e. SARA) of the organic matter in sedimentary rocks is the result of the original composition of the organic precursors and secondary biochemical processes altering it during sedimentation and diagenesis (Macko et al., 1998; Hayes et al., 1999). The carbon isotope composition of the Hekkingen Formation undergoes a gradual northwards change from heaviest in the Ringvassøy Loppa-High Fault Complex/southern Hammerfest Basin to lightest in the northern Bjarmeland Platform (Fig. 13A and B).

In an attempt to elucidate the effects of organic matter type (i.e. marine versus terrestrial) in the isotope signature, the relative maceral composition and the SARA isotope fractions of the reactive portion of the kerogen are cross plotted in Fig. 14. The plotted SARA isotope values indicate that samples containing different proportions of terrestrial- and marine-derived organic matter have a relatively uniform range of values. This suggests that although the primary composition of the organic matter has the main imprint on the original isotope signature, secondary processes may have altered it to different degrees.

Bacterial sulfate reduction is a complex biochemical process that not only releases sulfide but also alters the original isotopic composition of the organic matter owning to the preferential consumption of light isotopes (Jørgensen, 1982; Berner, 1984). By applying this logic, higher concentrations of pyrite indicate increasingly anoxic conditions leading to intensified bacterial activity and stronger isotope alteration towards heavier values. Cross-plots of pyrite and isotopes show that Alge samples from the Ringvassøy-Loppa Fault Complex and from the Hammerfest Basin record the highest pyrite contents and the heaviest isotopic composition (Fig. 15A and C). This correlation satisfactorily supports that accumulation of organic rich sediments within these areas occurred under more anoxic and stronger sulfate-reducing conditions relative to other areas in the dataset. The smaller variability in the content of pyrite and isotope values observed in the Krill Member (Fig. 15B and D) implies that although redox conditions seemingly changed across the Barents Sea during its deposition, the zonation in dissolved oxygen levels were not as significant as in Alge times. It is arguable that thermal maturity has shifted the original isotope composition to heavier (i.e. less negative) values. In such case, the degree of thermally-induced alteration would vary according to the stability of the different kerogen types. Nevertheless, the magnitude of this changes is not expected to be significant given the only marginal to mid-thermal maturity (Fig. 7; Table 1) of the samples plotted in Fig. 15.

Doerner et al. (2020) have considered the implications of organic matter lability in isotope alteration caused by sulfate-reducing bacteria. Sediments containing higher amounts of labile organic matter were found to have experienced heavier degradation by sulfate reducers. Samples from the Ringvassøy-Loppa Fault Complex and the Hammerfest Basin record high concentrations of labile marine liptinites relative to other areas (Fig. 7). This condition may have eventually prompted a more extensive alteration of the original carbon isotopic composition and, importantly, diminished the original hydrogen richness.

5. Discussion: relationships between paleogeography, macerals, and source rock potential variations

5.1. Sedimentation of the Alge Member

The paleogeographic scenario for the Late Jurassic in the Norwegian Barents Sea is from Marin et al. (2020). They interpret the Hekkingen Formation as part of an overall transgressive event with minor superimposed transgressive-regressive movements. In their model, regional flooding of the shelf begins in the Bathonian-Oxfordian with deposition of the Fuglen Formation. Further transgression during the Oxfordian–Kimmeridgian caused terrigenous sediments to be trapped

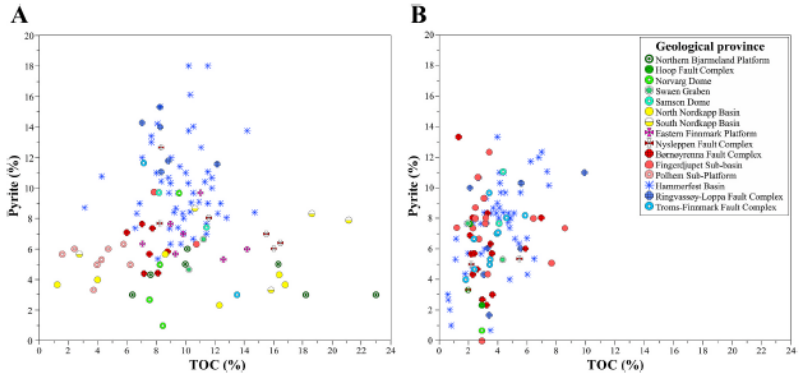

Fig. 12. Cross-plot of total organic carbon (TOC) weight percent versus whole rock volume percentage of pyrite (Pyrite %) for each of the samples from the Alge (**A**) and Krill (**B**) members. Samples are color-coded based on geological provinces. (For interpretation of the references to color in this figure legend, the reader is referred to the Web version of this article.)

landward with an associated drop in sedimentation rates farther offshore, marked by deposition of the black shales of the Alge Member. In the Hammerfest Basin and the Troms-Finnmark and Ringvassøy-Loppa fault complexes, outer shelf facies accumulated (Fig. 16A). This water mass transitioned westwards into the Tromsø Basin where cooler, deep marine facies were deposited. In these areas, a relatively high pyrite content and heavy isotopes (Fig. 15A) suggest a depositional environment with poorly oxygenated bottom waters. Under these conditions, intense degradation by sulfate-reducing bacteria is suspected to have decomposed the organic matter and probably depressed the HI values of preferentially algal debris (Littke et al., 1997; Luckge et al., 2002; Doerner et al., 2020). The westwards enrichment in marine organic components in the Hammerfest Basin reflects an increasing distance from the sources of land particles, which is inferred to be the Norwegian mainland.

The Loppa High remained under shallow water conditions and only uplifted footwall islands emerged above sea level (Fig. 16A). The higher content of colonial alginite recorded in the western Hammerfest Basin supports the existence of an inner shelf to transitional source area updip in the Loppa High. The isolated islands are likely sources for the abundant terrestrial organic matter in the Fingerdjupet Sub-basin, the Polhem Sub-platform, the Bjørnøyrenna Fault Complex, and the southern part of the Bjarmeland Platform. It is also possible that small islands established on top of the Samson and Norvarg domes and on top of uplifted footwalls around the Swaen Graben acted as additional sources of terrestrial debris in the southern Bjarmeland Platform.

Across most of the Nordkapp Basin, the Bjarmeland Platform, and the distal parts of the eastern Finnmark Platform, the Alge Member was deposited in an outer shelf setting with high inputs of terrestrial organic particles from the mainland and locally from islands formed on top of salt diapirs (Fig. 16A). In the Nordkapp Basin, marine liptinites possibly derived from autochthonous organisms living in semi-sealed mini basins formed between diapirs. Therein, the intermittent growth of salt diapirs (Rojo and Escalona, 2018; Cedeño et al., 2019) probably caused small-scale fluctuations in redox conditions and subjected the organic matter to reworking and degradation by aerobic bacteria, which consequently lowered HI (i.e. Fig. 10A) and increased the concentration of inertinite (i.e. Fig. 8E). Such fluctuations in dissolved oxygen content

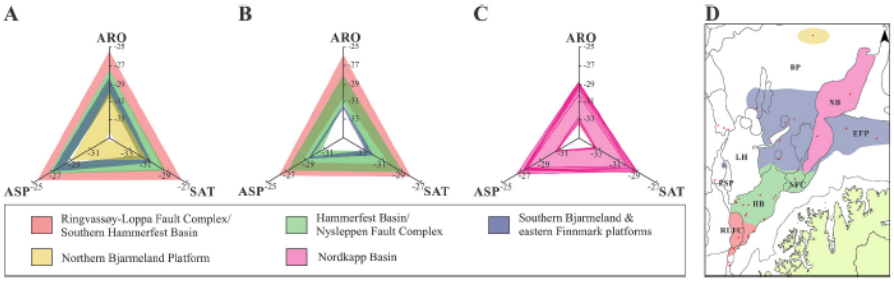

Fig. 13. North-south variability in carbon isotope composition within the Alge (**A**) and Krill (**B**) members. The isotope ranges displayed in the three-axes diagrams represent the minimum and maximum value for each of the SARA (Saturate, Aromatic, Asphaltene) fractions of samples in the corresponding region. **C.** Isotope ranges and samples of the Alge Member in the Nordkapp Basin are displayed. **D.** Map of the study area color-coded after the three-axes diagrams. Refer to Fig. 1 for abbreviations of the different geological provinces. (For interpretation of the references to color in this figure legend, the reader is referred to the Web version of this article.)

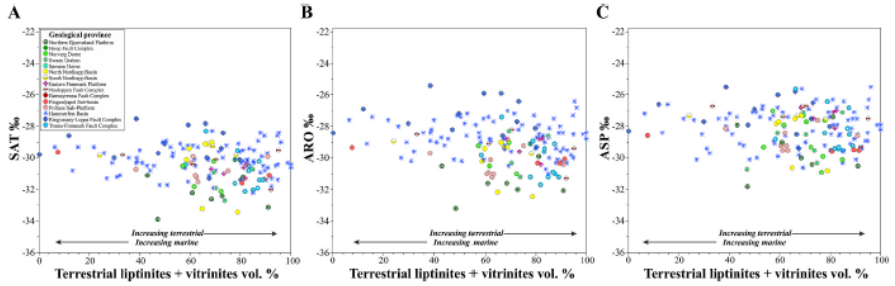

Fig. 14. Volume percentage of terrestrial macerals (i.e. vitrinite + terrestrial liptinites) cross-plotted versus isotope values of the saturate-SAT (**A**), aromatic-ARO (**B**), and asphaltenes-ASP (**C**) fractions of the studied source rock samples. Samples are color-coded based on geological provinces. (For interpretation of the references to color in this figure legend, the reader is referred to the Web version of this article.)

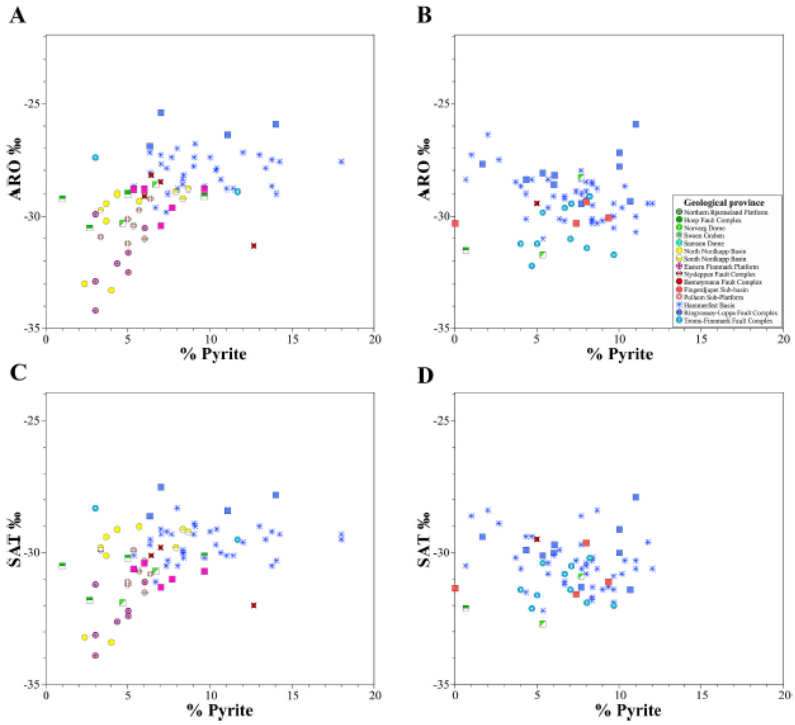

Fig. 15. Cross-plot of whole rock volume percentage of pyrite (Pyrite %) versus isotope values of the saturate (SAT) and aromatic (ARO) fractions of source rock from the Alge (**A** and **C**) and Krill (**B** and **D**) members, respectively. Samples are color-coded based on geological provinces. (For interpretation of the references to color in this figure legend, the reader is referred to the Web version of this article.)

in the Nordkapp Basin are probably responsible for the broad range of isotope values covering a span of up to 4.3‰ (Fig. 13C). Higher-than-average HI values in the eastern Finnmark, the northern Bjarmeland, and the Polhem Sub-platforms may be a result of less degradation by sulfate reducers under only modestly anoxic conditions. Lighter isotopes and lower contents of pyrite compared to the Hammerfest Basin and the Ringvassøy Fault Complex (Fig. 15A) suggest affinities with less anoxic bottom waters in the northern areas.

5.2. Sedimentation of the Krill Member

Increased tectonic activity during the late Kimmeridgian–Ryazanian brought about paleogeographic changes (Fig. 16B) that exerted important controls on the sedimentation of the Krill Member. Seawards migration of the shorelines and subaerial erosion of uplifted footwalls delivered higher volumes of coarse-grained sediments to the shelf, which locally increased sedimentation rates and diluted the organic matter. The generally coarse grain size of the clastic particles and the increased freshwater discharge imply a more energetic hydraulic regimen and greater contents of dissolved oxygen. This sedimentary background resulted in accumulation of the Krill Member under redox conditions that were generally more uniform across the different geological provinces compared to the accumulation during Alge times. Importantly, the biota sourcing the sedimentary organic matter remained essentially the same as in the underlying Alge Member, as discussed in section 4.2.

A set of normal faults caused further deepening of the shelf across the Ringvassøy-Loppa Fault Complex and development of deep marine environments (Fig. 16B). Most of the contiguous Hammerfest Basin remained under outer shelf conditions except for the Central High, which rose above sea level and shed terrestrial organic materials into the basin. Faulting along the Troms-Finnmark Fault Complex triggered the exhumation of the Finnmark Platform, followed by seaward migration of the shoreline and increased river runoff. Naturally, this caused the amount of terrestrial clastic and organic material delivered to the Hammerfest Basin and other areas adjacent to the Finnmark Platform to increase when compared to the underlying Alge Member (Fig. 16B). Sediments derived from the Norwegian mainland were probably deposited in delta and prodelta environments and were subsequently dispersed by turbiditic currents and hyperpycnal flows. Fewer inertinitic particles in the Hammerfest Basin and the Troms-Finnmark Fault Complex suggests short residence time in areas of oxic decomposition and supports the proximity of the continental source. Limited sulfate-reducing activity together with strong inputs of terrestrial organic matter, which is less susceptible to the attack by sulfate reducers, most likely prevented extensive decomposition of the organic matter and better preservation of the original hydrogen richness.

The Loppa High continued to be a tectonically active area and uplifted footwall islands became areally more extensive during Krill times (Fig. 16B). Shallow, inner shelf conditions existing in the Loppa High extended eastwards into the southern Bjarmeland Platform, the Nordkapp Basin, and the eastern Finnmark Platform. There, organic matter resided a longer time in the oxygenated uppermost sediment layer after deposition, where aerobic bacteria and bottom-dwelling fauna degraded all but the most resistant organic constituents. This lends itself to explaining a subtle increase in inertinite particles on the platforms, and possibly explains the lack of marine macerals.

5.3. Sedimentation within the Bjørnøyrenna Fault Complex

Subaqueous and subaerial degradation of uplifted footwalls in the Loppa High delivered increased volumes of clastic material to deep

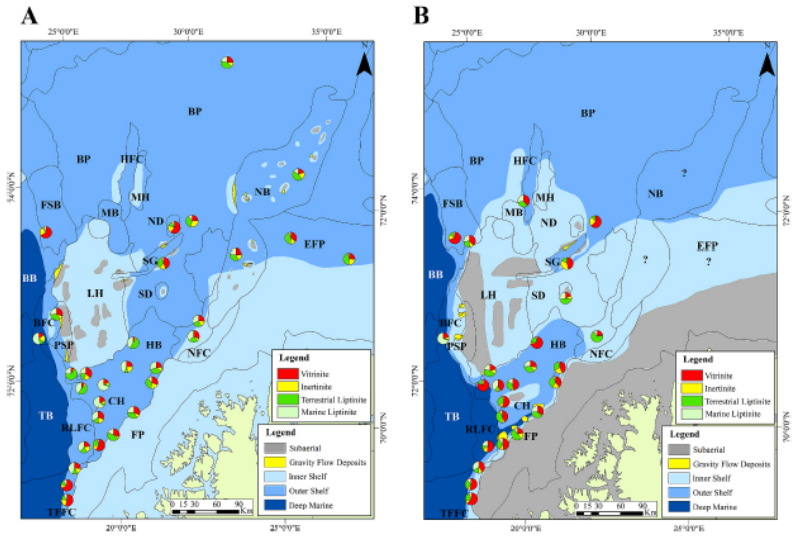

Fig. 16. Paleogeographic maps of the southwestern Barents Sea illustrating the variability in sedimentary environments within the Alge (**A**) and Krill (**B**) members. The paleogeographic maps are modified from Marin et al., (2020). The pie diagrams represent the average (i.e. per well) maceral compositions calculated from the microscopic analysis. See Table 1 for plotted values. Refer to Fig. 1 for abbreviations of geological provinces.

marine settings in the Bjørnøyrenna Fault Complex (Fig. 16B). Fig. 8A shows variability in organic facies reflected in shifts from high relative amounts of marine macerals (i.e. amorphinite) to high amounts of allochthonous terrestrial macerals (i.e. inertinite and vitrinite) within both members. This condition is consistent with short-lived, but frequent, changes in organic inputs and depositional conditions probably driven by submarine debris flows and turbiditic currents. These phenomena carried oxygenated waters and land plant-derived particles from proximal updip locations to deep sites where they disrupted the sedimentation of marine organic materials in oxygen-depleted waters. Oscillation in the concentration of pyrite and detrital quartz supports these interpretations (Figs. 12 and 8A). In this area of the Bjørnøyrenna Fault Complex, high sedimentation rates probably prevented oxidation and bacterial decomposition of the organic matter at the sediment-water interface.

6. Conclusions

The gross kerogen composition of the Hekkingen Formation is dominated by terrestrial organic matter. This conclusion arises from finding that vitrinitic and terrestrial liptinitic macerals predominate over marine macerals. Such preponderance of land-derived particles is more pronounced in the overlying Krill Member.

The abundance of marine macerals is higher in the central and western areas of the Hammerfest Basin and in well 7219/8-1 S in the Bjørnøyrenna Fault Complex. This suggests that authentic marine type II kerogens (i.e. ≤ 400 mgHC/gTOC) probably existed in these areas prior to thermal maturation.

The mapped shifts in the relative proportion of marine and allochthonous terrestrial macerals are ascribed to changes in the location of the depositional sites with respect to the sources of the terrestrial organic materials.

The highest levels of TOC (≥7 wt %t) occur within the Alge Member, but the more discrete and organically poorer beds of the Krill Member still contain sufficient organic carbon to be classified as petroleum source rocks (≥2 wt %).

Hydrogen indices between 50 and 400 mg HC/g TOC recorded throughout the entire formation indicate that both members have similar oil and gas generation capabilities. These HI values are characteristic of immature Type III to II-III kerogens and are generally consistent with the relatively high quantities of land-derived particles documented in this study.

Pyrite contents and carbon isotopes of the SARA fractions suggest that the degree of anoxia and bacterial sulfate reduction decreased gradually from south (i.e. Ringvassøy-Loppa Fault Complex/southern Hammerfest Basin) to north (i.e. Bjarmeland Platform). This zonation in redox conditions is more prominent in the Alge Member.

At least three factors controlled the detected variability in geochemical parameters: dilution rates of organic matter, varying proportions of terrestrial and marine organic particles, and the degree of preservation of the organic matter.

Declaration of competing interest

The authors declare that they have no known competing financial interests or personal relationships that could have appeared to influence the work reported in this paper.

Acknowledgments

The authors would like to thank the sponsors of the JuLoCrA project (https://wp.ux.uis.no/julocra/) for providing essential economic support. We are grateful to Integrated Geochemical Interpretation (IGI) for free software supply and to Applied Petroleum Technologies (APT) for analytical studies, especially to Per Erling Johansen. We sincerely thank the Norwegian Petroleum Directorate for providing sample material necessary to develop this research. The authors also thank reviewers Simon George, Dag Arild Karlsen, and Torbjørn Throndsen for their constructive reviews that greatly improved the manuscript.

References

Abay, T.B., Karlsen, D.A., Pedersen, J.H., Olaussen, S., Backer-Owe, K., 2017. Thermal maturity, hydrocarbon potential and kerogen type of some Triassic-Lower Cretaceous sediments from the SW Barents Sea and Svalbard. Petrol. Geosci. 24, 349–373. https://doi.org/10.1144/petgeo2017-035.

Århus, N., 1991. The transition from deposition of condensed carbonates to dark claystones in the Lower Cretaceous succession of the southwestern Barents Sea. Nor. Geol. Tidsskr. 71, 259–263.

Berglund, L., Augustson, J., Færseth, R., Gjelberg, J., Ramberg-Moe, H., 1986. The evolution of the Hammerfest Basin. Habitat of hydrocarbons on the Norwegian continental shelf 319–338.

Berner, R.A., Raiswell, R., 1983. Burial of organic carbon and pyrite sulfur in sediments over Phanerozoic time: a new theory. Geochem. Cosmochim. Acta 47, 855–862. https://doi.org/10.1016/0016-7037(83)90151-5.

Berner, R.A., 1984. Sedimentary pyrite formation: an update. Geochem. Cosmochim. Acta 48, 605–615. https://doi.org/10.1016/0016-7037(84)90089-9.

Berner, R.A., Kothavala, Z., 2001. GEOCARB III: a revised model of atmospheric CO2 over Phanerozoic time. Am. J. Sci. 301, 182–204.

Bjorøy, M., Hall, P.B., 1983. A rich Middle Triassic source rock in the Barents Sea area. In: Cheng, T.Y., Johnson, O.G. (Eds.), 3D Vector Forward Modeling – Proceedings of the 15th Annual Offshore Technology Conference. Society of Petroleum Engineers, Houston, Texas, pp. 379–392. https://doi.org/10.4043/4623-MS.

Blaich, O.A., Tsikalas, F., Faleide, J.I., 2017. New insights into the tectono-stratigraphic evolution of the southern Stappen high and its transition to Bjørnøya Basin, SW Barents Sea. Mar. Petrol. Geol. 85, 89–105. https://doi.org/10.1016/j.marpetgeo.2017.04.015.

Bugge, T., Elvebakk, G., Fanavoll, S., Mangerud, G., Smelror, M., Weiss, H.M., Gjelberg, J., Kristensen, S.E., Nilsen, K., 2002. Shallow stratigraphic drilling applied in hydrocarbon exploration of the Nordkapp Basin, Barents Sea. Mar. Petrol. Geol. 19, 13–37. https://doi.org/10.1016/S0264-8172(01)00051-4.

Cavanagh, A.J., Di Primio, R., Scheck-Wenderoth, M., Horsfield, B., 2006. Severity and timing of cenozoic exhumation in the southwestern Barents Sea. J. Geol. Soc. 163, 761–774. https://doi.org/10.1144/0016-76492005-146.

Cedeño, A., Rojo, L.A., Cardozo, N., Centeno, L., Escalona, A., 2019. The impact of salt tectonics on the thermal evolution and the petroleum system of confined rift basins: insights from basin modeling of the Nordkapp Basin, Norwegian Barents Sea. Geosciences 9. https://doi.org/10.3390/geosciences9070316.

Cedeño, A., Ohm, S., Escalona, A., Marín, D., Olaussen, S., Demchuck, T., 2021. SUBMITTED ALONG WITH THIS MS). Upper Cretaceous Source Rocks in the Norwegian Barents Sea, Part II: Insights from Open- and Closed-System Pyrolysis Experiments.

Clark, S., Glorstad-Clark, E., Faleide, J., Schmid, D., Hartz, E., Fjeldskaar, W., 2014. Southwest Barents Sea rift basin evolution: comparing results from backstripping and time-forward modelling. Basin Res. 26, 550–566. https://doi.org/10.1111/bre.12039.

Cornford, C., 1998. Source rocks and hydrocarbons of the north sea. In: Glennie, K.W. (Ed.), Petroleum Geology of the North Sea. Blackwell Science, Oxford, pp. 376–462. https://doi.org/10.1002/9781444313413.ch11.

Costa, L.I., Davey, R.J., 1992. Dinoflagellate cysts of the Cretaceous system. In: Powell, A.J. (Ed.), A Stratigraphic Index of Dinoflagellate Cysts. Chapman and Hall, London, pp. 99–131.

Dalland, A., Worsley, D., Ofstad, K., 1988. A lithostratigraphic scheme for the Mesozoic and Cenozoic succession offshore Norway north of 62 N. Norwegian Petrol. Dir. Bull. 4, 67.

Doemer, M., Berner, U., Erdmann, M., Barth, T., 2020. Geochemical characterization of the depositional environment of paleocene and eocene sediments of the tertiary central basin of Svalbard. Chem. Geol. 542 https://doi.org/10.1016/j.chemgeo.2020.119587.

Doré, A.G., Scotchman, I.C., Corcoran, D., 2000. Cenozoic exhumation and prediction of the hydrocarbon system on the NW European margin. J. Geochem. Explor. 69 (70), 615–618. https://doi.org/10.1016/S0375-6742(00)00137-0.

Dypvik, H., Mørk, A., Smelror, M., Sandbakken, P.T., Tsikalas, F., Vigran, J.O., Bremer, G.M.A., Nagy, J., Gabrielsen, R.H., Faleide, J.I., 2004. Impact breccia and ejecta from the Mjölnir crater in the Barents Sea-the Ragnarok Formation and Sindre bed. Norsk Geologisk Forening 84, 143–167.

Faleide, J.I., Gudlaugsson, S.T., Jacquart, G., 1984. Evolution of the western Barents Sea. Mar. Petrol. Geol. 1, 123–150. https://doi.org/10.1016/0264-8172(84)90082-5.

Faleide, J.I., Vågnes, E., Gudlaugsson, S.T., 1993. Late Mesozoic-Cenozoic evolution of the south-western Barents Sea in a regional rift-shear tectonic setting. Mar. Petrol. Geol. 10, 186–214. https://doi.org/10.1016/0264-8172(93)90104-Z.

Faleide, T.S., Middelsdal, I., Planke, S., Corseri, R., Faleide, J.I., Serck, C.S., Nystuen, J. P., 2019. Characterization and development of Early Cretaceous shelf platform deposition and faulting in the Hoop area, southwestern Barents Sea-constrained by high-resolution seismic data. Norw. J. Geol. 99, 3. https://doi.org/10.17850/njg99-3-7.

Gavshin, V.M., Zakharov, V.A., 1996. Geochemistry of the upper Jurassic - lower cretaceous Bazhenov Formation, West Siberia. Econ. Geol. 91, 122–133. https://doi.org/10.2113/gsecongeo.91.1.122.

Paper I

Georgiev, S.V., Stein, H.J., Hannah, J.L., Xu, G.P., Bingen, B., Weiss, H.M., 2017. Timing, duration, and causes for late Jurassic-early cretaceous anoxia in the Barents Sea. Earth Planet Sci. Lett. 461, 151–162. https://doi.org/10.1016/j.epsl.2016.12.035.
Gernigon, L., Brönner, M., Roberts, D., Olesen, O., Nasuti, A., Yamasaki, T., 2014. Crustal and basin evolution of the southwestern Barents Sea: from Caledonian orogeny to continental breakup. Tectonics 33, 347–373. https://doi.org/10.1002/2013TC003439.
Grace, J.D., Hart, G.F., 1986. Giant gas fields of northern West Siberia. AAPG (Am. Assoc. Pet. Geol.) Bull. 70, 830–852. https://doi.org/10.1306/94886358-1704-11D7-8645000102C1865D.
Gudlaugsson, S.T., 1993. Large impact crater in the Barents Sea. 2 Geology 21, 291–294. https://doi.org/10.1130/0091-7613(1993)021<0291:LICITB>2.3.CO.
Hayes, J.M., Strauss, H., Kaufman, A.J., 1999. The abundance of 13C in marine organic matter and isotopic fractionation in the global biogeochemical cycle of carbon during the past 800 Ma. Chem. Geol. 161, 103–125. https://doi.org/10.1016/S0009-2541(99)00083-2.
Helleren, S., Marín, D., Ohm, S., Augustsson, C., Escalona, A., 2020. Why does not lithology correlate with gamma-ray spikes in the shaley source rocks of the Upper Jurassic Alge Member (southwestern Barents Sea)? Mar. Petrol. Geol. 121 https://doi.org/10.1016/j.marpetgeo.2020.104623.
Henriksen, E., Ryseth, A., Larssen, G., Heide, T., Rønning, K., Sollid, K., Stoupakova, A., 2011a. Tectonostratigraphy of the greater Barents Sea: implications for petroleum systems. In: Spencer, A.M., Embry, A.F., Gautier, D.L., Stoupakova, A.V., Sørensen, K. (Eds.), Arctic Petroleum Geology, vol. 35. Geological Society, pp. 163–195. https://doi.org/10.1144/M35.10. London, Memoirs 2011.
Henriksen, E., Bjørnseth, H.M., Hals, T.K., Heide, T., Kiryukhina, T., Kløvjan, O.S., Larssen, G.B., 2011b. Uplift and erosion of the greater Barents Sea: impact on prospectivity and petroleum systems. In: Spencer, A.M., Embry, A.F., Gautier, D.L., Stoupakova, A.V., Sørensen, K. (Eds.), Arctic Petroleum Geology, vol. 35. Geological Society, pp. 271–281. https://doi.org/10.1144/M35.17. London, Memoirs 2011.
Indrevær, K., Gabrielsen, R.H., Faleide, J.I., 2017. Early Cretaceous synrift uplift and tectonic inversion in the Loppa High area, southwestern Barents Sea, Norwegian shelf. J. Geol. Soc. 174, 242–254. https://doi.org/10.1144/jgs2016-066.
Johansen, S.E., Ostisty, B.K., Birkeland, Ø., Fedorovsky, Y.F., Martirosjan, V.N., Bruun Christensen, O., Cheredeev, S.I., Ignatenko, E.A., Margulis, L.S., 1992. Hydrocarbon potential in the Barents Sea region: play distribution and potential. In: Vorren, T.O., Bergsager, E., Dahl-Stamnes, Ø.A., Holter, E., Johansen, B., Lie, E., Lund, T.B. (Eds.), Arctic Geology and Petroleum Potential, vol. 2. Norwegian Petroleum Society, Special Publication, pp. 273–320. https://doi.org/10.1016/B978-0-444-88943-0.50024-1.
Jørgensen, B.B., 1982. Mineralization of organic matter in the seabed - the role of sulphate reduction. Nature 296, 643–645.
Kairanov, B., Marín, D., Escalona, A., Cardozo, N., 2019. Growth and linkage of a Basin-bounding fault system: insights from the early cretaceous evolution of the northern Polheim Subplatform, SW Barents Sea. J. Struct. Geol. 124, 182–196. https://doi.org/10.1016/j.jsg.2019.04.014.
Kairanov, B., Escalona, A., Norton, I., Abrahamsson, P., 2021. Early cretaceous evolution of the Tromsø Basin, SW Barents Sea. Mar. Petrol. Geol. 123 https://doi.org/10.1016/j.marpetgeo.2020.104714.
Klemme, H.D., 1994. Petroleum systems of the world involving Upper Jurassic source rocks. In: Magoon, L.B., Dow, W.G. (Eds.), The Petroleum System: from Source to Trap, vol. 60. AAPG Memoir, pp. 51–72.
Knies, J., Matthiessen, J., Christoph, V., Laberg, J.S., Hjelstuen, B.O., Smelror, M., Larsen, E., Andreassen, K., Eidvin, T., Vorren, T.O., 2009. The Plio-Pleistocene glaciation of the Barents Sea–Svalbard region: a new model based on revised chronostratigraphy. Quat. Sci. Rev. 28, 812–829. https://doi.org/10.1016/j.quascirev.2008.12.002.
Leith, T., Weiss, H., Mørk, A., Elvebakk, G., Embry, A., Brooks, P., Verba, M., 1993. Mesozoic hydrocarbon source-rocks of the Arctic region. In: Vorren, T.O., Bergsager, E., Dahl-Stamnes, Ø.A., Holter, E., Johansen, B., Lie, E., Lund, T.B. (Eds.), Norwegian Petroleum Society Special Publications, vol. 2. Elsevier, pp. 1–25. https://doi.org/10.1016/B978-0-444-88943-0.50006-X.
Leventhal, J.S., 1983. An interpretation of carbon and sulfur relationships in Black Sea sediments as indicators of environments of deposition. Geochem. Cosmochim. Acta 47, 133–137. https://doi.org/10.1016/0016-7037(83)90097-2.
Littke, R., Luckge, A., Welte, D.H., 1997. Quantification of organic matter degradation by microbial sulphate reduction for Quaternary sediments from the northern Arabian Sea. Naturwissenschaften 84, 312–315. https://doi.org/10.1007/s001140050402.
Luckge, A., Horsfield, B., Littke, R., Scheeder, G., 2002. Organic matter preservation and sulfur uptake in sediments from the continental margin off Pakistan. Org. Geochem. 33, 477–488. https://doi.org/10.1016/S0146-6380(01)00171-1.
Macko, S.A., Engel, M.H., Freeman, K., 1998. Variability of isotope compositions in modern and fossil organic matter. Chem. Geol. 152, 1–2.
Marín, D., Escalona, A., Grundvåg, S.A., Olaussen, S., Sandvik, S., Śliwińska, K.K., 2018. Unravelling key controls on the rift climax to post-rift fill of marine rift basins: insights from 3D seismic analysis of the Lower Cretaceous of the Hammerfest Basin, SW Barents Sea. Basin Res. 30, 587–612. https://doi.org/10.1111/bre.12266.
Marín, D., Helleren, S., Escalona, A., Olaussen, S., Cedeño, A., Nøhr-Hansen, H., Ohm, S., 2020. The Middle Jurassic to lowermost Cretaceous in the SW Barents Sea: interplay between tectonics, coarse-grained sediment supply and organic matter preservation. Basin Res. https://doi.org/10.1111/bre.12504.
Mørk, A., Dallmann, W., Dypvik, H., Johannessen, E., Larssen, G., Nagy, J., Nøttvedt, A., Olaussen, S., Pchelina, T., Worsley, D., 1999. Mesozoic Lithostratigraphy. Lithostratigraphic Lexicon of Svalbard. Upper Paleozoic to Quaternary Bedrock. Review and Recommendations for Nomenclature Use, pp. 127–214.
Mulrooney, M.J., Leutscher, J., Braathen, A., 2017. A 3D structural analysis of the Goliat field, Barents Sea, Norway. Mar. Petrol. Geol. 86, 192–212. https://doi.org/10.1016/j.marpetgeo.2017.05.030.
Ohm, S.E., Karlsen, D.A., Austin, T., 2008. Geochemically driven exploration models in uplifted areas: examples from the Norwegian Barents Sea. AAPG (Am. Assoc. Pet. Geol.) Bull. 92, 1191–1223. https://doi.org/10.1306/06180808028.
Riis, F., Fjeldskaar, W., 1992. On the magnitude of the late tertiary and quaternary erosion and its significance for the uplift of Scandinavia and the Barents Sea. In: Larsen, R.M., Brekke, H., Larsen, B.T., Talleraas, E. (Eds.), Structural and Tectonic Modelling and its Application to Petroleum Geology, vol. 1. Norwegian Petroleum Society, Special Publication, pp. 163–185. https://doi.org/10.1016/B978-0-444-88607-1.50016-4.
Riis, F., 1996. Quantification of Cenozoic vertical movements of Scandinavia by correlation of morphological surfaces with offshore data. Global Planet. Change 331–357. https://doi.org/10.1016/0921-8181(95)00027-5.
Rojo, L.A., Escalona, A., 2018. Controls on minibasin infill in the Nordkapp Basin: evidence of complex Triassic synsedimentary deposition influenced by salt tectonics. AAPG Bull. 102 (7), 1239–1272. https://doi.org/10.1306/09261715243165523.
Rojo, L.A., Cardozo, N., Escalona, A., Koyi, H., 2019. Structural style and evolution of the Nordkapp Basin, Norwegian Barents Sea. AAPG (Am. Assoc. Pet. Geol.) Bull. 103 (9), 2177–2217. https://doi.org/10.1306/01301918023.
Scheidt, G., Littke, R., 1989. Comparative organic petrology of interlayered sandstones, siltstones, mudstones and coals in the Upper Carboniferous Ruhr basin, Northwest Germany, and their thermal history and methane generation. Geol. Rundsch. 78, 375–390. https://doi.org/10.1007/BF01988371.
Schlanger, S.O., Jenkyns, H.C., 1976. Cretaceous anoxic events: causes and consequences, Geologie. Mijnbouw 55, 179–184.
Sclater, J., Christie, P., 1980. Continental stretching: an explanation of post mid-Cretaceous subsidence of the central North Sea Basin. J. Geophys. Res. 85, 3711–3739. https://doi.org/10.1029/JB085iB07p03711.
Scotese, C.R., 2016. PALEOMAP PaleoAtlas for GPlates and the PaleoData Plotter Program. PALEOMAP Project. http://www.earthbyte.org/paleomap-paleoatlas-for-gplates/.
Serck, C.S., Faleide, J.I., Braathen, A., Kjølhamar, B., Escalona, A., 2017. Jurassic to early cretaceous basin configuration(s) in the Fingerdjupet Subbasin, SW Barents Sea. Mar. Petrol. Geol. 86, 874–891. https://doi.org/10.1016/j.marpetgeo.2017.06.044.
Smelror, M., Below, R., 1993. Dinoflagellate biostratigraphy of the toarcian to lower Oxfordian (Jurassic) of the Barents Sea region. In: Vorren, T.O. (Ed.), Arctic Geology and Petroleum Potential, vol. 2. NPF special publication, pp. 495–513. https://doi.org/10.1016/B978-0-444-88943-0.50035-6.
Smelror, M., Mørk, A., Mørk, M.B.E., Weiss, H.M., Løseth, H., 2001. Middle Jurassic-Lower Cretaceous transgressive-regressive sequences and facies distribution off northern Nordland and Troms, Norway, 10. Norwegian Petroleum Society Special Publications, pp. 211–232. https://doi.org/10.1016/S0928-8937(01)80015-1.
Sund, T., Skarpnes, O., Jensen, L.N., Larsen, R.M., 1986. Tectonic development and hydrocarbon potential offshore Troms, northern Norway. In: Halbouty, T.H. (Ed.), Future Petroleum Provinces of the World, vol. 40. AAPG Memoir. https://doi.org/10.1306/M40454C29.
Sweeney, R.E., Kaplan, I.R., 1980. Diagenetic sulphate reduction in marine sediments. Mar. Chem. 9, 165–174. https://doi.org/10.1016/0304-4203(80)90035-3.
Tsikalas, F., Gudlaugsson, S.T., Faleide, J.I., Eldholm, O., 1999. Mjolnir Structure, Barents Sea: a Marine Impact Crater Laboratory. Special Papers-Geological Society of America, pp. 193–204. https://doi.org/10.1130/0-8137-2339-6.193.
Tsikalas, F., Blaich, O.A., Faleide, J.I., Olaussen, S., 2021. Stappen High-Bjarmeya Tectono-Sedimentary Element, Barents Sea, vol. 57. Geological Society, London, Memoirs. https://doi.org/10.1144/M57-2016-24.
Weissert, H., McKenzie, J.A., Hochuli, P., 1979. Cyclic anoxic events in the early cretaceous tethys ocean. Geology 7, 147–151. https://doi.org/10.1130/0091-7613(1979)7<147:CAEITE>2.0.CO;2.
Weissert, H., Mohr, H., 1996. Late Jurassic climate and its impact on carbon cycling. Palaeogeogr. Palaeoclimatol. Palaeoecol. 122, 27–43. https://doi.org/10.1016/0031-0182(95)00088-7.
Wierzbowski, A., Smelror, M., 2020. The Bajocian to Kimmeridgian (middle to upper Jurassic) ammonite succession at Sentralbanken high (core 7533/3-U-1), Barents Sea, and its stratigraphical and palaeobiogeographical significance. Volumina Jurassica 18, 1–22. https://doi.org/10.7306/vj.18.1.
Worsley, D., 2008. The post-Caledonian development of Svalbard and the western Barents Sea. Polar Res. 27, 298–317. https://doi.org/10.3402/polar.v27i3.6197.
Zumberge, J., Harold, I., Lowell, W., 2016. Petroleum geochemistry of the cenomanian–turonian eagle Ford oils of south Texas. In: Breyer, J.A. (Ed.), The Eagle Ford Shale: A Renaissance in U.S. Oil Production, vol. 110. AAPG Memoir, pp. 135–165. https://doi.org/10.1306/13541960M110449.

Paper II

Upper Jurassic to Lower Cretaceous source rocks in the Norwegian Barents Sea, part II: Insights from open- and closed-system pyrolysis experiments

Andrés Cedeño [a], Sverre Ohm [a], Alejandro Escalona [a], Dora Marín [a], Snorre Olaussen [b], Thomas Demchuk [c]

[a] University of Stavanger, Norway

[b] The University Centre in Svalbard, Norway

[c] Louisiana State University, USA

Marine and Petroleum Geology 134 (2021) 105343
https://doi.org/10.1016/j.marpetgeo.2021.105343

Marine and Petroleum Geology 134 (2021) 105343

Contents lists available at ScienceDirect

Marine and Petroleum Geology

journal homepage: www.elsevier.com/locate/marpetgeo

Upper Jurassic to Lower Cretaceous source rocks in the Norwegian Barents Sea, part II: Insights from open- and closed-system pyrolysis experiments

Andrés Cedeño [a,*], Sverre Ohm [a], Alejandro Escalona [a], Dora Marín [a], Snorre Olaussen [b], Thomas Demchuk [c]

[a] University of Stavanger, Norway
[b] The University Centre in Svalbard, Norway
[c] Louisiana State University, USA

ARTICLE INFO

Keywords:
Source rock
Petroleum generation potential
GC-Pyrolysis
Bulk kinetics
Compositional kinetics
Barents sea
Hekkingen formation

ABSTRACT

The petroleum generation potential of Upper Jurassic to Lower Cretaceous organic rich shales from the southwestern Barents Sea was evaluated using bulk and quantitative pyrolysis analysis. Fifteen thermally-immature samples from the Hekkingen Formation with differing organic facies, as defined by maceral composition, were subjected to total organic carbon, Rock-Eval pyrolysis, pyrolysis gas chromatography, bulk kinetics, and micro-scale sealed vessel pyrolysis analyses. The results were employed to characterize differences in source rock kerogens, gross petroleum type, and the compositional evolution of the generated fluids as well as their physical properties (i.e. gas to oil ratio, saturation pressure, and formation volume factor) as a function of increasing maturity.

The investigated samples contain varying proportions of kerogen type II and III. Heterogeneities in the kerogen composition result in different orders of thermal stability, with the onset of petroleum generation predicted to occur over a high and broad temperature range from 123 °C to 144 °C (at 3.3C°/Ma). Reduced kerogen stability associated with elevated sulfur contents is only documented in a few samples. Most of the analyzed samples have the potential to generate low GOR oils of an intermediate to aromatic, low wax paraffinic-naphthenic-aromatic (P-N-A) composition and variable amounts of wet gas. Petroleums of similar compositional and physical properties are predicted to have been generated from the natural maturation sequence of various organic facies in thermally mature areas of the Hammerfest Basin and the Ringvassøy-Loppa High and Bjørnøyrenna fault complexes. Vitrinite-rich sources in the Fingerdjupet Sub-basin and the Troms-Finnmark Fault Complex have potential for gas and condensate generation.

1. Introduction

The Norwegian Barents Sea hosts various petroleum source rock intervals ranging in age from Carboniferous to Early Cretaceous (Henriksen et al., 2011a; Ohm et al., 2008; Abay et al., 2017). The clastic rocks of the Upper Jurassic Hekkingen Formation constitute the most widespread and one of the most prolific sourcing intervals. These extended deposits are records of a Late Jurassic epicontinental sea inundating vast areas of the western Barents Shelf (Fig. 1). Development of suboxic to anoxic conditions and the coincidental increase in biological carbon productivity favored accumulation of organic-carbon-rich sediments. Total organic carbon (TOC) values in the Alge Member are typically higher than in the overlying Krill Member as demonstrated by Cedeño et al., 2021 and affirmed by the general literature (Henriksen et al., 2011a; Ohm et al., 2008; Abay et al., 2017).

Geochemical characterization of oils in the southwestern Barents Sea has been conducted by Ohm et al. (2008), Duran et al. (2013a), Killops et al. (2014), Murillo et al. (2016) and Lerch et al. (2016). Their studies concluded that the organic-rich facies of the Hekkingen Formation provides a source for some of the migrated petroleum within the Snøhvit and Goliath fields, and various sub-commercial accumulations across the southwestern Barents Sea. These observations are also supported by the basin modelling work of Duran et al. (2013a and b).

Cedeño et al., 2021 analyzed the geochemistry and compositions of the solid organic matter constituents of more than 300 samples widely distributed across the southwestern Barents Sea to characterize the

* Corresponding author.
E-mail address: andres.f.cedenomotta@uis.com (A. Cedeño).

https://doi.org/10.1016/j.marpetgeo.2021.105343
Received 9 April 2021; Received in revised form 31 August 2021; Accepted 22 September 2021
Available online 1 October 2021

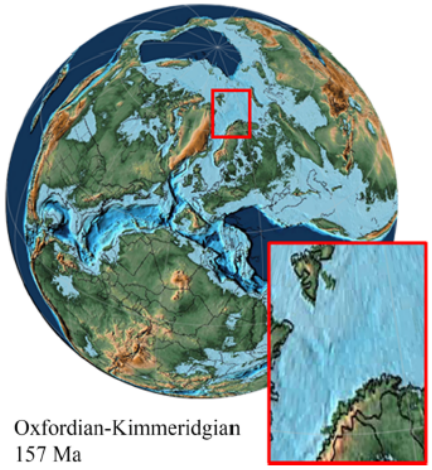

Fig. 1. Paleogeographic location of the Barents Sea within the northwestern European Shelf at the Oxfordian-Kimmeridgian boundary (Paleomap Project, Scotese, 2016).

depositional nature and organic facies variability within the Hekkingen Formation. This study recognized remarkably high contents of oil-prone amorphinite in the southern part of Bjørnøyrenna Fault Complex as well as a westwards enrichment in marine algae within the Hammerfest Basin, the latter being more pronounced within the Alge Member (Fig. 2). Their study also showed that the Hekkingen Formation in the Nordkapp Basin and the adjacent Bjarmeland and eastern Finnmark platforms contains mostly terrestrial-derived particles.

The generative potential of source rock kerogens depends essentially on the character of the primary biomass and dictates the gross composition of generated petroleum (Demaison and Moore, 1980; di Primio and Horsfield, 2006). Inherently, varying proportions of marine and terrestrial macerals reported within the Hekkingen Formation invokes heterogeneity in kerogen thermal stability and, importantly, in physicochemical properties of the generated petroleum. In this study, non-isothermal open-system pyrolysis is used for modeling bulk kinetic parameters of primary petroleum generation from fifteen samples chosen to capture the variability in organic facies, as defined by maceral compositions, within the Hekkingen Formation. Results from open pyrolysis-gas chromatography (Py-GC) and compositional kinetic models are employed to predict petroleum type and physical properties under increasing maturity. Additionally, the present study produces a map that illustrates the variation in kinetic parameters and predicted petroleum types generated from the natural maturation series of various organic facies across the southwestern Barents Sea. The results of this study can be readily implemented in basin and petroleum system studies of the Barents Sea and other basins alike.

2. Structural setting and stratigraphy

The western Barents Sea is divided into several basins (Hammerfest, Tromsø, Bjørnøya, Nordkapp, Fingerdjupet), platforms (Bjarmeland and Finnmark), and structural highs (Loppa and Central highs and Samson and Svalis domes) separated by major fault complexes (Troms-Finnmark, Ringvassøy-Loppa, Asterias, Bjørnøyrenna, Nysleppen and Hoop) (Fig. 2; Clark et al., 2014; Blaich et al., 2017; Indrevær et al., 2017; Mulrooney et al., 2017; Serck et al., 2017; Kairanov et al., 2019; Faleide et al., 2019; Tsikalas et al., 2021). Long term Cenozoic uplift in the greater Barents Sea has resulted in net erosion values that vary from 0 to more than 3000 m (Riis, 1996; Doré et al., 2000; Cavanagh et al., 2006; Henriksen et al., 2011b).

The geological evolution and deposition of Middle Jurassic to Lower Cretaceous successions within the western Barents Sea was largely controlled by a global eustatic sea level rise and renewed tectonic activity (Sund et al., 1986; Berglund et al., 1986; Faleide et al., 1993; Gernigon et al., 2014; Serck et al., 2017; Rojo et al., 2019; Kairanov et al., 2021). Development of an epicontinental sea and intensified organic carbon productivity during the Late Jurassic allowed for deposition and burial of organic rich sediments over vast areas of the continental shelf. These clastic sediments are collectively referred to as the Hekkingen Formation (Norwegian Petroleum Directorate, https://www.npd.no/en/). This formation has an unconformable basal contact with rocks of the Fuglen Formation, although it may locally grade to a conformable surface, and unconformably underlies the Lower Cretaceous units along the regionally extended Base Cretaceous Unconformity (Århus, 1991; Bugge et al., 2002; Marín et al., 2018; Wierzbowski and Smelror, 2020).

The sedimentary character of the Hekkingen Formation changes from a black shale-dominated succession at the base to a silt-dominated succession at the top, and is, therefore, subdivided into the Alge and Krill members, respectively (Dalland et al., 1988; Mørk et al., 1999). Based on palynological data, Dalland et al. (1988), Georgiev et al. (2017), Mørk et al. (1999), and Smelror et al. (2001) estimate an Oxfordian to Kimmeridgian age for the lower Alge Member and a Kimmeridgian to Ryazanian age for the upper Krill Member.

The Alge Member ranges in thickness from 35 m in the Hammerfest Basin to up to 185m (well 7129/8-1-s) in the Bjørnøyrenna Fault Complex (Mørk et al., 1999; Marín et al., 2020; Cedeño et al., 2021). These black shales are largely associated with deposition in an oxygen-depleted shelf (Mørk et al., 1999), but short phases of more oxygenated bottom water conditions have also been recognized. The Krill Member displays higher variations in thickness, from absent in some wells in the southwestern Barents Sea (e.g. 7120/2-3s) to over 600 m within the Bjørnøyrenna Fault Complex (Marín et al., 2020). These sediments were deposited in a wide range of bathymetric conditions ranging from a shallow shelf to deep marine environments (Mørk et al., 1999; Marín et al., 2020; Helleren et al., 2020). Marín et al. (2020) interpret the Krill Member to have been deposited during a more tectonically active period.

Total organic carbon data shows that the main section of enhanced organic richness occurs within the lower Alge Member (Henriksen et al., 2011a, 2011b; Marín et al., 2020; Cedeño et al., 2021). Hydrogen indices (HI) from 50 to 430 mg hydrocarbon per gram TOC (50–430 mg HC/g TOC) are recorded for Alge and Krill immature samples, which are typically associated with kerogen assemblages ranging from III to II. This suggests that both the Alge Member and the more discrete organic-rich Krill Member possess similar generative potential (Ohm et al., 2008; Henriksen et al., 2011a, 2011b; Cedeño et al., 2021). HI values in the central-western Hammerfest Basin and the Bjørnøyrenna Fault Complex are low owning to high thermal maturity. Cedeño et al., 2021 estimate an original HI value of 400 and at least 500 mg HC/g TOC for the Hekkingen members in these areas, respectively, which are consistent with Type II kerogens.

3. Samples and methods

A total of 235 cuttings and core samples from the Hekkingen Formation were collected from 35 oil and stratigraphic (i.e. IKU stratigraphic Drilling Projects) wells distributed across the southwestern areas of the Barents Sea (Fig. 2). All samples were obtained from the Norwegian Petroleum Directorate (NPD) and SINTEF well repositories.

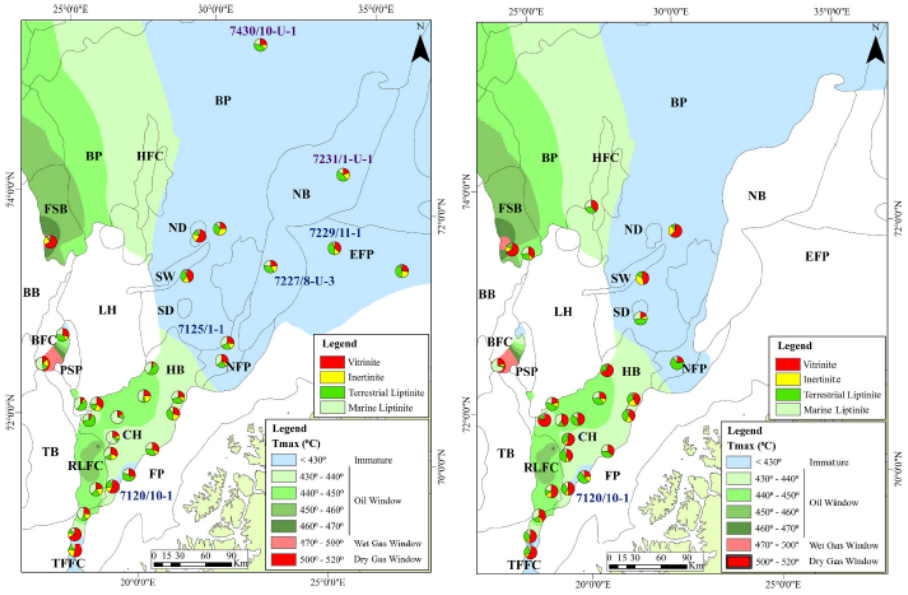

Fig. 2. Map of the southwestern Barents Sea illustrating the variability in maceral compositions within the Alge (A) and Krill (B) members across the various geological provinces. The pie diagrams represent the average (i.e. per well) maceral compositions calculated from the microscopic analysis in Cedeño et at. (2021). Relevant wells used in this study are shown (See Table 1). A present-day maturity overlay of the Hekkingen Formation calculated from Tmax Rock-Eval data is also displayed. BP= Bjarmeland Platform, HFC= Hoop Fault Complex. MB = Maud Basin, MH = Mercurius High, NB= Nordkapp Basin, EFP = eastern Finnmark Platform, ND= Norvarg Dome, SG= Swaen Graben, SD= Samson Dome, FSB= Fingerdjupet Sub-basin, BB= Bjørnøya Basin, BFC= Bjørnøya Fault Complex, PSP= Polhem Sub-platform, LH = Loppa High, NFC= Nysleppen Fault Complex, HB= Hammerfest Basin, CH= Central High, RLFC = Ringvassøy-Loppa Fault Complex, TB = Tromsø Basin, FP= Finnmark Platform, TFFC = Troms-Finnmark Fault Complex.

The sampled intervals were selected based on the stratigraphic boundaries of the Hekkingen Formation as defined by the NPD and preexisting geochemical results from well completion reports.

In an initial phase, samples underwent TOC and Rock-Eval analysis. Aliquots of each sample were pulverized and subdivided in two. The TOC content was quantified with a LECO SC-632 combustion oven tuned

Table 1
Sample information, whole rock and maceral composition, and bulk source rock geochemical results (i.e. Rock-Eval and TOC) of the fifteen studied samples. These samples were selected from a regional study documented in Cedeño et al., 2021.

ID	Well	Depth	Sample	Whole rock composition %						Maceral composition %				TOC	HI	Tmax
		m	type	Clay	Quarzt	Sulfides	Carbonates	Bitumen	Macerals	Mar. Lip	Terr. Lip	Inertinite	Vitrinite	%	mgHC/gTOC	°C
A	7120/10-1	1455	Cuttings	23	56	6	0	7	6	2	33	9	55	5.4	226	426
B	7120/10-1	1467	Cuttings	46	25	12	1	11	6	9	25	11	55	6.2	171	422
C	7120/10-1	1482	Cuttings	51	11	8	1	16	12	41	19	6	35	6.7	243	426
D	7125/1-1	1355	Cuttings	57	14	13	0	9	8	0	53	8	39	8.3	313	425
E	7125/1-1	1368	Cuttings	75	14	5	0	5	1	0	20	5	76	2.2	115	432
F	7125/1-1	1380	Cuttings	45	15	7	0	10	23	52	0	15	33	15.5	304	423
G	7125/1-1	1392	Cuttings	44	11	11	0	7	26	8	49	21	21	16.5	313	423
H	7220/5-2	1441	Cuttings	53	33	6	0	5	4	66	14	4	17	2.4	378	425
I	7227/8-U-3	39.9	Core	55	10	8	1	8	18	23	54	10	13	18.6	192	403
J	7227/8-U-3	44.0	Core	59	14	3	0	4	20	0	61	22	17	15.8	248	406
K	7227/8-U-3	48.78	Core	46	9	8	2	12	24	70	21	6	3	21.1	258	408
L	7229/11-1	1260	Cuttings	44	28	5	0	6	17	0	42	19	40	12.6	282	424
M	7231/1-U-1	65.5	Core	63	5	2	1	10	19	35	58	0	6	12.2	230	414
N	7430/10-U-1	44.1	Core	51	9	3	4	15	18	53	47	0	0	23.0	353	420
O	7430/10-U-1	46.95	Core	44	9	5	3	10	29	0	73	27	0	16.3	306	416

to an IR-detector. Rock-Eval pyrolysis was performed using a Rock-Eval 6 instrument, allowing direct measurement of free hydrocarbons (S_1), remaining hydrocarbon generative potential (S_2), carbon dioxide (CO_2) content produced during thermal cracking (S_3), and temperature of S_2 maxima (T_{max}) (Espitalié et al., 1977). All samples were also subjected to organic and mineral petrographic analysis following the methods described in Cedeño et al., 2021. Fifteen thermally-immature source rocks samples representing the most common maceral assemblages were selected for artificial maturation experiments (Table 1). To ensure thermal immaturity, sample selection was limited to wells drilled near structural highs (i.e. wells 7231-1-U-1, 7227/8-U-3, 7125/1-1) or well sections interpreted to have experienced significant organic matter dilution (i.e. well 7120/10–1; see Fig. 4 in Cedeño et al., 2021). Where available, core material was prioritized over cuttings.

Open-system pyrolysis-gas chromatography (Py-GC) was performed using a HP5890 II instrument with an MSSV injector and an FID. The column is a HP-1 (length 50 m, i.d. 0.32 mm, film thickness 0.52 μm) and the injector unit is from Margot Köhnen-Willsch Chromatographie & Software. An open sample tube containing 20 mg of pulverized whole rock was placed in the system injector at a preheated temperature of 300 °C and volatile compounds evaporated before the pyrolysis oven was closed. The oven temperature was increased to 600 °C at a rate of 25 °C/min. The pyrolysis products were collected in a liquid nitrogen-cooled trap for 10 min before being released into the GC column, whereupon there were released at an initial temperature of 40 °C (held 13 min), heated to 300 °C at 5 °C/min (held 25 min), and finally increased to 320 °C at 5 °C/min (held 10min). The pyrolysates were monitored on-line using a HP-1 capillary column (length 50m, i.d. 0.32 mm, film thickness 0.52 μm) on the GC that was equipped with a flame ionization detector (FID). Boiling ranges (C1, C2–C5, C6–C14, C15+) and individual compounds (n-alkenes, n-alkanes, alkylaromatic, and alkylthiophenes) were quantified using n-butane as an external standard. Response factors for all resolved compounds were assumed to be the same. In the case of methane, a response factor of 1.1 was assumed according to di Primio et al. (1998).

To constrain bulk kinetic parameters of primary kerogen to petroleum transformation, the 15 samples were subjected to non-isothermal open-system pyrolysis at five different heating rates (1 °C/min, 2 °C/min, 5 °C/min, 15 °C/min, 25 °C/min) using a Rock-Eval 6 instrument. Kinetics05 software from Lawrence Livermore National Laboratory (Burnham et al., 1987) was used to calculate a discrete activation energy distribution (E_A) and the frequency factor (A).

Non-isothermal, closed system pyrolysis-gas chromatography using micro-scaled sealed vessels (MSSV Closed-System Pyrolysis) was used for compositional kinetic modeling following the approach described by Horsfield et al. (1989) and Dieckmann and Keym (2006). Milligram amounts of five selected samples were sealed in glass capillary tubes (five tubes per sample) and heated at a single heating rate (0.7 °C/min) to final temperatures corresponding to preselected transformation ratios (10%, 30%, 50%, 70% and 90%). The temperatures corresponding to the selected transformation ratios were determined by simulated heating of the bulk kinetics parameters, as estimated from the Rock-Eval pyrolysis data, at the specified heating rate. The sample tubes were placed in the injector system and then broken when pressure had stabilized after 4 min. The composition of the generated hydrocarbon products was analyzed by thermovaporisation-gas chromatography (Tvap-GC) as described above. Compositional models with two (oil and gas), four (C_1, C_2–C_5, C_6–C_{14} and C_{15+}), and fourteen (C_1, C_2, C_3, i-C_4, n-C_4, i-C_5, n-C_5, pseudo-C_6, C_7–C_{15}, C_{16}–C_{25}, C_{26}–C_{35}, C_{36}–C_{45}, C_{46}–C_{55}, C_{56}–C_{80}) components were developed.

For prediction of petroleum physical properties such as saturation pressure (P_{sat}), gas to oil ratio (GOR), and formation volume factor (B_o), the Phase Kinetics approach by di Primio and Horsfield (2006) was followed. The estimation of petroleum phase was carried out using the fluid description consisting of 14 components, seven in the gas range (C_1, C_2, C_3, i-C_4, n-C_4, i-C_5, n-C_5) and seven in the liquid range (pseudo-C_6, C_7–C_{15}, C_{16}–C_{25}, C_{26}–C_{35}, C_{36}–C_{45}, C_{46}–C_{55}, C_{56}–C_{80}; di Primio and Horsfield, 2006).

The composition of pyrolysis gases differs substantially from natural gas (Mango, 1996, 2000, 2001). The most important difference is the comparably low content of methane in gases derived from pyrolysis experiment (di Primio and Horsfield, 2006). Methane is known to have the highest impact on the phase behavior (di Primio et al., 1998; di Primio and Skeie, 2004) and, therefore, its relative abundance needs to be corrected following the approach by di Primio and Horsfield (2006). The correcting procedure consisted in iterative adjustment of the methane to wet gas ratio, assuming decreasing gas wetness ratio for increasing transformation ratio, and shifting of the trends of P_{sat} against GOR and P_{sat} against B_o closer to the linear trends typically observed in natural petroleum systems (di Primio and Horsfield, 2006). The properties of the C_{7+} lumped fractions were then calculated from the corresponding properties for C_7 to C_{80} single carbon number groups by mass weighted averaging as described by Pedersen et al. (1985). The tuned component descriptions from MSSV closed-system pyrolysis were combined with the bulk kinetic model from open-system pyrolysis. The 14 components were allocated to the non-zero reaction weights from the bulk kinetic model, so that simulation of the resultant 14-component kinetic model best-fits the MSSV data. A coordinate-wise stochastic search algorithm (Zabinsky et al., 1993; Zabinsky, 1998) was used to compute a least-squares best-fit of the compositional kinetic model to the tuned compositional descriptions.

It is instructive to highlight that the accurate prediction of natural fluid properties is limited by the fundamental difference between the bulk composition of naturally generated petroleum and that of kerogen pyrolysates regardless of kerogen type or pyrolysis techniques (Karlsen and Larter, 1991; Larter and Horsfield, 1993; Horsfield, 1997). Natural oils are hydrocarbon-rich systems, while pyrolysates consist of comparatively higher proportions of aromatic and polar compounds (Urov, 1980; Castelli et al., 1990; Karlsen and Larter, 1991).

4. Results

4.1. Rock-Eval, TOC, and maceral assemblages

The TOC contents of the fifteen source rock samples selected for artificial maturation experiments range from 2.2 to 23 wt% with HI values in the range of 115–378 mg HC/g TOC (Table 1). High HI values are mostly associated with elevated TOC contents, while comparatively lower HI values correspond to low TOC contents (Fig. 3A). Sample H from well 7220/5-2 has a HI value of 378 mg HC/g TOC paired with a relatively low TOC content of 2.4% and, therefore, deviates from the main trend. When plotted on the pseudo-Van Krevelen diagram, the HI data indicates the presence of various proportions of mixed kerogen types II and III (Fig. 3B).

The investigated samples have not reached thermal stress levels required for petroleum generation and expulsion as indicated by their T_{max} Rock-Eval temperatures that are mostly equal or lower than 426 °C (Table 1). A T_{max} value of 432 °C was reported for sample E; however, based on its high relative abundances of thermally stable vitrinites (Table 1), it is interpreted to retain most of the original generative potential. Thus, the variations in TOC, HI, and maceral composition are expected to be primarily related to organic facies. This study did not find any detectable changes in the pyrolysis-gas chromatography data resulting from maturity variations in the sample set (i.e. T_{max} = 403–432 °C) that may affect the interpretations.

The maceral composition of the investigated samples comprises a wide range of assemblages ranging from terrestrial dominated (i.e. vitrinite and terrestrial-derived liptinite) to marine dominated (i.e. marine-derived liptinite) (Table 1). Fragments of detrovitrinite and primary vitrinite constitute the bulk of the vitrinite group, whereas sporinite, and only occasionally cutinite and resinite, predominates in the terrestrial liptinite sub-group. The marine liptinite sub-group consists mainly of

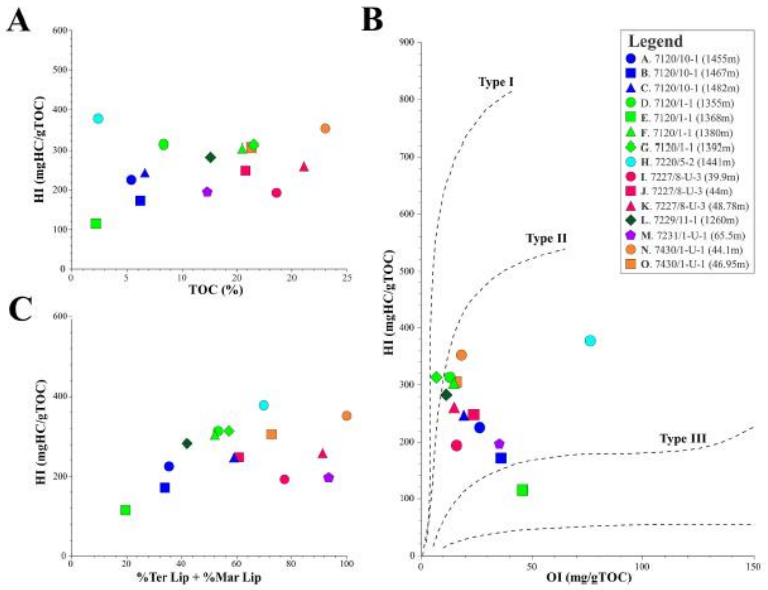

Fig. 3. Total organic carbon (**A**), oxygen index (**B**), and liptinites (**C**) versus hydrogen index cross-plots of studied samples. Maturation pathways for the three main kerogen types in plot B are shown after Cornford (1998).

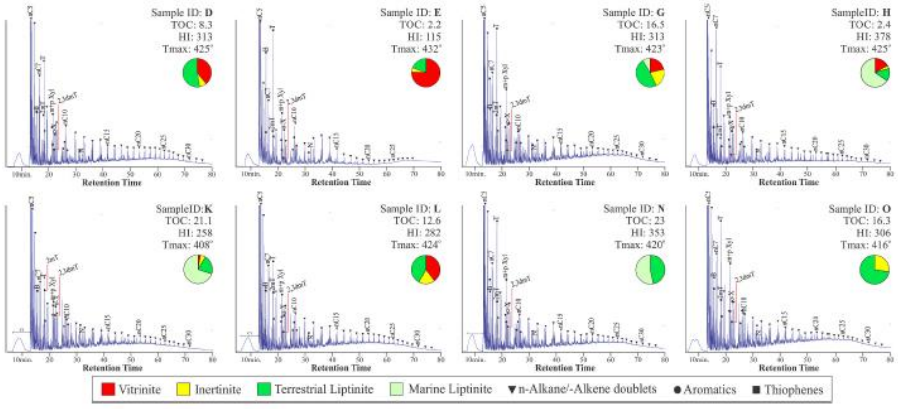

Fig. 4. Representative pyrolysis–gas chromatograms of eight selected source rocks samples. B = benzene, T = toluene, 2 mT = 2-methyl-thiophene, m + p xylene = meta + para-xylene, 2,3dmT = 2,3 dimethyl-thiophene, o-X = ortho-xylene, N = naphthalene. TOC = total organic carbon - wt%; HI = hydrogen index – mgHC/gTOC; Tmax = Tmax Rock-Eval - °C.

alginite particles (i.e. lamalginite, tasmanites, dinoflagellates). Only sample H contains elevated amounts of amorphinite, a marine kerogen maceral known to possess a high oil-proneness. A positive correlation between HI and liptinites is shown in Fig. 3C. The low to only modestly high hydrogen richness in the studied samples is coincident with the elevated inputs of autochthonous terrestrial inputs (see Cedeño et al., 2021).

4.2. Predicted petroleum type from Py-GC

Open system pyrolysis gas chromatography (Py-GC) was conducted on fifteen selected samples with distinctive maceral assemblages (Table 1) to characterize the macromolecular composition of kerogen pyrolysates and predict the generated petroleum types. Boiling ranges for C_1, C_2–C_5, C_6–C_{14} and C_{15+} and individual compounds were quantified up to n-C_{32} for most of the sample set (Fig. 4). Straight-chain aliphatic hydrocarbons, i.e. n-alkane/n-alkene doublets, dominate the pyrolysate. There is a systematic decrease in abundance of n-alkane/n-alkene doublets with increasing carbon number in the Py-GC traces. The precursors of aliphatic hydrocarbons in the source rock kerogens could be lipids inherited from aliphatic biopolymers (Tegelaar et al., 1989) or lipids incorporated through either condensation reactions (Tissot and Welte, 1984) or quenching of labile functionalized lipids with inorganic sulfur acting as a reactant during early diagenesis (Sinninghe Damste et al., 1989).

Besides aliphatic hydrocarbons, the most prominent individual compounds in the pyrolysate are, in descending order, mono-aromatic hydrocarbons (i.e. benzene, alkylbenzenes, trimethylbenzenes), sulfur-containing compounds (i.e. mostly alkylated thiophenes), and di-aromatic hydrocarbons (i.e. naphthalenes and methylnaphthalenes) (Fig. 4). Relatively high abundance of mono-aromatic hydrocarbons is often linked with terrestrial organic inputs (Tissot and Welte, 1984; Horsfield et al., 1992). In this study, such an assertion is supported by the relative abundance of toluene being greater than the C_7 n-alkyls in the more terrestrially-influenced samples (Fig. 4E), but are of similar or lower abundance in the marine liptinitic samples (Fig. 4H). Other mono-aromatic compounds such as benzene and meta + para-xylene sometimes occur in greater abundance than n-alkyls of the same carbon numbers. The most and least prominent thiophene compounds are 2-methyl-thiophene and 2,3-dimethylthiophene, respectively, but these are overall less abundant than the corresponding n-alkyls.

The amount of thiophenes generated during thermal degradation of kerogen under open-system pyrolysis can be used to assess the organic sulfur content of the organic matter (Eglinton et al., 1990). The ternary diagram in Fig. 5A uses a sulfur-bearing (i.e. 2,3-dimethylthiophene), an aromatic (i.e. ortho-xylene) and an aliphatic compound (i.e. n-alkene n-C9:1) for discriminating between freshwater lacustrine (Type I), terrestrial (Type III), clay-rich marine (Type II) and sulfur-containing carbonated environments (Type IIS). Twelve of the pyrolyzed samples yield varyingly low amounts of sulfur-bearing compounds, whereby they plot in the sulfur-poor kerogen type II and III fields. Kerogen pyrolysates falling in the kerogen type II field typically contain 50% by volume liptinitic macerals, either marine or terrestrial, and HI values generally higher than 250 mg HC/g TOC (Table 1). The pyrolysate products from sample E plot well into the kerogen type III field. This is consistent with the high concentrations of humic kerogen of a vitrinitic nature (i.e. 76%) and the very low HI value of 115 mg HC/g TOC (Table 1).

The kerogen pyrolysates of samples J, K, and L possess higher sulfur contents as compared to the other samples and plot in, or close to, the type IIS field (Fig. 5A). Pyrolysates with this relatively high thiophenic sulfur abundance are typically associated with clay-poor source rocks containing sulfur-rich kerogens (i.e. type IIS; Tissot et al., 1987; Eglinton et al., 1990; Braun et al., 1991; Tegelaar and Noble, 1994; Schaeffer et al., 1995; Orr, 1986; di Primio and Horsfield, 1996; Hartwig et al., 2012). The clastic mineralogy reported for these samples (Table 1) fails to support the composition derived from their pyrolysates. It is possible that the elevated concentration of 2,3-dimethylthiophene resulted from the early elimination of organically-bound sulfur occurring naturally in some terrestrial-derived materials (Eglinton et al., 1990, 1992). Alternatively, such a high concentration of thiophenic sulfur could originate from diagenetic incorporation of inorganic sulfur into unsaturated and functionalized lipids in the kerogen (i.e. sulfurization; Kaplan et al., 1963; Sinninghe Damste et al., 1989; Tegelaar et al., 1989; Eglinton et al., 1992).

The n-alkyl chain length distribution derived from source rocks during open system pyrolysis can be used to predict the likely petroleum types they generate throughout the entire natural maturation sequence (Horsfield et al., 1989; Horsfield, 1997). The ternary plot in Fig. 5B employs the total light gas fraction (i.e. Σ nC_1-C_5) and the intermediate (i.e. Σ n-C_6-C_{14}) and long-chained (i.e. Σ n-C_{15+}) n-alkyls to discriminate paraffinic (low and high wax varieties), paraffinic-naphthenic-aromatic (P–N-A) (low and high wax varieties), and the gas & condensate petroleum generating potentials. Based on the n-alkyl chain length distribution, most of the investigated samples are predicted to generate gross pyrolysates that fall within the Low Wax P–N-A oil generating facies.

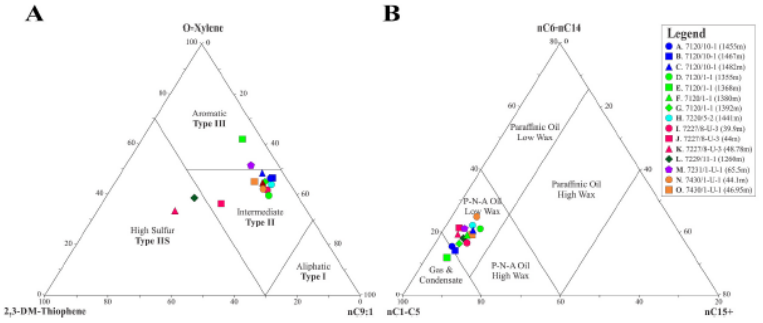

Fig. 5. A. Ternary diagram of n-C9 alkene (n-C9:1), ortho-xylene (O-Xylene), and 2,3 dimethyl-thiophene (2,3-DM-Thiophene) used for kerogen classification according to Eglinton et al. (1990). **B.** Ternary diagram of total C1–C5, C6–C14, and Σ n-C15+ n-alkanes + n-alkenes used for petroleum type prediction according to Horsfield et al. (1989).

Samples plotting well into the Low Wax P–N-A oil facies are compositionally rich in liptinitic particles. Only sample E plots in the gas and condensate field, whereas samples A and B plot on, or near, the boundary between the gas & condensate and Low Wax P–N-A fields. The higher proportions of short chained compounds in these samples are consistent with their high vitrinite contents and low HI values of 115, 171, and 225 mg HC/g TOC, respectively.

4.3. *Kinetic models of bulk petroleum generation*

Bulk kinetics analysis using non-isothermal open-system pyrolysis was performed to model the kinetic parameters, i.e. activation energy distribution and frequency factor, of bulk petroleum generation. The majority of the computed kinetic models show activation energies in the range of 45–70 kcal/mol (Table 2), with a gaussian-like shape (Fig. 6) commonly associated with marine-influenced kerogens (Braun et al., 1991; Tegelaar and Noble, 1994). This broad E_A reflects large variability in the composition of the organic constituents, intrinsically comprising a wide spectrum of chemical bond types and strengths. Associated frequency factors range between 2.80E+13/s and 1.96E+16/s (Table 2). The sample set was divided into three sub-sets according to the volumetrically predominant maceral (i.e. marine liptinites, terrestrial liptinites, vitrinites) and an average E_A distribution was computed for each sub-set. The average E_A distributions are displayed in Fig. 7 for the purpose of comparing the variability in activation energies linked to maceral compositions.

It is generally accepted that marine-rich kerogens often require lower activation energies than do terrestrial-rich kerogens (i.e. type II kerogen versus type III kerogens) to generate petroleum. This organic matter dependance in the present study is reflected in the fact that the lowest activation energy distributions occur in samples containing high relative abundances of marine liptinites, and increase gradually with increasing contents of terrestrial macerals (Fig. 6; Table 2). Samples K, H, and N, in which liptinites of marine origin account for 70%, 66% and 53%, have peak activation energies at 52 kcal/mol, 53–54 kcal/mol and 54 kcal/mol, respectively.

The more terrestrially influenced samples G, D, and E have activation energy maxima at 58 kcal/mol, 59 kcal/mol, and 60–61 kcal/mol, respectively (Fig. 6). The organic fraction (i.e. kerogen) in samples E and G is predominantly composed of vitrinite and terrestrial liptinite, respectively, while the kerogen in sample D has an intermediate composition. In comparing their maceral composition and their activation energy distributions, it is apparent that the vitrinite-rich sample requires slightly higher activation energies than the liptinite (terrestrial)-rich sample. This is further substantiated by Fig. 7 in which activation energy distributions of other vitrinitic kerogens in the sample set show dominant peaks between 59 and 61 kcal/mol compared to maxima between 56 and 59 kcal/mol recorded for the terrestrial liptinitic kerogens. It is interesting to note that the activation energy distribution of the more terrestrially influenced samples is overall broader than the more marine influenced samples. These observations reflect the more heterogeneous molecular composition of terrestrial organic matter compared to the marine organic matter (Tissot et al., 1987; Reynolds and Burnham, 1995; Schenk et al., 1997; Petersen and Rosenberg, 2000).

The low range of activation energies in sample L is an oddball among the data set. This sample is exclusively composed of terrestrial macerals yet exhibits a peak activation energy at 52 kcal/mol, 53 kcal/mol, and 54 kcal/mol (Fig. 6). This attribute could be the result of inorganic sulfur incorporation in reducing kerogen stability, as discussed in section 4.2.

4.4. *Petroleum formation and timing predictions*

The derived kinetic parameters provide the basis to estimate the temperatures of bulk petroleum generation and corresponding transformation ratio (TR; Fig. 8). A constant heating rate of 3.3 °C/Ma was assumed to extrapolate to geological heating conditions. The variability described in activation energy distributions and frequency factors is manifest in the temperatures at which the onset and peak petroleum generation occur. In Fig. 8, the onset of significant petroleum generation (10% TR) from least to most thermally stable kerogen varies from 123 °C to 144 °C. This temperature difference of up to 21 °C equates to a difference of up to 700m of burial if a geothermal gradient of 30 °C is assumed. These relatively high and different orders of thermal stability are consistent with the previously discussed mixtures of terrestrial and marine organic materials. A similar temperature range of 25 °C is observed at the peak of petroleum generation (i.e. 70 % TR), reflecting the involvement of relatively similar cracking reactions and conversion rates with increasing thermal stress regardless of the samples' different activation energy distributions and frequency factors.

The onset and peak petroleum generation from the more marine-influenced source rocks K, H, and N is predicted to occur at the lowest temperatures of 123 °C and 150 °C, respectively (Fig. 8). The early, low-temperature generation in these samples seems to be related with the

Table 2
Bulk kinetic parameters (i.e. activation energies and frequency factors) of the fifteen studied samples.

ID	A	B	C	D	E	F	G	H	I	J	K	L	M	N	O
Well	[illegible]	[illegible]	[illegible]	[illegible]	[illegible]	[illegible]	[illegible]	[illegible]	[illegible]	[illegible]	[illegible]	[illegible]	[illegible]	[illegible]	[illegible]
Depth	1435	1467	1482	1355	1368	1380	1392	1441	58.9	44	48.75	1760	65.5	44.1	47.08
A (s-1)	6.4058E+15	1.7117E+16	5.5906E+14	7.5211E+15	1.2766E+16	1.4940E+15	5.2815E+15	1.3700E+14	1.3120E+16	2.9104E+15	2.8073E+13	1.3340E+14	1.9602E+16	3.2568E+14	1.7877E+15
Ea (kcal/mol)															
40	0.0	0.0			0.1					0.0					
41	0.0	0.0			0.0					0.0					
42	0.0	0.0			0.0					0.0				0.0	
43	0.0	0.0			0.0					0.0	0.0			0.0	
44	0.0	0.0			0.0			0.0		0.1	0.0			0.0	
45	0.0	0.0	0.0		0.0			0.4		0.0	0.1			0.0	
46	0.0	0.1	0.0		0.0			0.5		0.0	0.0			0.0	
47	0.0	0.0	0.0		0.1			0.7		0.2	0.9			0.2	
48	0.0	0.0	0.2	0.0	0.0			0.7		0.0	0.9			0.2	
49	0.0	0.0	0.1	0.0	0.0	0.0		2.2		0.4	1.5			0.0	
50	0.1	0.1	0.0	0.1	0.1	0.1	0.0	0.5		0.5	8.8			0.6	0.0
51	0.0	0.0	0.5	0.0	0.3	0.1	0.0	4.8		1.2	19.2	0.0	0.0	2.8	0.7
52	0.3	0.3	0.3	0.1	0.0	0.0	0.2	4.9		1.7	29.5	24.0	0.2	11.5	0.6
53	0.3	0.1	6.8	0.6	0.6	0.5	0.0	30.9	0.0	4.9	11.8	20.9	0.0	14.3	5.0
54	0.0	1.0	14.7	0.0	0.4	6.0	0.0	31.2	1.2	7.9	12.3	25.1	1.6	26.2	11.9
55	0.9	0.2	25.2	0.4	1.1	16.6	1.3	11.6	2.9	15.1	6.9	10.6	1.9	19.5	9.1
56	2.6	2.9	20.3	0.4	1.9	22.5	8.4	5.4	10.8	18.6	1.2	10.9	5.9	10.2	23.8
57	10.4	6.1	14.4	8.1	4.2	19.5	17.8	4.3	17.3	21.3	2.5	8.1	10.2	7.2	18.1
58	19.6	12.8	7.6	17.4	6.9	13.5	22.3	1.7	19.1	15.6	1.6	5.9	14.9	1.2	11.0
59	21.6	18.8	2.3	23.4	13.0	8.6	17.9	0.1	18.1	6.2	0.2	0.7	18.9	2.6	4.6
60	17.1	20.2	6.3	17.6	18.8	5.0	11.2	0.0	13.0	4.2	0.7	0.7	23.3	0.5	1.8
61	11.8	15.8	0.2	14.0	17.9	1.6	8.3	0.0	7.4	1.6	0.0	0.7	13.5	1.4	1.3
62	3.7	10.3	1.4	7.3	13.5	4.0	4.2	0.0	4.4	0.1	0.0	0.1	3.8	0.0	0.9
63	4.4	4.8	0.1	1.7	8.3	0.2	1.7	0.6	1.3	0.4	0.0	0.2	1.4	0.8	0.3
64	4.4	2.0	0.6	5.8	4.5	1.1	4.0		2.4	0.0	2.1	0.0	1.5	0.1	0.4
65	0.0	3.3	0.0	0.0	1.5	0.3	0.4		0.5	0.0		0.0	0.1	0.1	0.0
66	1.0	0.9		1.3	3.3	0.0	0.8		0.5	0.0		0.2	0.4	0.5	0.3
67	0.5	0.2		0.9	0.6	0.1	0.7		0.5	0.0			0.0	0.0	0.0
68	0.0	0.0		0.0	0.0	0.1	0.0		0.0	0.0			0.1	0.0	0.0
69	0.1	0.5		0.0	0.8	0.4	0.0		0.0	0.0			0.2	0.0	0.0
70	0.5			0.3			0.4		0.5				0.0		0.3
71	0.0			0.0			0.0		0.1				0.0		
72	0.0			0.9			0.4		0.2				0.0		

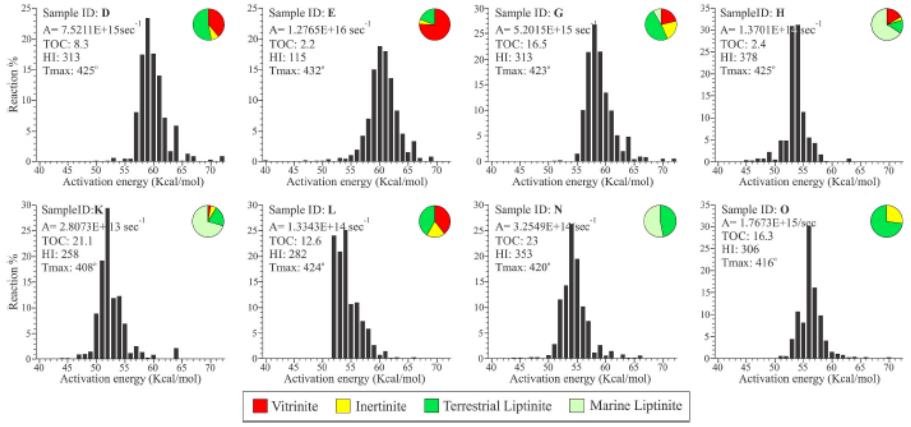

Fig. 6. Activation energy distribution of eight selected source rock samples. Pie diagrams represent the maceral composition of the corresponding sample. TOC = total organic carbon - wt%; HI = hydrogen index – mgHC/gTOC; Tmax = Tmax Rock-Eval - °C.

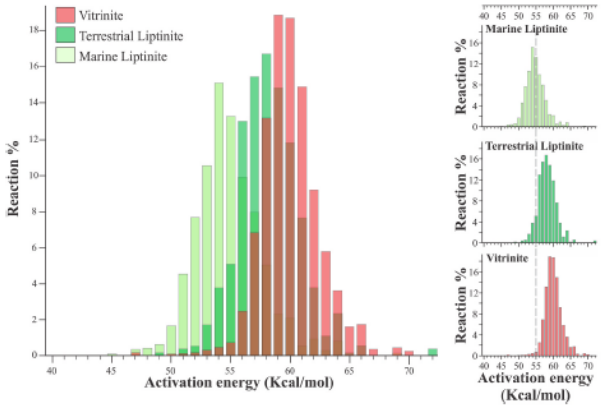

Fig. 7. Average activation energy distributions computed according to the volumetrically predominant maceral (i.e. marine liptinites, terrestrial liptinites, vitrinites) in each sample. Vitrinite subset = A, B, E; terrestrial liptinite subset = D, G, I, J, M, N; marine liptinite subset = C, F, H, K, N.

abundance of thermally labile marine particles. Sample K, interpreted to be enriched in thiophenic sulfur according to Fig. 5A, reaches onset and peak generation at temperatures within the same range as the other two sulfur-poor source rocks. This indicates that in this particular case sulfur richness has a minor impact on the timing of petroleum formation. Kinetic information from an average Type II North Sea (Tegelaar and Noble, 1994) and Type IIS source rock from the Campeche Basin (Santamaria Orozco, 2000) are plotted in Fig. 8 for comparison purposes.

Petroleum generation from source rock samples dominated by terrestrial macerals takes place at higher temperature ranges relative to marine-influenced sources. The onset of generation is predicted to occur at temperatures ranging from 139 °C for sample G to 144 °C for sample E (Fig. 8). The gas and condensate-prone sample E displays the highest stability at 70 and 90% conversion (i.e. generating petroleum up to 190 °C) as well as the broadest temperature range of generation. This demonstrates the slower conversion rates typically associated with vitrinitic type III kerogens.

In the case of the sulfur-rich L and J source rock samples, onset and peak generation occur at least 10 °C earlier than in other samples containing comparable maceral assemblages (Fig. 8). This generation at relatively low levels of maturity could be attributed to the break-down of weak carbon-sulfur bonds under less intense thermal stress (i.e. Orr, 1986; Tissot et al., 1987; di Primio and Horsfield, 1996; Van Dongen et al., 2003). The apparent lack of front-end activation energies in

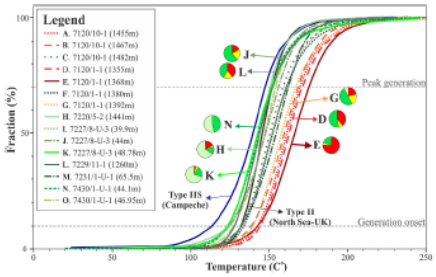

Fig. 8. Transformation rate curves calculated from bulk kinetic models of the sample set. A geological heating rate of 3.3 K/Ma is assumed. Relevant samples discussed in the text and corresponding kerogen compositions are displayed. The main petroleum generation events are shown. Transformation rate curves for a typical North Sea Type II kerogen (Tegelaar and Noble, 1994) and Type IIS kerogen from the Campeche Basin (Santamaria Orozco, 2000) are plotted for comparison purposes.

sample L (Fig. 6) implies that petroleum generation may have commenced at subsurface temperatures equivalent to Tmax values ≤ 424 °C (Table 1).

4.5. The PhaseKinetics approach: compositional kinetic models and fluid physical properties

The PhaseKinetics approach as defined by di Primio and Horsfield (2006) provides the basis to predict the compositional evolution and the physical properties (i.e. GOR, Bo, and Psat) of the generated fluids with increasing maturity. The five samples for MSSV-Py-GC-FID experiments were selected to represent most of the variability in maceral assemblages and kinetic parameters across the broader sample set. Three compositional models were constrained based on two components (C_1–C_5 and C_{6+}), four components (C_1, C_2–C_5, C_6–C_{14}, and C_{15+}), and 14 components (C_1, C_2, C_3, i-C_4, n-C_4, i-C_5, n-C_5, n-C_6, C_7–C_{15}, C_{16}–C_{25}, C_{26}–C_{35}, C_{36}–C_{45}, C_{46}–C_{55}, and C_{56}–C_{80}) (Table 3). The compositional kinetic models with 14 components are presented in Fig. 9.

Table 3
Compositional kinetic models with 2, 4, and 14 components calculated for five selected samples. Potentials are shown in weight percentage (wt-%).

ID	D	H	L	N	O
Well	7125/1-1	7220/5-2	7229/11-1	7430/10-1-3	7430/10-1-3
Depth	1355 m	1441 m	1260 m	44.1 m	46.95 m
Oil	65.0	63.7	67.7	74.7	74.1
Gas	35.0	36.3	32.3	25.3	25.9
C1	13.1	14.1	12.1	9.9	9.6
C2-C5	21.9	22.2	20.2	15.4	16.3
C6-C15	44.9	45.4	42.9	43.4	47.7
C15+	20.0	18.3	24.8	31.3	26.4
C1	13.1	14.1	12.1	9.9	9.6
C2	5.8	6.4	5.4	4.4	4.0
C3	6.1	5.7	5.8	4.6	4.5
iC4	1.2	1.6	1.1	1.0	0.8
nC4	3.7	4.1	3.7	3.2	2.9
iC5	2.5	2.1	1.9	1.5	2.0
nC5	2.8	2.3	2.3	0.8	2.0
C6	4.2	3.9	3.7	3.8	4.0
C7-15	40.8	41.5	39.2	39.6	43.7
C16-25	16.5	15.7	20.3	23.0	20.3
C26-35	3.0	2.3	3.7	5.7	4.7
C36-45	0.5	0.3	0.7	1.8	1.1
C46-55	0.1	0.0	0.1	0.6	0.2
C56-80	0.0	0.0	0.0	0.3	0.1

Hydrocarbons with six or more carbons ($\geq C_{6+}$) comprise 63.7 to 74.7 wt% of the total pyrolysates (Table 3). The remaining pyrolysate yield is composed of gaseous hydrocarbons (C_1–C_5). These compositional attributes show that the studied samples are capable of generating fluid and, in less proportions, gaseous hydrocarbons. Source rock samples N and O from well 7430/10-U-1 have the highest liquid generative potential with 74.7 and 74.1 wt%, respectively, but possess different kerogen maceral compositions. The shallower sample contains about equal amounts of marine and terrestrial liptinites (53% and 47%, respectively), while the deeper sample contains mostly terrestrial liptinite (73%; Table 1). Samples D, L, and H generate comparatively lower proportions of liquid hydrocarbons (65, 67.7 and 63.7 wt%, respectively). Sample H features an elevated abundance of marine-derived liptinites (66%) and similar amounts of vitrinite and terrestrial liptinite, whilst samples D and L possess exclusively terrestrial macerals in comparable proportions.

The n-C_7–C_{35} fraction constitutes most of the liquid portion of these Low Wax P–N-A oils (Table 3). Nevertheless, a closer look at the 14-component compositional kinetic models reveals distinct generative potentials within the liquid fraction. The lighter C_7–C_{15} liquids in the least oil-prone samples D, H, and L account for 62.1, 67.6, and 69.7 wt% of the n-C_7–C_{35} compositional fraction compared to lower values of 58 and 63.6 wt% in the most oil-prone samples (i.e. N, O). A waxier character of the most oil-prone samples is also manifest in a relative enrichment in the heavier C_{26}–C_{35} and C_{36}–C_{80} potentials (Table 3).

Predicted GORs, P_{sat}, and B_o of petroleum fluids increase as a function of increasing TR in all cases (Fig. 10; Table 4). The H source rock sample exhibits the highest GORs at all transformation ratios (Fig. 10A). It generates black oils (GOR <350 standard m3/m3) at TRs of 10 and 70% and light oils (350 < GOR <600 m3/m3) at TR of 90%. Additionally, this sample displays the highest gas generative potential (36.3 wt%; Table 3), which is consistent with the high GORs, P_{sat}, and B_o. The remaining samples display consistently lower GOR values with only black oils generated, except for some potential for light oils at late TR in sample D. This increase in GOR at higher conversion rates can be ascribed to either late generation of primary gas resulting from the breakdown of thermally stable vitrinites or to the initiation of secondary cracking of trapped gas with increasing thermal stress (Dieckmann et al., 1998). The most oil-prone samples from well 7430/10-U-1 (N and O) generate petroleum fluids with the lowest GORs, P_{sat}, and B_o values in this data set (Fig. 10; Table 4). This condition is consistent with their comparatively low gas generation potentials (25.3 and 25.9%, respectively; Table 3) and their waxier composition.

5. Discussion: organic facies variations and their impact on petroleum generation in the Barents Sea

5.1. Vertical organic facies variations

Pyrolysis data from well 7125/1-1 in the Nysleppen Fault Complex illustrates variations in thermal stability and geochemical composition inherited from differences in organic facies (Fig. 11B). Peak activation energies occur between 55 and 57 kcal/mol and 59–62 kcal/mol in the marine liptinite-rich (1380m, i.e. sample F) and the vitrinite-rich sample (1368m, i.e. sample E), respectively. As a consequence of the strong vitrinitic input, the latter sample has the potential to generate gas & condensate, whereas the remaining liptinitic kerogens (i.e. D, F, and G) generate intermediate, P–N-A low wax oils (Fig. 5). The bulk of the organic fraction throughout well 7120/10–1 consists of land-plant derived materials with comparable generation potentials (e.g. similar HI values) and peak activation energies at 59–60 kcal/mol (Fig. 11A). A moderate increase in the content of marine macerals at 1482m (i.e.

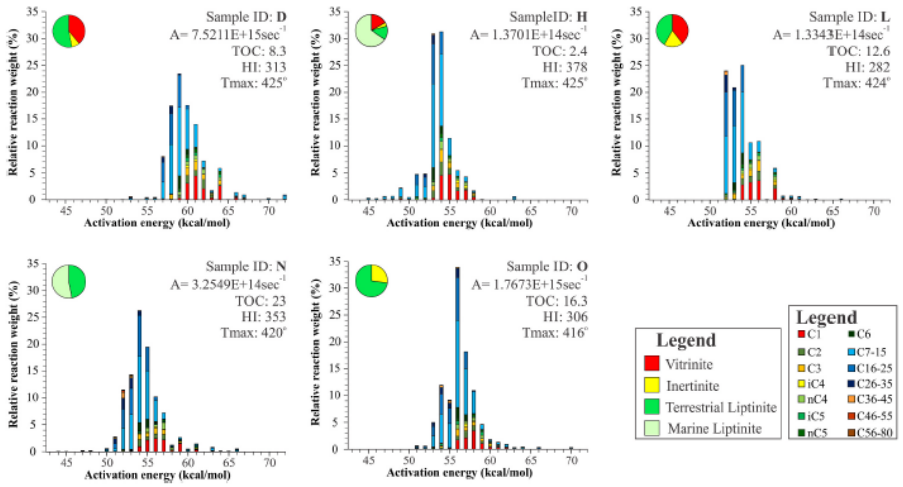

Fig. 9. Compositional kinetic models with fourteen components for five source rock samples. Pie diagrams represent the maceral composition of the corresponding sample. TOC = total organic carbon - wt%; HI = hydrogen index – mgHC/gTOC; Tmax = Tmax Rock-Eval - °C.

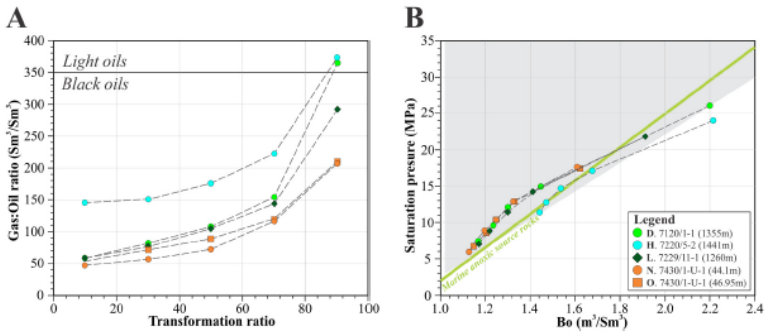

Fig. 10. Evolution of physical properties (i.e. gas to oil ration = GOR, volume factor = Bo, and saturation pressure = Psat) of generated fluids with increasing maturity calculated from micro-scaled sealed vessels (MSSV Closed-System Pyrolysis) experiments using the PhaseKinetics approach as defined by di Primio and Horsfield (2006). **A.** Cross-plot of transformation ratio versus GOR. **B.** Cross-plot of Bo versus Psat. The light grey area corresponds to naturally occurring petroleum fluids according to di Primio and Horsfield (2006).

sample C) causes the activation energy distribution to peak at 55–56 kcal/mol, and hence, 70% conversion takes place around 10 °C earlier relative to the vitrinitic samples A and B (Fig. 8).

Organic rich shales sampled at various depths from well 7227/8-U-3 in the neighboring Nordkapp Basin also display considerable differences in pyrolysis results relative to each other and with respect to other wells (Fig. 11C). The deepest, marine liptinite-rich sample (i.e. K), predicted to generate sulfur-rich, P–N-A low wax oils, exhibits a dominant activation energy peak at 52 kcal/mol and accordingly generates at one of the lowest temperature in the data set (Fig. 8). This sample has a relatively low HI value of 258 mg HC/g TOC given its elevated content of marine liptinites (Table 1). The E_A distribution derived for the shallower, more terrestrially influenced samples at 44m and 39.9m (i.e. J and I) shows dominant peaks in the range of 57–59 kcal/mol. These clay-rich rocks have the potential to generate intermediate, P–N-A low wax oils. Nevertheless, the sample at 44m produces a relatively higher content of sulfur-containing hydrocarbons (Fig. 5A) and starts generating at temperatures as low as those observed in the more marine, sulfur-rich sample K (Fig. 8). The elevated quantities of sulfur-bearing compounds were interpreted to result from diagenetic sulfurization of the organic matter brought about by sulfate reducing bacteria in anoxic settings. Changes in redox conditions triggered by the intermittent

Table 4
Fluid properties as a function of increasing maturity calculated from micro-scaled sealed vessels (MSSV Closed-System Pyrolysis) experiments for five selected samples.

ID	D			H			L			N			O		
	7125/1-1 (1355m)			7220/5-2 (1441m)			7229/11-1 (1260m)			7430/10-1-1 (44.1m)			7430/10-1-1 (46.95m)		
TR(%)	P_{sat} (MPa)	GOR (Sm3/Sm3)	Bo (m3/Sm3)	P_{sat} (MPa)	GOR (Sm3/Sm3)	Bo (m3/Sm3)	P_{sat} (MPa)	GOR (Sm3/Sm3)	Bo (m3/Sm3)	P_{sat} (MPa)	GOR (Sm3/Sm3)	Bo (m3/Sm3)	P_{sat} (MPa)	GOR (Sm3/Sm3)	Bo (m3/Sm3)
10	7.4	59.5	1.2	11.5	145.2	1.4	7.1	59.0	1.2	6.0	47.1	1.1	6.7	53.8	1.2
30	9.6	82.1	1.2	12.7	150.7	1.5	8.8	76.1	1.2	7.3	57.0	1.2	8.5	71.8	1.2
50	11.9	107.4	1.3	14.7	176.0	1.5	11.5	105.2	1.3	9.0	71.8	1.2	10.3	89.0	1.3
70	15.0	154.0	1.5	17.1	222.1	1.7	14.3	143.7	1.4	12.8	116.2	1.3	12.9	119.1	1.3
90	26.2	364.7	2.2	24.0	372.1	2.2	21.8	291.5	1.9	17.6	206.7	1.6	17.4	208.9	1.6

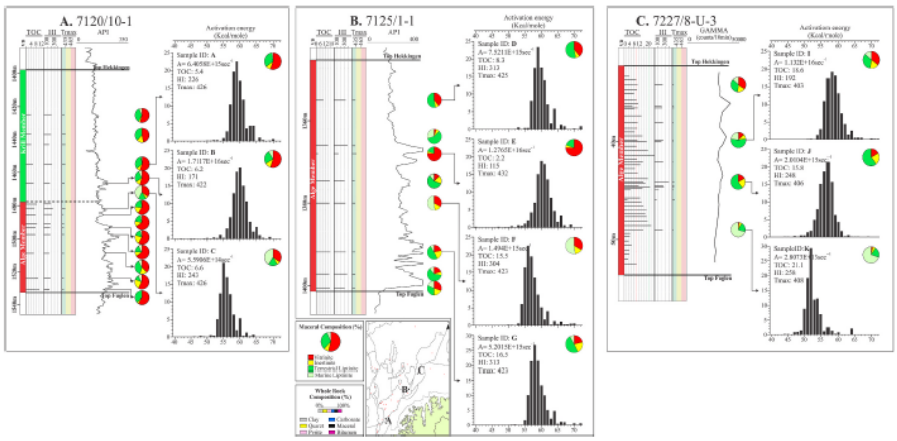

Fig. 11. Vertical variations in maceral composition and bulk kinetic parameters within the Hekkingen Formation at three different well locations: **A.** 7120/10-1 southern Hammerfest Basin; **B.** 7125/1-1 = Nysleppen Fault Complex; **C.** 7227/8-U-3 = Nordkapp Basin. TOC = total organic carbon - wt%; HI = hydrogen index – mgHC/gTOC; Tmax = Tmax Rock-Eval - °C.

growth of salt-diapirs in the Nordkapp Basin (Rojo et al., 2019; Cedeño et al., 2019) may have led to different degrees of sulfurization and hydrogen losses in the studied samples (Cedeño et al., 2021).

5.2. Sub-regional to regional organic facies variations

The documented variability in organic facies results from local to sub-regional geological and oceanographic controls on the sedimentation of organic-rich units across the Barents Sea (Cedeño et al., 2021). This ubiquitous heterogeneity cannot be described by bulk and quantitative pyrolysis analysis of just a few samples at different depths. Even more closely-spaced sampling intervals would only partly reproduce such variability. The current study assigns pyrolysis results from this data set to areas with comparable average maceral compositions from the subregional to regional characterization of organic facies by Cedeño et al. (2021; Fig. 2). This approach, although still uncertain, is able to more statistically and usefully reproduce changes in kinetics and petroleum type predictions. It is also important to point out that some of the pyrolyzed source rock samples in this data set come from wells drilled near structural highs (i.e. wells 7231-1-U-1, 7227/8-U-3, 7125/1-1; Fig. 2) or from well sections interpreted to have experienced substantial organic matter dilution during sedimentation (i.e. well 7120/10–1; see Fig. 4 in Cedeño et al., 2021); therefore, the generative potential in these areas may, to varying degrees, be less than that in deeper, more anoxic settings.

The maps in Fig. 12 illustrate the variations in kinetic models of bulk petroleum generation within the Alge and Krill members. The marine liptinite-rich shales of the Alge Member in the central Hammerfest Basin and their more terrestrial liptinitic equivalents to the west require the use of kinetic data derived from labile kerogen assemblages, similar to those in samples H and N (Table 2; Fig. 12A), respectively. According to the assigned parameters, the Alge Member in these marginal-to-thermally mature areas has the potential to generate intermediate, low wax P–N-A oils with overall low GOR (i.e. black oils). The high average contents of marine liptinites within both the Alge and Krill members in the Bjørnøyrenna Fault Complex, whose combined cumulative thickness exceeds 800m (Marín et al., 2020), permits the use of kinetic properties from sample H. Kinetic information from a more intermediate marine-terrestrial sample, and therefore a moderately more stable kerogen type (i.e. sample C), is assigned to the Alge source rocks in the Nysleppen Fault Complex as well as in the eastern margin of the Hammerfest Basin (Fig. 12A).

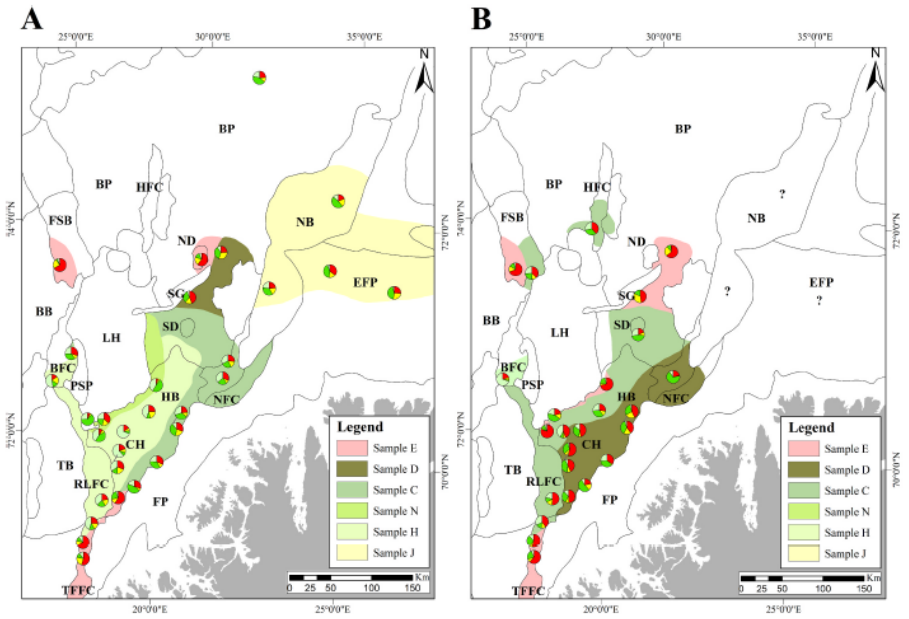

Fig. 12. Map of the southwestern Barents Sea illustrating the variability in kinetics models within the Alge (**A**) and Krill (**B**) members. Results from the current data set are assigned to areas with comparable maceral compositions from the subregional to regional characterization of organic facies by Cedeño et al., 2021.

The organic fraction within the Krill Member across most of the Hammerfest Basin consists predominantly of vitrinite and terrestrial liptinites (Fig. 12**B**). Thus, kinetic parameters describing the primary cracking from thermally more stable land-derived kerogens, like those in sample D, are suggested. These type III/II source rocks are expected to generate intermediate, black oils of a P–N-A low wax composition with potentially light oils generated at 90% transformation. The kinetic variability between the kerogen types assigned to the Alge and Krill members in the western-central Hammerfest Basin covers a temperature range of approximately 20 °C for the commencement of petroleum generation (Fig. 8). This shift in organic constituents within the Hammerfest Basin reflects the regional flooding that peaked during Alge times and subsequent sea level drop during Krill times.

Sources rocks of the Alge Member in the eastern Finnmark Platform feature maceral assemblages comparable to those within the Krill Member in the Hammerfest Basin (Fig. 12) and, therefore, assigning the kinetics derived from sample D seems logical. However, the pyrolysate of sample L from well 7229/11–1 in the eastern Finnmark Platform contains a high relative abundance of sulfur-bearing compounds, implying the existence, at least locally, of thermally less stable type IIS kerogens. Although both D and L samples have the potential to generate low wax P–N-A, black oils, the onset of generation in sample L takes place approximately 17 °C earlier than in sample D (Fig. 8), challenging the use of either set of kinetics. Additionally, it is possible that the sulfur content, and so the thermal stability, varies throughout the section as was the case in well 7227/8-U-3 from the Nordkapp Basin. This study provisionally assigns kinetics parameters from an organically comparable source rock sample with a sulfur content that is intermediate between sample L and D, that is, sample J.

The kerogen in both the Alge and Krill members within the Fingerdjupet Sub-basin and the Troms-Finnmark Fault Complex is composed mostly of hydrogen-poor vitrinitic macerals, which are at best only gas & condensate prone. In this case, kinetic parameters characteristic of the thermally very stable vitrinitic kerogen in sample E are suitable. Gas and condensate prone source rocks also occur within both members at some localities along the Hammerfest Basin-Loppa High boundary.

6. Conclusions

The investigated organic rich samples from the Hekkingen Formation contain varying proportions of kerogen type II and III, as demonstrated by their hydrogen richness and maceral assemblages. Heterogeneities in the kerogen composition result in different orders of kinetic stability, with the predicted onset of petroleum generation spread over a relatively high and wide temperature range from 123 °C to 144 °C (at 3.3C°/Ma). This temperature range equates to a difference of up to 700 m of burial if a thermal gradient of 30 °C is assumed.

With a few exceptions, the variability in activation energy distributions, and so in kerogen thermal stability, results from variations in the kerogen maceral composition. Marine liptinite-rich samples show a low and narrow range of activation energies relative to the higher and broader range described for the more terrestrial samples. Reduced kerogen stability associated with elevated sulfur contents is documented in a few samples.

The majority of the investigated samples have the potential to generate low GOR oils of an intermediate to aromatic, low wax P–N-A

composition along with variable amounts of wet gas in the range of 25–35%. Petroleum of similar compositional and physical properties is predicted to have been generated from the natural maturation series of various organic facies in mature areas of the Hammerfest Basin, the Ringvassøy-Loppa High and the Bjørnøyrenna fault complexes.

Upon maturation, it is likely that discreet intervals in the Nordkapp Basin and eastern Finnmark Platform may generate high-sulfur, low wax P–N-A oils with low GOR. Vitrinite-rich sources in the Fingerdjupet Subbasin and the Troms-Finnmark Fault Complex have a potential for gas and condensate generation at late maturities.

Declaration of competing interest

The authors declare that they have no known competing financial interests or personal relationships that could have appeared to influence the work reported in this paper.

Acknowledgments

The authors would like to thank the sponsors of the JuLoCrA project (https://wp.ux.uis.no/julocra/) for providing essential economic support. We are grateful to Integrated Geochemical Interpretation (IGI) for free software supply and to Applied Petroleum Technologies (APT) for analytical studies, particularly to Per Erling Johansen. The authors also thank reviewers Simon George and Dag Arild Karlsen for their constructive reviews that greatly improved the manuscript.

References

Abay, T.B., Karlsen, D.A., Pedersen, J.H., Olaussen, S., Backer-Owe, K., 2017. Thermal maturity, hydrocarbon potential and kerogen type of some Triassic-Lower Cretaceous sediments from the SW Barents Sea and Svalbard. Petrol. Geosci. 24, 349–373. https://doi.org/10.1144/petgeo2017-035.

Århus, N., 1991. The transition from deposition of condensed carbonates to dark claystones in the Lower Cretaceous succession of the southwestern Barents Sea. Nor. Geol. Tidsskr. 71, 259–263.

Berglund, L., Augustson, J., Færseth, R., Gjelberg, J., Ramberg-Moe, H., 1986. The evolution of the Hammerfest Basin. Habitat of hydrocarbons on the Norwegian continental shelf. Norsk Petroleumsforening 319–338.

Blaich, O.A., Tsikalas, F., Faleide, J.I., 2017. New insights into the tectono-stratigraphic evolution of the southern stappen high and its transition to Bjørnøya Basin, SW Barents Sea. Mar. Petrol. Geol. 85, 09–105. https://doi.org/10.1016/j.marpetgeo.2017.04.015.

Braun, R.L., Burnham, A.K., Reynolds, J.G., Clarkson, J.E., 1991. Pyrolysis kinetics for lacustrine and marine source rocks by programmed micropyrolysis. Energy Fuel. 5, 192–204. https://doi.org/10.1021/ef00025a033.

Bugge, T., Elvebakk, G., Fanavoll, S., Mangerud, G., Smelror, M., Weiss, H.M., Gjelberg, J., Kristensen, S.E., Nilsen, K., 2002. Shallow stratigraphic drilling applied in hydrocarbon exploration of the Nordkapp Basin, Barents Sea. Mar. Petrol. Geol. 19, 13–37. https://doi.org/10.1016/S0264-8172(01)00051-4.

Burnham, A.K., Braun, R.L., Gregg, H.R., Samoun, A.M., 1987. Comparison of methods for measuring kerogen pyrolysis rates and fitting kinetic parameters. Energy Fuel. 1, 452–458. https://doi.org/10.1021/ef00006a001.

Castelli, A., Chiaramonte, M.A., Beltrame, P.L., Camiti, P., Del Bianco, A., Stroppa, F., 1990. Thermal degradation of kerogen by hydrous pyrolysis. A kinetic study. Org. Geochem. 16, 75–82. https://doi.org/10.1016/0146-6380(90)90027-W.

Cavanagh, A.J., Di Primio, R., Scheck-Wenderoth, M., Horsfield, B., 2006. Severity and timing of cenozoic exhumation in the southwestern Barents Sea. J. Geol. Soc. 163, 761–774. https://doi.org/10.1144/0016-76492005-146.

Cedeño, A., Rojo, L.A., Cardozo, N., Centeno, L., Escalona, A., 2019. The impact of salt tectonics on the thermal evolution and the petroleum system of confined rift basins: insights from basin modeling of the Nordkapp Basin, Norwegian Barents Sea. Geosciences 9. https://doi.org/10.3390/geosciences9070316.

Cedeno, A., Ohm, S., Escalona, A., Marín, D., Olaussen, S., Demchuck, T., 2021. Upper Jurassic to Lower Cretaceous Source Rocks in the Norwegian Barents Sea, Part I: Organic Geochemical, Petrographic, and Paleogeographic Investigations.

Clark, S., Glorstad-Clark, E., Faleide, J., Schmid, D., Hartz, E., Fjeldskaar, W., 2014. Southwest Barents Sea rift basin evolution: comparing results from backstripping and time-forward modelling. Basin Res. 26, 550–566. https://doi.org/10.1111/bre.12059.

Cornford, C., 1998. Source rocks and hydrocarbons of the north sea. In: Glennie, K.W. (Ed.), Petroleum Geology of the North Sea. Blackwell Science, Oxford, pp. 376–462. https://doi.org/10.1002/9781444313413.ch11.

Dallmann, A., Worsley, D., Ofstad, K., 1988. A lithostratigraphic scheme for the Mesozoic and Cenozoic succession offshore Norway north of 62 N. Norwegian Petroleum Directorate Bulletin 4, 67.

Demaison, G.J., Moore, G.T., 1980. Anoxic environments and oil source bed genesis. AAPG (Am. Assoc. Pet. Geol.) Bull. 64, 1179–1209. https://doi.org/10.1306/2F91945E-16CE-11D7-8645000102C1865D.

di Primio, R., Horsfield, B., 1996. Predicting the generation of heavy oils in carbonate/evaporitic environments using pyrolysis methods. Org. Geochem. 24, 999–1016. https://doi.org/10.1016/S0146-6380(96)00116-7.

di Primio, R., Horsfield, B., 2006. From petroleum-type organofacies to hydrocarbon phase prediction. AAPG (Am. Assoc. Pet. Geol.) Bull. 90, 1031–1058. https://doi.org/10.1306/02140605129.

di Primio, R., Skeie, J.E., 2004. Development of a compositional kinetic model for hydrocarbon generation and phase equilibria modelling: a case study from Snorre field, Norwegian North Sea. In: Cubitt, J.M., England, W.A., Larter, S.R. (Eds.), Understanding Petroleum Reservoirs: towards an Integrated Reservoir Engineering and Geochemical Approach, vol. 237. Geological Society (London) Special Publication, pp. 157–174.

di Primio, R., Dieckmann, V., Mills, N., 1998. PVT and phase behavior analysis in petroleum exploration. Org. Geochem. 29, 207–222. https://doi.org/10.1016/S0146-6380(98)00102-8.

Dieckmann, V., Keym, M., 2006. A new approach to bridge the effect of organofacies variations on kinetic modelling and geological extrapolations. Org. Geochem. 37, 728–739. https://doi.org/10.1016/j.orggeochem.2005.12.008.

Dieckmann, V., Schenk, H.J., Horsfield, B., Welte, D.H., 1998. Kinetics of petroleum generation and cracking by programmed-temperature closed-system pyrolysis of Toarcian Shales. Fuel 77, 23–31. https://doi.org/10.1016/S0016-2361(97)00165-8.

Doré, A.G., Scotchman, I.C., Corcoran, D., 2000. Cenozoic exhumation and prediction of the hydrocarbon system on the NW European margin. J. Geochem. Explor. 69–70, 615–618. https://doi.org/10.1016/S0375-6742(00)00137-0.

Duran, E.R., di Primio, R., Anka, Z., Stoddart, D., Horsfield, B., 2013a. Petroleum system analysis of the Hammerfest Basin (southwestern Barents Sea): comparison of basin modelling and geochemical data. Org. Geochem. 63, 105–121. https://doi.org/10.1016/j.orggeochem.2013.07.011.

Duran, E.R., di Primio, R., Anka, Z., Stoddart, D., Horsfield, B., 2013b. 3D-basin modelling of the Hammerfest Basin (southwestern Barents Sea): a quantitative assessment of petroleum generation, migration, and leakage. Mar. Petrol. Geol. 45, 281–303. https://doi.org/10.1016/j.marpetgeo.2013.04.023.

Eglinton, T.I., Sinninghe Damsté, J.S., Kohnen, M.E.L., de Leeuw, J.W., Larter, S.R., Patience, R.L., 1990. Analysis of maturity-related changes in the organic sulfur composition of kerogens by flash pyrolysis–gas chromatography. In: Geochemistry of Sulfur in Fossil Fuels. American Chemical Society, pp. 529–565. https://doi.org/10.1021/bk-1990-0429.ch027.

Eglinton, T.I., Sinninghe Damsté, J.S., Pool, W., de Leeuw, J.W., Eijk, G., Boon, J.J., 1992. Organic sulphur in macromolecular sedimentary organic matter. II. Analysis of distributions of sulphur-containing pyrolysis products using multivariate techniques. Geochem. Cosmochim. Acta 56, 1545–1560. https://doi.org/10.1016/0016-7037(92)90224-7.

Faleide, J.I., Vågnes, E., Gudlaugsson, S.T., 1993. Late Mesozoic-Cenozoic evolution of the south-western Barents Sea in a regional rift-shear tectonic setting. Mar. Petrol. Geol. 10, 186–214. https://doi.org/10.1016/0264-8172(93)90104-Z.

Espitalié, J., Madec, M., Tissot, B.P., Menning, J.J., Leplat, P., 1977. Source Rock Characterization Method for Petroleum Exploration. Institut Francais du Petrole, Labofina, SA.

Faleide, T.S., Midtkandal, I., Planke, S., Corseri, R., Faleide, J.I., Serck, C.S., Nystuen, J. P., 2019. Characterisation and development of Early Cretaceous shelf platform deposition and faulting in the Hoop area, southwestern Barents Sea-constrained by high-resolution seismic data. Norw. J. Geol. 99, 3. https://doi.org/10.17850/njg99-3-7.

Georgiev, S.V., Stein, H.J., Hannah, J.L., Xu, G.P., Bingen, B., Weiss, H.M., 2017. Timing, duration, and causes for late jurassic-early cretaceous anoxia in the Barents Sea. Earth Planet Sci. Lett. 461, 151–162. https://doi.org/10.1016/j.epsl.2016.12.035.

Gernigon, L., Brönner, M., Roberts, D., Olesen, O., Nasuti, A., Yamasaki, T., 2014. Crustal and basin evolution of the southwestern Barents Sea: from Caledonian orogeny to continental breakup. Tectonics 33, 347–373. https://doi.org/10.1002/2013TC003439.

Hartwig, A., di Primio, R., Anka, Z., Horsfield, B., 2012. Source rock characteristics and compositional kinetic models of Cretaceous organic rich black shales offshore southwestern Africa. Org. Geochem. 51, 17–34. https://doi.org/10.1016/j.orggeochem.2012.07.003.

Helleren, S., Marín, D., Ohm, S., Augustsson, C., Escalona, A., 2020. Why does not lithology correlate with gamma-ray spikes in the shaley source rocks of the Upper Jurassic Alge Member (southwestern Barents Sea)? Mar. Petrol. Geol. 121 https://doi.org/10.1016/j.marpetgeo.2020.104623.

Henriksen, E., Ryseth, A., Larssen, G., Heide, T., Rønning, K., Sollid, K., Stoupakova, A., 2011a. Tectonostratigraphy of the greater Barents Sea: implications for petroleum systems. In: Spencer, A.M., Embry, A.F., Gautier, D.L., Stoupakova, A.V., Sørensen, K. (Eds.), Arctic Petroleum Geology, vol. 35. Geological Society, London, pp. 163–195. https://doi.org/10.1144/M35.10. Memoirs 2011.

Henriksen, E., Bjørnseth, H.M., Hals, T.K., Heide, T., Kiryukhina, T., Kløvjan, O.S., Larssen, G.B., 2011b. Uplift and erosion of the greater Barents Sea: impact on prospectivity and petroleum systems. In: Spencer, A.M., Embry, A.F., Gautier, D.L., Stoupakova, A.V., Sørensen, K. (Eds.), Arctic Petroleum Geology, vol. 35. Geological Society, London, pp. 271–281. https://doi.org/10.1144/M35.17. Memoirs 2011.

Horsfield, B., 1997. The bulk composition of first-formed petroleum in source rocks. In: Welte, D.H., Horsfield, B., Baker, D.R. (Eds.), Petroleum and Basin Evolution. Springer Verlag, Berlin, Heidelberg, pp. 337–402.

Horsfield, B., Disko, U., Leistner, F., 1989. The micro-scale simulation of maturation: outline of a new technique and its potential applications. Geol. Rundsch. 78, 361–374.
Horsfield, B., Schenk, H.J., Mills, N., Welte, D.H., 1992. An investigation of the inreservoir conversion of oil to gas: compositional and kinetic findings from closed-system programmed-temperature pyrolysis. Org. Geochem. 19, 191–204. https://doi.org/10.1016/0146-6380(92)90036-W.
Indrevær, K., Gabrielsen, R.H., Faleide, J.I., 2017. Early Cretaceous synrift uplift and tectonic inversion in the Loppa High area, southwestern Barents Sea, Norwegian shelf. J. Geol. Soc. 174, 242–254. https://doi.org/10.1144/jgs2016-066.
Kairanov, B., Marín, D., Escalona, A., Cardoso, N., 2019. Growth and linkage of a Basin-bounding fault system: insights from the early cretaceous evolution of the northern Polheim subplatform, SW Barents Sea. J. Struct. Geol. 124, 182–196. https://doi.org/10.1016/j.jsg.2019.04.014.
Kairanov, B., Escalona, A., Norton, I., Abrahamsson, P., 2021. Early cretaceous evolution of the Tromsø Basin, SW Barents Sea. Mar. Petrol. Geol. 123 https://doi.org/10.1016/j.marpetgeo.2020.104714.
Kaplan, I.R., Emery, K.O., Rittenbebg, S.C., 1963. The distribution and isotopic abundance of sulphur in recent marine sediments off southern California. Geochem. Cosmochim. Acta 27, 313–331. https://doi.org/10.1016/0016-7037(63)90074-7.
Karlsen, D.A., Larter, S.R., 1991. Analysis of petroleum fractions by TLC-FID: applications to petroleum reservoir description. Org. Geochem. 17 (5), 603–617. https://doi.org/10.1016/0146-6380(91)90004-4.
Killops, S., Stoddart, D., Mills, N., 2014. Inferences for sources of oils from the Norwegian Barents Sea using statistical analysis of biomarkers. Org. Geochem. 76, 157–166. https://doi.org/10.1016/j.orggeochem.2014.07.011.
Larter, S.R., Horsfield, B., 1993. Determination of structural components of kerogens by the use of analytical pyrolysis methods. In: Engel, M.H., Macko, S.A. (Eds.), Organic Geochemistry. Plenum Press, New York, pp. 271–287.
Lerch, B., Karlse, D.A., Matapour, Z., Seland, R., Backer-Owe, K., 2016. Organic geochemistry of Barents Sea petroleum: thermal maturity and alteration and mixing processes in oils and condensates. J. Petrol. Geol. 39, 125–147. https://doi.org/10.1111/jpg.12637.
Mango, F.D., 1996. Transition metal catalysis in the generation of natural gas. Org. Geochem. 24, 977–984. https://doi.org/10.1016/0016-7037(92)90153-A.
Mango, F.D., 2000. The origin of light hydrocarbons. Geochem. Cosmochim. Acta 64, 1265–1277. https://doi.org/10.1016/0016-7037(90)90156-P.
Mango, F.D., 2001. Methane concentrations in natural gas: the genetic implications. Org. Geochem. 32, 1283–1287. https://doi.org/10.1016/S0146-6380(01)00099-7.
Marín, D., Escalona, A., Grundvåg, S.A., Olaussen, S., Sandvik, S., Śliwińska, K.K., 2018. Unravelling key controls on the rift climax to post-rift fill of marine rift basins: insights from 3D seismic analysis of the Lower Cretaceous of the Hammerfest Basin, SW Barents Sea. Basin Res. 30, 587–612. https://doi.org/10.1111/bre.12266.
Marín, D., Helleren, S., Escalona, A., Olaussen, S., Cedeño, A., Nøhr-Hansen, H., Ohm, S., 2020. The Middle Jurassic to lowermost Cretaceous in the SW Barents Sea: interplay between tectonics, coarse-grained sediment supply and organic matter preservation. Basin Res. https://doi.org/10.1111/bre.12504.
Mørk, A., Dallmann, W., Dypvik, H., Johannessen, E., Larssen, G., Nagy, J., Nøttvedt, A., Olaussen, S., Pchelina, T., Worsley, D., 1999. Mesozoic Lithostratigraphy. Lithostratigraphic Lexicon of Svalbard. Upper Paleozoic to Quaternary Bedrock. Review and Recommendations for Nomenclature Use, pp. 127–214.
Mulrooney, M.J., Leutscher, J., Braathen, A., 2017. A 3D structural analysis of the Goliat field, Barents Sea, Norway. Mar. Petrol. Geol. 86, 192–212. https://doi.org/10.1016/j.marpetgeo.2017.05.033.
Murillo, W.A., Vieth-Hillebrand, A., Horsfield, B., Wilkes, H., 2016. Petroleum source, maturity, alteration and mixing in the southwestern Barents Sea: new insights from geochemical and isotope data. Mar. Petrol. Geol. 70, 119–143. https://doi.org/10.1016/j.marpetgeo.2015.11.009.
Ohm, S.E., Karlsen, D.A., Austin, T., 2008. Geochemically driven exploration models in uplifted areas: examples from the Norwegian Barents Sea. AAPG (Am. Assoc. Pet. Geol.) Bull. 92, 1191–1223. https://doi.org/10.1306/06180000028.
Orr, W.L., 1986. Kerogen/asphaltene/sulfur relationships in sulfur-rich Monterey oils. Org. Geochem. 10, 499–516. https://doi.org/10.1016/0146-6380(86)90049-5.
Pedersen, K.S., Thomassen, P., Fredenslund, A., 1985. Thermodynamics of petroleum mixtures containing heavy hydrocarbons. 3. Efficient flash calculation procedures using the SRK equation of state. Ind. Eng. Chem. Process Des. Dev. 24, 948–954. https://doi.org/10.1021/i200031a009.
Petersen, H., Rosenberg, P., 2000. The relationship between the composition and rank of humic coals and their activation energy distributions for the generation of bulk petroleum. Petrol. Geosci. 6, 137–149. https://doi.org/10.1144/petgeo.6.2.137.
Reynolds, J.G., Burnham, A.K., 1995. Comparison of kinetic analysis of source rockand kerogen concentrates. Org. Geochem. 23, 11–19. https://doi.org/10.1016/0146-6380(94)00114-G.
Riis, F., 1996. Quantification of Cenozoic vertical movements of Scandinavia by correlation of morphological surfaces with offshore data. Global Planet. Change 331–357. https://doi.org/10.1016/0921-8181(95)00027-5.
Rojo, L.A., Cardoso, N., Escalona, A., Koyi, H., 2019. Structural style and evolution of the Nordkapp Basin, Norwegian Barents Sea. AAPG (Am. Assoc. Pet. Geol.) Bull. 103 (9), 2177–2217. https://doi.org/10.1306/01301918028.
Santamaria Orozco, D.M., 2000. Organic geochemistry of tithonian source rocks and associated oils from the sonda de Campeche. Forschungszentrum Jülich GmbH Zentralbibliothek. Verlag Jülich, p. 201.
Schaeffer, P., Reiss, C., Albrecht, P., 1995. Geochemical study of macromolecular organic matter from sulfur-rich sediments of evaporitic origin (Messinian of Sicily) by chemical degradations. Org. Geochem. 23, 567–581. https://doi.org/10.1016/0146-6380(95)00045-G.
Schenk, H.J., Horsfield, B., Krooss, B., Schaefer, R.G., Schwochau, K., 1997. Kinetics of petroleum formation and cracking. In: Welte, D.H., Horsfield, B., Baker, D.R. (Eds.), Petroleum and Basin Evolution. Springer-Verlag, Berlin Heidelberg, pp. 231–270.
Scotese, C.R., 2016. PALEOMAP PaleoAtlas for GPlates and the PaleoData Plotter Program. PALEOMAP Project. http://www.earthbyte.org/paleomap-paleoatlas-for-gplates/.
Serck, C.S., Faleide, J.I., Braathen, A., Kjølhamar, B., Escalona, A., 2017. Jurassic to early cretaceous basin configuration(s) in the Fingerdjupet subbasin, SW Barents Sea. Mar. Petrol. Geol. 86, 874–891. https://doi.org/10.1016/j.marpetgeo.2017.06.044.
Sinninghe Damste, J.S., Eglington, T.I., de Leeuw, J.W., Schenck, P.A., 1989. Organic sulphur in macromolecular sedimentary organic matter: I. Structure and origin of sulphur-containing moieties in kerogen, asphaltenes and coal as revealed by flash pyrolysis. Geochem. Cosmochim. Acta 53, 873–889. https://doi.org/10.1016/0016-7037(89)90032-X.
Smelror, M., Mørk, A., Mørk, M.B.E., Weiss, H.M., Løseth, H., 2001. Middle Jurassic-Lower Cretaceous transgressive-regressive sequences and facies distribution off northern Nordland and Troms, Norway, 10. Norwegian Petroleum Society Special Publications, pp. 211–232. https://doi.org/10.1016/S0928-8937(01)80015-1.
Sund, T., Skarpnes, O., Jensen, L.N., Larsen, R.M., 1986. Tectonic development and hydrocarbon potential offshore Troms, northern Norway. In: Halbouty, T.H. (Ed.), Future Petroleum Provinces of the World, vol. 40. AAPG Memoir. https://doi.org/10.1306/M40454C29.
Tegelaar, E.W., Noble, R.A., 1994. Kinetics of hydrocarbon generation as a function of the molecular structure of kerogen as revealed by pyrolysis–gas chromatography. Org. Geochem. 22, 543–574. https://doi.org/10.1016/0146-6380(94)90125-2.
Tegelaar, E.W., de Leeuw, J.W., Derenne, S., Largeau, C., 1989. A reappraisal of kerogen formation. Geochem. Cosmochim. Acta 53, 3103–3106. https://doi.org/10.1016/0016-7037(89)90191-9.
Tissot, B.P., Welte, D.H., 1984. Petroleum Formation and Occurrence. Springer Verlag, Berlin.
Tissot, B.P., Pelet, R., Ungerer, P., 1987. Thermal history of sedimentary basins, maturation indices, and kinetics of oil and gas generation. AAPG (Am. Assoc. Pet. Geol.) Bull. 71, 1445–1466. https://doi.org/10.1306/703C80E7-1707-11D7-8645000102C1865D.
Tsikalas, F., Blaich, O.A., Faleide, J.I., Olaussen, S., 2021. Stappen High-Bjørnøya Tectono-Sedimentary Element, Barents Sea, vol. 57. Geological Society, London, Memoirs. https://doi.org/10.1144/M57-2016-24.
Uroy, K.E., 1980. Thermal decomposition of kerogens: mechanism and analytical application. J. Anal. Appl. Pyrol. 1, 323–338. https://doi.org/10.1016/0165-2370(80)80016-7.
Van Dongen, B.E., Schouten, S., Baas, M., Geenevasen, J.A.J., Sinninghe Damste, J.S., 2003. An Experimental Study of the Low-Temperature Sulfurisation of Carbohydrates. https://doi.org/10.1016/S0146-6380(03)00060-3.
Wierzbowski, A., Smelror, M., 2020. The bajocian to kimmeridgian (Middle to upper jurassic) ammonite succession at sentralbanken high (core 7533/3-U-1), Barents Sea, and its stratigraphical and palaeobiogeographical significance. Volumina Jurassica 18, 1–22. https://doi.org/10.7306/vj.18.1.
Zabinsky, Z.B., 1998. Stochastic methods for practical global optimization. J. Global Optim. 13, 433–444.
Zabinsky, Z.B., Smith, R.L., McDonald, J.F., Romeijn, H.E., Kaufman, D.E., 1993. Improving hit and run for global optimization. J. Global Optim. 3, 171–192.

Paper III

Facies Variations in the Upper Jurassic Source Rocks of the Norwegian North Sea; From Micro to Macro Scale

Guro Skarstein [a], Sverre Ohm [a], Andrés Cedeño [a], Alejandro Escalona [a]

[a] University of Stavanger, Norway

Marine and Petroleum Geology 145 (2022) 105856
https://doi.org/10.1016/j.marpetgeo.2022.105856

Paper III

Marine and Petroleum Geology 145 (2022) 105856

Contents lists available at ScienceDirect

Marine and Petroleum Geology

journal homepage: www.elsevier.com/locate/marpetgeo

Facies variations in the Upper Jurassic source rocks of the Norwegian North Sea; from micro- to macro scale

Guro Skarstein *, Sverre Ohm, Andres Cedeño, Alejandro Escalona

University of Stavanger, Norway

ARTICLE INFO

Keywords:
Upper Jurassic source rocks
Facies variations
Maceral composition
Isotopes for organofacies
Northern North Sea
Kimmeridge Clay

ABSTRACT

In the northern North Sea, the Upper Jurassic Kimmeridge Clay (KC) and its equivalents in the Norwegian sector (i.e., Mandal, Tau, and Draupne) are the most prolific source rocks. These source rock units are known to record both lateral and vertical heterogeneity in organofacies with increasing terrigenous organic inputs near highs and basin flanks. Existing interpretations rely predominantly on Rock-Eval data, but only a few authors validate their geochemical interpretations with maceral assessments. In this study, Upper Jurassic source rocks from fourteen wells in the northern North Sea were analysed for both organic petrography and geochemistry. A potential correlation between the maceral compositions and Rock-Eval, total organic carbon (TOC), and stable carbon isotopes (saturate and aromatic fractions) of source rock extracts was established. This correlation suggests that carbon isotopes mirror the organofacies, and inferred redox conditions during sedimentation, described for the studied source rocks.

Stable carbon isotopes of the saturate and aromatic fractions for 152 oils distributed across the Norwegian North Sea were compared to biomarker compounds sensitive to precursor organic material and oxygen abundance in the sedimentary environment. A correlation consistent with that observed between stable carbon isotopes and organofacies documented for the investigated source rocks is also observable in the oil dataset. Hence, the stable carbon isotope composition of the oils in the North Sea dataset appears to carry information related to the bulk organofacies and redox conditions prevailing during the sedimentation of their source. Oils often reflect the compositional attributes of their parental sources more efficiently than a single, or a set of rock extracts. Therefore, the stable carbon isotopes of migrated oils provide a means of inferring gross organofacies and redox conditions within different source rock kitchens in the study area.

1. Introduction

The Upper Jurassic Kimmeridge Clay (KC) and its Norwegian equivalents (i.e., Mandal, Tau and Draupne) are the most prolific petroleum source rocks in the northern North Sea, sourcing the majority of the fields (Barnard and Cooper, 1981; Cornford, 1998). Their importance as petroleum sources has motivated numerous studies focusing on assessing the variability in depositional environment and generation potential (e.g., Huc et al., 1985; Thomas et al., 1985; Cooper et al., 1995; Isaksen and Ledje, 2001; Kubala et al., 2003; Keym et al., 2006; Justwan and Dahl, 2005; Justwan et al., 2005; Petersen et al., 2016, 2017; Ziegs et al., 2017; Ponsaing et al., 2018; Misch et al., 2019; Ponsaing et al., 2020). These authors report the KC equivalent formations to record both vertical and lateral organofacies variations. Cornford (1998), Justwan et al. (2005), and Rossland et al. (2013) conclude that the organic-rich intervals are generally leaner and more terrigenous influenced in the vicinity of structural highs. The Late Jurassic marine transgression resulted in extensive anoxia and decreased clastic inputs, favouring accumulation and preservation of preferentially marine biomass (Huc et al., 1985; Cooper et al., 1995). Consequently, the uppermost interval is enriched in marine organic matter relative to deeper beds. The stacked source rock system has the potential to generate a wide spectrum of products ranging from gas, gas condensate, and waxy oils from the terrigenous rich intervals and light oil from the marine dominated intervals (Isaksen and Ledje, 2001; Justwan et al., 2005; Ponsaing et al., 2018).

Most published studies concerning the petroleum generation potential and, importantly, the composition of the organic matter of the Upper Jurassic source rocks rely on Rock-Eval pyrolysis. This type of analysis is a fast way of gaining information regarding the quality and generation

* Corresponding author.
E-mail address: guro.l.skarstein@uis.no (G. Skarstein).

https://doi.org/10.1016/j.marpetgeo.2022.105856
Received 22 February 2022; Received in revised form 2 August 2022; Accepted 3 August 2022
Available online 18 August 2022

potential of a given source rock sample (Peters, 1986), but lacks detailed information about the actual organic precursors (Barnard et al., 1981). Likewise, Rock-Eval results may be obscured by factors such as the presence of solid bitumen, oil based mud (OBM), or migrated hydrocarbons (Clementz, 1979). Maceral assessment is the conventional means of assessing the composition of solid organic particles preserved in organic-rich sediments. In the study area, however, a limited number of references report maceral compositions, and, when reported, only a few selected samples are discussed (e.g., Isaksen and Ledje, 2001; Ziegs et al., 2017; Misch et al., 2019).

Several authors have interpreted the variability in the composition of stable carbon isotopes of North Sea oils to reflect changes in the proportions of marine and terrigenous organic materials recorded in the Upper Jurassic shales (e.g., Grantham et al., 1980; Huc et al., 1985; Schou et al., 1985; Northam, 1985; Langrock et al., 2003; Justwan et al., 2005). Isotopically light oils (i.e., −30 to −25‰; Langrock et al., 2003) are interpreted to have originated from source rock facies dominated by marine organic matter, while comparatively heavier oils (i.e., −25 to −20‰; Langrock et al., 2003) are interpreted to have originated from terrigenous rich source rock facies.

This study collected 60 Upper Jurassic source rock samples from 14 wells across the northern North Sea, including samples from the British and Norwegian Central Graben, Ling Depression, Egersund Basin, Viking Graben, Tampen Spur, and Horda Platform (Fig. 1). The samples were analyzed for organic richness and generation potential (i.e., total organic carbon (TOC) and Rock-Eval), stable carbon isotopes, and maceral and mineral content (petrography). Integration of the acquired geochemical and petrographic data with geological constraints assists in producing an overview of the lateral and vertical variability in organofacies and source rock potential.

To test if the variations in organofacies observed in the analysed source rocks are reflected in the geochemical composition of oils, 20 crude oils from the Norwegian North Sea were sampled and analysed. Analytical data for 132 oils publicly available in the Integrated Geochemical Interpretation's (IGI) Norwegian Petroleum Directorate (NPD) Norwegian North Sea database (https://igiltd.com/news/official-release-of-igis-npd-norwegian-north-sea-database) was also employed. The oil database extends over a larger geographic area than the analysed source rocks and, therefore, provides an insight into the gross sourcing organofacies in areas where pertinent source rock data is absent.

2. Geological setting of Upper Jurassic source rocks

The North Sea Basin is a post-Caledonian graben system (Færseth, 1996). The present-day structural configuration developed during two major extensional phases: the Permo-Triassic rifting and the Middle Jurassic-Early Cretaceous rifting (Ziegler, 1992), followed by thermal cooling and subsidence (Badley et al., 1988; Færseth, 1996). During the Middle Jurassic to Early Cretaceous rift phase, a major marine transgression flooded vast areas of the shelf and triggered a rapid shift from fluvio-deltaic to deep marine conditions (Nøttvedt et al., 1995; Mannie et al., 2014; Fraser et al., 2002). During this time, organically enriched shales were deposited over the transgressed shelf. These clastic deposits comprise the Kimmeridge Clay and equivalent formations in the Norwegian sector: Mandal, Draupne and Tau formations (Figs. 1 and 2) and constitute the North Sea's primary source rocks (Gautier, 2005).

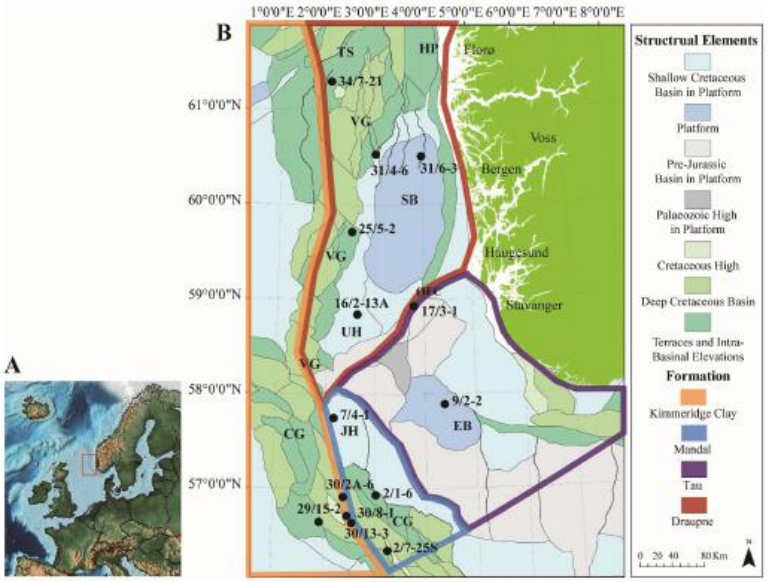

Fig. 1. A Location of study area (Paleomap Project; Scotese, 2016). B) Map of the northern North Sea showing the location of sampled wells and outlining the distribution of the various Kimmeridge Clay equivalents in the Norwegian sector. CG—Central Graben, JH — Jæren High, EB — Egersund Basin, UH—Utsira High, ØFC — Øygarden Fault Complex, VG—Viking Graben, SB—Stord Basin, TS — Tampen Spur, HP—Horda Platform.

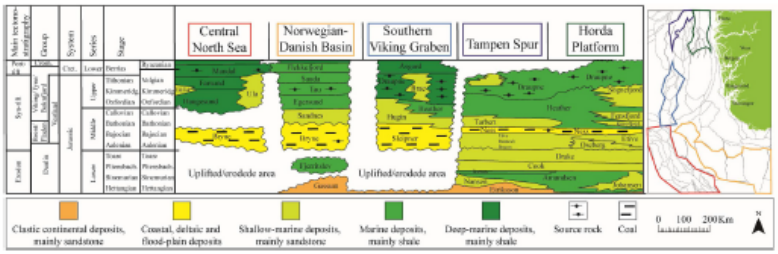

Fig. 2. Chronostratigraphic chart of the Kimmeridge Clay equivalent formations (Mandal, Tau and Draupne) in the Norwegian North Sea. The areal distribution of the different formations is outlined in colours. Modified from NPD (2014). (For interpretation of the references to colour in this figure legend, the reader is referred to the Web version of this article.)

2.1. Kimmeridge Clay Formation

The Kimmeridge Clay Formation constitutes one of the most prolific source rocks in the UK North Sea. The deposition of this mudstone-dominated unit took place within a series of tectonically controlled basins separated by structural highs (e.g., Ziegler, 1982; Scotchman, 1989; Oschmann, 1988) spanning from the Kimmeridgian to late Ryazanian. These organic-rich sediments contain autochthonous, algal-derived organic matter mixed with varying proportions of allochthonous, terrigenous components supplied by the surrounding highs (Macquaker and Gawthorpe, 1993). In the Norwegian sector, the Mandal, Tau, and Draupne formations are equivalent to the Kimmeridge Clay Formation (Fig. 2).

2.2. Mandal Formation

In the Norwegian Central Graben, source rocks of the Mandal Formation (Figs. 1 and 2) are broadly acknowledged as the major contributor to the petroleum accumulations. This unit consists of claystones deposited in a marine environment with anoxic bottom water conditions during the Volgian to Ryazian. The organic matter is predominantly composed of marine algal materials commonly regarded as kerogen Type II (Ziegs et al., 2017; Misch et al., 2019). Episodes of increased terrigenous inputs and coarser sediments sporadically occur within this unit as a consequence of erosion and re-deposition from the graben flanks and salt-related structures resulting from the reactivation of Zechstein evaporites (Ziegler, 1992; Rossland et al., 2013; Ziegs et al., 2017; Misch et al., 2019). The average TOC is 5 wt% with values as high as 12 wt% and average hydrogen index (HI) of 273 mg HC/g TOC and 516 mg HC/g TOC in the Søgne Basin (Ziegs et al., 2017), but may have values between 124 and 650 mg HC/g TOC (Cornford, 1994; Petersen et al., 2013).

2.3. Tau Formation

The Tau Formation (Figs. 1 and 2) occurs in the southeastern part of the Norwegian North Sea. Deposition of this unit occurred during the Kimmeridgian to early Volgian under anoxic marine environments established over an area affected by the Late Jurassic rifting event (Kalani et al., 2020). The Tau Formation consists of organic rich shales with TOC values in the range of 2 and 13 wt% and HI values in the range of 350–800 mg HC/g TOC (Ritter et al., 1987).

2.4. Draupne Formation

The Draupne Formation (Figs. 1 and 2) is regarded as one of the main contributors to the petroleum accumulations in the Viking Graben. This clay-dominated unit deposited during the time period spanning from the upper Oxfordian to Ryazanian in marine environments with increasing anoxia towards the top (Johansen et al., 2002). The depositional environment was locally affected by extension and fault rotation and thus development of major footwall islands (e.g., Nøttvedt et al., 2000; Ohm et al., 2006), leading to coarser sediments and increased terrigenous organic inputs (Thomas et al., 1985; Isaksen and Ledje, 2001; Justwan et al., 2005). Several authors (e.g., Isaksen and Ledje, 2001; Dahl, 2004; Justwan et al., 2005) have subdivided the Draupne Formation into a lower syn-rift section and an upper post-rift section. The lower section, having an age of upper Oxfordian to lower Volgian, is thicker than the upper unit (Dahl, 2004; Justwan et al., 2005). The upper section was deposited from the middle Volgian to Ryazanian and is organically richer than the lower section (Fraser et al., 2002; Dahl, 2004; Justwan et al., 2005). The lower Draupne section records average restored TOC and HI values of 4.1 wt% and 234.2 mg HC/g TOC, respectively. The average restored TOC and HI values of the upper Draupne section in the Viking Graben are 5.3 wt% and 300–450 mg HC/g TOC, respectively (Justwan et al., 2005); however, TOC values up to 12 wt% and HI up to 600 mg HC/g TOC have been reported (Goff, 1983; Thomas et al., 1985; Justwan et al., 2005).

3. Data and methodology

3.1. Dataset

A total of 60 source rocks from the KC and equivalent formations (i.e., Mandal, Draupne, Tau) were sampled. Twenty-five KC samples were collected from four wells in the British Central Graben and 33 samples were collected from the ten wells in the Norwegian North Sea (Fig. 1; Table 1). Sampling of wells in the Norwegian and British sectors was conducted at the NPD and Stratum Reservoir AS, Stavanger, Norway, and at Core Lab in Aberdeen, UK, respectively. Core samples were prioritized, but cuttings were sampled for denser vertical coverage. All source rock samples were submitted for both chemical and petrographic analyses. From the Norwegian North Sea, 20 crude oils were sampled and analysed for stable carbon isotopes of the saturate and aromatic fractions, as well as for gas chromatography (GC) and gas chromatography-mass spectrometry (GC-MS). Additional analytical data for 132 oils was retrieved from the IGI's NPD database (https://igiltd.com/news/official-release-of-igis-npd-norwegian-north-sea-database) for broader coverage of the Norwegian North Sea (Table 2).

3.2. Analyses

The source rock samples were analysed for organic carbon content (TOC) and generative potential (Rock-Eval) and extracted for stable

Table 1
Well locations, number of samples, and sampling depths. Sample depths in italic represent core samples. Ctry – Country, No–Norway, UK–United Kingdom M – Mandal Fm, T – Tau Fm, D – Draupne Fm, KCF–Kimmeridge Clay Fm.

Ctry	Coordinates		Well	Location	Fm	# of samples	Sample depth (m)
	X	Y					
No	501663.54	6308709.14	2/1-6	Cod Terrace	M	5	4115, *4127, 4147, 4153, 4161*
No	515353.49	6243336.31	2/7-25S	Feda Graben	M	4	4720, 4750, 4783, 4810
No	452016.11	6399820.83	7/4-1	Jæren High	M	3	2976, *2981, 2988.1*
No	583043.78	6416242.45	9/2-2	Egersund Basin	T	4	2964, 2991, 3021, 3054
No	479959.23	6521648.76	16/2-13A	Utsira High	D	2	*2588, 2595*
No	546414.75	6531280.15	17/3-1	Øygarden Fault Complex	T	2	2331, 2337
No	473870.96	6618657.96	25/5-2	Heimdal Terrace	D	5	3020, 3050, 3070, 3100, 3120
No	501794.95	6709625.47	31/4-6	Bjørgvin Arch	D	2	*2125, 2133*
No	554834.84	6707818.42	31/6-3	Stord Basin	D	4	1380-85, 1400-02, 1425-30,1485-90
No	450299.76	6796001.43	34/7-21	Tampen Spur	D	3	*2552, 2570, 2580*
UK	434064.82	6277704.92	29/15-2	Curlew-Puffin Platform	KCF	3	4587, 4621, 4648
UK	462624.47	6306855.78	30/2A-6	Breiflabb Basin	KCF	4	5230, 5252, 5273, 5291
UK	466936.08	6284626.88	30/8-1	Feda Graben	KCF	8	3716, 3743, 4191, 4246, 4292, 4392, 4462, 4478
UK	472651.52	6276323.72	30/13-3	Feda Graben	KCF	11	3901, 3932, 3962, 3972, 3981, 3990, 3996, 4008, 4017, 4026, 4036

carbon isotope measurements. All analyses were performed by Applied Petroleum Technology AS (APT), Oslo, Norway, following the Norwegian Industry Guide to Organic Geochemical Analysis (NIGOGA; Weiss et al., 2000). Maceral and mineral counting was performed by the RPS Group Inc, Kentucky, USA.

3.2.1. Maceral and mineral counting

To determine the maceral and mineral composition, the rock samples were crushed to pass through a 16-mesh sieve. The resulting material was embedded in thermoplastic epoxy in 2.54 cm moulds, which were left overnight to harden. These pellets were further ground and polished according to ASTM standards (ASTM, 2011). The samples were then investigated in white- and UV-light using a Zeiss Axio-Scope A1 at 500x (50x eyepiece, and 50x objective) in immersion oil. An X-Cite 120 LED light source provided with white and UV-light. A proprietary automated point-counter attached to the stage of the Zeiss Axio-Scope, was used for the point-counts, where the macerals and minerals were identified under the cross-hairs. Data of the maceral and minerals were captured using proprietary software; when a count was made, the computer and motorized stage automatically moved step-wise to a new, random field of view. A minimum of 300 counts were made of macerals and minerals for each sample. To obtain a statistical maceral dataset counting continued until 100 maceral particles had been registered. The resolution of the microscope was 1 μm (≥1 μm).

3.2.2. Rock-Eval

The Rock-Eval analysis was performed using a Rock-Eval 6 instrument for direct measurement of free hydrocarbons (S1), remaining hydrocarbon generative potential (S2), carbon dioxide (CO2) content produced during thermal cracking (S3), and temperature of S2 maxima (Tmax; Espitalié et al., 1977). The pyrolysis program started at 300 °C (held for 3 min) followed by an increased to 650 °C at 25 °C/min.

3.2.3. Total organic carbon (TOC)

For TOC analysis, the samples were first treated with diluted hydrochloric acid to remove carbonate minerals and then combusted in a LECO SC-632. The quantities of carbon in the sample was measured as carbon dioxide by an IR-detector.

3.2.4. Extraction

The source rock samples were extracted by using a Soxtec Tecator instrument. Thimbles were pre-extracted in dichloromethane with 7% (vol/vol) methanol, 10 min boiling and 20 min rinsing. The samples were weighed and boiled for 1 h and rinsed for 2 h in approximately 80 cc of dichloromethane with 7% (vol/vol) methanol. Copper blades activated in concentrated hydrochloric acid were added to the extraction cups to cause free sulphur to react with the copper. An aliquot of 10% of the extract was transferred to a pre-weighed bottle and evaporated to dryness. The amount of extractable organic matter was calculated from the weight of this 10% aliquot.

3.2.5. Deasphalting and quantitive medium performance liquid chromatography

Before oil and source rock extracts could be further analysed, the samples were deasphalted and separated into saturate, aromatic, and asphaltene fractions. For deasphalting, the aliquots were evaporated to almost dryness before a small amount of dichloromethane was added (3 times the amount of extractable organic matter (EOM)). Pentane was added in excess (40 times the volume of EOM/oil and dichloromethane) and the solution was stored in a dark place for 12 h before the solution was filtered or centrifuged and the weight of asphaltenes measured. Following, the saturate and aromatic fractions were separated employing the medium performance liquid chromatography (MPLC) set-up as described by Radke et al. (1980).

3.2.6. Isotope of saturate and aromatic fractions

The stable carbon isotope analysis of the saturate and aromatic hydrocarbon fractions was performed using a Thermo Fisher Scientific Elemental Analyser held at 1000 °C, increasing to 1700 °C as a result of the excess supply of oxygen to help flash combust the samples. Water was trapped on magnesium perchlorate, and a column separated CO_2 flashed into Delta V Plus IRMS (Isotope Ratio Mass Spectrometer via Conflo IV).

3.2.7. Gas chromatography (GC) of whole oil

Whole-oil gas chromatography was performed on an Agilent 7890 gas chromatograph coupled with a Hewlett Packard-PONA capillary column (50 m × 0.2 mm, film thickness = 0.50 μm). Oven temperature was programmed to run from 30 °C (held for 10 min) to 60 °C (held for 10 min) at 2 °C/min, then rise to 130 °C at 2 °C/min, and finally increase to 320 °C at 4 °C/min (held for 25 min). A constant flow of hydrogen carrier gas was used through the entire gas chromatographic run and 2-heptene was used as an internal standard.

3.2.8. Gas chromatography–mass spectrometry (GC-MS) of saturate and aromatic fractions

Gas chromatography-mass spectrometry (GC–MS) of saturate and aromatic fractions of whole oils were analysed using a Thermo Scientific DFS (double-focusing system) high-resolution gas chromatography–mass spectrometry instrument (GC–HRMS) from ThermoFisher. The instrument was tuned to a resolution of 3000, and data was acquired in selected ion recording (SIR) mode (GC-MS SIR). A CP-Sil-5 CB-MS capillary column (60 m × 0.25 mm, film thickness = 0.25 μm) was employed. Deuterated sterane (D4-27ααR) was used as an internal

standard for the saturate fraction and D8-naphthalene, D10-biphenyl, D10-phenanthrene and D12-chrysene were used for the aromatic fraction. The oven starting temperature was 50 °C and was programmed to rise from 50 °C to 120 °C at 20 °C/min, and then from 120 °C to 320 °C at 2 °C/min (held for 20 min). For the saturate fraction, ions with mass/charge (m/z) ratios of 177, 178, 191, 217, and 218 were monitored in both peak height and concentrations. As for the aromatic fraction, ions with m/z ratios of 178, 184, 192, 198, 231, 245, and 253 were monitored. The concentration of the peaks were used to calculate the hydrocarbon and biomarker ratios for the analysed oils. It should be mentioned that the dataset provided by the IOI and NPD has been collected over many years. Thus, the analyses have been conducted in several different laboratories, which may increase the uncertainty of the dataset. Values in the dataset represent a mixture of peak area and peak height. This, however, is not believed to comprise a problem as values used represent ratios.

4. Results and discussion

4.1. Source rock

4.1.1. Thermal maturity

Rock-Eval Tmax values generally lower than 435 °C (Table 3; Fig. 3) indicate that most source rock samples are thermally immature for petroleum generation (Peters et al., 2005a). Tmax values between 435 and 445 °C for some samples from wells 29/15-2, 30/2a-6, 30/8-1, 30/13-3, 2/1-6, and 9/2-2 suggest early maturity stages. Higher Tmax values of up to 450 °C in samples from well 2/1-6 are indicative of intermediate to late generation stages (Peters et al., 2005a). In the Central Graben, sample depths are generally greater than 3700 m, which is within the temperature range estimated for the early oil window as calibrated by Spencer et al. (1986) and Cornford (1994) for the Central Graben. Peak oil and late oil window temperatures occur, according to the same authors, at depths of about −4000 and −4200 m, respectively, while gas window temperatures occur at depths greater than 4500 m. Fig. 4 displays the thermal maturity distribution to the top of the Upper Jurassic source rocks in the northern North Sea after Pegrum and Spencer (1990).

The source rock samples collected from the Central Graben wells (i.e., 29/15-2, 30/2a-6, 30/8-1, 30/13-3, 2/1-6, 2/7-25S) do not follow the aforementioned trend. Interestingly, sediments sampled at depths greater than 4000 m exhibit Tmax values (~420-445 °C) that are consistent with immature or early oil window stages (Peters et al., 2005a). However, the thermal maturity map of Pegrum and Spencer (1990) indicates that the Upper Jurassic rocks in the Central Graben presently lie within the light oil/condensate or gas windows (Fig. 4). Yang and Horsfield (2020) describes several reasons for depressed Tmax values as observed in the presented dataset. Among these, the carry over effect of heavy oil or heavy bitumen may be a possible explanation, as heavy oil or bitumen are not always removed at 300 °C. In these cases, they are carried over into the S2 (Clements, 1979), which represents the remaining hydrocarbon generative potential (Espitalié et al., 1977), shifting it to lower temperature (lower Tmax). The heavy oil and bitumen may result from drilling additives, migrated- and/or *in situ* hydrocarbons (Gonçalves et al., 2013; Kus et al., 2016). The NPD fact pages confirm that the sampled interval in well 2/7-25S was drilled with OBM. For the UK wells no information regarding mud type used during drilling is revealed. The high production index (PI) values (>0.40) at low Tmax temperatures seemingly support this suspicion about the depressing effects of OBM, migrated- and/or *in situ* hydrocarbons (Fig. 3). Clements (1979), Peters (1986) and Petersen et al. (2017) document that contamination with OBM, migrated, and/or *in situ* oil may produce a shoulder adjacent to the S2 peak in the 350–450 °C temperature range, thus affecting the accuracy of Tmax and HI values. In the dataset, S2 shoulders are observed on several pyrograms from samples with a high PI. Fig. 5A displays a pronounced S2 peak while Fig. 5B displays an incipient S2 peak, hence implying possible contamination with OBM, migrated- and/or *in situ* hydrocarbons.

Carvajal-Ortiz and Gentzis (2015) and Rodriguez and Katz (2021) suggest that OBM contamination can be the reason for the high TOC values relative to low concentrations of organic materials (i.e., macerals) in their Eagle Ford dataset. In this study, such condition is displayed by some samples from the Central Graben (Fig. 6). Because contamination

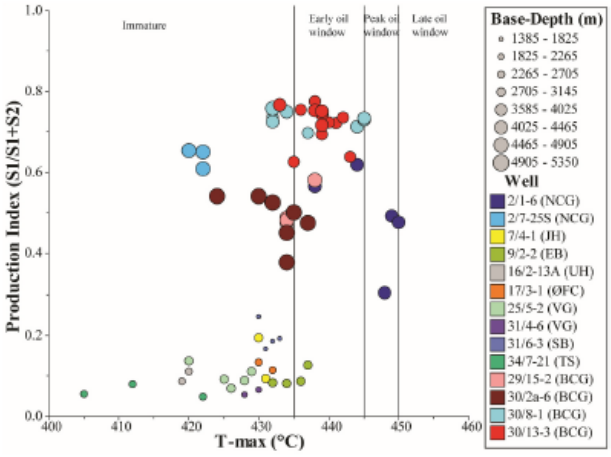

Fig. 3. Tmax (°C) values cross-plotted against production index (PI; S1/(S1+S2)) shows the Central Graben samples to have high PI at low Tmax. This may be a result of contamination with oil base mud and/or migrated or *in situ* hydrocarbons. BCG– British Central Graben, NCG– Norwegian Central Graben, JH – Jæren High, EB – Egersund Basin, UH–Utsira High, ØFC – Øygarden Fault Complex, VG–Viking Graben, SB–Stord Basin, TS – Tampen Spur.

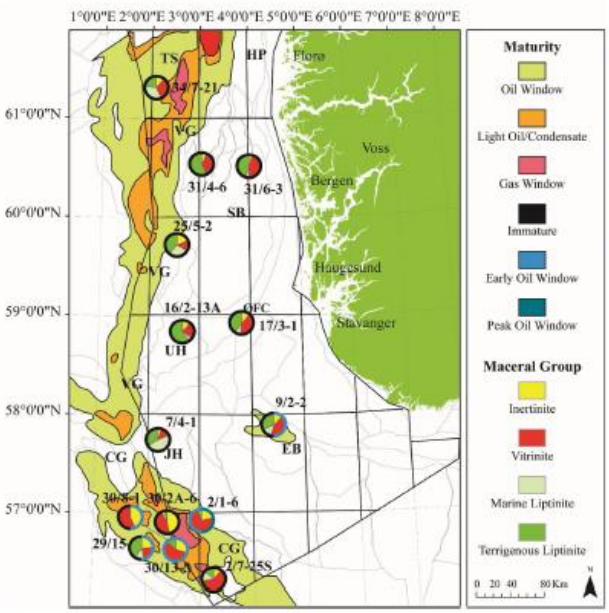

Fig. 4. Map shows estimates of the different hydrocarbon windows at the top of the Upper Jurassic source rock system. Modified from Pegrum and Spencer (1990). The authors modelled this maturity for the Base Cretaceous, thus, this figure shows the maturity of the top source rock interval (i.e., minimum maturity) according to the estimated vitrinite reflectance (%Ro; 0–0.6 %Ro = immature, 0.6–1.0 % Ro = oil, 1.0–1.3 %Ro = light oil/condensate, >1.3 % Ro = gas). The Pie charts show the average maceral composition per well. The circle around the pie charts indicates their estimated maturities according to the Tmax in Fig. 3. BCG= British Central Graben, NCG= Norwegian Central Graben, JH = Jæren High, EB = Egersund Basin, UH=Utsira High, ØFC = Øygarden Fault Complex, VG=Viking Graben, SB=Stord Basin, TS = Tampen Spur.

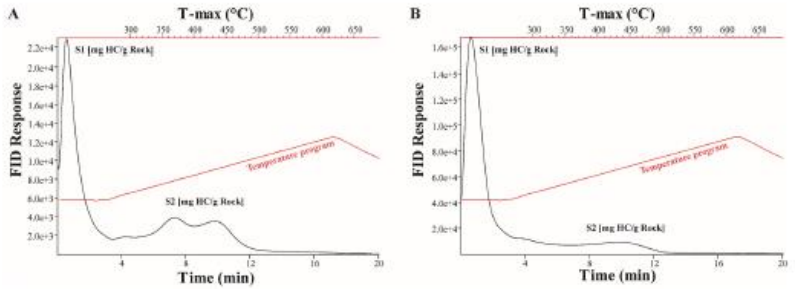

Fig. 5. Rock-Eval pyrograms showing the existence of a pronounced (A) and incipient (B) S2 shoulder possibly resulting from contamination with oil based mud, migrated hydrocarbons, solid bitumen and/or *in situ* hydrocarbons. Sample in A was collected from well 30/13-1 at 3901.4 m. Sample in B was collected from well 2/7-25S at 4782. 5m.

appears to be present in the Central Graben samples, they are not included in the following chapters for Rock-Eval and TOC data. As for the remaining samples, the positive correlation between organic materials (i.e., macerals and solid bitumen vo%) and TOC content suggests consistency between microscopic and geochemical analyses. Such correlation also indicates that much of the solid organic particles are larger than the resolution of the microscope (i.e., ≥ 1 μm; Scheidt and Littke, 1989).

4.1.2. Facies variations

Fig. 7 cross-plots TOC versus S2 values for thermally immature source rock samples (i.e., Tmax <435C°) in the dataset. The majority of the samples possess HI values in the range between 200 and 500 mg HC/g TOC and thus indicate that the samples are capable of generating both liquid and gaseous hydrocarbons. TOC contents ranging from 1.8 to 9.6 wt% further demonstrate the source rock variability in the sample set (Fig. 7; Table 3).

For the purpose of identifying variations in organic matter inputs and drawing inferences on the associated depositional environment, the bulk

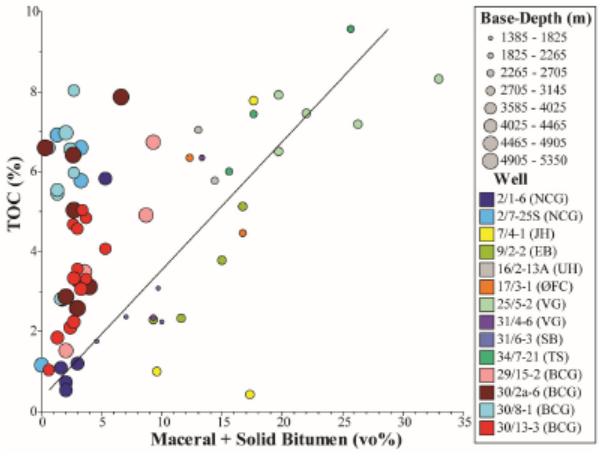

Fig. 6. TOC (wt.%) as a function of the maceral + solid bitumen content in volume percentage (vo%). Notice that samples from the Central Graben show high TOC values, whereas the organic content (i.e., maceral + solid bitumen) is low, suggesting contamination either by OBM or migrated hydrocarbons, alternatively *in situ* oil. BCG– British Central Graben, NCG– Norwegian Central Graben, JH – Jæren High, EB – Egersund Basin, UH–Utsira High, ØFC – Øygarden Fault Complex, VG–Viking Graben, SB–Stord Basin, TS – Tampen Spur.

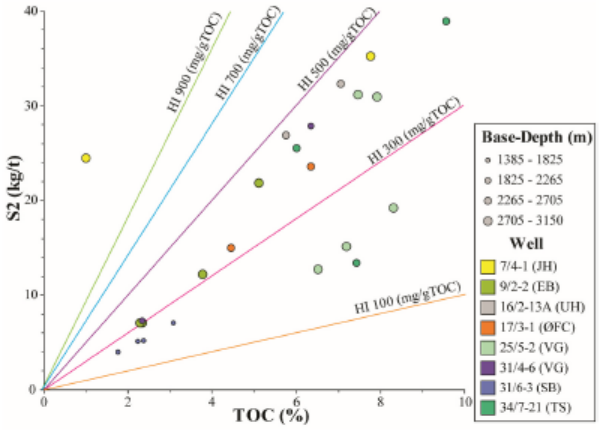

Fig. 7. TOC (wt.%) plotted against Rock-Eval S_2 (Kg/t). Hydrogen index (HI) trend lines ranging from 100 to 900 mg HC/g TOC are shown. BCG– British Central Graben, NCG– Norwegian Central Graben, JH – Jæren High, EB – Egersund Basin, UH–Utsira High, ØFC – Øygarden Fault Complex, VG–Viking Graben, SB–Stord Basin, TS – Tampen Spur.

maceral data was divided into inertinite, vitrinite, and liptinite groups. The liptinite group was further subdivided into a marine- and a terrigenous fraction (Figs. 8 and 9). Dinoflagellate cysts (i.e., alginate) dominate the marine liptinite sub-group, whereas the terrigenous liptinite sub-group comprises mostly sporinite and liptodetrinite (Fig. 10A, D-E). The vitrinite group is dominated by macerals of the detrovitrinite family with non-detrital vitrinite particles only constituting a minor part (Fig. 10B and C). Detrovitrinite and liptodetrinite are small particles (i.e., smaller than 10 μm in size) with unrecognisable structures within their respective vitrinite and liptinite groups (ICCP, 1998; Pickel et al., 2017). It is worth highlighting that the composition of each maceral group is relatively homogenous through the Upper Jurassic source rocks. This suggests that there are minor changes in the biota sourcing the organic matter and possibly some distance from land as one would expect larger variety of land-plants with closer proximity (Langrock et al., 2003). Variations in the relative abundance of each fraction are, however, observed.

The overall maceral composition shows vertical variations for most of the studied well sections (Figs. 8 and 9). The organic matter detectable under the microscope in wells 29/15-2, 30/8-1, 30/13-3, 2/1-6, 2,

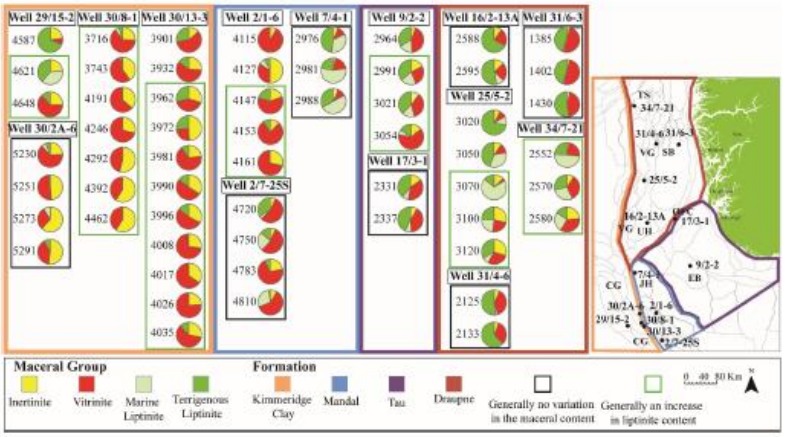

Fig. 8. Pie diagrams represent the maceral composition of the investigates samples. The corresponding sample depth is given in meters. Well locations and the distribution of the equivalent formations are indicated on the map. Both vertical and lateral organofacies variations are observed. CG—Central Graben, JH — Jæren High, EB — Egersund Basin, UH—Utsira High, ØFC — Øygarden Fault Complex, VG—Viking Graben, SB—Stord Basin, TS — Tampen Spur.

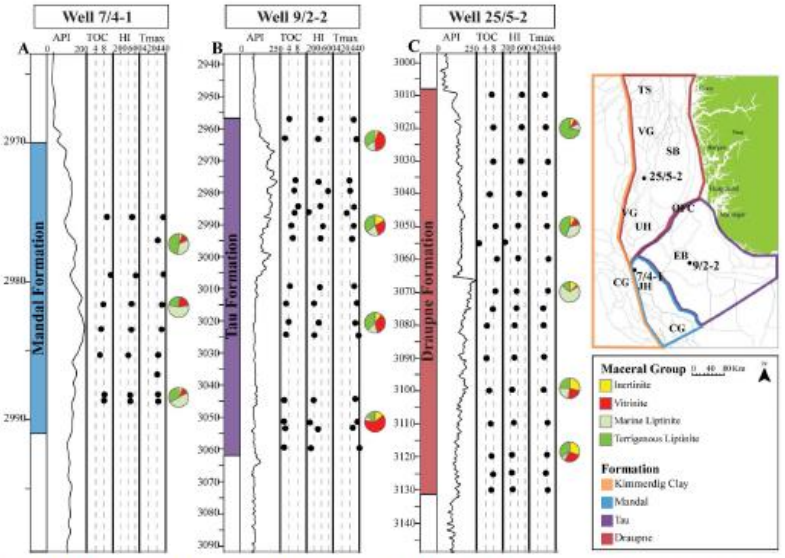

Fig. 9. Gamma Ray log (API), TOC (wt.%), hydrogen index (HI; mg HC/g TOC), Tmax (°C) values, and maceral compositions (in pie diagrams) for selected wells displaying the characteristic source rock patterns described in the text. The Rock-Eval data is supplemented with TOC, HI and Tmax values from the IGI dataset. A) Relatively homogeneous maceral composition with minor fluctuations in TOC and HI. B and C) General upward increase in the content of liptinitic macerals, TOC, and HI values topped by a subtle increase in vitrinite macerals and a decrease in TOC and HI values. CG—Central Graben, JH — Jæren High, EB — Egersund Basin, UH—Utsira High, ØFC — Øygarden Fault Complex, VG—Viking Graben, SB—Stord Basin, TS — Tampen Spur.

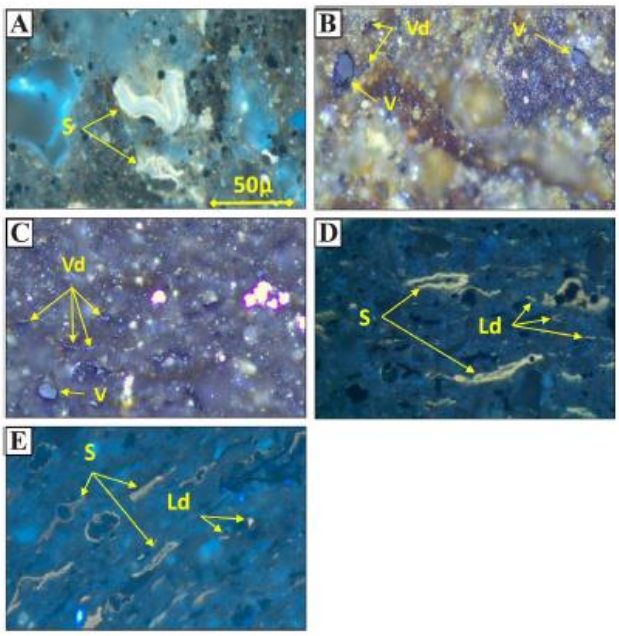

Fig. 10. Photos taken at 500X. A) Photo illustrating fluorescing sporinite (S) in UV-light from well 7/4-1 at 2998 m. The larger spore is likely a terrestrial microspore whereas the thin-walled sporinite may be a marine dinoflagellate. B) White-light photo, illustrating larger particles of vitrinite (V) and smaller particles of detrovitrinite (Vd) from well 25/5-2 at 3070 m. C-D) Paired photos in white- and UV-light photo from well 9/2-2 at 3021 m. (C) White-light photo illustrating larger particles of vitrinite (V) and smaller particles of detrovitrinite (Vd). D) UV-light photo illustrating fluorescing sporinite (S) and liptodetrinite (Ld), which is smaller dispersed particles of fluorescing organic matter (less than 10 µm in size) of unknown origin. E) UV-light photo illustrating several examples of fluorescing sporinite (S) and abundant liptodetrinite (Ld) in well 25/5-2 at 3120 m.

9/2-2, 25/5-2, and 34/7-21 is dominated by vitrinite and inertinite macerals in the deeper part of the investigated source intervals. The relative amount of marine and terrigenous liptinite particles increases gradually towards the top of the organic-rich interval (Fig. 8). This increase in liptinitic macerals is coincident with a subtle increase in TOC and HI values (Fig. 9B and C), which in turn implies an upward increase in the proportion of Type II kerogen. Huc et al. (1985), Dahl and Speers (1985), and Justwan et al. (2005) document a similar trend in the Viking Graben using Rock-Eval data, and Petersen et al. (2016) and Ponsaing et al. (2018, 2020) report this trend in the in the Danish Central Graben. The overall high content of terrigenous liptinites observed in the investigated organic-rich sediments suggests a continuous contribution of land-plant biomass from the surrounding highs despite of the regional transgressive event. In wells 2/1-6, 9/2-2, 25/5-2, 31/4-6 and 31/6-3 (Figs. 8 and 9B), an increase in the content of vitrinitic macerals paired with a slight decrease in TOC and HI are observed at the very top of the Upper Jurassic source rock interval. This coincides with a general decrease in the pyrite content (Table 4). These observations may suggest a shift back to higher levels of oxygen. Justwan and Dahl (2005) also notice this change at the top of the Draupne Formation in wells from the Viking Graben, and Langrock et al. (2003) report this change during the transition from Upper Jurassic to Lower Cretaceous in the Norwegian Sea.

The overall maceral composition in wells 30/2A-6, 2/7-25S 7/4-1, 17/3-1, 31/4-6, and 31/6-3 (Fig. 8) remains relatively constant through the studied section, suggesting minor changes in organic inputs and depositional environment at these locations. A slightly higher content of vitrinite particles may, however, be observed. This increase in higher-plant inputs is most likely due to mass flow deposits deriving from subaerially exposed highs (Fig. 8). Naturally, these wells also record less variations in TOC and HI values relative to wells with an upward increase in liptinite content (Fig. 9).

Fig. 4 shows the average maceral composition for each of the studied wells. The observed changes in the bulk maceral composition suggest that the different geographic areas have received varying contributions of marine and terrigenous organic inputs. The average values are computed from a limited number of samples from few wells, and therefore do not necessarily reflect the overall maceral composition across the study area. Fig. 8 displays the maceral composition for each of the analysed samples in representative wells from the KC, Mandal, Tau, and Draupne formations. Significant differences are observed between the different areas and vertically through the source rock interval.

A higher content of liptinite is observed within the Tau and Draupne formations, as well as in the Mandal Formation in well 7/4-1, compared to the KC and Mandal formations in the remaining wells (Fig. 8). It should be mentioned that the low content of liptinite preserved in source rock samples from the Central Graben buried to depths greater than 4000 m may have resulted from high thermal maturation or by drill-bit metamorphism. At elevated maturities, the fluorescence of liptinitic macerals decreases and eventually disappears, selectively preserving the most resistant macerals (i.e., vitrinite and inertinite; Misch et al., 2019; Al-Hajeri et al., 2021). Ziegs et al. (2017) and Misch et al. (2019) report a high content of terrigenous organic matter on the Cod Terrace where well 2/1-6 is located, hence, supporting the presented findings. Likewise, it cannot be ruled out that the very high content of inertinite reported in the investigated samples from the Central Graben (Fig. 8) is overestimated due to difficulties discriminating between minerogenic and organic matter.

Variations in the relative proportions of marine and terrigenous liptinite macerals are also detected in the sample set (Fig. 8). Wells 7/4-

1, 25/5-2 and 34/7-21 possess the highest content of marine liptinite macerals. This implies less contribution of terrigenous organic materials from the hinterland. The full variability in source rock facies within each well, and hence the likely petroleum blend to be generated, cannot be faithfully reproduced by a limited set of source rock samples. Analyzes of migrated oils may better reflect the compositional attributes of their parental sources as will be discussed in the following sections.

4.1.3. Relationship between total organic carbon and maceral compositions

The volume percentage of liptinitic (i.e., marine + terrigenous) macerals displays an overall positive correlation with TOC (Fig. 11A). On the other hand, the percentage of vitrinitic macerals, when cross-plotted against TOC, shows a negative correlation (Fig. 11B). This trend is similar to that Misch et al. (2019) describes for the Mandal Formation. The coexistence of decreasing TOC values with increasing vitrinite content is interpreted to result from higher oxidising conditions. Fig. 11C shows a positive correlation between increasing vitrinite content and increasing oxygen index (OI), substantiating that the detected higher inputs of land plant-derived organic material (i.e., vitrinite) occurred under relatively more oxygenated water conditions (Ziegs et al., 2017).

4.1.4. Relationship between pyrite, total organic carbon, and maceral composition

The volume percentage of pyrite relative to the total mineral count can be exploited as an indicator of oxygen availability during sedimentation and early diagenesis (Berner, 1984). Oxygen-depleted conditions in the top sediment act as a reductant for sulphate and favour the formation of sedimentary pyrite if a supply of reactive iron exists (Berner, 1984). A positive correlation between the volume percentage of pyrite and TOC (Fig. 12A) is observed in the dataset. This correlation implies that the accumulation and preservation of organic carbon increases proportionally with decreasing oxygen content, which in turn determines the availability of sulphide for pyrite formation (Berner, 1984; Raiswell et al., 1988; Lückge et al., 2002). The volume percentage of marine liptinite is also seen to positively correlate with the content of pyrite (Fig. 12B), which implies prevailing oxygen limited conditions in areas where marine liptinite was deposited and preserved. The fluorescence of liptinitic macerals decreases with increasing maturity and becomes unrecognisable in overmature source rocks (Misch et al., 2019;

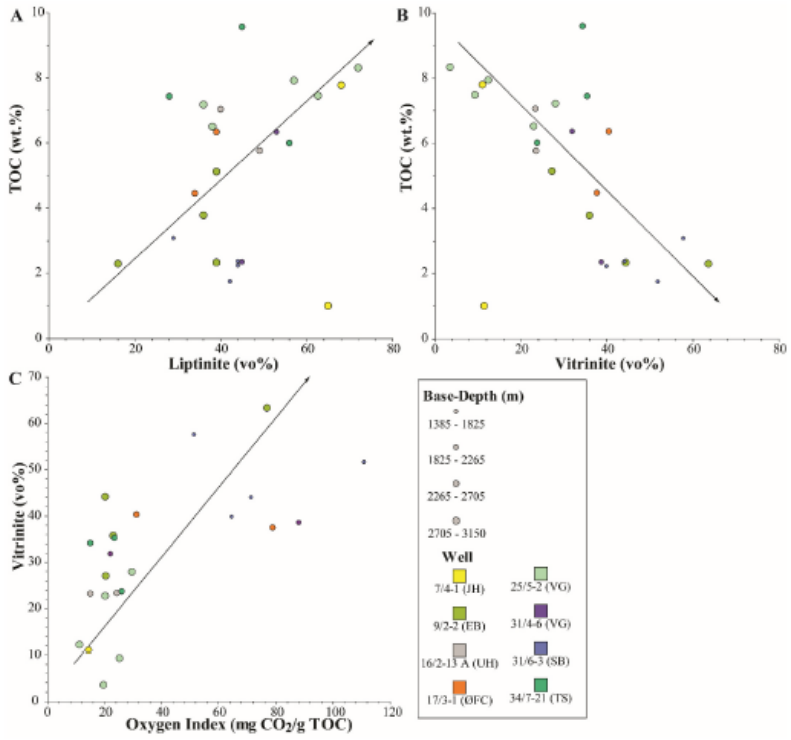

Fig. 11. A) Liptinite- and B) vitrinite content in volume percentage (vo%) plotted against TOC (wt.%). A) There is a positive correlation between TOC and liptinite (marine + terrigenous) content, whereas B) a negative correlation between TOC and vitrinite content. C) Oxygen index (mg CO_2/g TOC) plotted against vitrinite (vo %) displays increasing vitrinite content to coincide with increasing OI values. BCG– British Central Graben, NCG– Norwegian Central Graben, JH – Jæren High, EB – Egersund Basin, UH–Utsira High, ØFC – Øygarden Fault Complex, VG–Viking Graben, SB–Stord Basin, TS – Tampen Spur.

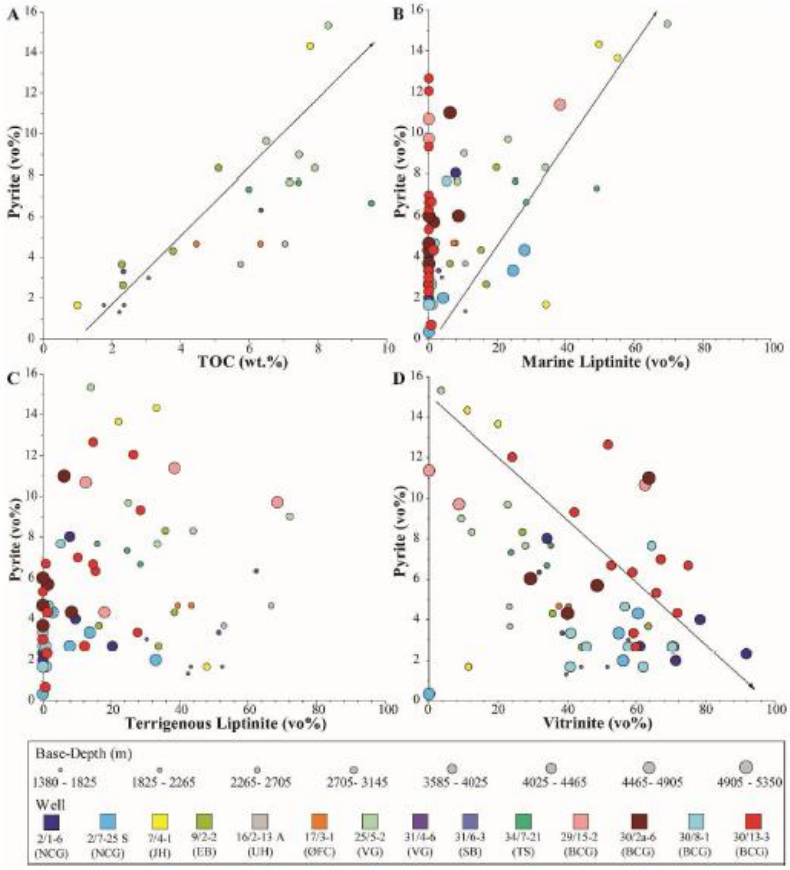

Fig. 12. Pyrite content in volume percentage (vo%) as a function of A) TOC (wt.%), B) marine liptinite (vo%), C) terrigenous liptinite (vo%), and D) vitrinite (vo%). The increase in pyrite is associated with higher levels of anoxia. Both TOC and marine liptinite content display a positive correlation with pyrite content, whereas vitrinite content shows a negative correlation. Terrigenous liptinite- versus pyrite content shows no trend. BCG— British Central Graben, NCG— Norwegian Central Graben, JH — Jæren High, EB — Egersund Basin, UH—Utsira High, ØFC — Øygarden Fault Complex, VG—Viking Graben, SB—Stord Basin, TS — Tampen Spur.

Al-Hajeri et al., 2021). This condition could provide an explanation for high pyrite concentrations associated with little to no marine liptinitic macerals in some of the deeply buried samples in the UK sector (Fig. 12B). Terrigenous liptinites may be transported and deposited in oxidising, coastal and more anoxic marine environments, which may explain the poor correlation with pyrite contents observed in Fig. 12C.

Similar to the cross-plot of vitrinite versus TOC (Fig. 11B), a negative correlation is observed between vitrinite and pyrite in Fig. 12D. Higher-plant derived vitrinitic material is normally deposited in coastal, near-shore environments where the content of dissolved oxygen in the water column and the top sediment is abundant. This condition does not favour the formation of pyrite and explains the negative correlation seen in Fig. 12D.

4.1.5. Stable carbon isotopes of source rock extracts and their relationship with pyrite content and maceral composition

Stable carbon isotopes of the saturate fraction of selected source rock extracts vary with respect to maceral composition and pyrite contents. In Fig. 13A, the stable carbon isotope composition of the saturate fraction is seen to become increasingly lighter with an increasing volume percentage of liptinitic macerals. This trend implies a positive correlation between the isotopic composition of the extractable organic matter and that of the macerals. Fig. 13B shows that stable carbon isotope values of the saturate fraction become heavier as the volume percentages of pyrite decreases. Although the stable carbon isotope compositions of organic matter in a source rock is not directly dependent on redox conditions during sedimentation, it is apparent that at least in this dataset lighter

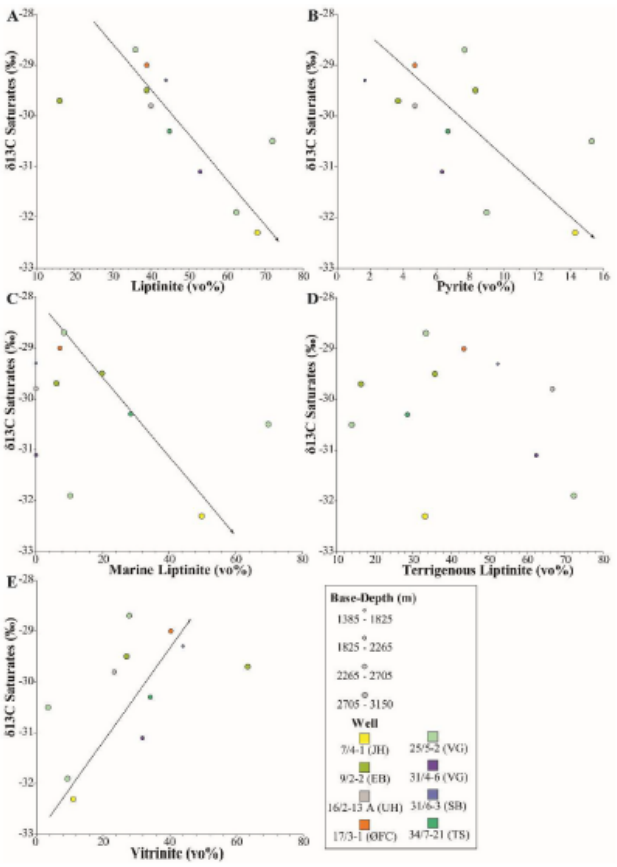

Fig. 13. A) Pyrite-, B) Bulk liptinite-, C) Marine liptinite-, D) Terrigenous liptinite-, and E) Vitrinite content in volume percentage (vo%) plotted against stable carbon isotope values (‰) of the saturate fraction of extracts from source rocks. Oils with isotopically lighter composition coexist with higher contents of pyrite and marine liptinite, whereas oils with comparatively heavier isotope values coincides with higher content of vitrinite. Terrigenous liptinite shows no correlation with the measured isotopes. BCG– British Central Graben, NCG– Norwegian Central Graben, JH – Jæren High, EB – Egersund Basin, UH–Utsira High, ØFC – Øygarden Fault Complex, VG–Viking Graben, SB–Stord Basin, TS – Tampen Spur.

isotope values are coincident with increasing liptinitic inputs interpreted to occur under decreasing oxygen contents (see discussion in section 4.2.1). The trend is less obvious when separating the liptinite group into marine (Fig. 13C) and terrigenous (Fig. 13D) sub-groups. This condition likely reflects the varying depositional conditions in which terrigenous liptinite can be deposited. In Fig. 13E, the isotopic composition of the analysed samples becomes increasingly heavier with increasing vitrinite content. The above observations support the findings by Justwan et al. (2005) and Langrock et al. (2003), which show a similar trend using Rock-Eval data. They associate light carbon isotope (saturate and aromatic fractions) compositions of source rock extracts with higher contents of kerogen Type II and comparatively heavier compositions with kerogen Type III.

4.2. Oil geochemistry

The results presented in this study demonstrating changes in organofacies within the Upper Jurassic source rock system support earlier work by various authors (e.g., Huc et al., 1985; Thomas et al., 1985; Cooper et al., 1995; Isaksen and Ledje, 2001; Kubala et al., 2003; Keym et al., 2006; Justwan and Dahl, 2005; Justwan et al., 2005; Petersen et al., 2016, 2017; Ziegs et al., 2017; Ponsaing et al., 2018; Misch et al., 2019; Ponsaing et al., 2020). Those changes are interpreted to indicate fluctuations in sedimentary environments with subsequent variations in oxygen content and organic matter inputs. Interpretations arising from the foregoing study and other works should be used with caution when predicting organofacies development at a regional scale due to the limited number of wells and samples analysed and their preferential locations in or near structural highs.

The geochemical composition of oils often reflects the average compositional attributes of their parental sources (i.e., the dominating type of organic material) more efficiently than a single, or a set of needlepoint rock samples (Zumberge et al., 2016). As such, the geochemical analyses of oils can be exploited as a supplement when assessing the regional development of source rock facies in the absence of pertinent source rock data.

4.2.1. Whole oil stable carbon isotopes and their significance in inferring source rock organofacies

The following approach relies on the premise that the Upper Jurassic source rocks system has sourced most of the produced oils in the North Sea as several authors suggest (e.g., Barnard and Cooper, 1981; Cornford, 1998; Cornford, 2018). The relative abundance of acyclic isoprenoids (i.e., Pristane (Pr) and Phytane (Ph)) is routinely employed as a proxy to determine organic inputs and redox conditions during sedimentation of source rocks and oils. High Pristane/Phytane (i.e., Pr/Ph > 3) ratios suggest terrigenous organic inputs commonly sedimented under oxidizing conditions. Low values (i.e., Pr/Ph < 0.8) of this ratio suggest anoxic, often hypersaline or carbonate environments (Peters et al., 2005b), typically associated with marine organic matter (e.g., Didyk et al., 1978; Hughes et al., 1995). Moderately high Pr/Ph ratios can equally be interpreted to indicate marine organic matter deposited under relatively oxidising environment. In Fig. 14A, a positive correlation between the Pr/Ph ratio and the carbon isotope composition of the saturate fraction of oils from the Norwegian North Sea data base is observed. Thus, increasing terrigenous organic inputs, possibly accumulated under oxidising conditions, are mirrored by successively heavier stable carbon isotopes.

Fig. 14B and C show cross-plots of homohopane and tricyclic terpane biomarker ratios sensitive to sedimentary conditions and organic matter inputs, respectively, versus carbon isotopes. A high abundance of the C35 homohopane relative to C34 homohopane reflects, according to Peters and Moldowan (1991), increasingly anoxic conditions. Fig. 14B shows that higher values of the C35/C34 ratio generally correlate with lighter isotope values. This substantiates the findings in Fig. 14A and further suggests the coincidental development of anoxic depositional environments and light isotope values in the current dataset. It can be argued that the C34/C35 homohopane ratio can equally be interpreted to indicate a carbonate lithology; however, none of the oil biomarker parameters in this study indicates a carbonate source.

The input of terrigenous organic matter to a source rock can be assessed using the abundance of C19 and C20 relative to that of the C21and C22 tricyclic terpanes as represented by the (C19+C20)/(C21+C22) ratio. High values of this ratio are indicative of high relative inputs of humic land-plant organic materials (Peters et al., 2005b). Increasingly higher values of this ratio in Fig. 14C are seen to correlate with successively heavier isotope values of the saturate fraction, which fortifies the observations from Fig. 14A. The ultimate isotope composition of an oil is primarily dependent on the initial isotope composition and molecular H/C ratio of its sourcing kerogen as well as secondary factors such as thermal maturity and expulsion efficiency. The H/C ratio is fundamentally related to a thermodynamically ordered intra- and intermolecular carbon isotope distribution prompted exclusively by biosynthesis (Galimov, 1980). Such a process is governed by the thermodynamic isotope exchange properties of each molecule, known as the β-factor. The lack of oxygen during diagenesis and early burial favours a better preservation of hydrogen and therefore higher H/C molecular ratios in kerogen. This condition may provide an explanation for the detected positive relationship between marine organic matter, which naturally possesses higher H/C ratios, anoxia, and stable carbon isotopes. Thus, the relationship between increasing anoxia and lighter carbon isotopes is at best indirect.

4.2.2. Thermal maturity and other potential factors altering the composition of stable carbon isotopes

The oils in the dataset are derived from various areas of the Norwegian North Sea and from kitchens buried to different depths.

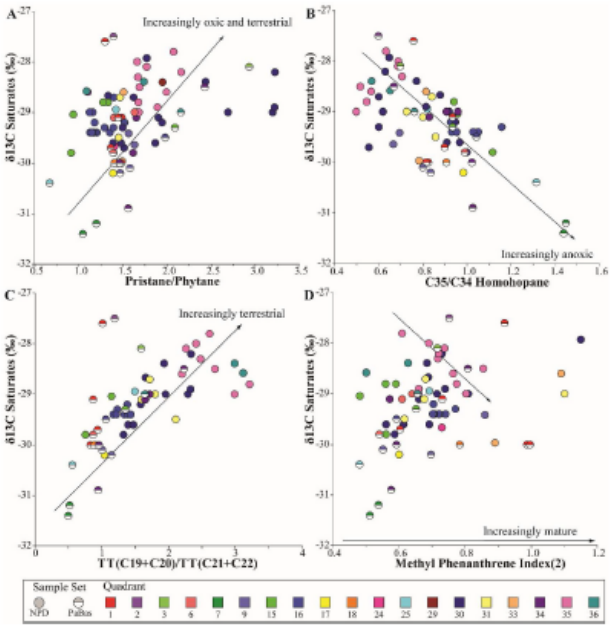

Fig. 14. A) Pristiane/Phytane ratio, B) C35/C34 homohopane ratio, C) C19+C20/C21+C22 tricyclic terpane ratio, and D) methyl phenanthrene index 2 (MPI (2)) plotted against stable carbon isotopes (‰) of the saturate fraction of the oils. The stable carbon isotope values become lighter with increasing marine organic matter, possibly deposited under anoxic conditions and heavier with more terrigenous organic matter, likely deposited under oxidising conditions. Thermal maturity appears to not influence the isotope values.

Therefore, the oils are inferred to have been generated and expelled from source rocks at a wide range of thermal maturities. In an attempt to test if thermal maturity is a major factor driving the isotopic composition of the studied oils, the methylphenanthrene index 2 (MPI (2) = 3(2-methylphenanthrene)/(phenanthrene+1- methylphenanthrene+9-methylphenanthrene); Radke et al., 1982) was plotted against stable carbon isotope values of the saturate fraction (Fig. 14D). The plotted data depicts a poor correlation trend in which the isotope compositions of oils become incipiently heavier with increasing maturity. This trend becomes less evident when comparing oils within the same quadrant. An example is the oils from quadrant 35, which show a negative correlation in Fig. 14D. It can be concluded that although maturity may have an impact on the isotope composition of expelled oils, it does not seem to be the main driving factor guiding the observed variability in the dataset. Other factors such as organic precursors appear to be the dominant imprint on the observed isotope values.

It is worth highlighting that a factor like seal and carrier bed permeability may have impacted the bulk composition of the oils and so that of the stable carbon isotopes. More volatile light fractions migrate faster and progressively fractionate, leaving behind a residue that is enriched in the heavier stable carbon isotope.

4.2.3. Oil grouping

Having established an empirical correlation between molecular and isotope compositions, this work divides the dataset into subgroups that reflect changes in the bulk organic matter composition and inferred sedimentary environments. It is achieved by cross plotting the isotopic composition of the saturate and aromatic fractions of the oils and arbitrarily grouping them in intervals set every 1‰. The groups are intended to reflect variations in the relative proportions of marine and terrigenous organic materials in the parental source rock. Group 1 oils are interpreted to derive from a source rock facies containing the highest proportion of marine organic materials, which decreases gradually and is lowest in the facies sourcing oils in Group 5. Based on the assessment of the oxygen content in the sedimentary environment using homohopane ratios (i.e., Fig. 14B), it is plausible to assume that the marine-rich facies sourcing Group 1 oils was deposited under relatively more anoxic conditions.

4.2.4. Comparison of interpreted facies from source rock and oils

The grouping based on stable carbon isotopes (Fig. 15A) was transferred to the northern North Sea map (Fig. 15B) to compare interpreted source rock organofacies with oil organofacies. Interpretation of gross source rocks organofacies from a limited number of samples from wells often drilled on structural highs are encumbered with large uncertainties as they may not be representative of the deep marine prolific facies. Oils, on the other hand, carry an average compositional view of the gross organofacies within their drainage area.

It cannot be ruled out that some oils may have contributions from source rocks other than the Upper Jurassic as Karlsen et al. (1993), Justwan et al. (2006), Pedersen et al. (2006) and Ohm et al. (2006, 2012) describe, thus affecting the oil composition and introducing uncertainty to the interpretation. However, relying on work by other authors (e.g., Barnard and Cooper, 1981; Cornford, 1998; Cornford, 2018) stating that the Upper Jurassic source rocks generated and expelled most of the oils in the North Sea, the following organofacies are suggested for the source rock system: A) more terrigenous organic matter, possibly associated with oxidising conditions, in the southern part of the Central Graben, North Viking Graben, and Horda Platform areas; and B) comparatively more marine organic matter, possibly associated with

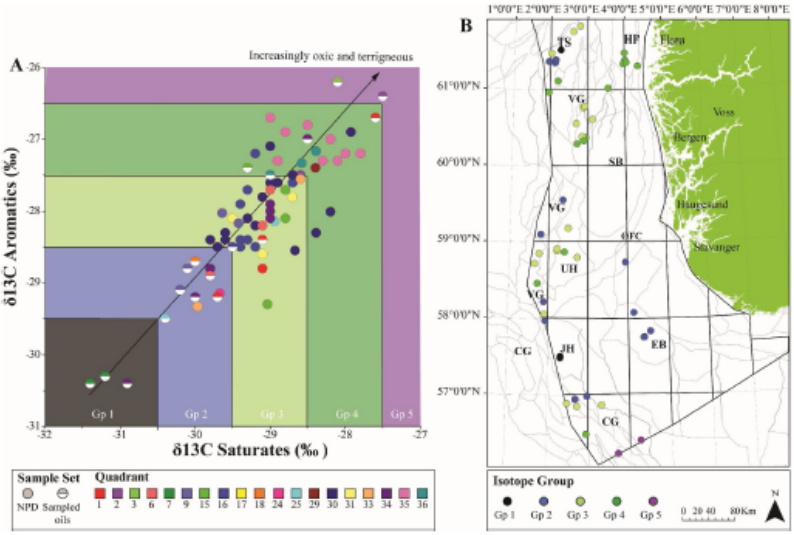

Fig. 15. A) Isotopes of the aromatic and saturate fractions of oils in the dataset. The oils were arbitrarily divided into groups by intervals of 1‰. Group 1 consist of the isotopically lightest oils, which becomes increasingly heavier, and is isotopically heaviest in Group 5. The isotopically lightest oils (Group 1) are associated with higher content of marine organic matter, possibly deposited under anoxic conditions. Successively more influence of terrigenous organic matter, likely deposited under oxidising conditions, is suggested to correspond to comparatively heavier isotope values (Group 5). B) Location of the oils coloured after their assigned groups in A). CG—Central Graben, JH — Jæren High, EB — Egersund Basin, UH—Utsira High, ØFC — Øygarden Fault Complex, VG—Viking Graben, SB—Stord Basin, TS — Tampen Spur, HP—Horda Platform.

anoxic conditions in the northern part of the Central Graben and South Viking Graben areas (Fig. 15B).

The average maceral composition measured in the source rock samples is generally consistent with the source organofacies interpreted from isotopes and molecular data of oils in the same area (Fig. 16). The isotopically lightest oils (Group 1 and 2) occur close to wells enriched in liptinitic macerals, for instance, oils near wells 7/4-1, 25/5-2, and 34/7-21. Intermediate isotope values reflected by Group 3 are found around wells 16/2A-13 and 31/4-6. The isotopically heaviest oils (Group 4 and 5) occur in the southern part of the Central Graben, where the analysed source rock samples have the highest content of vitrinite. However, as discussed in section 4.1.2, the high vitrinite content could be the result of high thermal maturity in this area, which has the potential to mask the liptinitic material. That may well be the case of wells 2/1-6 and 30/2A-6. Source rock samples in these wells exhibit high vitrinite content, but the surrounding oils are isotopically lighter than expected. This discrepancy may also be a result of lateral migration from different facies of their generating source. Deeper source rock units and multiple charging events may also have contributed to charging these traps, affecting the final total isotope compositions.

5. Conclusion

Petrographic and organic geochemical results of the Kimmeridge Clay (KC) equivalents in the northern North Sea show considerable lateral and vertical organofacies variations.

The preserved maceral content of the analysed KC equivalent formations consists mostly of terrigenous oil prone liptinite and varying contributions of vitrinite.

A general increase of liptinites and pyrite towards the top of the KC equivalent formations in seven of the fourteen wells indicates progressive deepening of the depositional sites and development of more anoxic conditions accompanied by enhanced organic matter preservation.

An increase of vitrinite coexisting with a decrease in pyrite content in the uppermost part of the source rock interval in four of the wells is interpreted as a shift back to more oxidising conditions and less favourable conditions for preservation of organic matter during the end of the Upper Jurassic.

The overall maceral composition is consistent with Rock-Eval and isotope data. Thus, source rock isotope data can be used to empirically predict organofacies and depositional environment in the study area.

The stable carbon isotope composition of oils in the dataset was found to carry organofacies information that can be linked to their generating source rocks, and can therefore be used to predict bulk source rock organofacies in areas where pertinent data is absent.

The studied oils suggest generation from more terrigenous influenced organofacies, possibly deposited under oxidising conditions, in the southern part of Central Graben, North Viking Graben, and Horda Platform. Comparatively more marine influenced organofacies, likely deposited under more anoxic conditions, sourced the oils in the northern part of the Central Graben and South Viking Graben.

Declaration of competing interest

The authors declare that they have no known competing financial interests or personal relationships that could have appeared to influence the work reported in this paper.

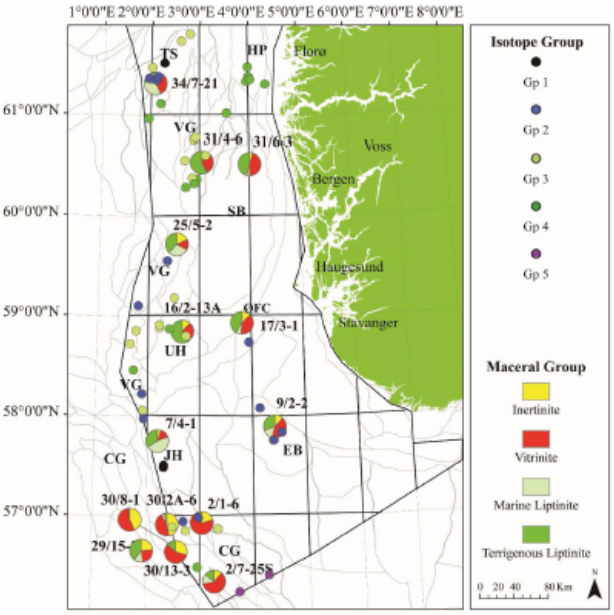

Fig. 16. Map of the Norwegian North Sea comparing the isotope grouping of oils with the average maceral content of source rocks. Lighter saturate fraction isotope values in the oils are observed in areas where source rock intervals contain higher contents of liptinite, and heavier isotopes correlate with increased amounts of vitrinite in the source rock intervals. CG—Central Graben, JH — Jæren High, EB — Egersund Basin, UH—Utsira High, ØFC — Øygarden Fault Complex, VG—Viking Graben, SB—Stord Basin, TS — Tampen Spur, HP—Horda Platform.

Data availability

The data that has been used is confidential.

Acknowledgment

This study is part of the PaBaz consortium (https://pabaz.ux.uis.no/). Acknowledgment goes to the companies sponsoring the project (Aker BP, DNO, Repsol, Vår Energi, Sval Energy and Wellesley). The authors would like to thank Integrated Geochemical Interpretation (IGI) for free software supply and the available dataset of the Norwegian North Sea, Applied Petroleum Technology AS (APT) for analytical studies and RPS Group for mineral and maceral interpretations. Special thanks to Per Erling Johansen (APT) and Thomas Demchuck (RPS Group). We are grateful for Norwegian Petroleum Directorate (NPD), Stratum, Reservoir AS and Core Lab (Aberdeen) for providing sample material. We would also like to thank the reviewers, Olaf Thießen and Dag Arild Karlsen, for the time invested to give constructive and helpful remarks, as well as suggestions to improve our manuscript.

A. Appendix

Table 2

Oil database with the following analytical results: 13C Sat – Isotope of the saturated fraction, 13C Aro – Isotope of the aromatic fraction, Pr/Ph – Pristiane/Phytane ratio, C34/C35 – C34/C35 homohopane ratio, TT ratio – C19 + 20/C21 + 22 tricyclic terpane ratio, MPI(2) – Methylphenanthrene Index 2. BB–Breiflabb Basin, CT–Cod Terrace, SH–Sørvestlandet High, MT – Maureen Terrace, EB – Egersund Basin, LD – Ling Depression, ViSb – Vilje Sub-basin, VeSb – Ve Sub-basin, GT – Gudrun Terrace, UH–Utsira High, VaSb – Vana Sub-basin, VoSb – Volve Sub-basin, BA–Bjørgbin Arch, HH–Heimdal High, FeSb–Fensal Sub-basin, BH–Brage Horst, OFB–Oseberg Fault Block, MFC – Mokkurkalve Fault Complex, LT – Lomre Terrace, MS – Måløye Slope, ØFC – Øygarden Fault Complex, HH–Hidra High, FG–Feda Graben, SB–Søgne Basin, JH – Jæren High, HT–Heimdalen Terrace.

Data Set	Well	Loc	Base Depth	Formation	Type	δ^{13}C SAT	δ^{13}C ARO	Pr/Ph	TT ratio	C35/C34	MPI (2)
NPD	1/2-1	BB	3137	Forties	Oil	−29.1	−28.8	1.5			
NPD	1/3-9 S	CT	4280	Ula	Oil			1.3	2.19	0.72	0.73
NPD	1/3-9 S	CT	4347	Ula	Oil			1.9		0.74	0.80
NPD	2/1-12	SH	3133	Tor	Oil	−28.6	−27.5	1.1			
NPD	2/1-12	SH	3133	Tor	Oil			1.4			
NPD	6/3-1	MT	2993	Skagerrak	DST	−29.0	−27.7	1.6			0.64
NPD	6/3-1	MT	3023	Skagerrak	DST	−29.1	−28.2	1.4			0.61
NPD	9/2-7 S	EB	3896	Sandnes	FMT	−29.6	−28.0	1.6		0.67	
NPD	9/2-7 S	EB	3896	Sandnes	FMT	−29.4	−28.2	1.6		0.69	0.86
NPD	15/12-12	MT	2895	Heather	MDT			1.6		1.24	0.53
NPD	15/12-23	LD	3191	Sleipner	Oil			1.1			
NPD	15/12-23	LD	3191	Sleipner	Oil	−29.8	−28.8	0.9	0.75	1.12	0.56
NPD	15/12-4	MT			Oil	−28.8	−28.1				0.59
NPD	15/12-9 S	MT			MDT					0.93	0.59
NPD	15/12-A-11	MT			MDT					1.00	0.60
NPD	15/3-7	ViSb	4224	Draupne	MDT	−28.8	−27.7	1.3		0.94	0.56
NPD	15/3-7	ViSb	4224	Draupne	MDT			1.4			0.67
NPD	15/5-5	VeSb	2158	Heimdal	MDT	−29.0	−29.3	0.9	1.15	0.96	0.48
NPD	15/5-5	VeSb	2183	Heimdal	DST			0.9		1.03	0.46
NPD	16/1-14	GT	2098	Heimdal	Oil			1.4			
NPD	16/1-14	GT	2098	Heimdal	Oil	−29.4	−28.5	1.2	1.17	1.05	0.74
NPD	16/1-14 T2	GT	2003	Balder	Oil			1.4			
NPD	16/1-14 T2	GT	2102	Heimdal	Oil			1.4			
NPD	16/1-14 T2	GT	2179	Aegard	Oil			1.5			
NPD	16/1-14 T2	GT	2003	Balder	Oil	−29.3	−28.4	1.3	1.23	1.16	0.77
NPD	16/1-14 T2	GT	2102	Heimdal	Oil	−29.4	−28.5	1.2	1.17	1.05	0.72
NPD	16/1-14 T2	GT	2179	Aegard	Oil	−29.4	−27.9	1.4	1.34	1.03	0.72
NPD	16/1-9	GT			Oil			1.4		0.94	0.77
NPD	16/1-9	GT			Oil	−29.3	−27.7	1.4			
NPD	16/2-4	UH	1728	Tor	Oil	−28.7	−27.6	1.4			
NPD	16/2-4	UH	1728	Tor	Oil			1.3		0.98	0.70
NPD	16/2-4	UH	1887	Basement	Oil			1.6		0.94	0.53
NPD	16/2-4	UH	1887	Basement	Oil	−29.2	−27.2	1.5			
NPD	16/2-4	UH	1898	Basement	Oil	−29.0	−28.0	1.2			
NPD	16/2-4	UH	1898	Basement	Oil			1.1		1.02	0.61
NPD	16/2-4	UH	1904	Basement	Oil	−29.0	−28.1	1.1			
NPD	16/2-4	UH	1904	Basement	Oil			1.1		1.01	0.60
NPD	16/3-4	UH	1929	Draupne	Oil			1.2			
NPD	16/3-4	UH	1929	Draupne	Oil	−29.4	−28.5	1.1	1.39	0.93	0.71
NPD	16/3-4	UH	1940	Draupne	Oil			1.2			
NPD	16/3-4	UH	1940	Draupne	Oil	−29.4	−28.4	1.2	1.22	0.95	0.70
NPD	16/3-4 A	UH	2079	Draupne	Oil			1.1			
NPD	16/3-4 A	UH	2079	Draupne	Oil	−29.4	−28.5	1.2	1.44	0.95	0.70
NPD	16/3-4 A	UH	3042	Basement	Oil	−29.2	−28.5	1.2	1.38	0.93	0.70
NPD	16/3-4 A	UH	3042	Basement	Oil			1.3			
NPD	17/12-1 R	EB	2325	Bryne	DST			1.3			
NPD	17/12-1 R	EB	2341	Bryne	DST			1.3			
NPD	17/12-2	EB	2162	Sandnes	DST			1.0			
NPD	17/6-1	LD	2631	Sandnes	Oil	−30.2	−29.1	1.4	1.04	0.98	0.60
NPD	17/6-1	LD	2631	Sandnes	Oil			1.5			
NPD	24/12-3 S	VaSb	2398	Heimdal	Oil	−29.7	−29.2	1.4			0.73
NPD	24/6-2	VoSb	2164	Heimdal	MDT			1.4		0.71	

(continued on next page)

Table 2 (*continued*)

Data Set	Well	Loc	Base Depth	Formation	Type	δ^{13}C SAT	δ^{13}C ARO	Pr/Ph	TT ratio	C35/C34	MPI (2)
NPD	24/6-2	VoSb	2166	Heimdal	DST			1.4		0.70	
NPD	24/6-2	VoSb	2167	Heimdal	MDT			1.4		0.68	
NPD	25/11-15	UH	1774	Heimdal	Oil	−28.9	−28.1	1.4	1.49	0.82	0.69
NPD	25/11-24	UH	2030	Statfjord Gp	Oil			1.4			
NPD	25/2-17	BA	1951	Frigg	MDT			1.5			
NPD	25/4-1	HH	2177	Heimdal	FIT			2.3			
NPD	25/4-1	HH	3188	Hugin	Oil			2.1			
NPD	25/4-1	HH	3194	Sleipner	Oil			2.5			
NPD	25/7-5	VaSb	2052	Hermod	DST			1.9			
NPD	25/7-5	VaSb	2116	Lista	Oil			1.3			
NPD	25/7-5	VaSb	2127	Heimdal	MDT			1.7			
NPD	29/3-1	TS			Oil	−28.4	−27.4	2.0			
NPD	30/10-2	FeSb	2063	Frigg	Oil			1.1			
NPD	30/11-8 A	FeSb	3810	Heather	Oil			4.3			
NPD	30/11-8 A	FeSb	3949	Tarbert	Oil			4.0			
NPD	30/11-8 A	FeSb	3992	Tarbert	Oil			4.3			
NPD	30/11-8 S	FeSb	3555	Tarbert	Oil			0.9			
NPD	30/11-8 S	FeSb	3615	Tarbert	Oil			0.9			
NPD	30/11-8 S	FeSb	3663	Tarbert	Oil			1.1			
NPD	30/11-8 S	FeSb	3748	Ness	Oil			4.4			
NPD	30/3-2 R	BH	2874	Ness	DST	−29.7	−28.5	1.5		0.56	
NPD	30/3-4	OFB	2882	Etive	DST	−29.6	−28.4	1.9			0.56
NPD	30/3-4	OFB	3096	Cook	DST	−29.1	−27.8	1.9			0.66
NPD	30/3-7 S	BH	3519	Jorsalfare	DST	−27.9	−26.9	1.8		0.65	1.15
NPD	30/3-A-1	BH	3088	Kyrre	DST	−29.3	−28.1	1.5		0.60	
NPD	30/3-A-1	BH	3250	Kyrre	DST	−28.7	−27.5	1.6		0.60	
NPD	30/6-27	MFC	3151	Statfjord Gp	MDT	−29.6	−28.3	1.4	1.39	0.91	0.69
NPD	30/6-27	MFC	3163	Statfjord Gp	MDT	−29.8	−28.4	1.4	1.32	1.00	0.59
NPD	30/6-27	MFC	3353	Statfjord Gp	MDT	−29.6	−28.3	1.5	1.48	0.97	0.61
NPD	30/9-10	OFB	2775	Draupne	RFT			1.9			
NPD	30/9-10	OFB	2822	Tarbert	RFT			1.9			
NPD	30/9-13 S	OFB	3073	Tarbert	DST			2.2			
NPD	30/9-15	BA	2264	Ness	MDT	−28.4	−28.3	2.4	1.94	0.77	0.68
NPD	30/9-16	BA	2753	Tarbert	DST			2.9			
NPD	30/9-20 S	BA	2766	Heather	MDT			1.7			
NPD	30/9-20 S	BA	2807	Tarbert	MDT			1.6			
NPD	30/9-22	BA	2830	Draupne	Oil	−29.0	−27.1	3.2	2.29	0.62	0.71
NPD	30/9-22	BA	2868	Tarbert	Oil	−28.9	−27.6	3.2	2.33	0.81	0.74
NPD	30/9-22	BA	2894	Tarbert	Oil	−29.0	−27.6	2.7	1.95	0.92	0.81
NPD	30/9-6	BA	2646	Ness	DST	−28.7	−28.6	1.3	1.66	0.88	0.69
NPD	30/9-8 R	OFB	2836	Tarbert	DST			2.1			
NPD	30/9-9	BA	2311	Tarbert	DST			3.8			
NPD	30/9-9	BA	2409	Rannoch	DST			3.8			
NPD	30/9-9	BA	2409	Rannoch	DST	−28.2	−28.0	3.2	2.34	0.63	0.73
NPD	30/9-F-19	OFB	3438	Ness	MDT	−29.2	−28.2	1.9	1.58	0.95	
NPD	31/4-11	BA	2183	Draupne	MDT	−29.5	−28.1	1.5	2.11	0.86	0.62
NPD	31/4-11	BA	2358	Fensfjord	MDT	−29.1	−28.6	1.5	1.60	0.80	0.68
NPD	31/4-11	BA	2372	Fensfjord	MDT	−28.7	−27.8	1.5	1.72	0.84	0.68
NPD	31/4-11	BA	2679	Ness	MDT	−29.0		1.7	1.80	0.73	1.10
NPD	33/9-19 S	TS	2701	Etive	Oil	−28.6	−27.6	1.5		0.81	1.09
NPD	33/9-G-4 H	TS			FMT	−30.0	−29.3	1.5		0.78	0.89
NPD	34/3-1 S	TS			Oil	−29.0	−27.9	1.7			
NPD	34/3-1 S	TS			Oil			1.7		0.72	0.66
NPD	34/5-1 S	TS	3648	Cook	Oil			1.8			
NPD	34/5-1 S	TS	3648	Cook	Oil	−29.1	−28.4	1.7	1.65	0.83	0.57
NPD	34/5-1 S	TS	3690	Cook	Oil	−29.0	−28.1	1.7	1.72	0.96	0.66
NPD	34/5-1 S	TS	3690	Cook	Oil			1.8			
NPD	34/5-1 S	TS	3690	Cook	Oil	−29.0	−28.0	1.7	1.66	0.91	0.64
NPD	34/5-1 S	TS	3690	Cook	Oil			1.8			
NPD	34/7-17 A	TS	2495	Tarbert	Oil	−29.8	−28.8	1.6			
NPD	34/7-26 A	TS	4180	Draupne	DST			1.5		0.68	0.36
NPD	34/7-26 A	TS	4180	Draupne	DST			1.4			
NPD	34/7-26 A	TS	4208	Draupne	DST			1.4		0.73	0.32
NPD	34/7-34	TS	2471	Statfjord Gp	Oil			1.5		1.00	0.55
NPD	34/7-34	TS	2503	Statfjord Gp	Oil			1.4		0.97	0.53
NPD	35/11-10	LT	1997	Sognefjord	MDT	−28.0	−27.2	1.7	2.41	0.69	0.69
NPD	35/11-10	LT	2049	Sognefjord	MDT	−28.1	−27.3	1.8	2.26	0.69	0.74
NPD	35/11-10	LT	2305	Fensfjord	MDT	−28.3	−27.3	1.7	2.48	0.71	0.72
NPD	35/11-10	LT	2680	Ness	MDT	−27.8	−27.2	2.1	2.61	0.63	0.61
NPD	35/11-12	LT			Oil			1.7		0.70	0.57
NPD	35/11-9	LT	2678	Heather	MDT	−28.6		2.0	2.20	0.57	0.76
NPD	35/9-1	MS	2292	Dunlin Gp	DST	−28.2	−27.0	2.2			0.72
NPD	35/9-2	MS	2342	Fensfjord	DST	−28.9	−27.3	1.9			0.66
NPD	35/9-3 T2	MS	2670	Agat	MDT	−28.5	−26.8	1.7	2.70	0.52	0.85
NPD	35/9-3 T2	MS	2677	Agat	MDT			1.7		0.53	0.82
NPD	35/9-3 T2	MS	2681	Agat	MDT	−28.8	−26.9	1.7	3.21	0.55	0.77

(continued on next page)

Table 2 (*continued*)

Data Set	Well	Loc	Base Depth	Formation	Type	δ^{13}C SAT	δ^{13}C ARO	Pr/Ph	TT ratio	C35/C34	MPI (2)
NPD	35/9-3 T2	MS	2684	Agat	MDT	−29.0	−26.7	1.7	2.99	0.50	0.80
NPD	35/9-3 T2	MS	2701	Agat	MDT			1.7		0.54	0.67
NPD	36/7-1	MS	2369	Fensfjord	DST	−28.4	−27.2	1.7	2.99	0.57	0.63
NPD	36/7-2	ØFC	935	Sognefjord	MDT	−28.6	−27.3	1.1	3.12	0.65	0.50
SO	1/3-3	CT	4214	Bryne	DST	−30.0	−29.2	1.5	0.91	0.83	0.99
SO	1/3-7	HiH	3216	Forties	DST	−29.1	−28.4	1.5	0.87	0.94	0.73
SO	1/2-1	BB	3137	Forties	DST	−29.7	−29.2	1.4	0.94	0.90	0.60
SO	1/3-9 ST2	CT	4347	Ula	Oil	−30.0	−29.2	1.5	0.83	0.81	1.00
SO	1/9-4	FG	3296	Tor	TEST	−27.6	−26.7	1.3	1.01	0.76	0.92
SO	2/12-1	FG	4647	Ula	DST	−27.5	−26.4	1.4	1.19	0.60	0.75
SO	3/7-4	SB	3470	Bryne	DST	−28.1	−26.2	2.9	1.59	0.70	0.72
SO	6/3-1	MT	3015	Skagerrak	TEST	−29.8	−28.9	1.4	0.87	0.99	0.54
SO	7/4-2	JH	3889	Ula	Oil	−31.2	−30.3	1.2	0.52	1.45	0.54
SO	7/7-2	JH	3342	Ula	TEST	−31.4	−30.4	1.1	0.50	1.44	0.51
SO	9/2-1	EB	3210	Sandnes	TEST	−30.1	−28.8	1.6	1.01	0.80	0.55
SO	9/2-3	EB	3268	Sandnes	TEST	−30.2	−29.1	1.5	1.15	0.84	0.70
SO	15/9-12	VeSb	3595	Hugin	TEST	−29.3	−27.4	2.1	1.35	0.94	0.65
SO	16/4-9 S	UH	1981	Hegre Gp	DST	−29.5	−28.5	2.0	1.06	1.04	0.59
SO	25/5-5	HT	2170	Heimdal	Oil	−30.4	−29.5	0.7	0.56	1.31	0.48
SO	18/10-1	EB	2402	Egersund	DST	−30.0	−28.7	1.4	0.89	0.91	0.78
SO	34/4-7	TS	2596	Lunde	DST	−30.9	−30.4	1.6	0.94	1.03	0.58
SO	34/7-16 R	TS	2458	Rannoch	DST	−30.0	−29.2	1.5	0.96	1.02	0.59
SO	34/10-36	TS	3373	Tarbert	TEST	−28.5	−27.0	2.4	2.23	0.67	0.81
SO	36/7-1	MS	2363	Fensfjord	DST	−29.0	−27.5	2.2	1.64	0.76	0.66

Table 3
Rock-Eval and isotope results of the source rock samples. M – Mandal Formation, T – Tau Formation, D – Draupne Formation, KCF–Kimmeridge Clay Formation, TOC – total organic carbon, HI – hydrogen index, OI – oxygen index, PI – production index, δ^{13}C Sat – stable carbon isotope of the saturated fraction, δ^{13}C Aro – stable carbon isotope of the aromatic fraction.

Fm	Type	Well	Depth	TOC	S1	S2	Tmax	HI	OI	PI	13 C SAT	13C ARO
M	DC	2/1-6	4115	1.1	2.3	1.7	438	157	74	0.57		
M	COCH	2/1-6	4127	5.8	7.0	15.9	448	274	12	0.31		
M	COCH	2/1-6	4147	1.2	1.7	1.8	449	147	175	0.49		
M	COCH	2/1-6	4153	0.7	0.7	0.8	450	107	77	0.48		
M	COCH	2/1-6	4161	0.5	0.7	0.4	444	78	72	0.62		
M	DC	2/7-25S	4720	5.8	35.1	22.5	422	390	42	0.61		
M	DC	2/7-25S	4750	6.6	39.5	21.3	422	323	34	0.65		
M	DC	2/7-25S	4783	2.8	17.2	5.8	267	206	12	0.75		
M	COCH	2/7-25S	4810	6.9	40.4	21.3	420	308	25	0.65		
M	DC	7/4-1	2976	1.0	5.9	24.5	430			0.19		
M	COCH	7/4-1	2981	0.4	0.1	0.1	475	33	195	0.30		
M	COCH	7/4-1	2988	7.8	3.6	35.2	431	453	14	0.09	−32.3	−31.5
T	DC	9/2-2	2964	2.3	1.0	7.1	437	303	20	0.13		
T	DC	9/2-2	2991	5.1	1.9	21.8	434	426	20	0.08	−29.5	−29.6
T	DC	9/2-2	3021	3.8	1.2	12.2	436	323	23	0.09		
T	DC	9/2-2	3054	2.3	0.6	7.0	432	307	77	0.08	−29.7	−28.9
D	COCH	16/2-13A	2588	7.1	3.1	32.3	419	459	15	0.09	−29.8	−31.6
D	COCH	16/2-13A	2595	5.8	3.4	26.9	420	467	24	0.11		
T	DC	17/3-1	2331	4.5	2.3	15.0	430	336	79	0.13		
T	DC	17/3-1	2337	6.3	3.0	23.6	432	372	31	0.11	−29	−28.4
D	DC	25/5-2	3020	7.5	2.4	31.2	426	418	25	0.07	−31.9	−31.5
D	DC	25/5-2	3050	7.9	3.9	30.9	429	390	11	0.11		
D	DC	25/5-2	3070	8.3	3.1	19.2	420	231	19	0.14	−30.5	−29.5
D	DC	25/5-2	3100	6.5	1.3	12.8	425	196	20	0.09		
D	DC	25/5-2	3120	7.2	1.5	15.1	428	210	29	0.09	−28.7	−26.7
D	DC	31/4-6	2125	2.3	0.4	7.3	428	311	88	0.05		
D	COCH	31/4-6	2133	6.4	2.0	27.8	430	438	22	0.07	−31.1	−31.4
D	DC	31/6-3	1380–85	1.8	1.3	4.0	430	226	111	0.25		
D	DC	31/6-3	1400–02	2.2	1.2	5.2	432	231	65	0.19		
D	DC	31/6-3	1425–30	2.4	1.2	5.2	433	220	71	0.19	−29.3	−31
D	DC	31/6-3	1485–90	3.1	1.4	7.1	431	229	51	0.17		
D	COCH	34/7-21	2552	6.0	1.3	25.6	422	426	26	0.05		
D	COCH	34/7-21	2570	9.6	3.4	39.0	412	408	15	0.08	−30.3	−29
D	COCH	34/7-21	2580	7.4	0.8	13.4	405	180	23	0.06		
KCF	DC	30/8-1	3716	8.0	59.1	21.2	432	264	43	0.74		
KCF	DC	30/8-1	3743	6.0	51.1	22.3	437	374	51	0.70		
KCF	DC	30/8-1	4191	6.6	51.8	20.9	444	317	44	0.71		
KCF	DC	30/8-1	4246	5.5	54.6	20.1	445	369	50	0.73		
KCF	DC	30/8-1	4292	5.5	53.8	19.4	445	351	52	0.73		
KCF	DC	30/8-1	4392	2.8	49.6	16.5	434	588	94	0.75		
KCF	DC	30/8-1	4462	6.6	50.6	19.2	432	293	57	0.73		

(*continued on next page*)

Table 3 (*continued*)

Fm	Type	Well	Depth	TOC	S1	S2	Tmax	HI	OI	PI	13 C SAT	13C ARO
KCF	DC	30/8-1	4478	7.0	50.1	16.0	432	230	58	0.76		
KCF	DC	29/15-2	4587	6.7	6.7	7.1	434	105	26	0.49		
KCF	DC	29/15-2	4621	4.9	6.0	6.6	434	134	40	0.48		
KCF	DC	29/15-2	4648	3.5	3.7	4.0	434	115	44	0.48		
KCF	DC	30/2A-6	5230	7.9	18.8	15.9	424	203	19	0.54		
KCF	DC	30/2A-6	5252	6.6	19.1	17.3	432	263	25	0.52		
KCF	DC	30/2A-6	5273	6.4	21.3	18.1	430	282	28	0.54		
KCF	DC	30/2A-6	5291	5.0	15.5	15.5	435	307	36	0.50		
KCF	DC	30/13-3	3901	1.0	2.2	1.8	371	173	112	0.55		
KCF	DC	30/13-3	3932	4.7	16.4	9.8	435	210	44	0.63		
KCF	DC	30/13-3	3962	4.8	22.6	12.8	443	265	34	0.64		
KCF	DC	30/13-3	3972	4.6	34.9	13.5	441	296	26	0.72		
KCF	DC	30/13-3	3981	3.6	31.4	12.1	440	338	46	0.72		
KCF	DC	30/13-3	3990	5.0	32.5	14.3	439	285	33	0.69		
KCF	DC	30/13-3	3996	3.3	32.4	11.6	442	358	54	0.74		
KCF	DC	30/13-3	4008	3.3	39.0	12.7	436	382	44	0.76		
KCF	DC	30/13-3	4017	4.1	47.5	13.7	438	337	84	0.78		
KCF	DC	30/13-3	4026	3.3	33.4	10.1	433	305	190	0.77		
KCF	DC	30/13-3	4036	2.1	33.2	11.4	439	547	129	0.74		

Table 4
The mineral and maceral composition. The maceral composition is shown as the volume percentage of each component in the samples. M – Mandal Formation, T – Tau Formation, D – Draupne Formation, KCF–Kimmeridge Clay Formation, %Q – %Quartz, %C – %Clay, %P – %Pyrite, %OM – %Other minerals, %M – Macerals, %SB – %Solid bitumen, %L – Liptinite, % L-M – % Marine Liptinite, %L-T – % Terrigenous Liptinite, % V – % Vitrinite, and I – % Inertinite. Depths are presented in metres.

Fm	Type	Well	Depth	% Q	% C	% P	% OM	% M	% SB	% M + SB	% L	% L-M	% L-T	% V	% I
M	DC	2/1-6	4115	89.3	6.7	2.3	2.3	1.3	0.3	1.6	0.0	0.0	0.0	91.8	8.2
M	COCH	2/1-6	4127	8.4	77.9	8.0	8.4	1.0	4.3	5.3	6.2	7.9	7.9	34.2	50.0
M	COCH	2/1-6	4147	51.2	42.8	2.7	3.0	1.7	1.3	3.0	15.6	0.0	20.3	60.9	18.8
M	COCH	2/1-6	4153	52.2	41.5	4.0	4.3	2.0	0.0	2.0	7.1	0.0	9.5	78.4	12.2
M	COCH	2/1-6	4161	61.5	34.5	2.0	2.0	0.0	2.0	2.0	0.0	0.0	0.0	71.4	28.6
M	DC	2/7-2SS	4720	84.3	10.3	2.0	2.0	3.0	0.3	3.3	33.0	4.1	33.0	56.2	6.7
M	DC	2/7-2SS	4750	70.7	22.7	3.3	3.3	3.0	0.3	3.3	35.3	24.7	13.7	54.9	6.6
M	DC	2/7-2SS	4783	63.3	31.7	2.7	3.3	0.7	1.0	1.7	4.1	0.0	7.8	70.6	21.6
M	COCH	2/7-2SS	4810	93.7	0.0	4.3	5.0	1.3	0.0	1.3	28.0	28.0	2.8	60.4	8.8
M	DC	7/4-1	2976	19.7	68.7	1.7	2.0	9.3	0.3	9.6	65.0	34.3	48.0	11.4	6.3
M	COCH	7/4-1	2981	22.7	45.3	13.7	14.7	14.0	3.3	17.3	58.0	55.2	22.1	20.0	2.7
M	COCH	7/4-1	2988	20.3	47.3	14.3	14.7	15.3	2.3	17.6	68.0	49.8	33.2	11.0	6.1
T	DC	9/2-2	2964	77.3	8.3	2.7	2.7	9.3	2.3	11.6	39.0	16.9	33.8	44.2	5.2
T	DC	9/2-2	2991	14.0	60.3	8.3	9.0	12.0	4.7	16.7	39.0	19.9	35.8	27.1	17.1
T	DC	9/2-2	3021	15.0	65.3	4.3	4.7	11.0	4.0	15.0	36.0	15.4	38.4	35.8	10.4
T	DC	9/2-2	3054	17.7	68.3	3.7	4.7	9.3	0.0	9.3	16.0	6.1	16.4	63.4	14.1
D	COCH	16/2-13A	2588	47.0	35.3	4.7	4.7	8.3	4.7	13.0	40.0	0.0	66.7	23.3	10.0
D	COCH	16/2-13A	2595	42.0	39.3	3.7	4.3	9.7	4.7	14.4	49.0	10.6	53.0	23.4	13.0
T	DC	17/3-1	2331	13.0	64.2	4.7	6.0	9.7	7.0	16.7	34.0	7.9	39.4	37.5	15.3
T	DC	17/3-1	2337	23.7	58.3	4.7	5.7	9.3	3.0	12.3	39.0	7.2	43.4	40.3	9.1
D	DC	25/5-2	3020	27.3	40.7	9.0	10.0	18.7	3.3	22.0	62.6	10.3	72.3	9.3	8.0
D	DC	25/5-2	3050	11.3	59.3	8.3	9.7	13.0	6.7	19.7	57.0	34.2	43.9	12.3	9.6
D	DC	25/5-2	3070	20.3	30.7	15.3	16.0	26.7	6.3	33.0	72.0	69.8	14.0	3.5	12.8
D	DC	25/5-2	3100	34.0	36.3	9.7	10.0	17.0	2.7	19.7	38.0	23.1	25.0	22.8	29.1
D	DC	25/5-2	3120	24.7	40.7	7.7	8.3	22.0	4.3	26.3	36.0	8.4	33.5	27.9	30.2
D	DC	31/4-6	2125	60.3	26.7	3.3	3.7	6.3	3.0	9.3	45.0	2.9	51.4	38.6	7.2
D	COCH	31/4-6	2133	64.0	16.3	6.3	6.3	10.0	3.3	13.3	53.0	0.0	62.4	31.8	5.9
D	DC	31/6-3	1380–85	27.0	66.7	1.7	1.7	3.3	1.3	4.6	42.1	1.9	43.3	51.6	3.2
D	DC	31/6-3	1400–02	13.7	74.3	1.3	2.0	7.7	2.3	10.0	44.0	10.6	42.4	39.8	7.2
D	DC	31/6-3	1425–30	6.3	84.7	1.7	2.0	6.0	1.0	7.0	44.0	0.0	52.4	44.0	3.6
D	DC	31/6-3	1485–90	7.7	79.7	3.0	3.0	7.7	2.0	9.7	29.0	3.8	30.3	57.6	8.2
D	COCH	34/7-21	2552	29.3	45.7	7.3	9.3	11.3	4.3	15.6	56.0	49.1	24.6	23.7	2.6
D	COCH	34/7-21	2570	24.3	42.3	6.7	7.7	16.7	9.0	25.7	45.0	28.5	28.5	34.2	8.9
D	COCH	34/7-21	2580	13.3	60.0	7.7	9.0	10.3	7.3	17.6	28.0	25.3	15.8	35.3	23.5
KCF	DC	30/8-1	3716	25.3	61.3	7.7	10.7	0.7	2.0	2.7	6.0	5.1	5.1	64.4	25.4
KCF	DC	30/8-1	3743	20.7	70.3	4.7	6.3	0.7	2.0	2.7	2.0	1.7	1.7	56.7	40.0
KCF	DC	30/8-1	4191	36.3	61.0	1.7	2.0	0.3	0.3	0.6	1.0	1.0	1.0	62.0	36.0
KCF	DC	30/8-1	4246	35.7	60.0	2.7	3.0	0.3	1.0	1.3	0.0	0.0	0.0	70.4	29.6
KCF	DC	30/8-1	4292	29.7	66.0	2.7	3.0	0.3	1.0	1.3	0.0	0.0	0.0	57.6	42.4
KCF	DC	30/8-1	4392	35.7	56.3	2.7	6.3	0.3	1.3	1.6	1.0	0.9	0.9	45.5	52.7
KCF	DC	30/8-1	4462	42.0	49.3	3.3	6.3	0.7	1.7	2.4	0.0	0.0	0.0	41.0	59.0
KCF	DC	30/8-1	4478	30.7	63.0	1.7	4.3	0.0	2.0	2.0	0.0	0.0	0.0	40.8	59.2
KCF	DC	29/15-2	4587	11.0	68.9	9.7	10.7	0.3	9.0	9.3	25.0	0.0	68.6	8.6	22.9
KCF	DC	29/15-2	4621	24.4	54.8	11.4	12.0	2.7	6.0	8.7	34.0	38.4	38.4	0.0	23.3
KCF	DC	29/15-2	4648	48.0	36.0	10.7	12.3	0.3	3.3	3.6	5.1	0.0	12.5	62.5	25.0

(*continued on next page*)

Table 4 (*continued*)

Fm	Type	Well	Depth	% Q	% C	% P	% OM	% M	% SB	% M + SB	% L	% L-M	% L-T	% V	% I
KCF	DC	30/2A-6	5230	18.0	63.3	11.0	12.0	1.3	5.3	6.6	4.0	6.1	6.1	63.6	24.2
KCF	DC	30/2A-6	5252	21.1	72.6	5.7	6.0	0.0	0.3	0.3	1.0	1.4	1.4	48.6	48.6
KCF	DC	30/2A-6	5273	25.4	65.2	6.0	6.7	1.3	1.3	2.6	5.0	8.6	0.0	29.3	62.1
KCF	DC	30/2A-6	5291	30.7	62.0	4.3	4.7	0.7	2.0	2.7	5.0	0.0	8.3	40.0	51.7
KCF	DC	30/13-3	3901	68.0	27.7	3.3	3.7	0.3	0.3	0.6	27.0	0.0	27.6	59.2	13.3
KCF	DC	30/13-3	3932	43.7	46.7	6.3	7.0	2.3	0.3	2.6	13.0	0.0	15.3	58.8	25.9
KCF	DC	30/13-3	3962	15.0	72.0	9.3	9.3	3.0	0.7	3.7	25.0	0.0	28.4	42.0	29.5
KCF	DC	30/13-3	3972	17.1	67.6	12.0	12.4	2.7	0.3	3.0	22.2	0.0	26.5	24.1	49.4
KCF	DC	30/13-3	3981	22.7	66.3	7.0	8.0	2.3	0.7	3.0	8.2	0.0	10.1	67.1	22.8
KCF	DC	30/13-3	3990	25.7	58.0	12.7	13.0	2.7	0.7	3.4	13.1	0.0	14.6	51.7	33.7
KCF	DC	30/13-3	3996	35.0	54.7	6.7	7.3	2.3	0.7	3.0	13.1	0.0	14.6	52.8	32.6
KCF	DC	30/13-3	4008	33.4	55.9	5.3	7.0	1.7	2.0	3.7	0.0	0.0	0.0	65.8	34.2
KCF	DC	30/13-3	4017	77.3	14.3	6.7	3.0	2.3	3.0	5.3	1.0	0.8	0.8	75.0	23.4
KCF	DC	30/13-3	4026	53.5	39.1	2.7	4.7	1.7	1.0	2.7	10.0	0.0	12.2	59.8	28.0
KCF	DC	30/13-3	4036	52.7	42.7	4.4	2.3	0.7	1.7	2.4	2.0	1.3	1.3	71.8	25.6

References

Al-Hajeri, M., Saucerer, B., Furmann, A., Amer, A., Al-Khamiss, A., Abdallah, W., 2021. Organic petrography and geochemistry of the prolific source rocks from the Jurassic Najmah and Cretaceous Makhul Formations in Kuwait–Validation and expansion of Raman spectroscopic thermal maturity applications. Int. J. Coal Geol. 236, 103654.

ASTM, 2011. D2799-11 Standard Test Method for Microscopical Determination of the Maceral Composition of Coal: Annual Book of ASTM Standards, Petroleum Products, Lubricants, and Fossil Fuels. Gaseous Fuels; Coal and Coke. ASTM International, West Conshohocken, PA.

Badley, M., Price, J., Dahl, C.R., Agdestein, T., 1988. The structural evolution of the northern Viking Graben and its bearing upon extensional modes of basin formation. J. Geol. Soc. 145, 455–472.

Barnard, P., Collins, A., Cooper, B., 1981. Identification and distribution of kerogen facies in a source rock horizon-examples from the North Sea basin. In: Brooks, J. (Ed.), Organic Maturation Studies and Fossil Fuel Exploration. Academic Press, London, pp. 271–282.

Barnard, P.C., Cooper, B.S., 1981. Oils and source rocks of the North Sea area. In: Illing, L.V., Hobson, G.D. (Eds.), Petroleum Geology of the Continental Shelf of North-West Europe: Proceedings of the 2nd Conference. Heyden and Son, London, pp. 169–175.

Berner, R.A., 1984. Sedimentary pyrite formation: an update. Geochem. Cosmochim. Acta 48, 605–615.

Carvajal-Ortiz, H., Gentzis, T., 2015. Critical considerations when assessing hydrocarbon plays using Rock-Eval pyrolysis and organic petrology data: data quality revisited. Int. J. Coal Geol. 152, 113–122.

Clementz, D., 1979. Effect of oil and bitumen saturation on source-rock pyrolysis. AAPG Bull. 63, 2227–2232.

Cooper, B., Barnard, P., Telnaes, N., 1995. The Kimmeridge Clay Formation of the north sea. In: Katz, B.J. (Ed.), Petroleum Source Rocks. Springer, Berlin, pp. 89–110.

Cornford, C., 1994. Mandal-ekofisk (!) petroleum system in the central graben of the north sea. In: Magoo, L.B., Dow, W.G. (Eds.), The Petroleum System - from Source to Trap. AAPG, Tulsa, pp. 537–571.

Cornford, C., 1998. Source rocks and hydrocarbons of the north sea. In: Glennie, K.W. (Ed.), Petroleum Geology of the North Sea: Basic Concepts Recent Advances, 4 ed. Blackwell Oxford, pp. 376–462.

Cornford, C., 2018. Petroleum systems of the south Viking graben. In: Turner, C.C., Cronin, B.T. (Eds.), Rift-related Coarsegrained Submarine Fan Reservoirs; the Brae Play, South Viking Graben, North Sea. AAPG Memoir, pp. 453–542.

Dahl, B., 2004. The use of bisnorhopane as a stratigraphic marker in the Oseberg back basin, North Viking graben, Norwegian North Sea. Org. Geochem. 35, 1551–1571.

Didyk, B., Simoneit, B., Brassell, S.t., Eglinton, G., 1978. Organic geochemical indicators of palaeoenvironmental conditions of sedimentation. Nature 272, 216–222.

Espitalié, J., Madec, M., Tissot, B., Mennig, J., Leplat, P., 1977. Source Rock Characterization Method for Petroleum Exploration. Offshore Technology Conference, OnePetro, pp. 439–448.

Fraser, S., Robinson, A., Johnson, H., Underhill, J., Kadolsky, D., Connell, R., Johannessen, P., Ravnås, R., 2002. Upper Jurassic. In: Evans, D., Graham, C., Armour, A., Bathurst, P. (Eds.), The Millennium Atlas: Petroleum Geology of the Central an Northern North Sea. Geological Society of London, London, pp. 157–189.

Færseth, R., 1996. Interaction of Permo-Triassic and Jurassic extensional fault-blocks during the development of the northern North sea. J. Geol. Soc. 153, 931–944.

Galimov, E., 1980. C13/C12 in Kerogen, Kerogen: Insoluble Organic Matter from Sedimentary Rocks. Editions Technip, Paris, pp. 271–299.

Gautier, D.L., 2005. Kimmeridgian Shales Total Petroleum System of the North Sea Graben Province. USGS Bulletin, pp. 1–24.

Grantham, P., Posthuma, J., De Groot, K., 1980. Variation and significance of the C27 and C28 triterpane content of a North Sea core and various North Sea crude oils. Phys. Chem. Earth 12, 29–38.

Gonçalves, P.A., Mendonça Filho, J.G., Mendonça, J.O., da Silva, T.F., Flores, D., 2013. Paleoenvironmental characterization of a Jurassic sequence on the Bombarral sub-basin (Lusitanian basin, Portugal): insights from palynofacies and organic geochemistry. Int. J. Coal Geol. 113, 27–40.

Huc, A., Irwin, H., Schoell, M., 1985. Organic matter quality changes in an Upper Jurassic shale sequence from the Viking Graben. In: Thomas, B.M., Dore, A.G., Eggen, S.S., Home, P.C., Larsen, R.M. (Eds.), Petroleum Geochemistry in Exploration of the Norwegian Shelf. Graham & Trotman Ltd., London, pp. 179–183.

Hughes, W.B., Holba, A.G., Dzou, L.I.P., 1995. The ratios of dibenzothiophene to phenanthrene and pristane to phytane as indicators of depositional environment and lithology of petroleum source rocks. Geochem. Cosmochim. Acta 59, 3581–3598.

ICCP, 1998. The new vitrinite classification (ICCP System 1994). Fuel 77, 349–358.

Isaksen, G.H., Ledje, K.H.I., 2001. Source rock quality and hydrocarbon migration pathways within the greater Utsira High area, Viking Graben, Norwegian North Sea. AAPG Bull. 85, 861–883.

Justwan, H., Dahl, B., 2005. Quantitative hydrocarbon potential mapping and organofacies study in the greater Balder area, Norwegian North Sea. In: Doré, A.G., Vining, B. (Eds.), Proceedings of the 6th Petroleum Geology Conference: North-West Europe and Global Perspectives. Geological Society London, pp. 1317–1329.

Justwan, H., Dahl, B., Isaksen, G., 2006. Geochemical characterisation and genetic origin of oils and condensates in the South Viking Graben, Norway. Mar. Petrol. Geol. 23, 213–239.

Justwan, H., Dahl, B., Isaksen, G., Meisingset, I., 2005. Late to middle Jurassic source facies and quality variations, South Viking graben, North Sea. J. Petrol. Geol. 28, 241–268.

Karlsen, D.A., Nedkvitne, T., Larter, S.R., Bjørlykke, K., 1993. Hydrocarbon composition of authigenic inclusions: application to elucidation of petroleum reservoir filling history. Geochem. Cosmochim. Acta 57, 3641–3659.

Keym, M., Dieckmann, V., Horsfield, B., Erdmann, M., Galimberti, R., Kus, L.-C., Leith, L., Podlaha, O., 2006. Source rock heterogeneity of the upper Jurassic Draupne formation, North Viking graben, and its relevance to petroleum generation studies. Org. Geochem. 37, 220–243.

Kubala, M., Bastow, M., Thompson, S., Scotchman, I., Oygard, K.J.T.M.A.P.G.o.t.C., 2003. Geothermal Regime, Petroleum Generation and Migration, vol. 289, p. 315. Northern North Sea. Geological Society, L.

Kus, J., Khanaqa, P., Mohialdeen, I., Kauffold, S., Babies, H., Meßner, J., Blumenberg, M., 2016. Solid bitumen, bituminite and thermal maturity of the upper Jurassic-lower Cretaceous Chia Gara formation, Kirkuk oil field, Zagros fold Belt, Kurdistan, Iraq. Int. J. Coal Geol. 165, 28–48.

Langrock, U., Stein, R., Lipinski, M., Brumsack, H.J., 2003. Late Jurassic to Early Cretaceous black shale formation and paleoenvironment in high northern latitudes: examples from the Norwegian-Greenland Seaway. Paleoceanography 18.

Lückge, A., Horsfield, B., Littke, R., Scheeder, G., 2002. Organic matter preservation and sulfur uptake in sediments from the continental margin off Pakistan. Org. Geochem. 33, 477–488.

Macquaker, J., Gawthorpe, R., 1993. Mudstone lithofacies in the Kimmeridge Clay Formation, Wessex Basin, southern England; implications for the origin and controls of the distribution of mudstones. J. Sediment. Res. 63, 1129–1143.

Mannie, A.S., Jackson, C.A.-L., Hampson, G.J., 2014. Structural controls on the stratigraphic architecture of net-transgressive shallow-marine strata in a salt-influenced rift basin: middle-to-Upper Jurassic Egersund Basin, Norwegian North Sea. Basin Res. 26, 675–700.

Misch, D., Riedl, F., Liu, B., Horsfield, B., Ziegs, V., Mendez-Martin, F., Vranjes-Wessely, S., Sachsenhofer, R.F., 2019. Petrographic and sorption-based characterization of bituminous organic matter in the Mandal Formation. Cent. Graben (Norway) 211, 103229.

Northam, M.A., 1985. Correlation of Northern North Sea oils: the different facies of their Jurassic source. In: Thomas, B.M., Dore, A.G., Eggen, S.S., Home, P.C., Larsen, R.M. (Eds.), Petroleum Geochemistry in Exploration of the Norwegian Shelf. Graham & Trotman Ltd., London, pp. 93–99.

NPD, 2014. Lithostratigraphic Chart, Norwegian North Sea. https://www.npd.no/globalassets/1-npd/fakta/geologi-eng/ns-od1409001.pdf.

Nøttvedt, A., Berge, A.M., Dawers, N.H., Færseth, R.B., Høiger, K.O., Mangerud, G., Puigdefabregas, C., 2000. Syn-rift evolution and resulting play models in the Snorre-H area, northern North Sea. Geol. Soc. Lond. Spec. Pub. 167, 179–218.
Nøttvedt, A., Gabrielsen, R., Steel, R., 1995. Tectonostratigraphy and sedimentary architecture of rift basins, with reference to the northern North Sea. Mar. Petrol. Geol. 12, 881–901.
Ohm, S., Beeley, H., Karlsen, D., Hall, P., Foss, A., 2006. An atypical early mature oil in Block 35/1, Norwegian North Sea–hypersaline, carbonate Jurassic environment? Petrol. Geosci. 12, 157–174.
Ohm, S.E., Karlsen, D.A., Phan, N.T., Strand, T., Iversen, G.J.A.b., 2012. Present Jurassic petroleum charge facing Paleozoic biodegraded oil: geochemical challenges and potential upsides, Embla field, north sea petroleum filling history of the Embla field. North Sea 96, 1523–1552.
Oschmann, W., 1988. Kimmeridge Clay sedimentation—a new cyclic model. Palaeogeogr. Palaeoclimatol. Palaeoecol. 65, 217–251.
Pedersen, J.H., Karlsen, D.A., Backer-Owe, K., Lie, J.E., Brunstad, H., 2006. The geochemistry of two unusual oils from the Norwegian North Sea: implications for new source rock and play scenario. Petrol. Geosci. 12, 85–96.
Pegrum, R., Spencer, A., 1990. Hydrocarbon plays in the northern North sea. In: Brooks, J. (Ed.), Classic Petroleum Provinces. Geological Society Special Publication, London, pp. 441–470.
Peters, K.E., 1986. Guidelines for evaluating petroleum source rock using programmed pyrolysis. AAPG Bull. 70, 318–329.
Petersen, H., Hertle, M., Juhasz, A., Krabbe, H., 2016. Oil family typing, biodegradation and source rock affinity of liquid petroleum in the Danish North Sea. J. Petrol. Geol. 39, 247–268.
Petersen, H., Hertle, M., Sulsbrück, H., 2017. Upper Jurassic–lowermost Cretaceous marine shale source rocks (Farsund Formation), North Sea: kerogen composition and quality and the adverse effect of oil-based mud contamination on organic geochemical analyses. Int. J. Coal Geol. 173, 26–39.
Petersen, H., Holme, A., Andersen, C., Whitaker, M., Nytoft, H., Thomsen, E., 2013. The Source Rock Potential of the Upper Jurassic–Lowermost Cretaceous in the Danish and Southern Norwegian Sectors of the Central Graben. North Sea. first break 31.
Pickel, W., Kus, J., Flores, D., Kalaitzidis, S., Christanis, K., Cardott, B., Misz-Kennan, M., Rodrigues, S., Hentschel, A., Hamor-Vido, M., 2017. Classification of liptinite–ICCP system 1994. Int. J. Coal Geol. 169, 40–61.
Ponsaing, L., Bojesen-Koefoed, J.A., Thomsen, E., Stemmerik, L., 2018. Temporal organic facies variations of upper Jurassic-lowermost Cretaceous source rocks in the Danish central graben, North Sea. Int. J. Coal Geol. 195, 217–237.
Ponsaing, L., Petersen, H., Bojesen-Koefoed, J., Nytoft, H., Schovsbo, N., Stemmerik, L., 2020. Source rock quality variations of Upper Jurassic–lowermost Cretaceous marine shales and their relationship to oils in the Valdemar Field, Danish North Sea. J. Petrol. Geol. 43, 49–74.
Radke, M., Welte, D.H., Willsch, H., 1982. Geochemical study on a well in the Western Canada Basin: relation of the aromatic distribution pattern to maturity of organic matter. Geochem. Cosmochim. Acta 46, 1–10.
Radke, M., Willsch, H., Welte, D.H., 1980. Preparative hydrocarbon group type determination by automated medium pressure liquid chromatography. Anal. Chem. 52, 406–411.
Raiswell, R., Buckley, F., Berner, R.A., Anderson, T., 1988. Degree of pyritization of iron as a paleoenvironmental indicator of bottom-water oxygenation. J. Sediment. Res. 58, 812–819.
Ritter, U., Leith, T.I., Griffiths, C.M., Schou, L., 1987. Hydrocarbon generation and thermal evolution in parts of the Egersund Basin, northern North sea. In: Beaumont, C., Tankard, A.J. (Eds.), Sedimentary Basins and Basin Forming Mechanism. Canadian Society of Petroleum Geology Calgary, pp. 75–85.
Rodriguez, N.D., Katz, B.J., 2021. The effect of oil-based drilling mud (OBM) on the assessment of hydrocarbon charge potential. Mar. Petrol. Geol. 133, 105312.
Rossland, A., Escalona, A., Rolfsen, R., 2013. Permian–holocene tectonostratigraphic evolution of the mandal high, central graben, North Sea. AAPG Bull. 97, 923–957.
Scheidt, G., Littke, R., 1989. Comparative organic petrology of interlayered sandstones, siltstones, mudstones and coals in the Upper Carboniferous Ruhr basin, Northwest Germany, and their thermal history and methane generation. Geol. Rundsch. 78, 375–390.
Schou, L., Eggen, S., Schoell, M., 1985. Oil—oil and oil—source rock correlation, Northern North Sea. In: Thomas, B.M., Dore, A.G., Eggen, S.S., Home, P.C., Larsen, R. M. (Eds.), Petroleum Geochemistry in Exploration of the Norwegian Shelf. Graham & Trotman Ltd., London, pp. 101–117.
Scotese, C.R., 2016. PALEOMAP PaleoAtlas for GPlates and the PaleoData Plotter Program. PALEOMAP Project. http://www.earthbyte.org/paleomap-paleoatlas-for-gplates/.
Scotchman, I., 1989. Diagenesis of the Kimmeridge Clay Formation, onshore UK. J. Geol. Soc. 146, 285–303.
Spencer, A., Home, P., Wiik, V., 1986. Habitat of hydrocarbons in the Jurassic Ula trend, central graben, Norway. In: Spencer, A. (Ed.), Habitat of Hydrocarbons on the Norvegian Continental Shelf. Graham & Trotman, London, p. 354.
Thomas, B., Møller-Pedersen, P., Whitaker, M., Shaw, N., 1985. Organic facies and hydrocarbon distributions in the Norwegian North Sea. In: Thomas, B.M., Dore, A.G., Eggen, S.S., Home, P.C., Larsen, R.M. (Eds.), Petroleum Geochemistry in Exploration of the Norwegian Shelf. Graham & Trotman London, pp. 3–26.
Weiss, H.M., Wilhelms, A., Mills, N., Scotchmer, J., Hall, P.B., Lind, K., Brekke, T., 2000. NIGOGA - the Norwegian Industry Guide to organic geochemical analyses 4.0. In: Norsk Hydro, Statoil, Geolab Nor, SINTEF Petroleum Research and the Norwegian Petroleum Directorate, p. 102. https://www.npd.no/globalassets/1-npd/regelverk/rapportering/bronner/eng/guide-organic-geochemical-analyses.pdf.
Yang, S., Horsfield, B., 2020. Critical review of the uncertainty of Tmax in revealing the thermal maturity of organic matter in sedimentary rocks. Int. J. Coal Geol. 225, 103500.
Ziegler, P., 1982. Geological Atlas of Western Europe. Shell International Petroleum, Maatschappij, BV, Amsterdam.
Ziegler, P., 1992. North Sea rift system. Tectonophysics 208, 55–75.
Ziegs, V., Horsfield, B., Skeie, J.E., Rinna, J., 2017. Petroleum retention in the mandal formation, central Graben, Norway. Mar. Petrol. Geol. 83, 195–214.
Zumberge, J., Illich, H., Waite, I., 2016. Petroleum geochemistry of the Cenomanian–Turonian Eagle Ford oils of south Texas. In: Breyer, J.A. (Ed.), The Eagle Ford Shale: A Renaissance in U.S. Oil Production. AAPG Memoir, pp. 135–166.

Further Reading

Goff, J., 1983. Hydrocarbon generation and migration from Jurassic source rocks in the E Shetland Basin and Viking Graben of the northern North Sea. Journal of the Geological Society 140, 445–474.
Johannesen, J., Hay, S., Milne, J., Jebsen, C., Gunnesdal, S., Vayssaire, A., 2002. 3D oil migration modelling of the Jurassic petroleum system of the Statfjord area, Norwegian North Sea. Petroleum Geoscience 8, 37–50.
Kalani, M., Faleide, J.I., Gabrielsen, R.H., 2020. Paleozoic-Mesozoic tectono-sedimentary evolution and magmatism of the Egersund Basin area, Norwegian central North Sea. Marine Petroleum Geology 122, 104642.
Peters, K., Moldowan, J., 1991. Effects of source, thermal maturity, and biodegradation on the distribution and isomerization of homohopanes in petroleum. Organic Geochemistry 17, 47–61.
Peters, K.E., Walters, C.C., Moldowan, J.M., 2005a. The Biomarker Guide: Volume I, Biomarkers and Isotopes in the environment and human history, second ed. Cambridge University Press, United Kingdom.
Peters, K.E., Walters, C.C., Moldowan, J.M., 2005b. The Biomarker Guide: Volume II, Biomarkers and Isotopes in Petroleum Exploration and Earth History, second ed. Cambridge University Press, United Kingdom.
Dahl, B., Speers, G., 1985. In: Thomas, B.M. (Ed.), Organic Geochemistry of the Oseberg Field (I). Dore, A.G., Eggen, S.S., Home, P.C., Larsen, R.M. (Eds.), Petroleum Geochemistry in Exploration of the Norwegian Shelf. Graham & Trotman London, pp. 185-195.

Paper IV

Barbados Petroleum and Its Role in Understanding Distribution of Cretaceous Source Rocks in the Southeastern Caribbean Margin: Insights from an Organic Geochemistry Study

Andrés Cedeño[1], Sverre Ohm[1], and Alejandro Escalona[1]

[1]University of Stavanger, Department of Energy Resources,

AAPG Memoir 123, p. 441–468.

DOI: 10.1306/13692254M1233854

This paper is not available in Brage due to copyright

Paper V

Source Rocks in the Guyana Basin: Insights from Geochemical Investigation of 15 Heavy Oils from Onshore Suriname

Andres Cedeño[1], Sverre Ohm[1], Alejandro Escalona[1], Eshita Narain[2], Jan de Jager[3]

[1]University of Stavanger, Department of Energy Resources
[2]Staasolie Hydrocarbon Institute
[3]Retired / Independent consultant

AAPG Memoir 123, p. 749–776.

DOI: 10.1306/13692312M1233854

Appendix 1

Analytical methods

Organic Geochemical Analyses

TOC and Rock-Eval

All samples were mechanically grounded to powder. The TOC content was quantified with a LECO SC-632 combustion oven tuned to an IR-detector. Rock-Eval pyrolysis was performed using a Rock-Eval 6 instrument, allowing direct measurement of free hydrocarbons (S1), remaining hydrocarbon generative potential (S2), carbon dioxide (CO_2) content produced during thermal cracking (S3), and temperature of S2 maxima (T_{max}) (Espitalie et al., 1977). The pyrolysis programme started at 300 °C (held for 3 min) and increased to 650 °C (held for 0 min) at 25 °C/min.

Pyrolysis-gas chromatography, Py-GC

Open-system pyrolysis-gas chromatography (Py-GC) was performed using a HP5890 II instrument with an MSSV injector and an FID. The column is a HP-1 (length 50 m, i.d. 0.32 mm, film thickness 0.52 μm) and the injector unit is from Margot Köhnen-Willsch Chromatographie & Software. An open sample tube containing 20 mg of pulverized whole rock was placed in the system injector at a preheated temperature of 300 °C and volatile compounds evaporated before the pyrolysis oven was closed. The oven temperature was increased to 600 °C at a rate of 25 °C/min. The pyrolysis products were collected in a liquid nitrogen cooled trap for 10 min before being released into the GC column, whereupon there were released at an initial temperature of 40 °C (held 13 min), heated to 300 °C at 5 °C/min (held 25 min), and finally increased to 320 °C at 5 °C/min (held 10min). The pyrolysates were monitored on-line using a HP-1 capillary column (length 50m, i.d. 0.32 mm, film thickness 0.52 μm) on the GC that was equipped with a flame ionization

detector (FID). Boiling ranges (C1, C2–C5, C6–C14, C15+) and individual compounds (n-alkenes, n-alkanes, alkylaromatic, and alkylthiophenes) were quantified using n-butane as an external standard. Response factors for all resolved compounds were assumed to be the same. In the case of methane, a response factor of 1.1 was assumed according to di Primio et al. (1998).

Bulk kinetics

Bulk kinetics uses a Rock-Eval 6 instrument at five different heating rates (1 °C/min, 2 °C/ min, 5 °C/min, 15 °C/min, 25 °C/min). Kinetics05 software from Lawrence Livermore National Laboratory (Burnham et al., 1987) was used to calculate a discrete activation energy distribution (EA) and the frequency factor (A).

Extraction

Isolation of the extractable organic matter (EOM) was performed using a Soxtec Tecator instrument. Thimbles were pre-extracted in dichloromethane with 7 % (vol/vol) methanol, 10 min boiling and 20 min rinsing. The sample was weighed accurately in the pre-extracted thimbles and boiled for 1 hour and rinsed for 2 hour in approximately 80cc of dichloromethane with 7 % (vol/vol) methanol. Copper blades activated in concentrated hydrochloric acid were added to the extraction cups to cause free sulfur to react with the copper.

Deasphalting and MPLC

For deasphalting, extracts were evaporated almost to dryness before a small amount of dichloromethane (3 times the amount of EOM) was added. Pentane was added in excess (40 times the volume of EOM and dichloromethane) and the solution was stored for at least 12 hours in a dark

place before the solution was filtered or centrifuged and the weight of the asphaltenes measured.

The saturate and aromatic fractions of oils and extracts were separated. The MPLC was constructed as described by Radke et al. (1980). Two HPLC pumps, a sample collector, and two packed columns were included in the system. The precolumn was filled with Kieselgel 100, which was heated at 600°C for 2 hours to deactivate it. The main column, a LiChroprep Si60 column, was heated at 120°C (held for 2 hours) with a helium flow to evacuate water. An aliquot of approximately 30 mg of deasphaltened oils and extracts diluted in 1 ml hexane was injected into a sample loop. The solvents used were hexane and dichloromethane.

Isotopes of SARA Fractions

The stable carbon isotope analysis of the saturate, aromatic, and asphaltene (SARA) fractions was performed using a Thermo Fisher Scientific Elemental Analyser held at 1020°C, rising to 1700°C to help flash-combust the samples. The produced water was trapped on Magnesium Perchlorate. CO_2 was separated by column and flashed into Delta V Plus Isotope Ratio Mass Spectrometer (IRMS, Thermo Fisher Scientific) via Conflo IV.

The deasphaltened samples were then loaded into an automatic sampler and placed in a combustion reactor (Thermo Fisher Scientific Elemental Analyzer) held at 1020 °C. The produced water was trapped on Magnesium Perchlorate.

MSSV Closed-System Pyrolysis

Compositional kinetic modeling follows the approach described by Horsfield et al. (1989) and Dieckmann and Keym (2006). Milligram

amounts were sealed in glass capillary tubes (five tubes per sample) and heated at a single heating rate (0.7 °C/min) to final temperatures corresponding to preselected transformation ratios (10%, 30%, 50%, 70% and 90%). The temperatures corresponding to the selected transformation ratios were determined by simulated heating of the bulk kinetics parameters, as estimated from the Rock-Eval pyrolysis data, at the specified heating rate. The sample tubes were placed in the injector system and then broken when pressure had stabilized after 4 min. The composition of the generated hydrocarbon products was analyzed by thermovaporisation-gas chromatography (Tvap-GC) as described above. Compositional models with two (oil and gas), four (C1, C2–C5, C6–C14 and C15+), and fourteen (C1, C2, C3, i-C4, n-C4, i-C5, n-C5, pseudo-C6, C7–C15, C16–C25, C26–C35, C36–C45, C46–C55, C56–C80) components were developed.

Prediction of petroleum physical properties

For prediction of petroleum physical properties such as saturation pressure (Psat), gas to oil ratio (GOR), and formation volume factor (Bo), the Phase Kinetics approach by di Primio and Horsfield (2006) was followed. The estimation of petroleum phase was carried out using the fluid description consisting of 14 components, seven in the gas range (C1, C2, C3, i-C4, n-C4, i-C5, n-C5) and seven in the liquid range (pseudo-C6, C7–C15, C16–C25, C26–C35, C36–C45, C46–C55, C56–C80; di Primio and Horsfield, 2006).

Because of the comparably low content of methane in gases derived from pyrolysis experiment and its impact on phase behavior (di Primio et al., 1998; di Primio and Skeie, 2004; di Primio and Horsfield, 2006), its relative abundance needs to be corrected following the approach by di Primio and Horsfield (2006). The correcting procedure consisted in iterative adjustment of the methane to wet gas ratio, assuming decreasing gas wetness ratio for

increasing transformation ratio, and shifting of the trends of Psat against GOR and Psat against Bo closer to the linear trends typically observed in natural petroleum systems (di Primio and Horsfield, 2006). The properties of the C7+ lumped fractions were then calculated from the corresponding properties for C7 to C80 single carbon number groups by mass weighted averaging as described by Pedersen et al. (1985). The tuned component descriptions from MSSV closed-system pyrolysis were combined with the bulk kinetic model from open-system pyrolysis. The 14 components were allocated to the non-zero reaction weights from the bulk kinetic model, so that simulation of the resultant 14-component kinetic model best-fits the MSSV data. A coordinate-wise stochastic search algorithm (Zabinsky et al., 1993; Zabinsky, 1998) was used to compute a least-squares best-fit of the compositional kinetic model to the tuned compositional descriptions.

Gas Chromatography of whole oil and EOM

Whole-oil gas chromatography was performed on an Agilent 7890 gas chromatograph coupled with a Hewlett Packard-PONA capillary column (50 m × 0.2mm, film thickness = 0.50 μm) used to resolve hydrocarbons to n-C40. A constant flow of hydrogen carrier gas was used through the entire gas chromatographic run. Components were detected by a flame ionization detector (FID). Oven temperature was programmed to run from 30°C (hold for 10 minutes) to 60°C (hold for 10 minutes) at 2°C/min, then rise to 130°C at 2°C/min, and finally increase to 320°C at 4°C/min (hold for 25 minutes). Prior to injection, oil samples were prepared for analysis by homogenization and addition of internal standards. The internal standard used was 2,2,4-tri-methyl-pentane.

As for the extracted samples, the Hewlett-Packard 7890 gas chromatograph was equipped with a FID and a CP-Sil-5 CB-MS column (30 m × 0.25 mm,

film thickness 0.25 μm). The oven temperature was programmed from 50°C to 320°C at 4°C/min (hold for 25 minutes).

Gas Chromatography-Mass Spectrometry

Gas Chromatography-Mass Spectrometry (GC–MS) was carried out on a Thermo Scientific TSQ Quantum instrument. A FactorFour VF-1ms column (60 m × 0.25 mm, film thickness = 0.25 μm) was used. The instrument was tuned to a resolution of 0.7 mass units. The collision energy was 15 V with Argon as the collision gas at a pressure of 1.0 mtorr. The oven starting temperature was 50°C (hold for 1 minute) and was programmed to rise from 50°C to 225°C at 20°C/min, then from 225°C to 300°C at 2°C/min, and finally from 300°C to 320°C at 20°C/min (hold for 20 minutes). The internal standard was d4-27ααR.

Petrographic Analyses

The samples for microscopy were crushed and sieved through a 16-mesh sieve, and then embedded in thermoplastic epoxy in 2.54 cm molds. The pellets were ground and polished according to ASTM standards (ASTM, 2011). All samples were investigated under both white and UV-light using a Zeiss Axio-Scope A1 at 500× (10× eyepiece, and 50× objective) in immersion oil. White- and UV-light was provided by an X-Cite 120 LED light source. Point-counts were conducted using a proprietary automated point-counter attached to the stage of the Zeiss Axio-Scope. As macerals and minerals were identified under the crosshairs in the field of view, data were captured using proprietary software: once the petrographer made a count, the computer and motorized stage would then automatically move step-wise to a new, random field of view. Three-hundred counts of macerals and minerals were made for each sample. If there was insufficient organic matter

after the 300 counts, counting was continued until 100 total counts of organic matter were collected. The resolution of the microscope is 1 μm (≥1 μm).